The Role of BldB in the Development of the Antibiotic-producing Bacteria *Streptomyces*

Marieta Marinova Avramova

A thesis submitted in fulfilment of the requirements for the degree of Doctor of Philosophy

December 2021

Page intentionally left blank

Abstract

The classical life cycle of *Streptomyces* is intricate, involving the generation of distinct developmental structures in response to environmental cues - the vegetative mycelium, the hydrophobic aerial hyphae, and mature spores. The production of clinically useful antibiotics is tightly coordinated with this complex life cycle.

Two families of developmental regulators control the life cycle transitions in *Streptomyces*. Bld regulators control the formation of the reproductive aerial hyphae, while Whi regulators control the differentiation of the reproductive structures into spores. This work focuses on BldB, whose function was a mystery. BldB has ten paralogues in *Streptomyces venezuelae*, all of which are encoded next to paralogues of the DNA-binding regulator WhiJ. Five of these BldB paralogues are encoded next to paralogues of the putative anti-sigma factor AbaA.

In this work I show that the deletion of *bldB* in *S. venezuelae* leads to a classical “bald” phenotype – the mutant cannot differentiate past vegetative growth. By screening a bacterial-two-hybrid library, I demonstrate that BldB strongly interacts with seven of its *S. venezuelae* BldB paralogues. The deletion of two of these paralogues results in sporulation-deficient phenotypes in *S. venezuelae*. RNA-seq showed a striking upregulation of all five *abaA* paralogues and the novel inhibitor of sporulation *iosA* in the *ΔbldB* mutant, suggesting that BldB indirectly represses the expression of these genes. I show that the tandem overexpression of *abaA6* and *iosA* recapitulates the *ΔbldB* mutant phenotype. The putative anti-sigma factor AbaA6 is involved in a network of protein interactions reminiscent of SigB-like partner-switching systems. I demonstrate that one of the WhiJ paralogues, WhiJ9, directly activates the expression of *iosA* by binding to direct repeats in the *iosA*-*whiJ9* intergenic region. Finally, I present evidence that BldB9 might be the protein that provides the biochemical link between BldB- and WhiJ9-mediated control of *iosA* expression.

This abstract is 296 words long. The whole thesis is 292 pages and 76,035 words long.

"*Mimi, I can help you with some of your problems, but not all of them.*"

Dr Govind Chandra, midway through RNA-seq analysis, 2018

Table of Contents

Abstract 3
Table of Contents 5
Table of Figures 9
Index of Tables 12
Acknowledgements 13
Abbreviations 16
1. General Introduction 17
The Importance of Being *Streptomyces* 17
The *Streptomyces* Life Cycle 19
Building *Streptomyces* Aerial Hyphae 22
Genes Required for Aerial Mycelium Formation in *Streptomyces* 27
Genes Required for Mature Spore Formation in *Streptomyces* 31
Project Aims 35
2. Materials and Methods 37
Bacterial and Bacteriophage Strains 37
Escherichia coli Strains 37
Streptomyces Strains 38
Bacteriophage Strains 39
Plasmids and Cosmids 40
Culture Media and Antibiotics 46
Solid Media 46
Liquid Media 48
Antibiotics and Substrates 49
Growth Conditions and Storage of Bacterial and Phage Strains 50
E. coli Strains 50
S. venezuelae Strains 50
Phage Strains 50
DNA Methods 52
Plasmid and Cosmid DNA Isolation from *E. coli* 52
General PCR 52
Colony PCR 52
Agarose Gel Electrophoresis 53
PCR Purification 53
Oligonucleotides 54
DNA Gel Extraction 74
DNA Restriction Enzyme Digestion 74

DNA Quantification 74
Vector DNA Dephosphorylation 74
Ligation 74
Golden Gate Cloning 75
Gibson Assembly 75
DNA Sequencing 75
ChIP-Seq Using Anti-BldB Polyclonal Antibody 76
ChIP-Seq Using Anti-FLAG Antibody 77
ChIP-Seq Analysis 79
RNA Methods 80
RNA Isolation 80
Quantitative Reverse Transcription PCR (qRT-PCR) 80
RNA-Seq Analysis 81
Microbiological Methods 82
Preparation and Transformation of Electrocompetent *E. coli* 82
Preparation and Transformation of Chemically Competent *E. coli* 82
Interspecies Conjugation from *E. coli* to *S. venezuelae* 83
Construction of *S. venezuelae* Mutants via Redirect 84
Phage Transduction 84
Construction of *S. venezuelae* Mutants via CRISPR/Cas9 85
Complementation of *S. venezuelae* Mutants 85
Generation of 3xFLAG Alleles 86
Gene Overexpression in *S. venezuelae* 86
Bacterial-Two-Hybrid Library Screens 87
β-Galactosidase Assays 88
Protein Methods 89
Protein Overexpression 89
Protein Purification 90
Protein Co-expression 90
SDS-PAGE 91
Protein Concentration Quantification 91
Western Blotting 92
Biochemical and Biophysical Methods 93
Surface Plasmon Resonance 93
X-ray Crystallography Screens 94
Bioinformatic Methods 95
Overall Data Analysis 95

Bacterial Genome Collection 95
Phylogenetic Analysis 95
Microscopy Methods 96
Scanning Electron Microscopy 96
3. BldB and Two BldB Homologues are Necessary for Sporulation in *Streptomyces venezuelae* 97
Introduction 97
The BldB Homologues and Their Role in *Streptomyces* Development 97
Results 104
BldB Has 10 Homologues in *Streptomyces venezuelae* 104
BldB is Necessary for Aerial Mycelium Formation and Sporulation in *S. venezuelae* 111
The Overexpression of *bldB* Has No Impact on *Streptomyces* Development 115
A Bacterial-Two-Hybrid Library Screen Identified Possible Protein Partners for BldB 117
BldB Interacts Strongly with 7 of the Non-Canonical BldB Homologues 120
Two Non-Canonical BldB Homologues are Necessary for Sporulation 122
Discussion 128
4. The Δ*bldB* Mutant Phenotype Is Recapitulated by Co-overexpression of *abaA6* and *iosA* 133
Introduction 133
Phosphorylation-dependent Regulation of Sigma Factor Activity in *Bacillus* 133
Bacillus SigB-like Systems in *Streptomyces* and Their Involvement in Development 135
The *abaA* Locus in *S. coelicolor* 139
Results 140
BldB is Abundant Throughout the *Streptomyces* Life Cycle 140
BldB Is Not a DNA-binding Protein 143
BldB Indirectly Represses the Expression of the *abaA* Homologues and *iosA* 147
Overexpression of *abaA6* or *iosA* Results in Sporulation-Deficient Phenotypes 159
The Double Overexpression of *abaA6* and *iosA* Recapitulates the *ΔbldB* Mutant Phenotype 161
Discussion 165
5. Protein-protein Interaction Network Involving the Putative Anti-Sigma Factor AbaA6 173
Introduction 173
The Role of Osmoregulation in Bacterial Growth 173
Osmotic Stress and Development in *Streptomyces* 174
The OsaABC System in *Streptomyces* 175

OsaC-Like Proteins in Bacteria 176
Results 178
A Bacterial-Two-Hybrid Library Screen Found Potential Anti-Sigma Antagonist Partners for AbaA6 178
AbaA6 Interacts with Two Predicted Anti-Sigma Factor Antagonists - AsfA1 and AsfA2 180
AbaA6 Does Not Interact with 7 SigB Homologues 181
AsfA1 and AsfA2 Interact with OsaC and OsaC2 184
OsaC Does Not Interact with SigB or BldB in a Bacterial-Two-Hybrid Experiment 186
The Involvement of the AsfA and OsaC Homologues in *Streptomyces* Development 188
Discussion 190
6. WhiJ9 is a Transcription Factor, which is Linked to BldB Function 195
Introduction 195
The HTH-Xre Family of Transcriptional Regulators in Bacteria 195
Regulators with HTH-Xre Motifs in *Streptomyces* 197
Results 199
The Deletion of Two *whiJ* Homologues Has No Impact on *Streptomyces* Development 199
The Overexpression of *whiJ9* Results in Impaired Sporulation 201
Protein Abundance Levels of the WhiJ6 and WhiJ9 Homologues 204
WhiJ9 is a DNA-binding Protein 207
WhiJ9 Acts as an Activator for the Expression of *iosA*, and a Repressor for Its Own Expression 219
WhiJ9 Binds 3 Direct Repeats in its Intergenic Region 240
Attempts to Crystallise a WhiJ9-DNA Complex 243
Discussion 244
7. Evidence that BldB9 is the Link Between BldB and WhiJ9 Function 251
Introduction 251
Results 252
WhiJ9 Did Not Interact with BldB or BldB9 in a Bacterial-Two-Hybrid Assay 252
Evidence that WhiJ9 Forms a Complex with BldB9 253
Evidence that BldB9 and WhiJ9 Control the Expression of *iosA* Together 256
Discussion 259
8. General Discussion 263
References 270

Table of Figures

Figure 1.1. The Classical *Streptomyces* Life Cycle. 20
Figure 1.2. The Cooperation of SapB, Chaplins and Rodlins Allows Aerial Hyphae Growth. 23
Figure 1.3. The Production of the SapB Surfactant. 24
Figure 1.4. Export and Polymerisation of the Chaplins in *Streptomyces*. 26
Figure 1.5. The *Streptomyces* Hydrophobic Sheath. 26
Figure 1.6. Regulators of Development in *Streptomyces*. 28
Figure 3.1. Type VII Secretion Clusters in *Streptomyces* Species. 100
Figure 3.2. The *bldB*, *whiJ* and *abaA orfA* Homologues in *Streptomyces coelicolor*. . 102
Figure 3.3. Presence or Absence of *bldB* Homologues in the 21/09/2021 Collection of Genomes. 104
Figure 3.4. Distribution of BldB Homologue Protein Length. 106
Figure 3.5. Distribution of *bldB* Homologues per Genome. 109
Figure 3.6. Genomic Arrangement of the *bldB*, *whiJ* and *abaA* Homologues in 110
Figure 3.7. The Bald Phenotype of the *S. venezuelae ΔbldB* Mutant. 113
Figure 3.8. Phenotype Characterisation of the *S. venezuelae ΔbldB* Mutant. 114
Figure 3.9. Validation of BldB Overexpression via Western Blot. 115
Figure 3.10. Overexpression of *bldB* in *S. venezuelae*. 116
Figure 3.11. Phenotypic Characterisation of the *S. venezuelae bldB* Overexpression Strain. 116
Figure 3.12. Interactions Between BldB and its 10 BldB Homologues. 121
Figure 3.13. The Mutant Phenotypes of the *S. venezuelae bldB* Homologues. 122
Figure 3.14. The Phenotypes of BldB6- and BldB9-related Strains. 123
Figure 3.15. Phenotypic Characterisation of BldB6-derived Strains. 124
Figure 3.16. Phenotypic Characterisation of BldB9-derived Strains. 124
Figure 3.17. Expression of *bldB6* and *bldB9* Throughout *S. venezuelae* Development. 125
Figure 3.18. Protein Sequence Alignment for the BldB Homologues. 127
Figure 3.19. BldB Homologue Phylogenetic Tree. 127
Figure 4.1. BldB Abundance Throughout *Streptomyces* Development. 141
Figure 4.2. Expression of *bldB* Throughout Development. 142
Figure 4.3. Polyclonal Anti-BldB ChIP-Seq Whole Genome Enrichment. 144
Figure 4.4. Anti-FLAG ChIP-Seq Whole Genome Enrichment. 145
Figure 4.5. 6xHis-BldB Does Not Bind Its Own Promoter. 146
Figure 4.6. Differential Gene Expression in the *ΔbldB* mutant from an RNA-seq Experiment. 149
Figure 4.7. Mutant Phenotypes for the *abaA* Homologues and *iosA*. 159

Figure 4.8. Overexpression Phenotypes for the *abaA* Homologues and *iosA*.....160
Figure 4.9. Phenotype Characterisation of the *abaA6* and *iosA* Single Overexpression Strains. 161
Figure 4.10. The Phenotype of the *abaA6 iosA* Double Overexpression Strain.....162
Figure 4.11. Phenotypic Characterisation of the *abaA6 iosA* Double Overexpression Strain. 163
Figure 4.12. The Phenotype of the *ΔabaA6 ΔiosA ΔbldB* Triple Mutant Strain. 164
Figure 4.13. Phenotypic Characterisation of the *ΔabaA6 ΔiosA ΔbldB* Triple Mutant.164
Figure 5.1. Interactions Between AbaA6, IosA and the AsfA Homologues. 180
Figure 5.2. Interactions Between AbaA6 and 7 SigB Homologues. 183
Figure 5.3. OsaC and OsaC2 Are Multidomain Proteins. 186
Figure 5.4. Interactions Between the AsfA Homologues and the OsaC Homologues.187
Figure 5.5. Interactions Involving the Multidomain Proteins OsaC and OsaC2. 188
Figure 5.6. Mutant and Overexpression Phenotypes for the *asfA* and *osaC* Homologues.....189
Figure 6.1. Mutant Phenotypes of the *ΔwhiJ6* and *ΔwhiJ9* Strains. 200
Figure 6.2. Phenotypic Characterisation of the *ΔwhiJ6* and *ΔwhiJ9* Mutant Strains. .201
Figure 6.3. Overexpression Phenotypes for *whiJ6* and *whiJ9*. 202
Figure 6.4. Phenotypic Characterisation of the *whiJ6* and *whiJ9* Overexpression Strains. 202
Figure 6.5. Overexpression Phenotypes for the 3xFLAG-tagged Alleles of *whiJ9*. 203
Figure 6.6. WhiJ6 and WhiJ9 Abundance Throughout Development.....205
Figure 6.7. WhiJ9 Abundance in WhiJ9 Overexpression Strains. 206
Figure 6.8. Anti-FLAG WhiJ6 ChIP-Seq Whole Genome Enrichment. 208
Figure 6.9. Anti-FLAG WhiJ9 ChIP-Seq Whole Genome Enrichment. 211
Figure 6.10. Anti-FLAG WhiJ9 ChIP-Seq Selected Peaks.....219
Figure 6.11. The WhiJ9 Binding Site on the *iosA-whiJ9* Intergenic Region.....220
Figure 6.12. Binding of 6xHis-WhiJ9 to 6 Overlapping Oligos from Its Promoter. 221
Figure 6.13. Mutant Phenotype of the *ΔwhiJ9 ΔbldB* Double Mutant Strain. 223
Figure 6.14. Phenotypic Characterisation of the *ΔwhiJ9 ΔbldB* Double Mutant. 223
Figure 6.15. Differential Gene Expression in the *ΔbldB* Mutant and the *ΔwhiJ9 ΔbldB* Double Mutant from an RNA-seq Experiment. 227
Figure 6.16. 6xHis-WhiJ9 'Footprinting' Using Surface Plasmon Resonance. 241
Figure 6.17. Binding of 6xHis-WhiJ9 to Direct Repeats from Its Promoter. 242
Figure 6.18. Protein-DNA Crystals of 6xHis-WhiJ9 Bound to DNA. 243
Figure 7.1. Interactions Between BldB and Proteins Encoded by the *iosA-bldB9-whiJ9* Locus. 253
Figure 7.2. Co-purification of a BldB9-WhiJ9 Complex from *E. coli*. 254

Figure 7.3. Binding of BldB9 to WhiJ9 Captured on DNA. 255
Figure 7.4. Mutant Phenotype of the *ΔbldB9 ΔwhiJ9* Strain. 256
Figure 7.5. Phenotypic Characterisation of the *ΔbldB9 ΔwhiJ9* Double Mutant Strain. 257
Figure 7.6. Expression of *iosA* in Mutant and Overexpression Strains for *bldB*, *bldB9* and *whiJ9*. 258
Figure 8.1. A Network of Interactions and Regulation Involving BldB 264

Index of Tables

Table 2.1. List of *E. coli* strains used in this study. 37
Table 2.2. List of *Streptomyces* strains used in this study. 38
Table 2.3. List of bacteriophages used in this study. 39
Table 2.4. List of plasmids used in this study. 40
Table 2.5. List of cosmids used in this study. 45
Table 2.6. Solid media used in this study. 46
Table 2.7. Liquid media used in this study. 48
Table 2.8. List of antibiotics and substrates used in this study. 49
Table 2.9. List of oligonucleotides used in this study. 54
Table 3.1. “Long” BldB Homologues with Alternative Domains. 107
Table 3.2. BldB Bacterial-Two-Hybrid Library Screen Results. 118
Table 4.1. BldB RNA-seq Results. 151
Table 5.1. AbaA6 and IosA Bacterial-Two-Hybrid Library Screen Results. 179
Table 5.2. List of Reciprocal Best Hits for Potential *S. venezuelae* SigB Homologues. 182
Table 5.3. AsfA1 and AsfA2 Bacterial-Two-Hybrid Library Screen Results. 185
Table 6.1. WhiJ9 ChIP-seq Results. 214
Table 6.2. WhiJ9 RNA-seq Results. 230

Acknowledgements

Despite the typical trials and tribulations of a PhD student (including a world pandemic in my case!), I had a wonderful time at the John Innes Centre. I would like to express my sincere gratitude to all people who supported me in my PhD endeavour, and to the BBSRC for funding my research.

A massive thank you goes to my main supervisor, Mark Buttner. Mark, you have been such a great role model and mentor. Thank you for always being available for chats, for guiding me back to the main road when I would get sidetracked, and for your overall enthusiastic encouragement and great advice. It has been an honour to be your last PhD student!

Thanks also go to my secondary supervisor, Barrie Wilkinson. Barrie, you were instrumental in getting me to move away from the nitty-gritty details and to focus on the bigger picture during our supervisory meetings. Thank you for your helpful input and interesting discussions!

Standing on the shoulders of giants, or in my case, two regular-sized 30-something postdocs, I would be a lesser scientist if it wasn't for Matt Bush and Neil Holmes. Matt, thank you for the welcome to the world of *Streptomyces venezuelae*. You do research with such precision, flourish and elegance, I hope I managed to soak up as much of your scientific wisdom as possible. Neil, thank you for our long conversations, whether they were about serious science business or just silly gossip. And thank you for making me an ÄKTA pro! It seems like I am going towards a protein biochemistry future, so you basically taught me how to earn my living.

Thank you to all past and present members of the Buttner lab and the Molecular Microbiology department as a whole! I am very sad to leave this wonderful environment and will miss you all greatly. Thank you to Susan Schlimpert for all of our science chats and for sharing the little experimental tricks to make my life easier! Susan, you made the journey from postdoc to group leader right in front of my eyes and it has been incredibly inspiring. I look forward to seeing more beautiful science coming from your lab! The dynamic duo, Kelley Gallagher and Félix Ramos-León, thank you both for helping me with my early protein work and phylogenetic analysis, and for being so fun to work with! Thank you to Joe Sallmen - Joe, you are such a delight to be around! I will miss your pep talks and hearing your voice all the way from the other side of the lab.

Thank you to Kathy Stratton, Max Jordan, Cat Thompson, Hannah McDonald, Rosaria Campilongo, Adam Jalal, Alba Pacheco Moreno, Ngat Tran, Tung Le, Marcelo Bueno Batista and Dave Widdick for all the scientific advice, shared laughs and good times!

A huge thank you goes to Govind Chandra - Govind, you should know by now that you are the most important person in the department. Thank you for all of your help with my bioinformatic analysis, whether you (patiently) taught me how to battle with Linux and R, or did it yourself.

My endeavours into the world of biophysics and structural biology would have been much more challenging without the support of the Biophysical and Crystallography Platforms, and in particular, Clare Stevenson, Julia Mundy and Dave Lawson. Clare, you were instrumental in the progress I made with my SPR experiments, thank you for your great advice and teaching. Julia and Dave, thank you for your help with my attempts to get a protein-DNA structure - even if it did not work out, it was a valuable learning experience for me. Thank you again to Tung Le, who gave me some great advice regarding all of my experiments, but especially the biophysics ones.

Thank you to Gerhard Saalbach and Carlo de Oliveira Martins, for processing my mass spectrometry samples and answering all of my questions in detail. Thank you to Kim Findlay, who taught me how cryo-SEM is done and took some of the beautiful microscopy images included in this thesis. Thank you to Sarah Tolland and Naomi Wang for being such wonderful rays of sunshine, and helping me with all admin work! A big thank you to the JIC Lab Support team - you made my work so much easier and faster by preparing all media and glassware. Dear Chatt Building, we love to joke about burning you down, but you hold so many memories and good times for me. I will miss you and your *Streptomyces* smell a lot.

Throughout the years, my slightly introverted self has been adopted into several tightly knit friend groups that I am happy to say keep in touch to this day, even if we are scattered around the world. Let’s keep it that way!

Arising from the 2017 intake of Chatt PhD students, thank you to the “Squat” - Isa, Lira and Raf for being my lunch and travel buddies. A shared struggle is a lesser one, and we all made it through the PhD despite the unique challenges we had. Thank you to the “Cringers” - my university friends and ex-housemates Gee and Maria, who I can always count on for a laugh and an adventure. Thank you to the “Lair” - Svet, Hudy and Misa, my high school friends of 10+ years, for all the wonderful times we have shared.

A heartfelt thank you to my partner in life James for being my source of strength, inspiration and tea. My loveliest, thank you for being my rock, especially during the thesis writing months! Thank you for not running away, even though I use words like “cloning” and “mutant bacteria” on a regular basis. Thank you for moving with me to Oxford and supporting me in my next scientific venture. Meeting you was the best, most significant outcome of this PhD.

Lastly, I would like to thank my family: my mum Galia, my dad Marin, my grandad Todor, and my not-so-little sister Radi. Thank you for raising me curious and driven. Thank you for accepting that I had to fly (quite far!) from the nest in order to grow. Thank you for investing your health, your money and your time into making my dreams happen and into making me who I am today. This work is for you, and because of you.

Този научен труд е посветен на семейството ми, което безрезервно ме е подкрепяло във всяко мое начинание. Благодаря ви, че ме окуражавахте да съм любопитна и устремена. Благодаря ви, че приехте че трябваше да отлетя (доста далече!) от гнездото за да порасна като човек. Благодаря ви, че жертвахте здравето си, парите си и времето си за да сбъднете мечтите ми и да ме направите това, което съм днес. Обичам ви!

Abbreviations

ABC	ATP-binding cassette
ATP	Adenosine triphosphate
bp	Base pairs
BSA	Bovine serum albumin
cAMP	Cyclic adenosine monophosphate
c-di-GMP	Cyclic diguanosine monophosphate
ChIP-seq	Chromatin immunoprecipitation sequencing
C-terminal	Carboxy-terminal
dH_2O	Distilled water
Da	Dalton
DMSO	Dimethylsulphoxide
DNA	Deoxyribonucleic acid
dNTP	Deoxynucleoside triphosphate
DTT	Dithiothreitol
ECF	Extracytoplasmic function
EDTA	Ethylene diamine tetraacetic acid
EMSA	Electrophoretic mobility shift assay
EtBr	Ethidium bromide
FDR	False discovery rate
FLAG	Polypeptide protein tag (N-DYKDDDDK-C)
GAF	cGMP-specific phosphodiesterases, adenylyl cyclases and FhlA
HTH	Helix-turn-helix
IPTG	Isopropyl-β-D-thiogalactopyranoside
kb	Kilobase pairs
kDa	Kilodalton
LB	Luria-bertani
LFC	Log_2 fold change
mb	Megabase pairs
MCS	Multiple cloning site
MYM	Maltose yeast extract malt extract medium
N-terminal	Amino-terminal
OD	Optical density
ONPG	Ortho-nitrophenyl-β-galactoside
ORF	Open reading frame
PAS	Per, ARNT and Sim
PCR	Polymerase chain reaction
PEG	Polyethylene glycol
RBS	Ribosome binding site
RNA	Ribonucleic acid
rpm	Revolutions per minute
SDS-PAGE	Sodium dodecyl sulphate polyacrylamide gel electrophoresis
SEM	Standard error of the mean / scanning electron microscopy
SFM	Soya mannitol flour medium
SPR	Surface plasmon resonance
TBE	Tris-Borate-EDTA
WT	Wild type
X-Gal	5-bromo-4-chloro-3-indolyl-β-D-galactopyranoside

1. General Introduction

In this chapter I give an overview into the biology of the antibiotic-producing bacteria *Streptomyces*, focusing on their developmental life cycle and the regulators required for their complex growth. I have also included an extended introduction in each Results chapter, in order to provide specific context related to the presented research.

The Importance of Being *Streptomyces*

Streptomycetes belong to the phylum Actinobacteria - one branch of Gram-positive bacteria, whose characteristic feature is the high GC content of their genomes (Lal *et al.*, 2016). *Streptomyces* are found most abundantly in soil and are responsible for soil's earthy scent through the production of the volatile secondary metabolite geosmin (Gerber, 1967). Apart from terrestrial and marine environments (Yang *et al.*, 2020), *Streptomyces* have also been shown to have roles as plant and animal symbionts (Seipke *et al.*, 2011; Worsley *et al.*, 2020; Park *et al.*, 2021). Though most species are not pathogenic, some important *Streptomyces* pathogens include the plant pathogen *Streptomyces scabies* (Loria *et al.*, 1997) and the human pathogen *Streptomyces somaliensis* (Kirby *et al.*, 2012). Among the most distinct characteristics of *Streptomyces* are their complex, fungus-like life cycle, and their prolific production of commercially useful secondary metabolites.

Interest in the study of streptomycetes arose after the antibiotic streptomycin, active against *Mycobacterium tuberculosis*, was isolated from *Actinomyces griseus*, which has been reclassified as *Streptomyces griseus* (Schatz, Bugle and Waksman, 1944). The Nobel Prize in Physiology or Medicine in 1952 was awarded to the lead investigator Selman Waksman "for his discovery of streptomycin, the first antibiotic effective against tuberculosis", which highlights the impact of the discovery, and illustrates the necessity for research on *Streptomyces*.

At that time, the taxonomic classification of actinomycetes was challenging. Some classified them as fungi due to their fungus-like life cycle, while others considered them bacteria, based on their size and susceptibility to antibacterial agents and bacteriophages (Waksman, 1957). There was also the attractive notion that actinomycetes are an intermediate life-form between bacteria and fungi, with most literature published between 1940 and 1970 making a clear distinction between spore-forming bacteria, actinomycetes, and fungi (Conn, 1948).

At the time when it became widely accepted that actinomycetes are indeed bacteria (Loening, 1968), the golden age of antibiotic discovery was still at its peak. The propensity of actinomycetes to produce a variety of natural products was (and still is) well-exploited - the majority of commercially available antibiotics have been isolated from actinomycetes (Tanaka and Omura, 1990; Hutchings, Truman and Wilkinson, 2019). It is generally accepted that the ability of *Streptomyces* to successfully inhabit various environments can be largely attributed to their secondary metabolite production. The released antibiotics allow *Streptomyces* to outcompete other soil-dwelling bacteria and fungi, to protect themselves against attacks by protists, and might also serve as signalling molecules (Yim, Wang and Davies, 2007).

Antibiotic resistance is currently a very urgent issue - in the year 2050, an estimated 10 million people will die from infections untreatable with antibiotics due to bacteria developing resistance (Review on Antimicrobial Resistance, 2014). Although their secondary metabolite production has been well-harnessed over the years, *Streptomyces* are far from an exhausted resource. Genes encoding different components necessary for the biosynthesis of a given secondary metabolite are typically found close to each other in the genome, forming secondary metabolite clusters (such as the actinorhodin biosynthetic gene cluster in the model organism *Streptomyces coelicolor*; Malpartida and Hopwood, 1984). Based on this knowledge, advances in bioinformatics have allowed us to mine *Streptomyces* genomes for novel antibiotic clusters (Blin *et al.*, 2019). Most of these clusters are designated “cryptic” because the metabolites they are hypothesised to produce have not been detected under laboratory conditions. For example, *S. coelicolor* has 27 predicted secondary metabolite gene clusters (Blin *et al.*, 2019), but under laboratory conditions, is only able to produce actinorhodin, undecylprodigiosin, calcium-dependent antibiotic (CDA), and methylenomycin.

Current research on natural product biosynthesis focuses on studying these cryptic secondary metabolite clusters, and bioengineering novel antibiotics based on known structures and modes-of-action (Rutledge and Challis, 2015). This work still very much involves *Streptomyces*, with research into the developmental biology of streptomycetes helping to elucidate the link between their complex life cycle and antibiotic production.

The *Streptomyces* Life Cycle

Rather than dividing by binary fission, *Streptomyces* grow several different structures before giving rise to mature spores (Flärdh and Buttner, 2009). The classical model of the *Streptomyces* life cycle (**Fig. 1.1**) sets off with the germination of spores. Once favourable environmental conditions have been found, spores swell, and germ tubes emerge from them. These germ tubes grow by apical tip extension into vegetative hyphae, which further branch and form a proliferative vegetative mycelium. These vegetative hyphae are multigenomic - several copies of the chromosome can be found in each hyphal compartment, which is defined by the formation of vegetative cross-walls. Cryo-electron tomography performed on *Streptomyces albus* revealed the presence of septal junctions in the vegetative cross-walls, which might have a role in transport of molecules between the vegetative compartments (Sexton and Tocheva, 2020).

The depletion of nutrients triggers a switch in the developmental programme - reproductive aerial hyphae form, coated with a hydrophobic sheath (composed of proteins from the chaplin and rodlin families), which allows the hyphae to grow into the air, breaking surface tension. At this stage of development secondary metabolism is initiated and most antibiotics produced - a process found to be driven by phosphate depletion in particular (Nieselt *et al.*, 2010).

The aerial hyphae then begin to differentiate - chromosomes replicate and segregate at regular intervals along the length of each hypha. Sporulation septa form, marking the generation of pre-spore compartments. The spores become rounded, their walls thicken, and a spore pigment is synthesised, giving the spore chains a characteristic colour - grey in the case of *S. coelicolor*, and green in *Streptomyces venezuelae*. Unigenomic spores are then released to disperse into the environment, completing the life cycle (Flärdh and Buttner, 2009).

Interestingly, the dispersal of spores was shown to be facilitated by springtails - a species of arthropod found in soil (Ruddick and Williams, 1972; Becher *et al.*, 2020). Springtails were shown to be specifically attracted to the scent of geosmin and 2-methylisoborneol (2-MIB) released by *Streptomyces* spores (Becher *et al.*, 2020). The spores were found to be dispersed in the faeces of the springtails and by sticking to the springtail cuticle (Becher *et al.*, 2020). More recently, *S. coelicolor* were demonstrated to be transported over short distances by motile bacteria, such as *Bacillus subtilis* in a process designated “microbial hitchhiking” (Muok, Claessen and Briegel, 2021).

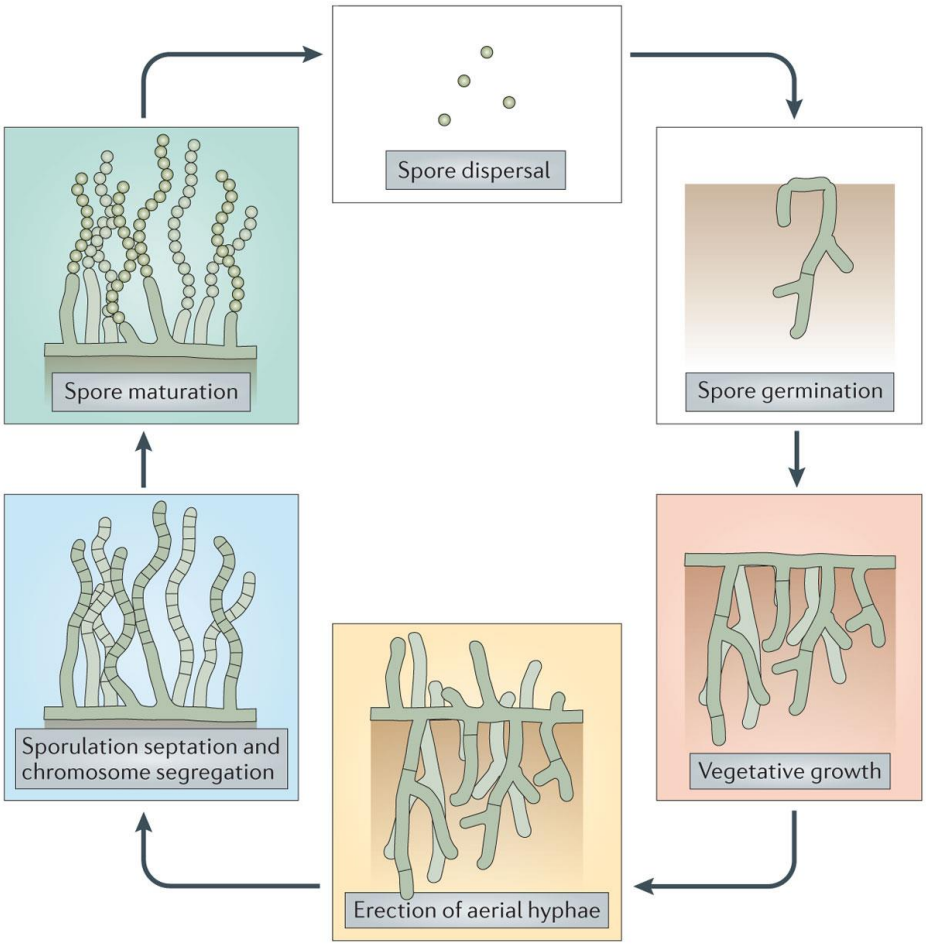

Figure 1.1. The Classical *Streptomyces* Life Cycle.

Streptomyces spores swell and germinate, vegetative hyphae emerge, grow by tip extension and branch to develop the vegetative mycelium. Nutrient limitation drives the formation of reproductive aerial hyphae. The chromosome is replicated, and copies are segregated into pre-spore compartments divided by sporulation septa. The resulting spores mature and are released into the surrounding environment. Figure reproduced with permission from Bush *et al.*, (2015).

This classical life cycle is observed when *Streptomyces* species are grown isolated, under laboratory conditions. In external environments, their growth is thought to be radically different due to interactions with different organisms - something that *Streptomyces* microbial ecologists are just beginning to appreciate. In recent studies it was discovered that *Streptomyces* are also able to colonise new environments through the formation of explorer cells - a new mode of growth initiated independently from the classical life cycle (Jones *et al.*, 2017). The authors observed this new type of development when they grew *S. venezuelae* in close proximity to the model fungal species *Saccharomyces cerevisiae*.

They found that the volatile organic compound trimethylamine (TMA) released by *Streptomyces* explorer cells, which had been co-cultured with *S. cerevisiae,* was able to induce this exploration phenotype in *S. venezuelae* grown isolated in a separate plate compartment. Explorer growth was also observed to be facilitated by either high pH, low iron, or low glucose levels in the solid media (Jones *et al.*, 2017, 2019). This new type of growth, dependent on chemical signals along with the presence of a different organism, adds a new mode of short-distance motility and another layer of complexity to the developmental biology of *Streptomyces*.

Early work on the regulation of *Streptomyces* development predominantly used *Streptomyces coelicolor* as a model species. However, the use of *S. coelicolor* for developmental studies was not ideal because *S. coelicolor* does not differentiate in liquid culture, preventing representative sampling of the various developmental stages. When grown on agar, the separation of a sporulating colony into its constituent vegetative mycelium, aerial mycelium and spores is a technical challenge. For this reason, many studies noted that no separation of developmental structures was performed, meaning that any late developmental samples consisted of a heterogeneous mix of vegetative, aerial and sporulation growth, which is not ideal for gene expression studies in particular.

Streptomyces venezuelae was proposed as a new model species for studying *Streptomyces* development (Flärdh and Buttner, 2009), and has been widely adopted. *S. venezuelae* is able to complete its entire life cycle in liquid culture, which allows for easy sampling from different time points, greatly enhancing the capacity for performing large-scale transcriptomic and proteomic studies. It also allows for timelapse microscopy to be performed in microfluidics experiments and the subcellular localisation of fluorescently tagged proteins to be determined throughout the life cycle (Schlimpert, Flärdh and Buttner, 2016).

Building *Streptomyces* Aerial Hyphae

Focusing on the *Streptomyces* classical life cycle, the major developmental transitions are marked by the formation of 3 different structures - the vegetative mycelium, the aerial mycelium, and the mature spores. These transitions are governed by two main classes of developmental regulators - the Bld regulators, which control the formation of aerial hyphae, and the Whi regulators, which control the partitioning of these aerial hyphae into mature spores. The Bld and Whi regulators will be discussed in detail later in this chapter.

Vegetative mycelium formation begins with the formation of 1 or 2 germ tubes, following the germination of single spores (**Fig. 1.1**). These germ tubes extend into a branched vegetative mycelium, which grows across the surface of the solid medium and can penetrate deeply into it.

Hyphal growth in *Streptomyces* occurs by tip extension, as exemplified by the incorporation of tritiated GlcNAc or fluorescent derivatives of vancomycin only into the cell wall of the tips of growing hyphae (Gray, Gooday and Prosser, 1990; Daniel and Errington, 2003). This tip extension growth is coordinated by the coiled-coil cytoskeletal protein DivIVA, which is essential in *Streptomyces* (Flärdh, 2003). DivIVA forms foci at growing hyphal tips and also at future branch points on the lateral walls (Flärdh, 2003; Hempel *et al.*, 2008, 2012). This activity is dependent on the complete *Streptomyces* “polarisome”, which consists of DivIVA and its interacting proteins - the scaffold protein Scy and the intermediate filament-like protein FilP (Bagchi *et al.*, 2008; Fuchino *et al.*, 2013; Holmes *et al.*, 2013; Fröjd and Flärdh, 2019). The polarisome serves as a recruitment hub for proteins involved in cell wall biosynthesis, such as the cellulose synthase-like protein CslA (Xu *et al.*, 2008).

Interestingly, cell division and apical tip growth do not appear to be essential for one another, as loss of the major divisome determinant FtsZ does not impact hyphal tip growth (McCormick *et al.*, 1994; Santos-Beneit *et al.*, 2017). In contrast, there is a link between chromosome segregation and tip extension, in the form of the interaction of the polarisome protein Scy with the chromosome partitioning ATPase ParA (Ditkowski *et al.*, 2013).

Upon nutrient depletion, the reproductive growth of *Streptomyces* is initiated, leading to the formation of aerial hyphae (**Fig. 1.1**). Aerial hyphae break the surface tension of the aqueous milieu of vegetative mycelium and extend into the air. This requires the coating of the aerial hyphae with a hydrophobic sheath and, on rich media specifically, the production of the surfactant peptide SapB (**Fig. 1.2**).

The production of the surfactant SapB was found to be significantly decreased in a series of *bld* mutants, but not in the *whi* mutants in *S. coelicolor* (Willey *et al.*, 1991). The extracellular complementation with SapB-producing *Streptomyces*, or addition of purified SapB peptide restored aerial mycelium formation to the *bld* mutants, which led to the conclusion that SapB has an important role in the erection of aerial hyphae (Willey *et al.*, 1991). The precise mode and regulation of SapB production eluded researchers for over a decade. It is now known that SapB is the product of the *ram* gene cluster, the designation standing for **r**apid **a**erial **m**ycelium formation, as increased expression of the *ram* genes resulted in accelerated formation of aerial hyphae in *Streptomyces lividans* (Ma and Kendall, 1994). The deletion of the *ram* cluster resulted in a bald phenotype on rich media (Keijser *et al.*, 2002; Nguyen *et al.*, 2002).

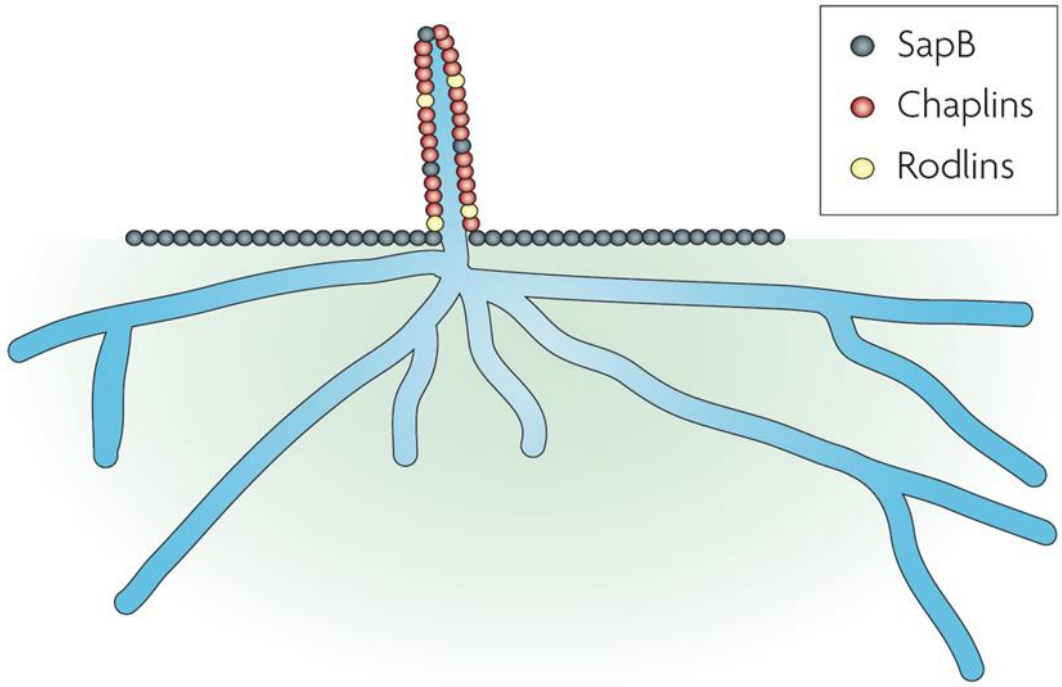

Figure 1.2. The Cooperation of SapB, Chaplins and Rodlins Allows Aerial Hyphae Growth.

The surfactant peptide SapB is secreted to the surface of the colony. The chaplins and rodlins are also exported to the hyphal surface, where they arrange in a basketweave pattern to form the hydrophobic sheath, which is anchored to the cell wall via covalent interactions with the long chaplins. Figure reproduced with permission from Flärdh and Buttner (2009).

The *ram* gene cluster was observed to have similarity with components of lantibiotic biosynthetic gene clusters - this similarity allowed for the full characterisation of SapB production and processing (Kodani *et al.*, 2004). The production of SapB is illustrated in **Figure 1.3** and is briefly discussed below.

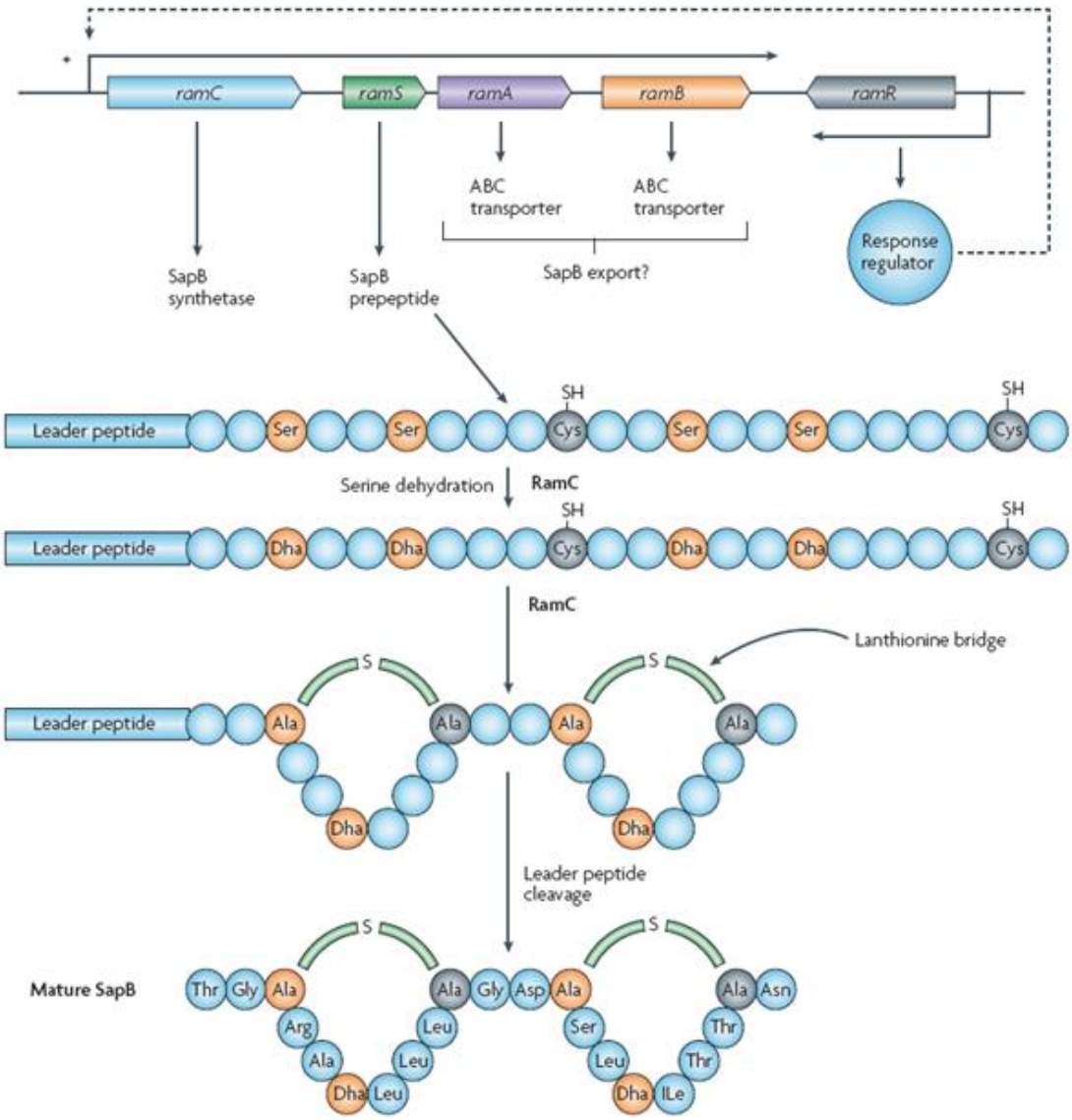

Figure 1.3. The Production of the SapB Surfactant.

The SapB pre-peptide encoded by *ramS* is post-translationally modified by the SapB synthetase RamC and an unknown protease to yield the mature SapB peptide. The ABC transporters RamA and RamB are thought to be involved in the export of SapB. Figure reproduced with permission from Flärdh and Buttner (2009).

RamR is a response regulator, which activates the expression of the convergently transcribed *ramCSAB* operon (Keijser *et al.*, 2002; O'Connor, Kanellis and Nodwell, 2002; Kodani *et al.*, 2004). The 42-amino-acid SapB pre-peptide is encoded by the *ramS* gene. The pre-peptide is processed in several post-translational modification steps, resulting in the final lantibiotic-like SapB peptide (Kodani *et al.*, 2004). First, the lantibiotic synthetase homologue RamC converts 4 serines in the pre-peptide to dehydroalanines. Two of these dehydroalanines then form lanthionine rings via reactions with two cysteine thiols - a reaction also catalysed by RamC. The leader peptide is then cleaved off, which yields the mature 21-amino-acid SapB peptide (Kodani *et al.*, 2004). The ABC transporters RamA and RamB have been proposed to export the mature SapB surfactant peptide to the surface of the hyphae (Kodani *et al.*, 2004).

Irrespective of growth medium, *Streptomyces* also utilise another structure to build their aerial hyphae - the hydrophobic sheath, which is composed of the chaplins and the rodlins. There are 5 "short" (ChpDEFGH) and 3 "long" (ChpABC) chaplins in *S. coelicolor* (**Fig. 1.4**), all of which share a hydrophobic chaplin domain and a Sec signal peptide for export to the hyphal surface (Claessen *et al.*, 2003; Elliot *et al.*, 2003). The "long" chaplins also contain a second chaplin domain and a sorting signal (Claessen *et al.*, 2003; Elliot *et al.*, 2003). Sortases recognise the sorting signal and covalently link the long chaplins to the peptidoglycan (**Fig. 1.4**), thus anchoring the whole hydrophobic sheath to the hyphal surface (Claessen *et al.*, 2003; Elliot *et al.*, 2003). A mixture of purified chaplins in aqueous solution assembled into amyloid-like fibrils at the water-air interface (Claessen *et al.*, 2003). Therefore, the chaplins were able to assemble into chaplin filaments *in vitro* without the presence of the rodlins (Claessen *et al.*, 2003). Out of the *S. coelicolor* chaplins, ChpC, ChpE and ChpH were shown to be crucial for aerial mycelium formation, as a "minimal chaplin strain" lacking all other chaplins except these three was still able to form robust aerial hyphae (Di Berardo *et al.*, 2008). ChpH was shown to be the most important determinant for this activity (Di Berardo *et al.*, 2008). *In vitro* and *in vivo* experiments showed that ChpH has 2 amyloid domains, with only the C-terminal one playing a role in rodlet assembly (Capstick *et al.*, 2011).

There are 2 rodlins in *S. coelicolor* - RdlA and RdlB (Claessen *et al.*, 2002, 2004). Loss of RdlAB does not prevent the construction of aerial hyphae in *Streptomyces*, but it results in a hydrophobic sheath with a disordered pattern of chaplin filaments, as opposed to the regular basketweave-like pattern (**Fig. 1.5**) (Claessen *et al.*, 2002, 2004). Thus, the rodlins are responsible for the large-scale structural organisation of the chaplin filaments (Claessen *et al.*, 2002, 2004).

Strikingly, *chpE* was found to be essential in wild-type *S. coelicolor*, but not in the *rdlAB* mutant, the *tat* mutant or the full chaplin mutant (Di Berardo *et al.*, 2008)**.** This link between the Tat secretion system and hydrophobic sheath formation is indirect, as neither the chaplins nor the rodlins were found to be exported via the Tat system (Di Berardo *et al.*, 2008)**.**

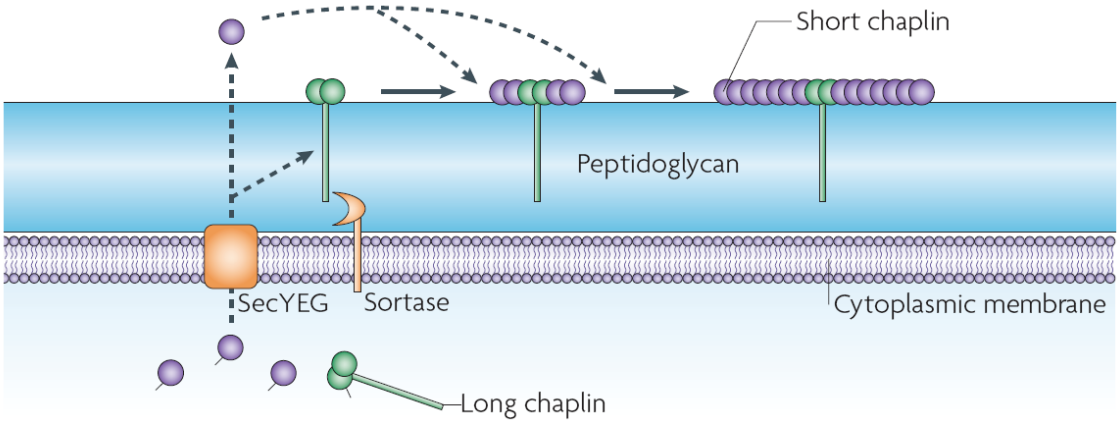

Figure 1.4. Export and Polymerisation of the Chaplins in *Streptomyces*.

Chaplins are exported through the Sec system. Sortases recognise the sorting signals in the long chaplins and covalently bind these chaplins to the cell wall. The long and short chaplins form chaplin filaments on the spore surface. Figure reproduced with permission from Flärdh and Buttner (2009).

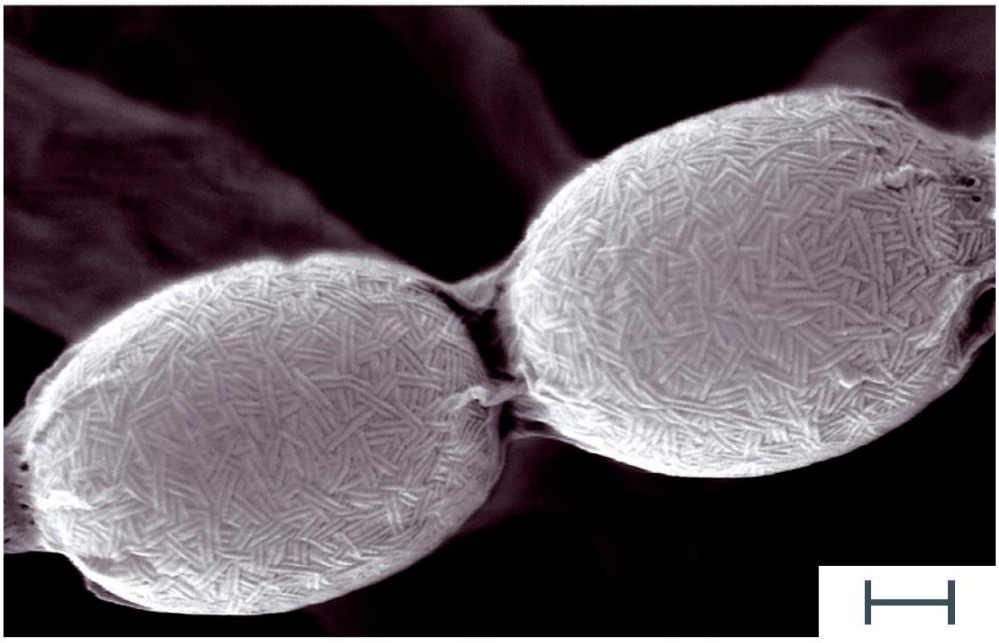

Figure 1.5. The *Streptomyces* Hydrophobic Sheath.

Scanning electron micrograph showing the basketweave pattern of the hydrophobic sheath of wild-type *S. coelicolor* M600 spores. Bar indicates 200 nm. Figure reproduced with permission from Di Berardo *et al.*, (2008).

Genes Required for Aerial Mycelium Formation in *Streptomyces*

The regulators responsible for different stages of development in *Streptomyces* form a complex network - the interactions of some of the gene products discussed in this chapter are represented in **Figure 1.6**.

The first linkage map of the *S. coelicolor* genome provided an initial insight into one gene responsible for the complex developmental biology of streptomycetes (Hopwood, 1967). In this study, *S. coelicolor* mutants were generated via exposure to UV light or chemical mutagens such as N-methyl-N'-nitro-N-nitrosoguanidine. Among a list of auxotrophic, UV-sensitive and temperature-sensitive mutants, a morphological mutant was also isolated. The mutation, labelled S48, conferred an inability to raise an aerial mycelium and to produce the pigmented antibiotics actinorhodin and undecylprodigiosin to the mutant (Hopwood, 1967). Further studies found mutations in different genes, which resulted in the same phenotype - designated “bald” due to the soft, non-fuzzy appearance of the non-sporulating mutant colonies (Merrick, 1976). As was custom, the newly mapped genes were named for the phenotype of the mutants. Hence, the S48 locus was renamed *bldA* - the first of a series of genes whose products are necessary for aerial mycelium formation.

Null mutations in *bld* loci prevent the formation of aerial hyphae for one of two diametrically opposite reasons: either because they block differentiation (mutations in activators) or because they cause precocious hypersporulation, bypassing the formation of aerial hyphae (mutations in repressors). In general, most *bld* genes encode transcriptional regulators, *bldA* being a notable exception. *bldA* encodes the only tRNA able to efficiently translate the UUA mRNA codon to leucine (Leskiw *et al.*, 1991). As *Streptomyces* genomes are GC-biased, TTA codons are rare. The presence of TTA codons in genes required for the biosynthesis of all 4 of the well-characterised *S. coelicolor* antibiotics explains the lack of antibiotic production in the *ΔbldA* mutant (Fernández-Moreno *et al.*, 1991; White and Bibb, 1997; Chater, 2006; O’Rourke *et al.*, 2009). The inability of the *ΔbldA* mutant to form an aerial mycelium is proposed to be directly caused by another developmental gene, *bldH* (also called *adpA*), having a TTA codon (Nguyen *et al.*, 2003; Takano *et al.*, 2003).

The main subject of this thesis - BldB is discussed in greater detail in Chapter 3. Briefly, the biochemical function of BldB is still unknown, with several studies proposing that BldB is a transcription factor (Pope, Green and Westpheling, 1998; Mishig-Ochiriin *et al.*, 2003).

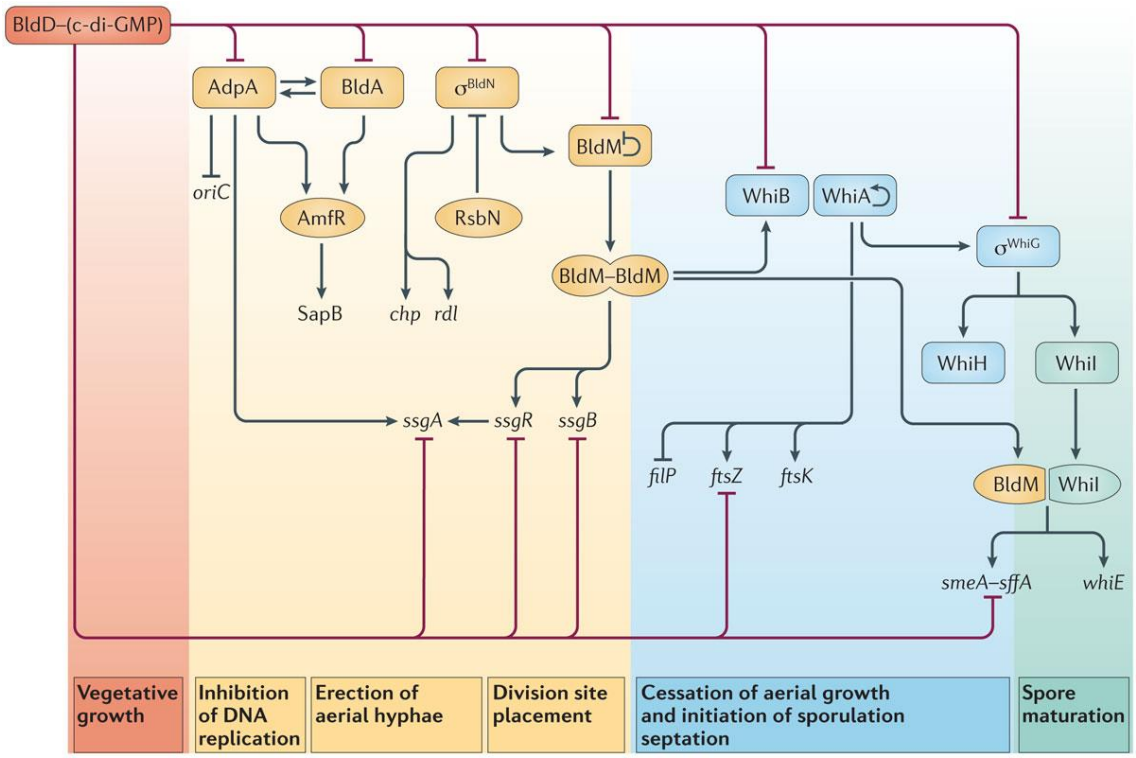

Figure 1.6. Regulators of Development in *Streptomyces*.

Proteins of the Bld and Whi families regulate development in *Streptomyces*. Figure reproduced with permission from Bush *et al.*, (2015).

BldC is a DNA-binding protein, whose wHTH domain has structural similarity to that of MerR-family transcription factors. It was shown that BldC monomers cooperatively bind DNA in a head-to-tail manner, and their oligomerisation bends the helix (Schumacher, den Hengst, *et al.*, 2018). The same study found that in *S. coelicolor* BldC bound the promoters of developmental genes such as *bldM*, *whiB, whiD, whiH, whiI, sigF, smeA, hupS* and *bldC* itself (Schumacher, den Hengst, *et al.*, 2018). ChIP-seq and RNA-seq experiments in *S. venezuelae* led to the full characterisation of the BldC regulon, which included more than 300 direct gene targets, and revealed that BldC can equally act as an activator and a repressor of transcription (Bush *et al.*, 2019). The loss of BldC in *S. venezuelae* led to an interesting phenotype - rather than forming a vegetative mycelium that is unable to further differentiate, the *ΔbldC* mutant was found to sporulate precociously, bypassing the formation of aerial hyphae (Bush *et al.*, 2019). Therefore, BldC is suggested to be one of several developmental “brakes” (Flärdh and McCormick, 2017), and to be important for sustaining vegetative growth before sporulation (Bush *et al.*, 2019). Furthermore, the production of actinorhodin in *S. coelicolor* has been shown to be indirectly affected by BldC (Hunt *et al.*, 2005).

Another such developmental brake is the DNA-binding protein BldD (Elliot and Leskiw, 1999). BldD monomers are able to dimerise via their C-terminal domains through the binding of an unprecedented tetrameric form of the secondary messenger cyclic-di-GMP, thus forming a $BldD_2$-$(c\text{-}di\text{-}GMP)_4$ complex (Tschowri *et al.*, 2014; Schumacher *et al.*, 2017). In a chromatin immunoprecipitation microarray (ChIP-chip) experiment comparing expression levels in the *ΔbldD* mutant to wild-type *S. coelicolor*, it was discovered that BldD regulates the expression of almost 170 genes (Den Hengst *et al.*, 2010). This includes the developmental genes *bldA, bldC, bldD, bldH, bldM, bldN, ssgA, ssgB, ftsZ, whiB, whiG, smeA-ssfA, sigH*, and the antibiotic production genes *bldA, nsdA* and conservon *cvn9*, highlighting the role of BldD as a master regulator of development in *Streptomyces* (Den Hengst *et al.*, 2010). The *ΔbldD* mutant displays a similar precocious sporulation phenotype to the *ΔbldC* mutant, meaning that BldD has a similar function as a repressor of premature *Streptomyces* sporulation (Tschowri *et al.*, 2014).

BldG was proposed to be an anti-sigma factor antagonist, due to the similarity of its protein sequence to those of known anti-sigma factor antagonists, such as SpoIIAA and RsbV in *Bacillus subtilis* (Bignell *et al.*, 2000). It was shown that the phosphorylation-deficient *bldG* mutant (in which the serine in BldG that is predicted to be phosphorylated was exchanged for an alanine) had a similar phenotype to the null *ΔbldG* mutant, suggesting that phosphorylation is necessary for the activity of BldG in *S. coelicolor* (Bignell *et al.*, 2003). BldG has been proposed to control the activity of the sigma factors SigF and SigH via binding of their respective anti-sigma factors RsfA and RshA (Takano *et al.*, 2011; Mingyar *et al.*, 2014).

Not much work has been done on *bldH* in *S. coelicolor*, but its orthologue *adpA* in *S. griseus* is a transcriptional regulator, activating the expression of developmental genes such as *adsA* (orthologue of the *S. coelicolor bldN*) and *ssgA* (Yamazaki, Ohnishi and Horinouchi, 2000, 2003).

Similarly, not much is known about *bldI*. It was first discovered in a study of the wider *bldB* region in *S. coelicolor*, where *bldI* was proposed to be a second gene, located near *bldB*, also necessary for development (Harasym *et al.*, 1990). It was suggested that BldI activates the expression of the *bldA* tRNA, though the mechanisms of this process have not been studied extensively (Leskiw and Mah, 1995).

An oligopeptide signalling molecule produced directly or indirectly by BldJ [the *bldJ* gene was designated *bld261* at its discovery (Willey, Schwedock and Losick, 1993)] was suggested to be transported by the oligopeptide ABC membrane transporter BldK (Nodwell, McGovern and Losick, 1996), and to be the first signal required to activate a developmental extracellular signalling cascade necessary for aerial mycelium formation (Nodwell and Losick, 1998). The bald phenotypes of the *S. coelicolor ΔbldJ* and *ΔbldK* mutants were partially restored to wild-type levels of differentiation by the supplementation of iron in the media, which was suggested to be dependent on the activation of *bldN* expression by iron (Traxler *et al.*, 2012; Lambert *et al.*, 2014). BldK has also been implicated in the transport of S-adenosylmethionine, thus affecting the methylation state of the cell (Park *et al.*, 2005). In *S. griseus*, the expression of the *bldK* operon was indirectly regulated by the BldH orthologue AdpA (Akanuma *et al.*, 2011). The function of BldL is still unknown (Nodwell *et al.*, 1999).

BldM is an atypical two-component response regulator (Molle and Buttner, 2000). BldM could not be phosphorylated *in vitro*, and an allele with an aspartate-to-alanine substitution in its phosphorylation pocket restored sporulation to the *S. coelicolor ΔbldM* mutant, highlighting that phosphorylation of BldM is not essential for its function (Molle and Buttner, 2000). BldM directly regulates the expression of two classes of developmental genes, the first through forming a BldM-BldM homodimer, and the second through forming a functional heterodimer with another atypical response regulator - WhiI (Al-Bassam *et al.*, 2014). The Group I genes activated by the BldM-BldM homodimer include *whiB* and *ssgR*, and the Group II genes activated by the BldM-WhiI heterodimer include *smeA-sffA* and *whiE* (Al-Bassam *et al.*, 2014). Interestingly, the *S. venezuelae ΔbldM* mutant, was found to constitutively produce a cryptic antibiotic, which was designated venemycin (Thanapipatsiri *et al.*, 2016).

BldN is an extracytoplasmic function (ECF) sigma factor, initially synthesised as a longer, pro-protein (pro-σ^{BldN}), which is later cleaved to produce the mature sigma factor (Bibb and Buttner, 2003). The transcription of *bldN* was found to depend on BldG and BldH in *S. coelicolor* (Bibb, Molle and Buttner, 2000). BldN is regulated post-translationally by its cognate transmembrane anti-sigma factor, RsbN (Bibb *et al*., 2012). The major function of BldN appears to be the transcriptional activation of all the protein components of the hydrophobic sheath, presumably in response to a signal that results in the proteolytic inactivation of RsbN and the processing of pro-σ^{BldN} (Bibb *et al*., 2012). The target genes that are directly activated by BldN include all the chaplin and rodlin genes, *bldM*, and the gene encoding the BldN-specific anti-sigma factor *rsbN* (Bibb *et al.*, 2012).

The deletion of *rsbN* results in accelerated sporulation in *S. venezuelae* (Bibb *et al.*, 2012). The crystal structure of BldN in complex with the cytoplasmic domain of RsbN revealed that RsbN defines a new structural class of anti-σ factor, having no structural similarity with previously characterised anti-σ factors (Schumacher *et al.*, 2018).

The *bldO* gene in *S. venezuelae* was identified fairly recently - its expression was discovered to be directly activated by WhiA and WhiB in cooperation (Bush *et al.*, 2017). Interestingly, BldO, which is a member of the MerR family of regulators, was discovered to be a dedicated transcriptional repressor of *whiB*, creating a developmental feedback loop. The *S. venezuelae ΔbldO* mutant displayed a precocious sporulation phenotype, like the *ΔbldC* and *ΔbldD* mutants. The same phenotype was seen when WhiB was overexpressed under the strong constitutive *ermE** promoter, bypassing BldO repression (Bush *et al.*, 2017).

Genes Required for Mature Spore Formation in *Streptomyces*

The other major family of developmental regulators is the Whi (white) proteins. Like the *bld* genes, *whi* genes typically encode DNA-binding transcriptional regulators, acting on different developmental pathways in *Streptomyces* (Flärdh and Buttner, 2009). *whi* mutants are arrested at different stages of post-aerial-mycelium differentiation and are unable to form mature spores. On solid media, *whi* mutants form fuzzy white colonies - fuzzy due to their intact aerial mycelium, and white because they fail to synthesise the polyketide pigment associated with mature spores. Under the microscope, different *whi* mutants display varying degrees of progress through development, from a complete failure to initiate sporulation septation right through to the production of chains of unpigmented but morphologically wild-type spores (Flärdh and Buttner, 2009).

The first set of *whi* mutants in *S. coelicolor* was identified in a mutagenesis screen identical to the one that discovered the first *bld* mutants (Chater, 1972). The genes discovered in the screen were mapped and designated *whiA-I* (Chater, 1972). A second such screen was performed - it expanded the list of *whi* genes with the additions of *whiJ-O* (Ryding *et al.*, 1999). Out of those mutants, the *whiC* mutant was lost, and *whiF* was found to be an allele of *whiG* (Ryding *et al.*, 1999). Out of the remaining Whi regulators, WhiL, WhiM and WhiO have not been investigated further. The full deletions of *whiK* and *whiN* resulted in bald phenotypes (rather than the white phenotypes of the point mutants from the initial mutagenesis screens), and so the genes were re-designated *bldM* and *bldN* respectively (Bibb, Molle and Buttner, 2000; Molle and Buttner, 2000).

WhiA is a transcription factor with an N-terminal degenerate endonuclease domain and a C-terminal helix-turn-helix domain (Knizewski and Ginalski, 2007). Interestingly, it is found in virtually all Gram-positive bacteria, even in non-sporulating species (Aínsa *et al.*, 2000). The function of WhiA is closely linked to that of another Whi regulator, WhiB (Davis and Chater, 1992).

The earliest connection made between the functions of WhiA and WhiB was their identical mutant phenotypes in *S. coelicolor* - this was later observed in *S. venezuelae* as well. *whiA* and *whiB* mutants fail to halt aerial growth, to initiate sporulation septation, or to partition their chromosomes - instead, the cells keep growing, producing long aerial hyphae devoid of sporulation septa and containing uncondensed DNA (Flärdh, Findlay and Chater, 1999; Aínsa *et al.*, 2000; Bush *et al.*, 2013, 2016). These identical phenotypes arise because WhiA and WhiB are transcription factors that function cooperatively to control the expression of a common set of WhiAB target genes.

In *S. venezuelae*, WhiA was shown to directly bind the promoters of genes important for development and chromosome segregation, such as *ftsZ*, *ftsK, ftsW, filP* and *whiG* (Bush *et al.*, 2013). Looking at the transcriptional profile of WhiA target genes in the wild type and the *ΔwhiA* mutant throughout *S. venezuelae* development revealed that WhiA acts as an activator of some of its target genes and a repressor of others (Bush *et al.*, 2013).

In Actinobacteria, WhiB has multiple homologues, which were designated Wbl (**W**hi**B-l**ike) (Soliveri *et al.*, 2000; Bush, 2018). A characteristic feature of the Wbl proteins is the presence of a [4Fe-4S] iron-sulfur cluster (Bush, 2018). WhiB was shown to be a transcription factor and its regulon was found to completely overlap with the regulon of WhiA, suggesting that the two proteins jointly regulate the expression of their target genes (Bush *et al.*, 2013, 2016). However, a direct protein-protein interaction between WhiA and WhiB has not been demonstrated yet, neither *in vivo* nor *in vitro*, as the iron-sulfur cluster of WhiB makes *in vitro* work difficult. Substituting the 4 key cysteines in WhiB for either serines or alanines results in a loss of DNA binding, proving that the iron-sulfur cluster is essential for its transcription factor activity (Bush *et al.*, 2016). Among the more recently identified targets of WhiA and WhiB are the genes encoding the developmental regulator BldO (which itself represses *whiB* expression), the cell division protein SepH (Bush *et al.*, 2017; Ramos-León *et al.*, 2021) and the cell division protein SepX (Bush *et al.*, 2022).

Another member of the Wbl family of proteins is WhiD. The *S. coelicolor ΔwhiD* mutant was able to form spores, but those spores were irregularly sized and prone to lysis, with the presence of small, anucleate spores (Molle *et al.*, 2000). WhiD has the characteristic iron-sulfur cluster (Crack *et al.*, 2009), which was shown to be essential for its function, as the *ΔwhiD* mutant could not be complemented with *whiD* variants lacking any of the 4 cysteines necessary for [4Fe-4S] binding (Jakimowicz *et al.*, 2005). In *S. venezuelae*, WhiD was shown to exist in a monomer-dimer equilibrium and its homodimerisation was dependent on the C-terminus of the protein - a feature not present in the *S. coelicolor* orthologue (Stewart *et al.*, 2020). WhiD binds domain 4 of principal sigma factor HrdB *in vivo* and *in vitro* and this interaction also depends on the iron-sulfur cluster (Stewart *et al.*, 2020).

The *whiE* designation was given to an 8-gene locus (*orfI* - *orfVIII*), which is involved in the synthesis of the spore pigment in *Streptomyces*. The homology of these genes to those in certain secondary metabolite gene clusters led to the realisation that the spore pigment is in fact a polyketide (Davis and Chater, 1990). Expression of the *whiE* genes was shown to be greatly reduced or overall abolished in the mutants for *whiA*, *whiB*, *whiG*, *whiH*, *whiI*, and *whiJ*, demonstrating the involvement of these regulators in the final step of spore maturation (Kelemen *et al.*, 1998). Mutations in *whiE orfI-VII* resulted in strains with classical white phenotypes (Yu and Hopwood, 1995).

A mutation in *whiE orfVIII* in *S. coelicolor* was found to result in the synthesis of a green spore pigment rather than the grey pigment characteristic of the wild type (Yu and Hopwood, 1995). WhiE OrfVIII is a hydroxylase tailoring enzyme, responsible for the final step of pigment synthesis. Expression of *whiE orfVIII* was shown to be dependent on the sporulation sigma factor SigF - as a result, the *S. coelicolor ΔsigF* mutant exhibited a green spore phenotype (Kelemen *et al.*, 1998). Interestingly, the green spore pigment of the *S. venezuelae* NRRL B-65442 strain used in this study differs from the grey pigment of its parent *S. venezuelae* strain ATCC 10712. The full genome sequence of NRRL B-65442 revealed that the green spore pigment of the strain was caused by a spontaneous point mutation resulting in a tryptophan-to-arginine substitution in WhiE OrfVIII (Gomez-Escribano *et al.*, 2021).

The sigma factor WhiG belongs to the flagellar clade of sigma factors, which includes SigD (Sigma 28) in *B. subtilis* and FliA in enteric bacteria (Chater *et al.*, 1989). The *S. coelicolor ΔwhiG* mutant exhibited the growth of straight aerial hyphae without any sporulation septation or spore pigment formation (Mendez and Chater, 1987; Flärdh, Findlay and Chater, 1999). In comparison, the *S. venezuelae ΔwhiG* mutant showed a mixture of undifferentiated hyphae and hyphae bearing chains of immature spores (Gallagher *et al.*, 2020). The overexpression of *whiG* in *S. coelicolor* results in hypersporulation, showing that WhiG is a positive regulator of sporulation (Chater *et al.*, 1989). In *S. venezuelae*, the *whiG* overexpression phenotype was characterised in greater detail - the hypersporulation of the strain resulted from a precocious sporulation of the vegetative hyphae, bypassing aerial hyphae formation (Gallagher *et al.*, 2020). This resulted in a bald hypersporulation phenotype, related to the phenotypes of the *ΔbldC*, *ΔbldD* and *ΔbldO* mutants.

In *S. venezuelae*, WhiG directly activates transcription of only three genes. One of these genes, *vnz15005*, encodes a membrane protein of unknown function and deletion of *vnz15005* has no obvious phenotypic consequences (Gallagher *et al*., 2020). The other two WhiG targets are the key late developmental regulators *whiH* and *whiI*, and through them WhiG indirectly affects the expression of more than 100 late sporulation genes (Gallagher *et al.*, 2020). In *S. coelicolor*, *whiG* was found to be expressed during the entire developmental life cycle, which pointed to its post-transcriptional regulation (Kelemen *et al.*, 1996). An anti-sigma factor for WhiG was discovered and designated RsiG (standing for **r**egulator of **s**igma Whi**G**) (Gallagher *et al.*, 2020). The novel crystal structure of the WhiG-RsiG complex revealed that a dimer of c-di-GMP was bound to the middle of the resulting RsiG–$(c\text{-di-GMP})_2$–WhiG complex, and biochemical and genetic analysis showed that c-di-GMP was required for stable assembly of the sigma-anti-sigma complex (Gallagher *et al.*, 2020). An ancestral form of RsiG from *Rubrobacter radiotolerans* was found to bind WhiG as a dimer instead of a monomer, resulting in a $(RsiG)_2$-$(c\text{-di-GMP})_2$-WhiG complex (Schumacher *et al.*, 2021). Through its involvement in BldD and WhiG function, c-di-GMP emerged as an important determinant of *Streptomyces* sporulation (Tschowri *et al.*, 2014; Schumacher *et al.*, 2017; Gallagher *et al.*, 2020).

WhiH is a transcriptional regulator of the GntR family, which regulates its own expression (Ryding *et al.*, 1998; Persson, Chater and Flärdh, 2013). The *S. coelicolor ΔwhiH* mutant showed the formation of mostly undifferentiated hyphae, with some exhibiting occasional sporulation septation (Flärdh, Findlay and Chater, 1999). A similar phenotype was found in the *S. venezuelae ΔwhiH* mutant - whenever septation did take place, it resulted in long spore-like compartments with multiple condensed chromosomes (Schlimpert *et al.*, 2017). ChIP-seq on 3xFLAG-WhiH revealed many enrichment peaks next to late sporulation genes (Matt Bush, unpublished; dataset deposited in ArrayExpress under the accession number E-MTAB-6702). WhiH was shown to indirectly activate the expression of the dynamin-like genes *dynA* and *dynB*, which encode important components of the *Streptomyces* divisome (Schlimpert *et al.*, 2017).

WhiI is an atypical response regulator, which was found to lack key phosphorylatable residues (Aínsa, Parry and Chater, 1999; Tian *et al.*, 2007). Point mutations in the abnormal phosphorylation pocket of WhiI only resulted in a lack of spore pigment formation, as opposed to the sporulation defects caused by the deletion of the whole gene (Tian *et al.*, 2007). As already discussed, WhiI was observed to form a heterodimer with another atypical response regulator - BldM (Al-Bassam *et al.*, 2014). The BldM-WhiI complex directly bound the promoters of several known sporulation genes, such as the *whiE* locus and the *smeA-sffA* operon (Al-Bassam *et al.*, 2014). There is no set of genes regulated by a WhiI homodimer - WhiI functions solely as an auxiliary protein to modulate BldM binding specificity through heterodimerization. This contrasts with BldM, which functions as a homodimer in early development and as a BldM-WhiI heterodimer in late development (Al-Bassam et al., 2014).

Project Aims

The transition between vegetative and aerial growth in *Streptomyces* marks an impactful shift towards dispersal and scavenging for nutrition via the formation of complex new structures - the aerial hyphae. Since the discovery of the Bld developmental regulators that are necessary for aerial mycelium formation, many of them have been functionally characterised as direct regulators of the transcription of sporulation-related genes. A notable exception is BldB, whose function in development was still a mystery. In this thesis, I present an investigation of the molecular function of BldB and its role in aerial mycelium formation in *Streptomyces venezuelae*.

Page intentionally left blank

2. Materials and Methods

Bacterial and Bacteriophage Strains

The bacterial and bacteriophage strains used in this study are listed in **Tables 2.1**, **2.2** and **2.3**.

Escherichia coli Strains

The *E. coli* strains used for general cloning and transformation, Redirect, bacterial-two-hybrid assays, and protein overexpression and purification are listed in **Table 2.1.**

Table 2.1. List of *E. coli* strains used in this study.

Strain	Genotype	Source
DH5α	F', *supE44*, *lacU169*, (*Φ80lacZΔM15*), *ΔhsdR17*, *recA1*, *endA1*, *gyrA96*, *thi-1*, *relA1*	Hanahan (1983)
TOP10	F^-, *mcrA*, Δ(*mrr-hsdRMSmcrBC*), *Φ80lacZΔM15*, Δ*lacX74*, *recA1*, *araD139*, Δ(*ara-leu*)*7697*, *galU*, *galK*, *rpsL*, *galE15*, *galK16*, *λ-endA1*, *nupG* (Str^R)	ThermoFisher Scientific (Waltham, MA, USA)
BW25113	Δ(*araD-araB*)*567*, Δ*lacZ4787*(*::rrnB-4*) *lacIp-4000*(*lacI*^{Q}) *λ-*, *rpoS369*(*Am*), *rph-1*, Δ(*rhaD-rhaB*)*568*, *hsdR514*	Datsenko and Wanner, (2000)
ET12567	F', *dam13::Tn9*, *dcm6*, *hsdM*, *hsdR*, *recF143::Tn10*, *galK2*, *galT22*, *ara-14*, *lacY1*, *xyl-5*, *leuB6*, *thi-1*, *tonA31*, *rpsL136*, *hisG4*, *tsx-78*, *mtl-1*, *glnV44* (Cam^R, Tet^R); carries RK2 derivative with defective *oriT* for plasmid mobilisation (Kan^R)	MacNeil *et al.*, (1992); Flett, Mersinias and Smith, (1997)
BTH101	F^-, *cya-99*, *araD139*, *galE15*, *galK16*, *rpsL1*, *hsdR2*, *mcrA1*, *mcrB1* (Str^R)	Karimova, Ullmann and Ladant, (2000)
BL21 DE3 pLysS Rosetta	F^-, *ompT*, *gal*, *dcm*, *hsdS*$_B$(r_B^- m_B^-), λ(DE3 [*lacI lacUV5-T7 gene1 ind1 sam7 nin5*]), pLysSRARE^6 (Cam^R)	Novagen (Merck, Nottingham, UK)

Strain	Genotype	Source
BL21 DE3 NiCo	*can::CBD fhuA2 [lon] ompT gal (λ DE3) [dcm] arnA::CBD slyD::CBD glmS6Ala ΔhsdS λ DE3 = λ sBamHIo ΔEcoRI-B int::(lacI::PlacUV5::T7 gene1) i21 Δnin5* (Cam^R)	NEB (Ipswich, MA, USA)

***Streptomyces* Strains**

The *S. venezuelae* mutants generated in this study, as well as the wild-type *S. venezuelae* strain are listed in **Table 2.2.**

Table 2.2. List of *Streptomyces* strains used in this study.

Strain	Description	Source
S. venezuelae NRRL B-65442	Wild-type *Streptomyces venezuelae*	Ehrlich *et al.*, (1948)
SV100	Δ*bldB::apr* (Apr^R)	This study
SV101	*ΔbldB2::apr* (Apr^R)	This study
SV102	*ΔbldB3::apr* (Apr^R)	This study
SV103	*ΔbldB4::apr* (Apr^R)	This study
SV104	*ΔbldB5::apr* (Apr^R)	This study
SV105	*ΔbldB6::apr* (Apr^R)	This study
SV106	*ΔbldB7::apr* (Apr^R)	This study
SV107	*ΔbldB8::apr* (Apr^R)	This study
SV108	*ΔbldB9::apr* (Apr^R)	This study
SV109	*ΔbldB10::apr* (Apr^R)	This study
SV110	*ΔbldB11::apr* (Apr^R)	This study
SV111	*ΔabaA3::apr* (Apr^R)	This study
SV112	*ΔabaA4::apr* (Apr^R)	This study
SV113	*ΔabaA6::apr* (Apr^R)	This study

Strain	Description	Source
SV114	*ΔabaA7::apr* (Apr^R)	This study
SV115	*ΔabaA10::apr* (Apr^R)	This study
SV116	*ΔiosA::apr* (Apr^R)	This study
SV117	*ΔwhiJ6::apr* (Apr^R)	This study
SV118	*ΔwhiJ9::apr* (Apr^R)	This study
SV119	*ΔasfA1::apr* (Apr^R)	This study
SV120	*ΔasfA2::apr* (Apr^R)	This study
SV121	*ΔosaC::apr* (Apr^R)	This study
SV122	*ΔosaC2::apr* (Apr^R)	This study
SV123	*ΔsigB::apr* (Apr^R)	This study
SV124	*ΔabaA6 ΔiosA ΔbldB::apr* (Apr^R)	This study
SV125	*ΔwhiJ9 ΔbldB::apr* (Apr^R)	This study
SV126	*ΔbldB9 ΔwhiJ9::apr* (Apr^R)	This study

Bacteriophage Strains

Table 2.3. List of bacteriophages used in this study.

Strain	Genotype	Source
SV1	Genome available at http://phagesdb.org/phages/SV1/	Stuttard, (1982); Smith *et al.*, (2013)

Plasmids and Cosmids

The plasmids and cosmids used and generated in this study are listed in **Tables 2.4** and **2.5**.

Table 2.4. List of plasmids used in this study.

Plasmid	Description	Source
BT340	Temperature-sensitive FLP recombination plasmid (Cam^R)	Datsenko and Wanner, (2000)
pIJ773	Plasmid template for the amplification of the *apr-oriT* cassette for Redirect P1-FRT-*oriT-aac(3)IV*-FRT-P2 (Apr^R)	Gust *et al.*, (2003)
pIJ790	Modified λ RED recombination plasmid [*oriR101*] [*repA101*(ts)] *araBp-gam-be-exo* (Cam^R)	Gust *et al.*, (2003)
pUZ8002	Non-transmissible *oriT*-mobilising plasmid (Kan^R)	Paget *et al.*, (1999)
pIJ10770/ pSS170	Plasmid cloning vector for the conjugal transfer of DNA from *E. coli* to *Streptomyces* spp. Integrates site specifically at the ΦBT1 attachment site. *ori*, pUC18, hyg, *oriT*, RK2, int ΦBT1 Δ*aac(3)IVp* (Hyg^R)	Susan Schlimpert, referenced in Bush *et al*., (2017)
pIJ10927	pSS170 carrying *bldB* driven from its native promoter	This study
pIJ10928	pSS170 carrying *bldB* with an N-terminal 3xFLAG tag driven from its native promoter	This study
pIJ10929	pSS170 carrying *whiJ6* with an N-terminal 3xFLAG tag driven from its native promoter	This study
pIJ10930	pSS170 carrying *whiJ6* with a C-terminal 3xFLAG tag driven from its native promoter	This study

Plasmid	Description	Source
pIJ10931	pSS170 carrying *whiJ9* with an N-terminal 3xFLAG tag driven from its native promoter	This study
pIJ10932	pSS170 carrying *whiJ9* with a C-terminal 3xFLAG tag driven from its native promoter	This study
pIJ10500	A modified version of the integrative pMS82 vector containing a *Streptomyces* codon usage-optimised 3xFLAG epitope cassette (Hyg^R)	Chris den Hengst, referenced in Pullan *et al.*, (2011)
pIJ10933	pIJ10500 carrying *bldB* with a C-terminal 3xFLAG tag driven from its native promoter	This study
pIJ10257	Plasmid integrating at the ΦBT1 attachment site of *S. venezuelae* and containing the strong *ermE** promoter for the overexpression of a target gene (Hyg^R)	Hong *et al.*, (2005)
pIJ10934	pIJ10257 carrying *bldB*	This study
pIJ10935	pIJ10257 carrying *bldB6*	This study
pIJ10936	pIJ10257 carrying *bldB9*	This study
pIJ10937	pIJ10257 carrying *abaA3*	This study
pIJ10938	pIJ10257 carrying *abaA4*	This study
pIJ10939	pIJ10257 carrying *abaA6*	This study
pIJ10940	pIJ10257 carrying *abaA7*	This study
pIJ10941	pIJ10257 carrying *abaA10*	This study
pIJ10942	pIJ10257 carrying *iosA*	This study
pIJ10943	pIJ10257 carrying *whiJ6*	This study
pIJ10944	pIJ10257 carrying *whiJ9*	This study
pIJ10945	pIJ10257 carrying *asfA1*	This study
pIJ10946	pIJ10257 carrying *asfA2*	This study
pIJ10947	pIJ10257 carrying *osaC*	This study

Plasmid	Description	Source
pIJ10948	pIJ10257 carrying *osaC2*	This study
pIJ10949	pIJ10257 carrying *sigB*	This study
pIJ10950	pIJ10257 carrying *abaA6* and *iosA*, separated by an RBS	This study
pIJ10951	pIJ10257 carrying *whiJ9* with an N-terminal 3xFLAG tag	This study
pIJ10952	pIJ10257 carrying *whiJ9* with a C-terminal 3xFLAG tag	This study
pET15b	Protein expression vector for expression of a target gene with an N-terminal 6xHis tag under the control of a T7 promoter (Amp^R)	Novagen (Merck, Nottingham, UK)
pIJ10953	pET15B carrying *bldB* with an N-terminal 6xHis tag	This study
pIJ10954	pET15B carrying *bldB9* with an N-terminal 6xHis tag	This study
pIJ10955	pET15B carrying *whiJ6* with an N-terminal 6xHis tag	This study
pIJ10956	pET15B carrying *whiJ9* with an N-terminal 6xHis tag	This study
pCOLA-Duet1	Protein expression vector for coexpression of two target genes, each under the control of a T7 promoter (Kan^R)	Novagen (Merck, Nottingham, UK)
pIJ10957	pCOLA-Duet1 carrying untagged *whiJ9* and *bldB9* with an N-terminal 6xHis tag	GenScript (Piscataway, NJ, USA)
pUT18	Two-hybrid plasmid, C-terminal CyaAT18 fusion (Amp^R)	Karimova *et al.*, (1998)
pUT18C	Two-hybrid plasmid, N-terminal CyaAT18 fusion (Amp^R)	Karimova *et al.*, (1998)
pKT25	Two-hybrid plasmid, N-terminal CyaAT25 fusion (Kan^R)	Karimova *et al.*, (1998)
pKNT25	Two-hybrid plasmid, C-terminal cyaAT25 fusion (Kan^R)	Karimova *et al.*, (1998)

Plasmid	Description	Source
pIJ10958	pUT18 carrying *bldB*	This study
pIJ10959	pUT18C carrying *bldB*	This study
pIJ10960	pKT25 carrying *bldB*	This study
pIJ10961	pKNT25 carrying *bldB*	This study
pIJ10962	pUT18C carrying *bldB2*	This study
pIJ10963	pKNT25 carrying *bldB2*	This study
pIJ10964	pUT18C carrying *bldB3*	This study
pIJ10965	pKNT25 carrying *bldB3*	This study
pIJ10966	pUT18C carrying *bldB4*	This study
pIJ10967	pKNT25 carrying *bldB4*	This study
pIJ10968	pUT18C carrying *bldB5*	This study
pIJ10969	pKNT25 carrying *bldB5*	This study
pIJ10970	pUT18C carrying *bldB6*	This study
pIJ10971	pKNT25 carrying *bldB6*	This study
pIJ10972	pUT18C carrying *bldB7*	This study
pIJ10973	pKNT25 carrying *bldB7*	This study
pIJ10974	pUT18C carrying *bldB8*	This study
pIJ10975	pKNT25 carrying *bldB8*	This study
pIJ10976	pUT18C carrying *bldB9*	This study
pIJ10977	pKNT25 carrying *bldB9*	This study
pIJ10978	pUT18C carrying *bldB10*	This study
pIJ10979	pKNT25 carrying *bldB10*	This study
pIJ10980	pUT18C carrying *bldB11*	This study
pIJ10981	pKNT25 carrying *bldB11*	This study
pIJ10982	pUT18 carrying *abaA6*	This study
pIJ10983	pKT25 carrying *abaA6*	This study
pIJ10984	pUT18 carrying *iosA*	This study

Plasmid	Description	Source
pIJ10985	pKT25 carrying *iosA*	This study
pIJ10986	pUT18 carrying *whiJ6*	This study
pIJ10987	pKT25 carrying *whiJ6*	This study
pIJ10988	pUT18 carrying *whiJ9*	This study
pIJ10989	pKT25 carrying *whiJ9*	This study
pIJ10990	pUT18 carrying *asfA1*	This study
pIJ10991	pKT25 carrying *asfA1*	This study
pIJ10992	pUT18 carrying *asfA2*	This study
pIJ10993	pKT25 carrying *asfA2*	This study
pIJ10994	pUT18 carrying *osaC*	This study
pIJ10995	pKT25 carrying *osaC*	This study
pIJ10996	pUT18 carrying *osaC2*	This study
pIJ10997	pKT25 carrying *osaC2*	This study
pIJ10998	pUT18 carrying *sigB*	This study
pIJ10999	pKT25 carrying *sigB*	This study
pUT18::*sigB2*	pUT18 carrying *sigB2*	This study
pKT25::*sigB2*	pKT25 carrying *sigB2*	This study
pUT18::*sigB3*	pUT18 carrying *sigB3*	This study
pKT25::*sigB3*	pKT25 carrying *sigB3*	This study
pUT18::*sigI*	pUT18 carrying *sigI*	This study
pKT25::*sigI*	pKT25 carrying *sigI*	This study
pUT18::*sigN*	pUT18 carrying *sigN*	This study
pKT25::*sigN*	pKT25 carrying *sigN*	This study
pUT18::*sigF*	pUT18 carrying *sigF*	This study
pKT25::*sigF*	pKT25 carrying *sigF*	This study
pUT18::*sigH*	pUT18 carrying *sigH*	This study
pKT25::*sigH*	pKT25 carrying *sigH*	This study

Table 2.5. List of cosmids used in this study.

Cosmid	Start in Genome	End in Genome	Purpose
PL1_B10	5811852	5851919	Generation of the *ΔbldB* mutant in *S. venezuelae*
3I07	5796574	5838390	
PL1_L16	3343938	3390700	Generation of the *ΔbldB2* mutant in *S. venezuelae*
PL2_C23	6391668	6430432	Generation of the *ΔbldB3* mutant and the *ΔabaA3* mutant in *S. venezuelae*
PL1_H19	5568759	5610177	Generation of the *ΔbldB4* mutant and the *ΔabaA4* mutant in *S. venezuelae*
PL2_K3	4493600	4540862	Generation of the *ΔbldB5* mutant in *S. venezuelae*
1-C4	2219566	2260643	Generation of the *ΔbldB6* mutant, the *ΔwhiJ6* mutant and the *ΔabaA6* mutant in *S. venezuelae*
PL1_C12	3575127	3614619	Generation of the *ΔbldB7* mutant and the *ΔabaA7* mutant in *S. venezuelae*
PL2_D11	6187362	6231453	Generation of the *ΔbldB8* mutant in *S. venezuelae*
PL2_H18	3689751	3733133	Generation of the *ΔbldB9* mutant, the *ΔwhiJ9* mutant, the *ΔiosA* mutant and the *ΔbldB9 ΔwhiJ9* double mutant in *S. venezuelae*
Pl1_A8	6939255	6976491	Generation of the *ΔbldB10* mutant and the *ΔabaA10* mutant in *S. venezuelae*
PL2_E5	6210531	6252891	Generation of the *ΔbldB11* mutant in *S. venezuelae*
PL2_G7	876389	918137	Generation of the *ΔasfA1* mutant in *S. venezuelae*
PL1_E13	2357474	2398938	Generation of the *ΔasfA2* mutant in *S. venezuelae*
3J08	5829495	5864615	Generation of the *ΔosaC* mutant in *S. venezuelae*
Sv-4-D07	3840807	3880157	Generation of the *ΔosaC2* mutant in *S. venezuelae*
Sv-5-C07	380346	421756	Generation of the *ΔsigB* mutant in *S. venezuelae*

Culture Media and Antibiotics

All media were prepared according to pre-established protocols (Kieser *et al.*, 2000), or according to the manufacturer's instructions, as described in **Tables 2.6** and **2.7**. Antibiotics and substrates were prepared as described in **Table 2.8**.

Solid Media

LB agar, MacConkey agar and M63 agar were used to culture *E. coli* strains. Soya flour mannitol agar (SFM), Difco nutrient agar (DNA), soft nutrient agar (SNA) and MYM agar were used to culture *Streptomyces* strains and the SV1 phage.

Table 2.6. Solid media used in this study.

Medium	Composition		Preparation
LB Agar	Agar	11.0 g	The ingredients, except agar, were dissolved in deionised water and 200 mL aliquots were dispensed into 250 mL Erlenmeyer flasks containing 2.2 g agar. The flasks were closed and autoclaved.
	Tryptone	10.0 g	
	Yeast extract	5.0 g	
	NaCl	10.0 g	
	dH_2O to	1000 mL	
MacConkey Agar	MacConkey Agar	52.0 g	The ingredients were dissolved in deionised water and 200 mL aliquots were dispensed into 250 mL Erlenmeyer flasks. The flasks were closed and autoclaved.
	dH_2O to	1000 mL	
M63 Agar	Agar	15.0 g	The agar was dissolved in deionised water and 200 mL aliquots were dispensed into 250 mL Erlenmeyer flasks. The flasks were closed and autoclaved. Sterile 5X M63 was added to a 1X final concentration.
	5X M63	250 mL	
	dH_2O to	1000 ml	
SFM Agar	Agar	15.0 g	Ingredients were dissolved in tap water and 200 mL aliquots poured into 250 mL Erlenmeyer flasks. The flasks were autoclaved twice (115°C, 15 minutes), with gentle shaking between the two runs.
	D-Mannitol	15.0 g	
	Soya flour	15.0 g	
	H_2O to	750 mL	

Medium	Composition		Preparation
DNA (Difco Nutrient Agar)	Difco Nutrient Agar dH_2O to	4.6 g 200 mL	Difco Nutrient Agar was placed in each 250 mL Erlenmeyer flask and deionised water was added. The flasks were closed and autoclaved.
SNA	Difco Nutrient Broth Agar dH_2O to	8.0 g 7.0 g 1000 mL	The ingredients, except agar, were dissolved in deionised water and 50 mL aliquots were dispensed into 100 mL narrow-necked conical flasks containing 0.35 g agar. The flasks were closed and autoclaved.
MYM Agar	Difco Bacto Agar Maltose Yeast extract Oxoid Malt extract H_2O to	20.0 g 4.0 g 4.0 g 10.0 g 1000 mL	The ingredients, except agar, were dissolved in a 1:1 mix of regular tap water and deionised water. 200 mL aliquots were dispensed into 250 mL Erlenmeyer flasks containing 4 g agar. The flasks were closed and autoclaved. To aid sporulation of *Streptomyces*, a 1:500 dilution of trace elements was added to the molten agar before pouring plates.

Liquid Media

LB broth, SOC medium and M63 minimal medium were used to culture *E. coli* strains. Difco nutrient broth (DNB) and MYM medium were used to culture *Streptomyces* strains.

Table 2.7. Liquid media used in this study.

Medium	Composition		Preparation
LB Broth	Tryptone	10.0 g	The ingredients were dissolved in deionised water and aliquots dispensed and autoclaved.
	Yeast extract	5.0 g	
	NaCl	10.0 g	
	dH_2O to	1000 mL	
SOC	Tryptone	20.0 g	The ingredients were dissolved in deionised water and aliquots dispensed and autoclaved. After autoclaving, the appropriate quantities of sterile glucose and $MgCl_2$ were added.
	Yeast extract	5.0 g	
	NaCl	0.58 g	
	KCl	0.186 g	
	$MgCl_2 . 6H_2O$	2.03 g	
	$MgSO_4 . 7H_2O$	2.46 g	
	Glucose	3.6 g	
	dH_2O to	1000 mL	
5xM63 Minimal Medium	$(NH_4)_2SO_4$	5.0 g	The ingredients were dissolved in deionised water, pH was adjusted to 7.0 with KOH, aliquots were dispensed and autoclaved.
	KH_2PO_4	34.0 g	
	$FeSO_4$-$7H_2O$	1.25 mg	
	Vitamin B1 (thiamine)	2.5 mg	
	dH_2O to	500 mL	
DNB	Difco Nutrient Broth	8.0 g	The ingredients were dissolved in deionised water and aliquots dispensed and autoclaved.
	dH_2O to	1000 mL	

MYM	Maltose	4.0 g	The ingredients were dissolved in a 1:1 mix of regular tap water and deionised water. The Duran bottles were closed and autoclaved. To aid sporulation of *Streptomyces*, a 1:500 dilution of trace elements was added before inoculation.
	Yeast extract	4.0 g	
	Oxoid Malt extract	10.0 g	
	H_2O to	1000 mL	
Trace Elements	$ZnCl_2$	40.0 mg	The ingredients were dissolved in 1L of dH_2O, dispensed in 10 mL aliquots and autoclaved.
	$FeCl_3 . 6H_2O$	200.0 mg	
	$CuCl_2 . 2H_2O$	10.0 mg	
	$MnCl_2 . 4H_2O$	10.0 mg	
	$Na_2B_4O_7 . 10H_2O$	10.0 mg	
	$(NH_4)_6Mo_7O_{24} . 4H_2O$	10.0 mg	
	dH_2O to	1000 mL	

Antibiotics and Substrates

Table 2.8. List of antibiotics and substrates used in this study.

Antibiotic / Substrate	**Final concentration in media (µg/mL)**
Apramycin (Apr)	50
Kanamycin (Kan)	50
Carbenicillin (Carb)	100
Hygromycin (Hyg)	25
Nalidixic Acid (Nal)	25
Chloramphenicol (Cam)	25
X-Gal	40
IPTG	0.5 - 1 mM

Growth Conditions and Storage of Bacterial and Phage Strains

E. coli Strains

In general, *E. coli* strains were either plated on solid media, or inoculated in liquid media shaking at 250 rpm. Appropriate antibiotics were added to the media, and strains were incubated overnight at 30-37°C. Glycerol stocks were prepared from fresh liquid cultures, by adding sterile 40% (v/v) glycerol to an equal volume of overnight bacterial culture, and stored at -80°C.

S. venezuelae Strains

S. venezuelae strains were either plated on solid media or inoculated in liquid media shaking at 250 rpm. When grown on agar, strains were incubated at 28°C for 3 - 5 days. When growth in liquid culture was required, strains were grown at 28°C for 18 - 24 hours in 250 mL Erlenmeyer flasks, or 30 mL glass universals containing metal springs for better aeration and homogenisation.

For sporulating *S. venezuelae* strains, spores were harvested from confluent MYM plates using sterile cotton pads. The cotton pad was placed on the bacterial lawn, folded over, and 3 mL of 20% (v/v) glycerol was pipetted on the pad. Using sterile forceps, the cotton pad was gently pushed across the lawn to gather the spores on the underside. The spores were collected through the pad using a 2 mL syringe and stored at -80°C.

Non-sporulating *S. venezuelae* strains were grown in liquid MYM cultures (incubated as outlined above) and centrifuged at 3,000 rpm. The superfluous medium was discarded, the resulting mycelium resuspended in 20% glycerol, and stored at -80°C.

Phage Strains

The temperate SV1 phage was used for generalised transduction in this study (Stuttard, 1982). To prepare a high-titre phage stock (Kieser *et al.*, 2000), serial dilutions of SV1 (10^{0} – 10^{-10}) in DNB medium were prepared in 100 µL aliquots. Soft nutrient agar (SNA) was melted, 800 µL volumes were added to Eppendorf tubes, which were cooled to and maintained at 40 - 45°C, to prevent the medium from solidifying at this stage.

Difco nutrient agar (DNA) plates supplemented with 10 mM $MgSO_4$, 10 mM $Ca(NO_3)_2$, and 0.5% (w/v) glucose were prepared. The SV1 phage dilution aliquots, along with 6 µL wild-type *S. venezuelae* spores were added to the SNA Eppendorfs, mixed, and the total volume was poured on the DNA plates, and gently swirled to cover the whole plate surface. The plates were incubated at 28°C overnight.

On the following day, near-confluent plates were flooded with 2 mL DNB and left to soak for 2 - 5 hours at room temperature. The DNB containing SV1 phage was collected from these plates and passed through a 0.45 µm filter to remove any *Streptomyces* mycelial fragments. The resulting high-titre phage lysate was stored at 4°C.

DNA Methods

Plasmid and Cosmid DNA Isolation from *E. coli*

Plasmids were extracted using QIAprep Spin Miniprep kits (QIAGEN, Manchester, UK) according to the manufacturer's instructions. Plasmid DNA was eluted in 50 µL dH_2O and stored at -20°C. Cosmids were extracted using Wizard® Plus SV Minipreps DNA Purification System kits (Promega, Madison, WI, USA) following the manufacturer's instructions. Cosmid DNA was eluted in 100 µL dH_2O, and stored at -20°C.

General PCR

Q5 High-Fidelity DNA Polymerase (NEB, Ipswich, MA, USA) was used to produce high-quality PCR products for use in later experiments (*e.g.*, for cloning). A full list of oligos used for PCR is included in **Table 2.9.** Reactions were typically run in 50 µL volumes, containing the following components (final concentration): 1X Q5 Reaction Buffer, 1X Q5 High GC Enhancer, 200 µM dNTPs, 0.5 µM of each primer, 100 - 500 ng of template DNA, 3% DMSO and 0.02 U/µL Q5 High-Fidelity DNA Polymerase.

All PCR reactions were performed in a thermal cycler. After an initial denaturation phase (98°C for 30 sec), the samples went through 30 cycles of denaturation (98°C for 10 sec), annealing (estimated T_m for each primer pair, for 30 sec) and extension (72°C for 30 sec/kb - calculated based on expected size of PCR product). This was followed by a final extension phase (72°C for 2 min). PCR products were analysed by agarose gel electrophoresis, and stored at -20°C.

Colony PCR

Colony PCR was used to confirm whether clones with the desired DNA sequences were obtained after cloning and transformation in E*. coli*. The low-fidelity GoTaq® Green Master Mix polymerase (Promega, Madison, WI, USA) was used. A full list of oligos used for colony PCR is included in **Table 2.9.** Reactions were run in 20 µL volumes, containing the following components (final concentration): 0.5 µM of each primer, 7% DMSO and 1X GoTaq® Green Master Mix. Single colonies were picked with sterile pipette tips and material was deposited into each PCR tube. The tips were then put in fresh PCR tubes containing 50 µL LB for later inoculation.

All PCR reactions were performed in a thermal cycler. After the initial denaturation phase (95°C for 5 min), the samples were put through 25 cycles of denaturation (95°C for 30 sec), annealing (estimated T_m for each primer pair, for 30 sec) and extension (72°C for 1 min/kb - calculated based on expected size of PCR product). This was followed by a final extension phase (72°C for 5 min). PCR products were analysed by gel electrophoresis. Colonies that yielded the expected PCR product sizes were grown in liquid cultures for the preparation of glycerol stocks and plasmid isolation.

Agarose Gel Electrophoresis

Gels were prepared with 1% agarose and 1X Tris Borate EDTA (TBE) buffer (Severn Biotech, Kidderminster, UK). Ethidium bromide (EtBr) was added to the gels to a final concentration of 0.5 - 1 µg/mL. A pre-mixed loading buffer (6X Gel Loading Dye, Purple, NEB, Ipswich, MA, USA) was added to DNA samples to a 1X final concentration. To determine fragment sizes, one of the following ladders was run alongside the samples: 100 bp DNA Ladder or 1 kb Plus DNA Ladder (NEB, Ipswich, MA, USA). Electrophoresis was carried out at 100 -120 V for ~1 hour. Gels were visualised under UV light using a gel imaging system.

PCR Purification

PCR-amplified DNA was purified using the QIAquick PCR purification kit (QIAGEN, Manchester, UK) according to the manufacturer's instructions. PCR purification was also carried out to remove unwanted reagents from preceding reactions (*e.g.,* restriction enzymes). Purified DNA was eluted in 50 µL dH_2O, and stored at -20°C.

Oligonucleotides

All oligonucleotides used in this study were synthesised by either Eurofins Genomics (Ebersberg, Germany) or IDT (Leuven, Belgium) and listed in **Table 2.9**.

Table 2.9. List of oligonucleotides used in this study.

Name	Sequence (5' - 3')	Digestion Sites	Purpose
pUT18_F	CCAGGCTTTACACTTTATGCTTCC	-	Sequencing and verification of insertion into the pUT18 vector.
pUT18_R	GACGCGCCTCGGTGCCCACTGC	-	
pUT18C_F	GTGCCGAGCGGACGTTCGA	-	Sequencing and verification of insertion into the pUT18C vector.
pUT18C_R	TCAGCGGGTGTTGGCGGGTGTC	-	
pKT25_F	CGGTGACCAGCGGCGATT	-	Sequencing and verification of insertion into the pKT25 vector.
pKT25_R	CCGCCGGACATCAGCGCCATTC	-	
pKNT25_F	CCCAGGCTTTACACTTTATGCTTCC	-	Sequencing and verification of insertion into the pKNT25 vector.
pKNT25_R	GTTTTTTTCCTTCGCCACGGCCTTG	-	
pET15B_F	TATGCTAGTTATTGCTCAGCGGT	-	Sequencing and verification of insertion into the pET15B vector.
pET15B_R	AAATTAATACGACTCACTATAGGGG	-	
pCOLADuet1_MCS1_F	GGATCTCGACGCTCTCCCT	-	Sequencing and verification of insertion into the MCS1 of the pCOLA-Duet1 vector.
pCOLADuet1_MCS1_R	GATTATGCGGCCGTGTACAA	-	
pCOLADuet1_MCS2_F	TTGTACACGGCCGCATAATC	-	Sequencing and verification of insertion into the MCS2 of the pCOLA-Duet1 vector.
pCOLADuet1_MCS2_R	GCTAGTTATTGCTCAGCGG	-	
pSS170_F	CCTAGATCCTTTTGGTTCATGTGCAGCTCC	-	Sequencing and verification of insertion into the pSS170 vector.
pSS170_R	TATCACCGCAGATGGTTACCTCGCC	-	
pIJ10257_F	ACGTCCATGCGAGTGTCC	-	Sequencing and verification of insertion into the pIJ10257 vector.
pIJ10257_R	CCAAACGGCATTGAGCGTC	-	
19760_F	ATGGACGCGCAGACGATCGC	-	Tracing the unintended deletion in the *ΔabaA6 ΔiosA ΔbldB* triple mutant.
19760_R	TCAGTGTGTGTTGCGCCTGCC	-	
BldB_BACTH_F	ctgaggatcccATGACCGACGCAGACACCA	BamHI	Cloning *bldB* (*vnz26620*) into the BACTH vectors (PCR product is full gene without stop codon).
BldB_BACTH_R	ccggtacccgCCGCAGGTCGAACTCGCC	KpnI	

Name	Sequence (5' - 3')	Digestion Sites	Purpose
BldB2_BACTH_F	ctgaggatcccATGGCGATTATTCAGGGTGGCAC	BamHI	Cloning *bldB2* (*vnz15145*) into the BACTH vectors (PCR product is full gene without stop codon).
BldB2_BACTH_R	ccggtacccgGAGGGCCCCGTTGCTCAC	KpnI	
BldB3_BACTH_F	ctgaggatcccATGAGCACCACTGACCTGGCCT	BamHI	Cloning *bldB3* (*vnz29075*) into the BACTH vectors (PCR product is full gene without stop codon).
BldB3_BACTH_R	ccggtacccgCGCCAGCCGGGCGAGGAA	KpnI	
BldB4_BACTH_F	ctgaggatcccATGAGCGCAGCAGCACTTTCGT	BamHI	Cloning *bldB4* (*vnz25555*) into the BACTH vectors (PCR product is full gene without stop codon).
BldB4_BACTH_R	ccggtacccgGTTCGCCGCGCCGACGAA	KpnI	
BldB5_BACTH_F	ctgaggatcccATGGGGACCGGATCGAGCATGA	BamHI	Cloning *bldB5* (*vnz20565*) into the BACTH vectors (PCR product is full gene without stop codon).
BldB5_BACTH_R	ccggtacccgGAACCGCCCCTGCGCGG	KpnI	
BldB6_BACTH_F	ctgaggatcccATGGAGACCAACCAGAACCTGGC	BamHI	Cloning *bldB6* (*vnz09895*) into the BACTH vectors (PCR product is full gene without stop codon).
BldB6_BACTH_R	ccggtacccgGCGACTGCCGATGCGCCC	KpnI	
BldB7_BACTH_F	AACTGCAGCGTGCATCATGCGCATCGTGCG	PstI	Cloning *bldB7* (*vnz16140*) into the BACTH vectors (PCR product is full gene without stop codon).
BldB7_BACTH_R	ccggtacccgCACCAGGTGGTCGAACTCCC	KpnI	
BldB8_BACTH_F	ctgaggatcccGTGGAAGACCAGCTCGAATACT	BamHI	Cloning *bldB8* (*vnz28285*) into the BACTH vectors (PCR product is full gene without stop codon).
BldB8_BACTH_R	ccggtacccgGATCACGCCTTGATCCACCG	KpnI	
BldB9_BACTH_F	ctgaggatcccATGAGCGACACCCTGCACTG	BamHI	Cloning *bldB9* (*vnz16680*) into the BACTH vectors (PCR product is full gene without stop codon).
BldB9_BACTH_R	ccggtacccgCTGCCACGCGACGAAAGC	KpnI	
BldB10_BACTH_F	ctgaggatcccATGGATCGCATATACAACGGCA	BamHI	Cloning *bldB10* (*vnz31505*) into the BACTH vectors (PCR product is full gene without stop codon).
BldB10_BACTH_R	ccggtacccgGGTGAGCAGAAAGTCAGCC	KpnI	
BldB11_BACTH_F	ctgaggatcccGTGAAGCCCGTGTCCCAACC	BamHI	Cloning *bldB11* (*vnz28375*) into the BACTH vectors (PCR product is full gene without stop codon).
BldB11_BACTH_R	ccggtacccgCGGGCGCTTGATCGCCTC	KpnI	
AbaA6_BACTH_F	ctgaggatcccATGAATCAGGCAACAGACCTCT	BamHI	Cloning *abaA6* (*vnz09905*) into the BACTH vectors (PCR product is full gene without stop codon).
AbaA6_BACTH_R	ccggtacccgCGCGTCGCACTCGAACCA	KpnI	
IosA_BACTH_F	ctgaggatcccGTGAATGAAGAGAATCGGGAAGTA	BamHI	Cloning *iosA* (*vnz16670*) into the BACTH vectors (PCR product is full gene without stop codon).
IosA_BACTH_R	ccggtacccgGGACCCGCCGCTGAACAG	KpnI	
WhiJ6_BACTH_F	gctctagagGTGGTCAACATCCGCAGCCTG	XbaI	Cloning *whiJ6* (*vnz09900*) into the BACTH vectors (PCR product is full gene without stop codon).
WhiJ6_BACTH_R	ccggtacccgCGCCAGCGCGCTCCCGCCA	KpnI	
WhiJ9_BACTH_F	AACTGCAGCATGGCGCGTGCGGAGAACA	PstI	Cloning *whiJ9* (*vnz16675*) into the BACTH vectors (PCR product is full gene without stop codon).
WhiJ9_BACTH_R	GCTCTAGAGCTCTTTGTTCTCCCGCCAACTC	XbaI	
AsfA1_BACTH_F	gctctagagATGCAGCTGATCCCCCGTCATG	XbaI	Cloning *asfA1* (*vnz03680*) into the BACTH vectors (PCR product is full gene without stop codon).
AsfA1_BACTH_R	ccggtacccgGTCGGGGTTCGCCGCCCA	KpnI	

Name	Sequence (5' - 3')	Digestion Sites	Purpose
AsfA2_BACTH_F	ctgaggatcccATGCCCTGGGACGATGCTGC	BamHI	Cloning *asfA2* (*vnz10850*) into the BACTH vectors (PCR product is full gene without stop codon).
AsfA2_BACTH_R	ccggtacccgGCCGGCGACGGCGTCGG	KpnI	
OsaC_T18Gibson_F	TGCCTGCAGGTCGACTCTAGAGGATATGGCAGAG CCGGGCGTCGAGACGC	-	Cloning *osaC* (*vnz26705*) into the T18 vector via Gibson assembly.
OsaC_T18Gibson_R	TGGCGGCTGAATTCGAGCTCGGTACGCGGTCGTC CGGCTCCCGCAGGCGCA	-	
OsaC_T25Gibson_F	GGCTGCAGGGTCGACTCTAGAGGATATGGCAGAG CCGGGCGTCGAGACGC	-	Cloning *osaC* (*vnz26705*) into the T25 vector via Gibson assembly.
OsaC_T25Gibson_R	gccgaattcttagTTACTTAGGTACGCGGTCGTCCGGCT CCCGCAGGCGCA	-	
OsaC2_BACTH_F	ctgaggatcccATGCGCACCGAGGACGTCCTG	BamHI	Cloning *osaC2* (*vnz17535*) into the BACTH vectors (PCR product is full gene without stop codon).
OsaC2_BACTH_R	ccggtacccgCGGCCTGTCGTCCCCCGG	KpnI	
SigB_BACTH_F	ctgaggatcccGTGACGCTCACCACCATGTCG	BamHI	Cloning *sigB* (*vnz01715*) into the BACTH vectors (PCR product is full gene without stop codon).
SigB_BACTH_R	ccggtacccgGCCGGTCTCCAGGAGGCC	KpnI	
SigB2_BACTH_F	ctgaggatcccGTGCGGACCGAACCGGC	BamHI	Cloning *sigB2* (*vnz01090*) into the BACTH vectors (PCR product is full gene without stop codon).
SigB2_BACTH_R	ccggtacccgGTCGTCCGTCCCCGTCTC	KpnI	
SigB3_BACTH_F	ctgaggatcccATGTCGAACCACCGCACCACC	BamHI	Cloning *sigB3* (*vnz02255*) into the BACTH vectors (PCR product is full gene without stop codon).
SigB3_BACTH_R	ccggtacccgGGTCCGCTTCGCGGCGAC	KpnI	
SigI_BACTH_F	ctgaggatcccATGTCACCCCGGCTCGACG	BamHI	Cloning *sigI* (*vnz13800*) into the BACTH vectors (PCR product is full gene without stop codon).
SigI_BACTH_R	ccggtacccgTTCCTCCAGAGTGAGCCCCC	KpnI	
SigN_BACTH_F	ctgaggatcccATGTCCACAGAACTGGGCAGC	BamHI	Cloning *sigN* (*vnz18615*) into the BACTH vectors (PCR product is full gene without stop codon).
SigN_BACTH_R	ccggtacccgGTCCGCGATGAGGCCCTC	KpnI	
SigF_BACTH_F	ctgaggatcccGTGCCGGCCAGTACAGCAC	BamHI	Cloning *sigF* (*vnz18620*) into the BACTH vectors (PCR product is full gene without stop codon).
SigF_BACTH_R	ccggtacccgCGCCTCGATTCTGTTTGCGGAT	KpnI	
SigH_BACTH_F	ctgaggatcccGTGAGGCGCGGGGACGC	BamHI	Cloning *sigH* (*vnz24270*) into the BACTH vectors (PCR product is full gene without stop codon).
SigH_BACTH_R	ccggtacccgCTCCTCGACCAGAAGCTTCTCC	KpnI	
BldB_pET15B_F	GGGAATTCCATATGACCGACGCAGACACCAG	NdeI	Overexpression of *bldB* in *E. coli* for protein purification. PCR product was cloned into pET15B.
BldB_pET15B_R	CCGCTCGAGTCACCGCAGGTCGAACTCG	XhoI	
BldB9_pET15B_F	GGAATTCCATATGAGCGACACCCTGCACTG	NdeI	Overexpression of *bldB9* in *E. coli* for protein purification. PCR product was cloned into pET15B.
BldB9_pET15B_R	CCGCTCGAGCTACTGCCACGCGACGAAAG	XhoI	

Name	Sequence (5' - 3')	Digestion Sites	Purpose
WhiJ6_pET15B_F	GCGGCCTGGTGCCGCGCGGCAGCCACGTGGTCAACATCCGCAGCCTGGA	-	Overexpression of *whiJ6* in *E. coli* for protein purification. PCR product was cloned into pET15B via Gibson assembly.
WhiJ6_pET15B_R	TCGGGCTTTGTTAGCAGCCGGATCCTTACGCCAGCGCGCTCCCGCCAGGTT	-	
WhiJ9_pET15B_F	GCGGCCTGGTGCCGCGCGGCAGCCACATGGCGCGTGCGGAGAACAAGG	-	Overexpression of *whiJ9* in *E. coli* for protein purification. PCR product was cloned into pET15B via Gibson assembly.
WhiJ9_pET15B_R	TCGGGCTTTGTTAGCAGCCGGATCCTCATCTTTGTTCTCCCGCCAACTCC	-	
BldB_Red_F	GAGGGACCGCCGTACCACCGCGAAGGGAACGCGCCGATGATTCCGGGGATCCGTCGACC	-	Redirect deletion of *bldB* (*vnz26620*).
BldB_Red_R	CGTACGACGGGCCACCCCCTCACGCGTGTCCGCGGCTCATGTAGGCTGGAGCTGCTTC	-	
BldB_Red_Ext_F	ACATCCTCGGCAACGTCCGG	-	External primers for confirmation of the Redirect deletion of *bldB* (*vnz26620*).
BldB_Red_Ext_R	CCCAGCTCCTCGACGAGTC	-	
BldB2_Red_F	GCGCGACAACCACTGGCAGAACCGGAGCTGAGCAGCATGATTCCGGGGATCCGTCGACC	-	Redirect deletion of *bldB2* (*vnz15145*).
BldB2_Red_R	TGCTGGTCGTGCGCGAGACGGCTCGGGCGACGGGGCTCATGTAGGCTGGAGCTGCTTC	-	
BldB2_Red_Ext_F	GTACGGTACACCGCGTAATC	-	External primers for confirmation of the Redirect deletion of *bldB2* (*vnz15145*).
BldB2_Red_Ext_R	TGGACCAGCTGCGCTGAG	-	
BldB3_Red_F	CGTGAGCCTGCTGCGGGAGATCCGAGGAGCACTATGAGCATTCCGGGGATCCGTCGACC	-	Redirect deletion of *bldB3* (*vnz29075*).
BldB3_Red_R	TGGAGGGCAGGTACACGCATCCTGCCAGACGCGTTCTCATGTAGGCTGGAGCTGCTTC	-	
BldB3_Red_Ext_F	TACTGCGAGGGCCAGGAGAC	-	External primers for confirmation of the Redirect deletion of *bldB3* (*vnz29075*).
BldB3_Red_Ext_R	CCGGCCGATGCCGGAACT	-	
BldB4_Red_F	CATGGGCCTGCTGGAACGCCTGGCAGGAGTGACATGAGCATTCCGGGGATCCGTCGACC	-	Redirect deletion of *bldB4* (*vnz25555*).
BldB4_Red_R	ACACACGGCCGGGGCACAGGGTTGCCCCGGCCGGCGTCATGTAGGCTGGAGCTGCTTC	-	
BldB4_Red_Ext_F	ACGAGCACGTCGCCTACATC	-	External primers for confirmation of the Redirect deletion of *bldB4* (*vnz25555*).
BldB4_Red_Ext_R	TGGCCGGGGTGGTGAGCT	-	

Name	Sequence (5' - 3')	Digestion Sites	Purpose
BldB5_Red_F	GGGACCGGATCGAGCATGACCAGCGTGGAGTGGC GTAAGATTCCGGGGATCCGTCGACC	-	Redirect deletion of *bldB5* (*vnz20565*).
BldB5_Red_R	CGTCAGCGGGGACTGACGCCCCTCATTCGGGCCG GATCATGTAGGCTGGAGCTGCTTC	-	
BldB5_Red_Ext_F	ACGGCCGATCTGGACACGCT	-	External primers for confirmation of the Redirect deletion of *bldB5* (*vnz20565*).
BldB5_Red_Ext_R	ACCGCTGCCGGTGGTGCT	-	
BldB6_Red_F	GAGACCAACCAGAACCTGGCGGGAGCGCGCTGG CGTAAGATTCCGGGGATCCGTCGACC	-	Redirect deletion of *bldB6* (*vnz09895*).
BldB6_Red_R	TGGCGAGGATCATCGTCCCTATGAGCGTCGCCAT GATCATGTAGGCTGGAGCTGCTTC	-	
BldB6_Red_Ext_F	TTCAGGGAGGGGTCGCTCC	-	External primers for confirmation of the Redirect deletion of *bldB6* (*vnz09895*).
BldB6_Red_Ext_R	GCGGCTGGGGCAGTTCGT	-	
BldB7_Red_F	GTTGACACCTGCACCAAGCAACTCGGGGAGCTAC CAGTGATTCCGGGGATCCGTCGACC	-	Redirect deletion of *bldB7* (*vnz16140*).
BldB7_Red_R	TGTACGTCTCCGGAGGCACGCGCACGTACGCGGG TCTCATGTAGGCTGGAGCTGCTTC	-	
BldB7_Red_Ext_F	AGATCAGAACCCGTAGGGTGAG	-	External primers for confirmation of the Redirect deletion of *bldB7* (*vnz16140*).
BldB7_Red_Ext_R	TTCCGGATCGGCCCGGAGT	-	
BldB8_Red_F	ATGCGCGTGATCGATTCCTGCAGCTCGCAAGTAAG TAGAATTCCGGGGATCCGTCGACC	-	Redirect deletion of *bldB8* (*vnz28285*).
BldB8_Red_R	CAGGGAGGCGCCGGGCCGACACAGGTGGGGCAG GGGTCATGTAGGCTGGAGCTGCTTC	-	
BldB8_Red_Ext_F	TCTGGAGCACCAGACCGGC	-	External primers for confirmation of the Redirect deletion of *bldB8* (*vnz28285*).
BldB8_Red_Ext_R	GGGCTTGTCCGCATGAACAGAT	-	
BldB9_Red_F	GGGTCTCATCGAGGAGTTGGCGGGAGAACAAAGA TGAGCATTCCGGGGATCCGTCGACC	-	Redirect deletion of *bldB9* (*vnz16680*).
BldB9_Red_R	GCGTCCCCGCCGGGTCGAACCTGTCCTGCTAGTC GGCTATGTAGGCTGGAGCTGCTTC	-	
BldB9_Red_Ext_F	CGTCACCTACCTCGAGATCCA	-	External primers for confirmation of the Redirect deletion of *bldB9* (*vnz16680*).
BldB9_Red_Ext_R	GGCTTCGGCCAGACCATCT	-	

Name	Sequence (5' - 3')	Digestion Sites	Purpose
BldB10_Red_F	AAGGAGATTCTCCGGAATCTCCGCAAGGAGCTGT GAATGATTCCGGGGATCCGTCGACC	-	Redirect deletion of *bldB10* (*vnz31505*).
BldB10_Red_R	AAGAGTTACGCGACGGTAGGGGTGGGGCGGAAG GGGTCATGTAGGCTGGAGCTGCTTC	-	
BldB10_Red_Ext_F	CCGGACATGGTCTACAGCGA	-	External primers for confirmation of the Redirect deletion of *bldB10* (*vnz31505*).
BldB10_Red_Ext_R	CAGGAACCAGTCGTACATCCG	-	
BldB11_Red_F	AGCAACACGCAGGGCGGCGACTGCGTAGAGATCG CTGACATTCCGGGGATCCGTCGACC	-	Redirect deletion of *bldB11* (*vnz28375*).
BldB11_Red_R	CGACCGAGACGCGCAGGGGCGCGCCCCGGTGAG CGATCATGTAGGCTGGAGCTGCTTC	-	
BldB11_Red_Ext_F	GCAGAGTACGTACTGGCACT	-	External primers for confirmation of the Redirect deletion of *bldB11* (*vnz28375*).
BldB11_Red_Ext_R	TCAGGATTGCAGTCCTGTCG	-	
AbaA3_Red_F	CTGGTAACTGCCCTCGGGCGGCGCCACATTGGCC CCATGATTCCGGGGATCCGTCGACC	-	Redirect deletion of *abaA3* (*vnz29085*).
AbaA3_Red_R	TGGATCACCGGGACGCCCTTCTGACCCACCGCCG GTTCATGTAGGCTGGAGCTGCTTC	-	
AbaA3_Red_Ext_F	TTCGGAACCTCGTCCGTCAC	-	External primers for confirmation of the Redirect deletion of *abaA3* (*vnz29085*).
AbaA3_Red_Ext_R	CGTGCAACTCCGGCCTGA	-	
AbaA4_Red_F	GGGGCGGGTGGGCCGCCGCAGGCCACCGTGAGC GTCATGATTCCGGGGATCCGTCGACC	-	Redirect deletion of *abaA4* (*vnz25565*).
AbaA4_Red_R	AGCGGACGCAAGACCGCATGACCCGCGGGAACAC GGCTATGTAGGCTGGAGCTGCTTC	-	
AbaA4_Red_Ext_F	GTACGTACTCGACGCGTTCC	-	External primers for confirmation of the Redirect deletion of *abaA4* (*vnz25565*).
AbaA4_Red_Ext_R	CCTGAATCTCGCATGACCCTC	-	
AbaA6_Red_F	TAGCCGAGCGTAACGAACCGAGCCCACTCTGGTG GCATGATTCCGGGGATCCGTCGACC	-	Redirect deletion of *abaA6* (*vnz09905*).
AbaA6_Red_R	ACTGGCGGGTACGCGGGTGACGGCGCCCATCGT GCCCTATGTAGGCTGGAGCTGCTTC	-	
AbaA6_Red_Ext_F	GCGGAGTTCGTACCCGTAGT	-	External primers for confirmation of the Redirect deletion of *abaA6* (*vnz09905*).
AbaA6_Red_Ext_R	CTCACCGACGGGCATGAAC	-	

Name	Sequence (5' - 3')	Digestion Sites	Purpose
AbaA7_Red_F	GTCGCACCACAGTCGCGATTCCCGGGAGTGCCTC GCATGATTCCGGGGATCCGTCGACC	-	Redirect deletion of *abaA7* (*vnz16135*).
AbaA7_Red_R	TTCCATGTTCCGTACGCGCCGCCCGGGGCGACGC GGCTATGTAGGCTGGAGCTGCTTC	-	
AbaA7_Red_Ext_F	GCATCCAGTGGTCGCATTCG	-	External primers for confirmation of the Redirect deletion of *abaA7* (*vnz16135*).
AbaA7_Red_Ext_R	GTGCCTCCGGAGACGTACA	-	
AbaA10_Red_F	AACGCGCAGCCTTCAGGTCTCATGAGTCCCCGAG TCATGATTCCGGGGATCCGTCGACC	-	Redirect deletion of *abaA10* (*vnz31495*).
AbaA10_Red_R	GCGGGATCATGCGGGTGGCCATCGACCTCAGCAC GGTTCTGTAGGCTGGAGCTGCTTC	-	
AbaA10_Red_Ext_F	GACAGTGTTCCGGTGAACCAG	-	External primers for confirmation of the Redirect deletion of *abaA10* (*vnz31495*).
AbaA10_Red_Ext_R	GGATCTTGAAGCCGAAGCGG	-	
IosA_Red_F	TGGAAAACGCTAGCGCCGGCGCGGGAACATGTCC TCGTGATTCCGGGGATCCGTCGACC	-	Redirect deletion of *iosA* (*vnz16670*).
IosA_Red_R	ATGTATGTAGCTGGCCTTGCGACCCTCGCGGGGT GGTCATGTAGGCTGGAGCTGCTTC	-	
IosA_Red_Ext_F	GCCATTCACGTTCCCCATTCG	-	External primers for confirmation of the Redirect deletion of *iosA* (*vnz16670*).
IosA_Red_Ext_R	TGATGATCGCCAGGTCCTCG	-	
WhiJ6_Red_F	AACGCCTCACCGCGTGAACTTGGGGGTGACCTCG CCGTGATTCCGGGGATCCGTCGACC	-	Redirect deletion of *whiJ6* (*vnz09900*).
WhiJ6_Red_R	CACCTCCGACCCTCCGACTTCCTGACGCAAGGCC GCCTCTGTAGGCTGGAGCTGCTTC	-	
WhiJ6_Red_Ext_F	AGTGCTCACCGACGGTGAAC	-	External primers for confirmation of the Redirect deletion of *whiJ6* (*vnz09900*).
WhiJ6_Red_Ext_R	CTGGACGAAGTCCTCGGTGT	-	
WhiJ9_Red_F	CGGTTGAGATCGGTTGAGTCCGAATGGGGAACGT GAATGATTCCGGGGATCCGTCGACC	-	Redirect deletion of *whiJ9* (*vnz16675*).
WhiJ9_Red_R	GATCGGCCTCCTCAGCACCGACTCGTCGAGGATC AGCTCTGTAGGCTGGAGCTGCTTC	-	
WhiJ9_Red_Ext_F	TCACGAGGACATGTTCCCGC	-	External primers for confirmation of the Redirect deletion of *whiJ9* (*vnz16675*).
WhiJ9_Red_Ext_R	GCAGCACCTGAAGGTTCACG	-	

Name	Sequence (5' - 3')	Digestion Sites	Purpose
AsfA1_Red_F	CGAAGCGACACATGGAGCCACCCTGTGGAGCGTC CGATGATTCCGGGGATCCGTCGACC	-	Redirect deletion of *asfA1* (*vnz03680*).
AsfA1_Red_R	ACGCCCCCGCCGCCACGGAATTCGGCCCGCCGG CCGTCATGTAGGCTGGAGCTGCTTC	-	
AsfA1_Red_Ext_F	GTTCACCGATTCAGGTGACAG	-	External primers for confirmation of the Redirect deletion of *asfA1* (*vnz03680*).
AsfA1_Red_Ext_R	ACGAGGTGGTCACGGCGT	-	
AsfA2_Red_F	CCCCCTCGCGCGAGGGGCGCCGGAGGGAGTACA CGCATGATTCCGGGGATCCGTCGACC	-	Redirect deletion of *asfA2* (*vnz10850*).
AsfA2_Red_R	GGCTGCGCAGTAGCCGCATGATCGGCCGGACAAG TCCTATGTAGGCTGGAGCTGCTTC	-	
AsfA2_Red_Ext_F	GCGTTCGGATTGTCCGCAATA	-	External primers for confirmation of the Redirect deletion of *asfA2* (*vnz10850*).
AsfA2_Red_Ext_R	GATCACCTGCCGGTGGTTC	-	
OsaC_Red_F	AACGACCACCGGGCAGCGGGGAGGGACAGACCG AGCATGATTCCGGGGATCCGTCGACC	-	Redirect deletion of *osaC* (*vnz26705*).
OsaC_Red_R	AGCCGGCGATCCCCGCACGGGGGATCGCCGGCA TCGTCATGTAGGCTGGAGCTGCTTC	-	
OsaC_Red_Ext_F	CGCGTGGACGGTGAAGGTA	-	External primers for confirmation of the Redirect deletion of *osaC* (*vnz26705*).
OsaC_Red_Ext_R	CGGTAGAGCGTCTCCATGGT	-	
OsaC2_Red_F	TGGCGACCTGCTGTCCGATATTCATAAAGTGGGGC AATGATTCCGGGGATCCGTCGACC	-	Redirect deletion of *osaC2* (*vnz17535*).
OsaC2_Red_R	CCCGGGGGAGGGACGCGCGCGATGACCCCGGCC CCGCTATGTAGGCTGGAGCTGCTTC	-	
OsaC2_Red_Ext_F	CGTTCATCCAGTCTTCGGGAT	-	External primers for confirmation of the Redirect deletion of *osaC2* (*vnz17535*).
OsaC2_Red_Ext_R	GACCTTGTGGGTGTCCATGG	-	
SigB_Red_F	ATGACCGGTTCGGGACACACGTGAAAGGAGAACG GCGTGATTCCGGGGATCCGTCGACC	-	Redirect deletion of *sigB* (*vnz01715*).
SigB_Red_R	AGGAGCCTTCGCGGACGGGCGAGAGGGGACGAC GGATCATGTAGGCTGGAGCTGCTTC	-	
SigB_Red_Ext_F	GATCGACGGCGAATTCGTCG	-	External primers for confirmation of the Redirect deletion of *sigB* (*vnz01715*).
SigB_Red_Ext_R	CAGTTGCTCGTACCGGCGT	-	

Name	Sequence (5' - 3')	Digestion Sites	Purpose
AbaA6_CRISPR_Frag1_F	tgccgccgggcgttttttatCGACGCCGGTCTCGCGTCCCTGTAC	-	Amplification and cloning of repair flanking regions for *abaA6* in pCRISPomyces-2 via Gibson assembly.
AbaA6_CRISPR_Frag1_R	ATCGTGCCCTACGCGTCGCATGCCTGATTCATGCCACCAG	-	
AbaA6_CRISPR_Frag2_F	GTGGCATGAATCAGGCATGCGACGCGTAGGGCACGATGGG	-	
AbaA6_CRISPR_Frag2_R	ctttttacggttcctggcctTCGCGGCCGACGGCGCCCG	-	
AbaA6_sgRNA_F	ACGCTCGCAAGTACCGCAGGATAG	BbsI	Cloning of a protospacer for *abaA6* in pCRISPomyces-2 via Golden Gate cloning.
AbaA6_sgRNA_R	AAACCTATCCTGCGGTACTTGCGA	BbsI	
IosA_CRISPR_Frag1_F	ttgccgccgggcgttttttatGACCGCCTCGCACAACGGC	-	Amplification and cloning of repair flanking regions for *iosA* in pCRISPomyces-2 via Gibson assembly.
IosA_CRISPR_Frag1_R	CGGGGTGGTCAGGACCCGCCCTCTTCATTCACGAGGACAT	-	
IosA_CRISPR_Frag2_F	GTCCTCGTGAATGAAGAGGGCGGGTCCTGACCACCCCGCG	-	
IosA_CRISPR_Frag2_R	ccttttttacggttcctggcctCGGGCCATGGCCATCTTGT	-	
IosA_sgRNA_F1	ACGCGGTGAGCGCCTCCATCAAGG	BbsI	Cloning of a protospacer for *iosA* in pCRISPomyces-2 via Golden Gate cloning.
IosA_sgRNA_R1	AAACCCTTGATGGAGGCGCTCACC	BbsI	
IosA_sgRNA_F2	ACGCGGGGGGAAGCGCCAGGACAG	BbsI	Cloning of a protospacer for *iosA* in pCRISPomyces-2 via Golden Gate cloning.
IosA_sgRNA_R2	AAACCTGTCCTGGCGCTTCCCCCC	BbsI	
WhiJ9_CRISPR_Frag1_F	tgccgccgggcgttttttatCGCATCGAACCGGGCCACGC	-	Amplification and cloning of repair flanking regions for *whiJ9* in pCRISPomyces-2 via Gibson assembly.
WhiJ9_CRISPR_Frag1_R	GACTCGTCGAGGATCAGCTCCATTCACGTTCCCCATTCGGAC	-	
WhiJ9_CRISPR_Frag2_F	CCGAATGGGGAACGTGAATGGAGCTGATCCTCGACGAGTCGG	-	
WhiJ9_CRISPR_Frag2_R	gcggccttttttacggttcctggcctCGCAAGCTGGTCACCTCACTG	-	
WhiJ9_sgRNA_F1	ACGCCGCCCAGGACGCGTTCGAGC	BbsI	Cloning of a protospacer for *whiJ9* in pCRISPomyces-2 via Golden Gate cloning.
WhiJ9_sgRNA_R1	AAACGCTCGAACGCGTCCTGGGCG	BbsI	
WhiJ9_sgRNA_F2	ACGCGCCACCGCCTTCTGTTCGAT	BbsI	Cloning of a protospacer for *whiJ9* in pCRISPomyces-2 via Golden Gate cloning.
WhiJ9_sgRNA_R2	AAACATCGAACAGAAGGCGGTGGC	BbsI	
BldB_Comp_F	GCAGAAGCTTGACGTCGGCATCCGCTTCAT	HindIII	Complementation of the Δ*bldB* mutant with *bldB in trans*. PCR product was cloned into pSS170.
BldB_Comp_R	GGCGGTACCGCTCACCGCAGGTCGAACT	KpnI	

Name	Sequence (5' - 3')	Digestion Sites	Purpose
BldB_NFLAG_F	GCGGAAGCTTGACGTCGGCATCCGCTTCAT	HindIII	Fusion of an N-terminal 3xFLAG-tag to BldB. Overlap PCR (F+1)+(2+R) yielded a long PCR product, which was cloned into pSS170.
BldB_NFLAG_1	TCGATGTCGTGGTCCTTGTAGTCGCCGTCGTGGTC CTTGTAGTCCATCGGCGCGTTCCCTTC	-	
BldB_NFLAG_2	CGACTACAAGGACCACGACATCGACTACAAGGAC GATGACGACAAGACCGACGCAGACACCAGCA	-	
BldB_NFLAG_R	GCCGGTACCGCTCACCGCAGGTCGAACT	KpnI	
BldB_CFLAG10500_F	GGAATTCCATATGGACGTCGGCATCCGCTTCAT	NdeI	Fusion of a C-terminal 3xFLAG-tag to BldB. PCR product was cloned into pIJ10500.
BldB_CFLAG10500_R	CCGCTCGAGCCGCAGGTCGAACTCGCC	XhoI	
WhiJ6_NFLAG_F	GCGGAAGCTTGTACGGCTCGCGCAGGATC	HindIII	Fusion of an N-terminal 3xFLAG-tag to WhiJ6. Overlap PCR (F+1)+(2+R) yielded a long PCR product, which was cloned into pSS170.
WhiJ6_NFLAG_1	TCGATGTCGTGGTCCTTGTAGTCGCCGTCGTGGTC CTTGTAGTCCACGGCGAGGTCACCCCC	-	
WhiJ6_NFLAG_2	CGACTACAAGGACCACGACATCGACTACAAGGAC GATGACGACAAGGTCAACATCCGCAGCCTGGAT	-	
WhiJ6_NFLAG_R	GCCGGTACCACTTACGCCAGCGCGCTCC	KpnI	
WhiJ6_CFLAG_F	GGCGAAGCTTGTACGGCTCGCGCAGGATC	HindIII	Fusion of an C-terminal 3xFLAG-tag to WhiJ6. Overlap PCR (F+1)+(2+R) yielded a long PCR product, which was cloned into pSS170.
WhiJ6_CFLAG_1	TCGATGTCGTGGTCCTTGTAGTCGCCGTCGTGGTC CTTGTAGTCCGCCAGCGCGCTCCCGCC	-	
WhiJ6_CFLAG_2	CGACTACAAGGACCACGACATCGACTACAAGGAC GATGACGACAAGTAAGTCCTCGTTCAGCGGCG	-	
WhiJ6_CFLAG_R	GGCGGTACCTCGCCATGATCAGCGACTGC	KpnI	
WhiJ9_NFLAG_F	GCGGAAGCTTCCTCGATCACGACGGGCCC	HindIII	Fusion of an N-terminal 3xFLAG-tag to WhiJ9. Overlap PCR (F+1)+(2+R) yielded a long PCR product, which was cloned into pSS170.
WhiJ9_NFLAG_1	TCGATGTCGTGGTCCTTGTAGTCGCCGTCGTGGTC CTTGTAGTCCATTCACGTTCCCCATTCGGAC	-	
WhiJ9_NFLAG_2	CGACTACAAGGACCACGACATCGACTACAAGGAC GATGACGACAAGGCGCGTGCGGAGAACAAGG	-	
WhiJ9_NFLAG_R	GGAATTCCATATGGCTCATCTTTGTTCTCCCGCCA	NdeI	

Name	Sequence (5' - 3')	Digestion Sites	Purpose
WhiJ9_CFLAG_F	GGCGAAGCTTCCTCGATCACGACGGGCCC	HindIII	Fusion of a C-terminal 3xFLAG-tag to WhiJ9. Overlap PCR (F+1)+(2+R) yielded a long PCR product, which was cloned into pSS170.
WhiJ9_CFLAG_1	TCGATGTCGTGGTCCTTGTAGTCGCCGTCGTGGTC CTTGTAGTCTCTTTGTTCTCCCGCCAACTCC	-	
WhiJ9_CFLAG_2	CGACTACAAGGACCACGACATCGACTACAAGGAC GATGACGACAAGTGAGCGACACCCTGCACTGG	-	
WhiJ9_CFLAG_R	GGAATTCCATATGCCTGCTAGTCGGCTACTGCC	NdeI	
WhiJ9_NFLAG_OE_F	GGGAATTCCATATGGACTACAAGGACCACGACG	NdeI	Overexpression of N-terminally 3xFLAG-tagged *whiJ9* in *S. venezuelae*. PCR product was cloned into pIJ10257.
WhiJ9_NFLAG_OE_R	GTCCAAGCTTTCATCTTTGTTCTCCCGCCAAC	HindIII	
WhiJ9_CFLAG_OE_F	GGGAATTCCATATGGCGCGTGCGGAGAACAA	NdeI	Overexpression of C-terminally 3xFLAG-tagged *whiJ9* in *S. venezuelae*. PCR product was cloned into pIJ10257.
WhiJ9_CFLAG_OE_R	GTCCAAGCTTTCACTTGTCGTCATCGTCCTTG	HindIII	
BldB_OE_F	GGGAATTCCATATGACCGACGCAGACACCAG	NdeI	Overexpression of *bldB (vnz26620)* in *S. venezuelae*. PCR product was cloned into pIJ10257.
BldB_OE_R	TCCAAGCTTTCACCGCAGGTCGAACTCG	HindIII	
BldB6_OE_F	GGGAATTCCATATGGAGACCAACCAGAACCTGG	NdeI	Overexpression of *bldB6 (vnz09895)* in *S. venezuelae*. PCR product was cloned into pSS170 and pIJ10257.
BldB6_OE_R	GTCCAAGCTTTCAGCGACTGCCGATGCGC	HindIII	
BldB9_OE_F	GGGAATTCCATATGAGCGACACCCTGCACTG	NdeI	Overexpression of *bldB9 (vnz16680)* in *S. venezuelae*. PCR product was cloned into pSS170 and pIJ10257.
BldB9_OE_R	GTCCAAGCTTCTACTGCCACGCGACGAAAG	HindIII	
AbaA3_OE_F	GGGAATTCCATATGACCTCCCCCGTGACCC	NdeI	Overexpression of *abaA3 (vnz29085)* in *S. venezuelae*. PCR product was cloned into pIJ10257.
AbaA3_OE_R	GTCCAAGCTTTCAGGGAACCACGAGGTCGAG	HindIII	
AbaA4_OE_F	GGGAATTCCATATGAGCGACGAACTCCCCCTG	NdeI	Overexpression of *abaA4 (vnz25565)* in *S. venezuelae*. PCR product was cloned into pIJ10257.
AbaA4_OE_R	GTCCAAGCTTCTAGGGGCTGTCCGGGAAG	HindIII	
AbaA6_OE_F	GGGAATTCCATATGAATCAGGCAACAGACCTCT	NdeI	Overexpression of *abaA6 (vnz09905)* in *S. venezuelae*. PCR product was cloned into pIJ10257.
AbaA6_OE_R	GTCCAAGCTTCTACGCGTCGCACTCGAA	HindIII	
AbaA7_OE_F	GGGAATTCCATATGGGGACGAATGGATCGACC	NdeI	Overexpression of *abaA7 (vnz16135)* in *S. venezuelae*. PCR product was cloned into pIJ10257.
AbaA7_OE_R	GTCCAAGCTTCTACTCCGGGCCGATCCG	HindIII	

Name	Sequence (5' - 3')	Digestion Sites	Purpose
AbaA10_OE_F	CCGCTCGAGATGGCCCAGCGCCCGCAG	XhoI	Overexpression of *abaA10 (vnz31495)* in *S. venezuelae*. PCR product was cloned into pIJ10257.
AbaA10_OE_R	GTCCAAGCTTTCAGCACGGTTCCCCCATGC	HindIII	
IosA_OE_F	GGGAATTCCATATGGTGAATGAAGAGAATCGGGAAGT	NdeI	Overexpression of *iosA (vnz16670)* in *S. venezuelae*. PCR product was cloned into pIJ10257.
IosA_OE_R	GTCCAAGCTTTCAGGACCCGCCGCTGAA	HindIII	
WhiJ6_OE_F	CCGCTCGAGGTGGTCAACATCCGCAGCCTG	XhoI	Overexpression of *whiJ6 (vnz09900)* in *S. venezuelae*. PCR product was cloned into pIJ10257.
WhiJ6_OE_R	GTCCAAGCTTTTACGCCAGCGCGCTCCCG	HindIII	
WhiJ9_OE_F	GGGAATTCCATATGGCGCGTGCGGAGAACA	NdeI	Overexpression of *whiJ9 (vnz16675)* in *S. venezuelae*. PCR product was cloned into pIJ10257.
WhiJ9_OE_R	GTCCAAGCTTTCATCTTTGTTCTCCCGCCAAC	HindIII	
AsfA1_OE_F	GGGAATTCCATATGCAGCTGATCCCCCGTCA	NdeI	Overexpression of *asfA1 (vnz03680)* in *S. venezuelae*. PCR product was cloned into pIJ10257.
AsfA1_OE_R	GTCCAAGCTTTCAGTCGGGGTTCGCCGC	HindIII	
AsfA2_OE_F	GGGAATTCCATATGCCCTGGGACGATGCTGC	NdeI	Overexpression of *asfA2 (vnz10850)* in *S. venezuelae*. PCR product was cloned into pIJ10257.
AsfA2_OE_R	GTCCAAGCTTCTAGCCGGCGACGGCGTC	HindIII	
OsaC_OE_F	GGGAATTCCATATGGCAGAGCCGGGCGTC	NdeI	Overexpression of *osaC (vnz26705)* in *S. venezuelae*. PCR product was cloned into pIJ10257.
OsaC_OE_R	GTCCAAGCTTTCAGCGGTCGTCCGGCTC	HindIII	
OsaC2_OE_F	GGGAATTCCATATGCGCACCGAGGACGTCC	NdeI	Overexpression of *osaC2 (vnz17535)* in *S. venezuelae*. PCR product was cloned into pIJ10257.
OsaC2_OE_R	GTCCAAGCTTCTACGGCCTGTCGTCCCC	HindIII	
SigB_OE_F	GGGAATTCCATATGGTGACGCTCACCACCATGTC	NdeI	Overexpression of *sigB (vnz01715)* in *S. venezuelae*. PCR product was cloned into pIJ10257.
SigB_OE_R	GTCCAAGCTTTCAGCCGGTCTCCAGGAG	HindIII	

Name	Sequence (5' - 3')	Digestion Sites	Purpose
AbaA6_IosA_2xOE_Frag1_F	gtctagaacaggaggccccatATGAATCAGGCAACAGACCTCTAT	-	Tandem overexpression of *abaA6 (vnz09905) and iosA (vnz16670)* in *S. venezuelae*. PCR product was cloned into pIJ10257 via Gibson assembly. An RBS was placed between the two genes.
AbaA6_IosA_2xOE_Frag1_R	ACggcttacctccgatgttgagCTACGCGTCGCACTCGAACCACA	-	
AbaA6_IosA_2xOE_Frag2_F	TAGctcaacatcggaggtaagccGTGAATGAAGAGAATCGGGAAGT	-	
AbaA6_IosA_2xOE_Frag2_R	tgagaaccctaggggatccaTCAGGACCCGCCGCTGAACAGC	-	
IosA_qRTPCR_F	GACCTGGCCGCTGTCCTG	-	For amplification of a fragment of the *iosA* (*vnz16670*) gene in qRT-PCR.
IosA_qRTPCR_R	GGACCCGCCGCTGAACAG	-	
HrdB_qRTPCR_F	TGTTCTGCGCAGCCTCAATCAG	-	For amplification of a fragment of the *hrdB* gene in qRT-PCR.
HrdB_qRTPCR_R	CTCTTCGCTGCGACGCTCTT	-	
BldB_ReDCaT_F1	CGGTGCTGGTGGAGAACCTGCCGTTCGCGCGGGACGTCGG	-	Testing if BldB binds overlapping dsDNA oligos from its promoter region via ReDCaT.
BldB_ReDCaT_R1	CCGACGTCCCGCGCGAACGGCAGGTTCTCCACCAGCACCGcctaccctacgtcctcctgc	-	
BldB_ReDCaT_F2	CGCGCGGGACGTCGGCATCCGCTTCATCGTGGCGCGCAAC	-	Testing if BldB binds overlapping dsDNA oligos from its promoter region via ReDCaT.
BldB_ReDCaT_R2	GTTGCGCGCCACGATGAAGCGGATGCCGACGTCCCGCGCGcctaccctacgtcctcctgc	-	
BldB_ReDCaT_F3	ATCGTGGCGCGCAACGCCGCGGGCGCCTCCCGGGCGATGT	-	Testing if BldB binds overlapping dsDNA oligos from its promoter region via ReDCaT.
BldB_ReDCaT_R3	ACATCGCCCGGGAGGCGCCCGCGGCGTTGCGCGCCACGATcctaccctacgtcctcctgc	-	
BldB_ReDCaT_F4	CCTCCCGGGCGATGTACGAGCCGTTCATGCAGCGGATGAG	-	Testing if BldB binds overlapping dsDNA oligos from its promoter region via ReDCaT.
BldB_ReDCaT_R4	CTCATCCGCTGCATGAACGGCTCGTACATCGCCCGGGAGGcctaccctacgtcctcctgc	-	
BldB_ReDCaT_F5	CATGCAGCGGATGAGGGAGCTGGGCGCGCAGGGCGTGCTG	-	Testing if BldB binds overlapping dsDNA oligos from its promoter region via ReDCaT.
BldB_ReDCaT_R5	CAGCACGCCCTGCGCGCCCAGCTCCCTCATCCGCTGCATGcctaccctacgtcctcctgc	-	

Name	Sequence (5' - 3')	Digestion Sites	Purpose
BldB_ReDCaT_F6	GCGCAGGGCGTGCTGCTCTCCGGCGATCCGGGCGAGGGCG	-	Testing if BldB binds overlapping dsDNA oligos from its promoter region via ReDCaT.
BldB_ReDCaT_R6	CGCCCTCGCCCGGATCGCCGGAGAGCAGCACGCCCTGCGCcctaccctacgtcctcctgc	-	
BldB_ReDCaT_F7	ATCCGGGCGAGGGCGACATCCTCGGCAACGTCCGGGCGCG	-	Testing if BldB binds overlapping dsDNA oligos from its promoter region via ReDCaT.
BldB_ReDCaT_R7	CGCGCCCGGACGTTGCCGAGGATGTCGCCCTCGCCCGGATcctaccctacgtcctcctgc	-	
BldB_ReDCaT_F8	CAACGTCCGGGCGCGGCCGATGCCTCCGGGCCGGGGCACG	-	Testing if BldB binds overlapping dsDNA oligos from its promoter region via ReDCaT.
BldB_ReDCaT_R8	CGTGCCCCGGCCCGGAGGCATCGGCCGCGCCCGGACGTTGcctaccctacgtcctcctgc	-	
BldB_ReDCaT_F9	CCGGGCCGGGGCACGTTCGTGTCGCGGAAGCGGGGCACGC	-	Testing if BldB binds overlapping dsDNA oligos from its promoter region via ReDCaT.
BldB_ReDCaT_R9	GCGTGCCCCGCTTCCGCGACACGAACGTGCCCCGGCCCGGcctaccctacgtcctcctgc	-	
BldB_ReDCaT_F10	GGAAGCGGGGCACGCCGCTGGTGCAGCTGGGCTGGCTGCC	-	Testing if BldB binds overlapping dsDNA oligos from its promoter region via ReDCaT.
BldB_ReDCaT_R10	GGCAGCCAGCCCAGCTGCACCAGCGGCGTGCCCCGCTTCCcctaccctacgtcctcctgc	-	
BldB_ReDCaT_F11	GCTGGGCTGGCTGCCGGAACAGCACTGATCGGGTGCGGCG	-	Testing if BldB binds overlapping dsDNA oligos from its promoter region via ReDCaT.
BldB_ReDCaT_R11	CGCCGCACCCGATCAGTGCTGTTCCGGCAGCCAGCCCAGCcctaccctacgtcctcctgc	-	
BldB_ReDCaT_F12	TGATCGGGTGCGGCGGTCCCACTACTGTGGGAGGGACCGC	-	Testing if BldB binds overlapping dsDNA oligos from its promoter region via ReDCaT.
BldB_ReDCaT_R12	GCGGTCCCTCCCACAGTAGTGGGACCGCCGCACCCGATCAcctaccctacgtcctcctgc	-	
BldB_ReDCaT_F13	TGTGGGAGGGACCGCCGTACCACCGCGAAGGGAACGCGCC	-	Testing if BldB binds overlapping dsDNA oligos from its promoter region via ReDCaT.
BldB_ReDCaT_R13	GGCGCGTTCCCTTCGCGGTGGTACGGCGGTCCCTCCCACAcctaccctacgtcctcctgc	-	

Name	Sequence (5' - 3')	Digestion Sites	Purpose
BldB_ReDCaT_F14	GTGGGAGGGACCGCCGTACCACCGCGAAGGGAACGCGCCG	-	Testing if BldB binds overlapping dsDNA oligos from its promoter region via ReDCaT.
BldB_ReDCaT_R14	CGGCGCGTTCCCTTCGCGGTGGTACGGCGGTCCCTCCCACcctaccctacgtcctcctgc	-	
AbaA6_WhiJ6_ReDCaT_F1	ATGCCACCAGAGTGGGCTCGGTTCGTTACGCTCGG	-	Testing if WhiJ6 binds overlapping dsDNA oligos from the *abaA6-whiJ6* intergenic region via ReDCaT.
AbaA6_WhiJ6_ReDCaT_R1	CCGAGCGTAACGAACCGAGCCCACTCTGGTGGCATcctaccctacgtcctcctgc	-	
AbaA6_WhiJ6_ReDCaT_F2	GTTCGTTACGCTCGGCTACGGCCTGAATACAACGC	-	Testing if WhiJ6 binds overlapping dsDNA oligos from the *abaA6-whiJ6* intergenic region via ReDCaT.
AbaA6_WhiJ6_ReDCaT_R2	GCGTTGTATTCAGGCCGTAGCCGAGCGTAACGAACcctaccctacgtcctcctgc	-	
AbaA6_WhiJ6_ReDCaT_F3	GCCTGAATACAACGCCTCACCGCGTGAACTTGGGG	-	Testing if WhiJ6 binds overlapping dsDNA oligos from the *abaA6-whiJ6* intergenic region via ReDCaT.
AbaA6_WhiJ6_ReDCaT_R3	CCCCAAGTTCACGCGGTGAGGCGTTGTATTCAGGCcctaccctacgtcctcctgc	-	
AbaA6_WhiJ6_ReDCaT_F4	ACGCCTCACCGCGTGAACTTGGGGGTGACCTCGCC	-	Testing if WhiJ6 binds overlapping dsDNA oligos from the *abaA6-whiJ6* intergenic region via ReDCaT.
AbaA6_WhiJ6_ReDCaT_R4	GGCGAGGTCACCCCCAAGTTCACGCGGTGAGGCGTcctaccctacgtcctcctgc	-	
IosA_WhiJ9_ReDCaT_F1	TCACGTTCCCCATTCGGACTCAACCGATCTCAACCGGTCT	-	Testing if WhiJ9 binds overlapping dsDNA oligos from the *iosA-whiJ9* intergenic region via ReDCaT.
IosA_WhiJ9_ReDCaT_R1	AGACCGGTTGAGATCGGTTGAGTCCGAATGGGGAACGTGAcctaccctacgtcctcctgc	-	
IosA_WhiJ9_ReDCaT_F2	GATCTCAACCGGTCTCAACTGCTCCCCGCCGAATTCGACT	-	Testing if WhiJ9 binds overlapping dsDNA oligos from the *iosA-whiJ9* intergenic region via ReDCaT.
IosA_WhiJ9_ReDCaT_R2	AGTCGAATTCGGCGGGGAGCAGTTGAGACCGGTTGAGATCcctaccctacgtcctcctgc	-	
IosA_WhiJ9_ReDCaT_F3	CCGCCGAATTCGACTGCACACGAGGGGCGTTGGTGCAGGT	-	Testing if WhiJ9 binds overlapping dsDNA oligos from the *iosA-whiJ9* intergenic region via ReDCaT.
IosA_WhiJ9_ReDCaT_R3	ACCTGCACCAACGCCCCTCGTGTGCAGTCGAATTCGGCGGcctaccctacgtcctcctgc	-	

Name	Sequence (5' - 3')	Digestion Sites	Purpose
IosA_WhiJ9_ReDCaT_F4	GGCGTTGGTGCAGGTCGAGGGGTTACCGACGCGCCCGCCA	-	Testing if WhiJ9 binds overlapping dsDNA oligos from the *iosA-whiJ9* intergenic region via ReDCaT.
IosA_WhiJ9_ReDCaT_R4	TGGCGGGCGCGTCGGTAACCCCTCGACCTGCACCAACGCCcctaccctacgtcctcctgc	-	
IosA_WhiJ9_ReDCaT_F5	CCGACGCGCCCGCCACAGTCGTGGAAAACGCTAGCGCCGG	-	Testing if WhiJ9 binds overlapping dsDNA oligos from the *iosA-whiJ9* intergenic region via ReDCaT.
IosA_WhiJ9_ReDCaT_R5	CCGGCGCTAGCGTTTTCCACGACTGTGGCGGGCGCGTCGGcctaccctacgtcctcctgc	-	
IosA_WhiJ9_ReDCaT_F6	GTCGTGGAAAACGCTAGCGCCGGCGCGGGAACATGTCCTC	-	Testing if WhiJ9 binds overlapping dsDNA oligos from the *iosA-whiJ9* intergenic region via ReDCaT.
IosA_WhiJ9_ReDCaT_R6	GAGGACATGTTCCCGCGCCGGCGCTAGCGTTTTCCACGACcctaccctacgtcctcctgc	-	
IosA_WhiJ9_O1O2_LH_F	TTCCCCATTCGGACTCAACCGATCTCAACCGGTCTCAACT	-	Finding a minimal binding site for WhiJ9 in the *iosA-whiJ9* intergenic region via ReDCaT footprinting.
IosA_WhiJ9_O1O2_LH_R	AGTTGAGACCGGTTGAGATCGGTTGAGTCCGAATGGGGAAcctaccctacgtcctcctgc	-	
IosA_WhiJ9_O1O2_LH_minus2_F	CCCCATTCGGACTCAACCGATCTCAACCGGTCTCAACT	-	Finding a minimal binding site for WhiJ9 in the *iosA-whiJ9* intergenic region via ReDCaT footprinting.
IosA_WhiJ9_O1O2_LH_minus2_R	AGTTGAGACCGGTTGAGATCGGTTGAGTCCGAATGGGGcctaccctacgtcctcctgc	-	
IosA_WhiJ9_O1O2_LH_minus4_F	CCATTCGGACTCAACCGATCTCAACCGGTCTCAACT	-	Finding a minimal binding site for WhiJ9 in the *iosA-whiJ9* intergenic region via ReDCaT footprinting.
IosA_WhiJ9_O1O2_LH_minus4_R	AGTTGAGACCGGTTGAGATCGGTTGAGTCCGAATGGcctaccctacgtcctcctgc	-	
IosA_WhiJ9_O1O2_LH_minus6_F	ATTCGGACTCAACCGATCTCAACCGGTCTCAACT	-	Finding a minimal binding site for WhiJ9 in the *iosA-whiJ9* intergenic region via ReDCaT footprinting.
IosA_WhiJ9_O1O2_LH_minus6_R	AGTTGAGACCGGTTGAGATCGGTTGAGTCCGAATctaccctacgtcctcctgc	-	
IosA_WhiJ9_O1O2_LH_minus8_F	TCGGACTCAACCGATCTCAACCGGTCTCAACT	-	Finding a minimal binding site for WhiJ9 in the *iosA-whiJ9* intergenic region via ReDCaT footprinting.
IosA_WhiJ9_O1O2_LH_minus8_R	AGTTGAGACCGGTTGAGATCGGTTGAGTCCGAcctaccctacgtcctcctgc	-	
IosA_WhiJ9_O1O2_LH_minus10_F	GGACTCAACCGATCTCAACCGGTCTCAACT	-	Finding a minimal binding site for WhiJ9 in the *iosA-whiJ9* intergenic region via ReDCaT footprinting.
IosA_WhiJ9_O1O2_LH_minus10_R	AGTTGAGACCGGTTGAGATCGGTTGAGTCCctaccctacgtcctcctgc	-	

Name	Sequence (5' - 3')	Digestion Sites	Purpose
IosA_WhiJ9_O1O2_LH_minus12_F	ACTCAACCGATCTCAACCGGTCTCAACT	-	Finding a minimal binding site for WhiJ9 in the *iosA-whiJ9* intergenic region via ReDCaT footprinting.
IosA_WhiJ9_O1O2_LH_minus12_R	AGTTGAGACCGGTTGAGATCGGTTGAGTcctaccctacgtcctcctgc	-	
IosA_WhiJ9_O1O2_LH_minus14_F	TCAACCGATCTCAACCGGTCTCAACT	-	Finding a minimal binding site for WhiJ9 in the *iosA-whiJ9* intergenic region via ReDCaT footprinting.
IosA_WhiJ9_O1O2_LH_minus14_R	AGTTGAGACCGGTTGAGATCGGTTGAcctaccctacgtcctcctgc	-	
IosA_WhiJ9_O1O2_LH_minus16_F	AACCGATCTCAACCGGTCTCAACT	-	Finding a minimal binding site for WhiJ9 in the *iosA-whiJ9* intergenic region via ReDCaT footprinting.
IosA_WhiJ9_O1O2_LH_minus16_R	AGTTGAGACCGGTTGAGATCGGTTcctaccctacgtcctcctgc	-	
IosA_WhiJ9_O1O2_LH_minus18_F	CCGATCTCAACCGGTCTCAACT	-	Finding a minimal binding site for WhiJ9 in the *iosA-whiJ9* intergenic region via ReDCaT footprinting.
IosA_WhiJ9_O1O2_LH_minus18_R	AGTTGAGACCGGTTGAGATCGGcctaccctacgtcctcctgc	-	
IosA_WhiJ9_O1O2_LH_minus20_F	GATCTCAACCGGTCTCAACT	-	Finding a minimal binding site for WhiJ9 in the *iosA-whiJ9* intergenic region via ReDCaT footprinting.
IosA_WhiJ9_O1O2_LH_minus20_R	AGTTGAGACCGGTTGAGATCcctaccctacgtcctcctgc	-	
IosA_WhiJ9_O1O2_LH_minus22_F	TCTCAACCGGTCTCAACT	-	Finding a minimal binding site for WhiJ9 in the *iosA-whiJ9* intergenic region via ReDCaT footprinting.
IosA_WhiJ9_O1O2_LH_minus22_R	AGTTGAGACCGGTTGAGAcctaccctacgtcctcctgc	-	
IosA_WhiJ9_O1O2_LH_minus24_F	TCAACCGGTCTCAACT	-	Finding a minimal binding site for WhiJ9 in the *iosA-whiJ9* intergenic region via ReDCaT footprinting.
IosA_WhiJ9_O1O2_LH_minus24_R	AGTTGAGACCGGTTGAcctaccctacgtcctcctgc	-	
IosA_WhiJ9_O1O2_LH_minus26_F	AACCGGTCTCAACT	-	Finding a minimal binding site for WhiJ9 in the *iosA-whiJ9* intergenic region via ReDCaT footprinting.
IosA_WhiJ9_O1O2_LH_minus26_R	AGTTGAGACCGGTTcctaccctacgtcctcctgc	-	
IosA_WhiJ9_O1O2_RH_F	AGTTGAGACCGGTTGAGATCGGTTGAGTCCGAATGGGGAA	-	Finding a minimal binding site for WhiJ9 in the *iosA-whiJ9* intergenic region via ReDCaT footprinting.
IosA_WhiJ9_O1O2_RH_R	TTCCCCATTCGGACTCAACCGATCTCAACCGGTCTCAACTcctaccctacgtcctcctgc	-	
IosA_WhiJ9_O1O2_RH_minus2_F	TTGAGACCGGTTGAGATCGGTTGAGTCCGAATGGGGAA	-	Finding a minimal binding site for WhiJ9 in the *iosA-whiJ9* intergenic region via ReDCaT footprinting.
IosA_WhiJ9_O1O2_RH_minus2_R	TTCCCCATTCGGACTCAACCGATCTCAACCGGTCTCAAcctaccctacgtcctcctgc	-	

Name	Sequence (5' - 3')	Digestion Sites	Purpose
IosA_WhiJ9_O1O2_RH_minus4_F	GAGACCGGTTGAGATCGGTTGAGTCCGAATGGGGAA	-	Finding a minimal binding site for WhiJ9 in the *iosA-whiJ9* intergenic region via ReDCaT footprinting.
IosA_WhiJ9_O1O2_RH_minus4_R	TTCCCCATTCGGACTCAACCGATCTCAACCGGTCTCcctaccctacgtcctcctgc	-	
IosA_WhiJ9_O1O2_RH_minus6_F	GACCGGTTGAGATCGGTTGAGTCCGAATGGGGAA	-	Finding a minimal binding site for WhiJ9 in the *iosA-whiJ9* intergenic region via ReDCaT footprinting.
IosA_WhiJ9_O1O2_RH_minus6_R	TTCCCCATTCGGACTCAACCGATCTCAACCGGTCcctaccctacgtcctcctgc	-	
IosA_WhiJ9_O1O2_RH_minus8_F	CCGGTTGAGATCGGTTGAGTCCGAATGGGGAA	-	Finding a minimal binding site for WhiJ9 in the *iosA-whiJ9* intergenic region via ReDCaT footprinting.
IosA_WhiJ9_O1O2_RH_minus8_R	TTCCCCATTCGGACTCAACCGATCTCAACCGGcctaccctacgtcctcctgc	-	
IosA_WhiJ9_O1O2_RH_minus10_F	GGTTGAGATCGGTTGAGTCCGAATGGGGAA	-	Finding a minimal binding site for WhiJ9 in the *iosA-whiJ9* intergenic region via ReDCaT footprinting.
IosA_WhiJ9_O1O2_RH_minus10_R	TTCCCCATTCGGACTCAACCGATCTCAACCcctaccctacgtcctcctgc	-	
IosA_WhiJ9_O1O2_RH_minus12_F	TTGAGATCGGTTGAGTCCGAATGGGGAA	-	Finding a minimal binding site for WhiJ9 in the *iosA-whiJ9* intergenic region via ReDCaT footprinting.
IosA_WhiJ9_O1O2_RH_minus12_R	TTCCCCATTCGGACTCAACCGATCTCAAcctaccctacgtcctcctgc	-	
IosA_WhiJ9_O1O2_RH_minus14_F	GAGATCGGTTGAGTCCGAATGGGGAA	-	Finding a minimal binding site for WhiJ9 in the *iosA-whiJ9* intergenic region via ReDCaT footprinting.
IosA_WhiJ9_O1O2_RH_minus14_R	TTCCCCATTCGGACTCAACCGATCTCcctaccctacgtcctcctgc	-	
IosA_WhiJ9_O1O2_RH_minus16_F	GATCGGTTGAGTCCGAATGGGGAA	-	Finding a minimal binding site for WhiJ9 in the *iosA-whiJ9* intergenic region via ReDCaT footprinting.
IosA_WhiJ9_O1O2_RH_minus16_R	TTCCCCATTCGGACTCAACCGATCcctaccctacgtcctcctgc	-	
IosA_WhiJ9_O1O2_RH_minus18_F	TCGGTTGAGTCCGAATGGGGAA	-	Finding a minimal binding site for WhiJ9 in the *iosA-whiJ9* intergenic region via ReDCaT footprinting.
IosA_WhiJ9_O1O2_RH_minus18_R	TTCCCCATTCGGACTCAACCGAcctaccctacgtcctcctgc	-	
IosA_WhiJ9_O1O2_RH_minus20_F	GGTTGAGTCCGAATGGGGAA	-	Finding a minimal binding site for WhiJ9 in the *iosA-whiJ9* intergenic region via ReDCaT footprinting.
IosA_WhiJ9_O1O2_RH_minus20_R	TTCCCCATTCGGACTCAACCcctaccctacgtcctcctgc	-	
IosA_WhiJ9_O1O2_RH_minus22_F	TTGAGTCCGAATGGGGAA	-	Finding a minimal binding site for WhiJ9 in the *iosA-whiJ9* intergenic region via ReDCaT footprinting.
IosA_WhiJ9_O1O2_RH_minus22_R	TTCCCCATTCGGACTCAAcctaccctacgtcctcctgc	-	

Name	Sequence (5' - 3')	Digestion Sites	Purpose
IosA_WhiJ9_O1O2_RH_minus24_F	GAGTCCGAATGGGGAA	-	Finding a minimal binding site for WhiJ9 in the *iosA-whiJ9* intergenic region via ReDCaT footprinting.
IosA_WhiJ9_O1O2_RH_minus24_R	TTCCCCATTCGGACTCcctaccctacgtcctcctgc	-	
IosA_WhiJ9_O1O2_RH_minus26_F	GTCCGAATGGGGAA	-	Finding a minimal binding site for WhiJ9 in the *iosA-whiJ9* intergenic region via ReDCaT footprinting.
IosA_WhiJ9_O1O2_RH_minus26_R	TTCCCCATTCGGACcctaccctacgtcctcctgc	-	
IosA_WhiJ9_DR123_F	TACGGACTCAACCGATCTCAACCGGTCTCAACAT	-	Characterisation of WhiJ9 binding to direct repeats in the *iosA-whiJ9* intergenic region via ReDCaT.
IosA_WhiJ9_DR123_R	ATGTTGAGACCGGTTGAGATCGGTTGAGTCCGTAc ctaccctacgtcctcctgc	-	
IosA_WhiJ9_DR12_F	TACGGACTCAACCGATCTCAACCATGCAGCGGAT	-	Characterisation of WhiJ9 binding to direct repeats in the *iosA-whiJ9* intergenic region via ReDCaT.
IosA_WhiJ9_DR12_R	ATCCGCTGCATGGTTGAGATCGGTTGAGTCCGTAc ctaccctacgtcctcctgc	-	
IosA_WhiJ9_DR23_F	TACATGCAGCGGCGATCTCAACCGGTCTCAACAT	-	Characterisation of WhiJ9 binding to direct repeats in the *iosA-whiJ9* intergenic region via ReDCaT.
IosA_WhiJ9_DR23_R	ATGTTGAGACCGGTTGAGATCGCCGCTGCATGTAc ctaccctacgtcctcctgc	-	
IosA_WhiJ9_DR13_F	TACGGACTCAACCATGCAGCGGCGGTCTCAACAT	-	Characterisation of WhiJ9 binding to direct repeats in the *iosA-whiJ9* intergenic region via ReDCaT.
IosA_WhiJ9_DR13_R	ATGTTGAGACCGCCGCTGCATGGTTGAGTCCGTAc ctaccctacgtcctcctgc	-	
IosA_WhiJ9_DR1only_F	TACGGACTCAACCATGCAGCGGATGAGGGAGCAT	-	Characterisation of WhiJ9 binding to direct repeats in the *iosA-whiJ9* intergenic region via ReDCaT.
IosA_WhiJ9_DR1only_R	ATGCTCCCTCATCCGCTGCATGGTTGAGTCCGTAc ctaccctacgtcctcctgc	-	
IosA_WhiJ9_DR2only_F	TACATGCAGCGGCGATCTCAACATGAGGGAGCAT	-	Characterisation of WhiJ9 binding to direct repeats in the *iosA-whiJ9* intergenic region via ReDCaT.
IosA_WhiJ9_DR2only_R	ATGCTCCCTCATGTTGAGATCGCCGCTGCATGTAcc taccctacgtcctcctgc	-	
IosA_WhiJ9_DR3only_F	TACATGCAGCGGATGAGGGAGCCGGTCTCAACAT	-	Characterisation of WhiJ9 binding to direct repeats in the *iosA-whiJ9* intergenic region via ReDCaT.
IosA_WhiJ9_DR3only_R	ATGTTGAGACCGGCTCCCTCATCCGCTGCATGTAc ctaccctacgtcctcctgc	-	
WhiJ9_22bp_blunt_F	CCGATCTCAACCGGTCTCAACT	-	Use in crystallisation screens in an attempt to obtain crystals of 6xHis-WhiJ9 bound to DNA.
WhiJ9_22bp_blunt_R	AGTTGAGACCGGTTGAGATCGG	-	
WhiJ9_22bp_5'A_F	ACCGATCTCAACCGGTCTCAACT	-	Use in crystallisation screens in an attempt to obtain crystals of 6xHis-WhiJ9 bound to DNA.
WhiJ9_22bp_5'T_R	TAGTTGAGACCGGTTGAGATCGG	-	

Name	Sequence (5' - 3')	Digestion Sites	Purpose
WhiJ9_22bp_5'T_F	TCCGATCTCAACCGGTCTCAACT	-	Use in crystallisation screens in an attempt to obtain crystals of 6xHis-WhiJ9 bound to DNA.
WhiJ9_22bp_5'A_R	AAGTTGAGACCGGTTGAGATCGG	-	
WhiJ9_32bp_5'A_F	ATCGGACTCAACCGATCTCAACCGGTCTCAACT	-	Use in crystallisation screens in an attempt to obtain crystals of 6xHis-WhiJ9 bound to DNA.
WhiJ9_32bp_5'T_R	TAGTTGAGACCGGTTGAGATCGGTTGAGTCCGA	-	
WhiJ9_30bp_5'A_F	AGGACTCAACCGATCTCAACCGGTCTCAACT	-	Use in crystallisation screens in an attempt to obtain crystals of 6xHis-WhiJ9 bound to DNA.
WhiJ9_30bp_5'T_R	TAGTTGAGACCGGTTGAGATCGGTTGAGTCC	-	
WhiJ9_28bp_5'A_F	AACTCAACCGATCTCAACCGGTCTCAACT	-	Use in crystallisation screens in an attempt to obtain crystals of 6xHis-WhiJ9 bound to DNA.
WhiJ9_28bp_5'T_R	TAGTTGAGACCGGTTGAGATCGGTTGAGT	-	
WhiJ9_24bp_5'A_F	AAACCGATCTCAACCGGTCTCAACT	-	Use in crystallisation screens in an attempt to obtain crystals of 6xHis-WhiJ9 bound to DNA.
WhiJ9_24bp_5'T_R	TAGTTGAGACCGGTTGAGATCGGTT	-	
WhiJ9_20bp_5'A_F	AGATCTCAACCGGTCTCAACT	-	Use in crystallisation screens in an attempt to obtain crystals of 6xHis-WhiJ9 bound to DNA.
WhiJ9_20bp_5'T_R	TAGTTGAGACCGGTTGAGATC	-	
WhiJ9_18bp_5'A_F	ATCTCAACCGGTCTCAACT	-	Use in crystallisation screens in an attempt to obtain crystals of 6xHis-WhiJ9 bound to DNA.
WhiJ9_18bp_5'T_R	TAGTTGAGACCGGTTGAGA	-	

DNA Gel Extraction

Agarose gels were loaded and run as described above. DNA bands were visualised using long-wavelength UV light (310 nm) to minimise breaking of the DNA molecules. Desired fragments were excised with a clean razor blade and then extracted using the QIAquick Gel Extraction Kit (QIAGEN, Manchester, UK) according to the manufacturer's instructions. DNA was eluted in 30 µL dH_2O, and stored at -20°C.

DNA Restriction Enzyme Digestion

Restriction enzyme digestion of plasmids and PCR products was carried out according to the enzyme manufacturer's instructions. Digestion reactions were typically carried out for at least 3 hours at 37°C.

DNA Quantification

The concentration of isolated DNA was determined using a Nanodrop spectrophotometer (ThermoFisher Scientific, Waltham, USA) or a Qubit 2.0 fluorometer using the Qubit Broad Range Assay kit (ThermoFisher Scientific, Waltham, USA).

Vector DNA Dephosphorylation

Dephosphorylation of vector DNA was carried out, to remove the 5' phosphate from digested linearised vectors prior to ligation. This served to prevent any re-circularisation of the digested vector and make the ligation of an insert more efficient. Samples were incubated with rAPid Alkaline Phosphatase (Sigma-Aldrich, Gillingham, UK) and a 1X final concentration of the rAPid Alkaline Phosphatase buffer for 1 hour at 37°C and then for 20 minutes at 65°C to deactivate the phosphatase.

Ligation

Ligation of digested vectors and inserts was performed using a T4 DNA Ligase kit (NEB, Ipswich, MA, USA) according to the manufacturer's instructions. An insert:vector ratio of 5:1 (taking DNA length into account) was used with 20 - 50 ng of dephosphorylated vector DNA in the reaction. Ligation reactions (with the appropriate negative controls) were incubated at 16°C overnight, and the products from those reactions were transformed into suitable bacterial hosts.

For most cloning, *E. coli* TOP10 competent cells were used for plasmid transformation. Assembled plasmids were isolated from *E. coli* and sequenced to verify insertion.

Golden Gate Cloning

Golden Gate Cloning was used to insert a protospacer into the pCRISPomyces-2 vector for use in CRISPR/Cas9-mediated gene deletion in *Streptomyces* (Cobb, Wang and Zhao, 2015). Briefly, 100 ng of the vector was mixed with 0.3 µL of the 10x diluted PCR-amplified insert. The mixture was incubated with 2 µL of 10X T4 ligase buffer (NEB, Ipswich, MA, USA), 1 µL of T4 DNA ligase (NEB), 1 µL of BbsI (NEB), and dH_2O topped up to a 20 µL volume. The reaction was run in a thermocycler using the following program: 10 cycles of 10 minutes at 37°C and 10 minutes at 16°C, followed by 5 minutes at 50°C and 20 minutes at 65°C. The mixture was transformed into *E. coli* - after blue-white screening, the assembled plasmids were isolated and verified by sequencing.

Gibson Assembly

Gibson assembly (Gibson *et al.*, 2009) was used to achieve seamless integration of up to 2 DNA fragments into a vector without the need for restriction enzymes. Gibson assembly was performed using a Gibson Assembly Cloning Kit (NEB, Ipswich, MA, USA) according to the manufacturer's instructions. Oligos were designed to anneal to the ends of 2 adjacent DNA fragments, with at least 20 bp overlap with either fragment. Fragments were then amplified via PCR. Vectors were linearised either by restriction digestion or by PCR amplification. The linearised vector and 0.02–0.5 pmols of the PCR-amplified DNA fragments (with a vector: inserts ratio - 1:3) were incubated with Gibson Assembly Master Mix at 50°C for 1 hour. Samples were then transformed into *E. coli*. Assembled plasmids were isolated from *E. coli* and sequenced to verify insertion.

DNA Sequencing

All small-scale DNA sequencing was performed by Eurofins Genomics (Ebersberg, Germany) using their Mix2Seq Sanger sequencing service. Sequencing primers were typically designed to bind ~150-200 bp upstream of the desired sequence. Depending on the template, 50 - 100 ng of DNA was added, along with 2 µL of sequencing primer at a 10 µM concentration. Finally, dH_2O was added to the reactions for a final volume of 17 µL. DNA sequences were analysed and aligned using SnapGene.

ChIP-Seq Using Anti-BldB Polyclonal Antibody

In order to assess whether BldB binds DNA, a ChIP-seq experiment using the generated anti-BldB polyclonal antibody (Cambridge Research Biochemicals, Billingham, UK) was undertaken. Cultures of wild-type *S. venezuelae* and the *ΔbldB* mutant strain were grown in 30 mL volumes of liquid MYM medium at 28˚C, shaking at 250 rpm. For this ChIP-Seq experiment, duplicate wild-type *S. venezuelae* cultures from 3 different time points were prepared - sampled at 10-, 14- and 22-hours post-inoculation. Duplicate *ΔbldB* mutant cultures were sampled at 14 hours and used as a negative control.

All cultures were examined under a light microscope to determine if they were at the expected developmental stage. To crosslink proteins bound to DNA, formaldehyde was added to the cultures at a final concentration of 1% (v/v), and incubation was continued for another 30 minutes. To stop the crosslinking reaction, glycine was then added to the cultures at a final concentration of 125 mM, and all cultures were incubated for 5 min at RT. The bacteria were harvested via centrifugation at 4˚C at 7,000 rpm for 5 min and washed twice with ice-cold PBS (pH - 7.4).

The resulting pellets were resuspended in 0.75 mL lysis buffer [10 mM Tris HCl pH 8.0, 50 mM NaCl, with 10 mg/mL lysozyme and EDTA-free protease inhibitor (Roche, Basel, Switzerland) added], and incubated for 25 min at 37˚C. Following lysis, an equal volume of IP buffer (100 mM Tris HCl pH 8, 250 mM NaCl, 0.5% Triton X-100, 0.1% SDS, with protease inhibitor added) was added to the samples, which were then incubated on ice for 2 min. The samples were sonicated at an 8-micron amplitude (8 cycles: 20 sec on/1 min off) on ice, resulting in chromosomal DNA fragments ranging from 300 - 1,000 bp in size, centered on ~600 bp - as confirmed by agarose gel electrophoresis. The sonicated samples were centrifuged twice at 13,000 rpm at 4˚C to remove unlysed cells and debris. The resulting supernatants were incubated with 10% (v/v) equilibrated 50% protein A-Sepharose (Sigma-Aldrich, Gillingham, UK) for 1 hr on a rotating wheel, in order to remove non-specifically bound proteins. The samples were then centrifuged at 13,000 rpm for 15 min to isolate the supernatants from the beads; supernatants were then incubated with 10% (v/v) anti-BldB antibody overnight at 4˚C on a rotating wheel.

On the following day, 10% (v/v) of equilibrated 50% protein A-Sepharose was added to the samples and incubated for 4 hr to recover the anti-BldB antibodies with bound protein and DNA. The samples were centrifuged for 5 min at 3,500 rpm at 4˚C, the supernatant was discarded, and the pellets were washed twice with 0.5x IP buffer, and then twice more with 1x IP buffer.

To elute the DNA, the bead pellets were resuspended in 150 µL IP elution buffer (50 mM Tris HCl pH 7.6, 10 mM EDTA, 1% SDS), and incubated overnight at 65˚C. The samples were then centrifuged for 5 min at 13,000 rpm to pellet the beads. The supernatants were retained, and the pellets were re-extracted using 50 µL TE buffer (10 mM Tris HCl pH 7.4, 1 mM EDTA). The resulting supernatants were incubated with 3 µL 10 mg/mL proteinase K for 2 hr at 55˚C, to remove the bound proteins. Two consequent phenol-chloroform (equal volumes) extractions, followed by a chloroform-only extraction were performed, and the resulting DNA was further purified using a QiaQuick kit (QIAGEN, Manchester, UK), and eluted in 50 µL EB buffer. Library construction and sequencing were performed by the Earlham Institute (Norwich, UK), using Illumina HiSeq 2500. ChIP-seq results were analysed as described later in this section.

ChIP-Seq Using Anti-FLAG Antibody

In order to assess whether 3xFLAG-BldB, 3xFLAG-WhiJ6 and 3xFLAG-WhiJ9 bind DNA, separate ChIP-seq experiments using an anti-FLAG antibody were undertaken. Cultures of wild-type *S. venezuelae* and the appropriate strains producing 3xFLAG-tagged proteins were grown in 30 mL volumes of liquid MYM medium at 28˚C, shaking at 250 rpm.

For the BldB experiment, the 3xFLAG-BldB strain (*ΔbldB* mutant complemented with 3xFLAG-BldB, produced from its native promoter) was inoculated to yield duplicate cultures - sampled at 10-, 14- and 22-hours post-inoculation. Duplicate wild-type *S. venezuelae* cultures were sampled at 14 hours only and used as a negative control.

For the WhiJ6 experiment, the 3xFLAG-WhiJ6 strain (*ΔwhiJ6* mutant complemented with 3xFLAG-WhiJ6, produced from its native promoter) was inoculated to yield duplicate cultures - sampled at 10-, 16- and 22-hours post-inoculation. Duplicate wild-type *S. venezuelae* cultures were sampled at 16 hours only and used as a negative control.

For the WhiJ9 experiments, the 3xFLAG-WhiJ9 complementation strain (*ΔwhiJ9* mutant complemented with 3xFLAG-WhiJ9, produced from its native promoter), and the 3xFLAG-WhiJ9 overexpression strain (wild-type *S. venezuelae* overproducing 3xFLAG-WhiJ9 from the *ermE** promoter) were inoculated to yield duplicate cultures - sampled at 10-, 16- and 22-hours post-inoculation. Duplicate wild-type *S. venezuelae* cultures were sampled at 16 hours only and used as a negative control.

All cultures were examined under a light microscope to determine if they were at the expected developmental stage. To crosslink proteins bound to DNA, formaldehyde was added to the cultures at a final concentration of 1% (v/v), and incubation was continued for another 30 minutes. To stop the crosslinking reaction, glycine was then added to the cultures at a final concentration of 125 mM, and all cultures were incubated for 5 min at RT. The bacteria were harvested via centrifugation at 4˚C at 7,000 rpm for 5 min and washed twice with ice-cold PBS (pH - 7.4).

The resulting pellets were resuspended in 0.75 mL lysis buffer [10 mM Tris HCl pH 8.0, 50 mM NaCl, 0.8% Triton X-100, with 14 mg/mL lysozyme and EDTA-free protease inhibitor (Roche, Basel, Switzerland)], and incubated for 25 min at 37˚C. Following lysis, an equal volume of IP buffer (50 mM Tris HCl pH 8, 250 mM NaCl, 0.8% Triton X-100, with protease inhibitor added) was added to the samples, which were then incubated on ice for 2 min. The samples were sonicated at an 8-micron amplitude (8 cycles: 20 s on/1 min off) on ice, resulting in chromosomal DNA fragments ranging from 100 - 900 bp in size, centered on ~400-500 bp - as confirmed by agarose gel electrophoresis. The sonicated samples were centrifuged twice at 13,000 rpm at 4˚C to remove unlysed cells and debris. The resulting supernatants were incubated with 40 µL of prepared ANTI-FLAG® M2 Affinity Gel suspension (Sigma-Aldrich, Gillingham, UK) per 1 mL of supernatant overnight at 4˚C on a rotating wheel to isolate protein-DNA complexes. On the following day, the samples were centrifuged for 30 sec at 4,500 rpm at 4˚C, the supernatant was discarded, and the pellets were washed 4 times with 1x IP buffer.

To elute the DNA, the bead pellets were resuspended in 100 µL IP elution buffer (50 mM Tris HCl pH 7.6, 10 mM EDTA, 1% SDS), and incubated overnight at 65˚C. The samples were then centrifuged for 5 min at 13,000 rpm to pellet the beads. The supernatants were retained, and the pellets were re-extracted using 50 µL TE buffer (10 mM Tris HCl pH 7.4, 1 mM EDTA). The resulting supernatants were incubated with 3 µL 10 mg/mL proteinase K for 2 hr at 55˚C, to remove the bound proteins. Two consequent phenol-chloroform (equal volumes) extractions, followed by a chloroform-only extraction were performed, and the resulting DNA was further purified using a QiaQuick kit (QIAGEN, Manchester, UK), and eluted in 50 µL EB buffer.

For the 3xFLAG-BldB samples and their negative controls, library construction and sequencing were performed by the Earlham Institute (Norwich, UK), using Illumina HiSeq 2500. For the 3xFLAG-WhiJ6 and 3xFLAG-WhiJ9 samples and their negative controls, library construction and sequencing were performed by Genewiz (NJ, USA), using their Illumina HiSeq platforms. ChIP-seq results were analysed as below.

ChIP-Seq Analysis

All ChIP-seq analysis was performed by Dr. Govind Chandra. The reads in the fastq files received from the sequencing contractors were aligned to the *S. venezuelae* genome (GenBank: CP018074) using the most current version of the bowtie2 software. This resulted in one SAM (.sam) file for each fastq file for all BldB ChIP-seq samples, where single-ended sequencing was performed. Paired-end sequencing was performed for the 3xFLAG-WhiJ6 and 3xFLAG-WhiJ9 ChIP-seq samples, so one SAM file was generated for each pair of fastq files. For each SAM file, the *depth* command of *samtools* was used to arrive at the depth of sequencing at each nucleotide position of the *S. venezuelae* genome. From the sequencing depths at each nucleotide position determined in the previous step, a local enrichment was calculated in a moving window of 30 nucleotides moving in steps of 15 nucleotides as (the mean depth at each nucleotide position in the 30-nucleotide window) divided by (the mean depth at each nucleotide position in a 3000-nucleotide window centered around the 30-nucleotide window). This resulted in an enrichment ratio value for every 15 nucleotides along the genome. Enrichment for the control samples was subtracted from the enrichment for each sample. Significance of enrichment values were calculated assuming normal distribution of the enrichment values. Genomic positions were ordered from low to high P values. Association of regions of enrichment with P values below 1E-4 with genes on the chromosome was done by simply listing genes left and right of the region. Rows of lower significance with the same context of genes were removed to leave the most significant row for each combination of left, right and within genes. Genes had to be in the right orientation and within 500 nucleotides of the enriched region for association with the region. The final list of genes was checked by visual inspection of enrichment in the region in Integrated Genome Browser (IGB).

RNA Methods

RNA Isolation

RNA extractions were performed as described by Bush *et al.* (2019). *S. venezuelae* cultures were grown in triplicate (for RNA-seq) or duplicate (for qRT-PCR) in liquid MYM medium. For the earliest time point (10 hours post inoculation), 5 mL of culture was pelleted to gain enough biomass, whereas for the later time points 2 mL of culture was pelleted and the medium supernatant was discarded. The pellets were washed in PBS and resuspended in 900 µL lysis solution [400 µL phenol at pH - 4.3, 100 µL chloroform:isoamyl alcohol (24:1) and 400 µL RLT buffer (QIAGEN, Manchester, UK)]. The samples were transferred to lysing matrix B tubes (MP Biomedicals, Irvine, CA, USA) and homogenized using a FastPrep FP120 Cell Disruptor (Thermo Savant). Two 30-second pulses at a 6.0 intensity were applied, with cooling down for 1 min on ice between pulses. Supernatants were centrifuged for 15 min at full-speed on a bench-top centrifuge at 4°C and then processed according to the instructions given in the RNEasy Kit (QIAGEN, Manchester, UK). The RNA samples were treated with on-column DNase I (QIAGEN, Manchester, UK), followed by an additional DNase I treatment (Turbo DNA-free Kit, Ambion). RNA concentration was determined using a Qubit® 2.0 Fluorometer (ThermoFisher Scientific, Waltham, MA, USA).

Quantitative Reverse Transcription PCR (qRT-PCR)

qRT-PCR was performed to quantify the levels of *iosA* expression in *Streptomyces* strains. Equal amounts (1 µg) of total RNA from each sample was converted to cDNA using SuperScript™ II Reverse Transcriptase and Random Primers (ThermoFisher Scientific, Waltham, MA, USA). 2 µL of 10-fold diluted cDNA was then used as a template in qRT-PCR. The experiment was conducted twice independently, and 3 technical replicates were performed for each of the 2 biological replicates. Primers iosA_qRTPCR_F and iosA_qRTPCR_R were used to amplify the *iosA* gene, and primers hrdB_qRTPCR_F and hrdB_qRTPCR_R were used to amplify the *hrdB* reference gene (**Table 2.9**). The primers were designed using Primer3Plus with the following parameters: 95 - 105 bp fragment size, 18 - 22 bp primer length, 62 - 65°C melting temperature. General PCR using *S. venezuelae* genomic DNA was used to validate that only 1 product per primer pair was produced.

During each qRT-PCR experiment a standard curve was constructed using serial dilutions of *S. venezuelae* chromosomal DNA to normalize for differing primer efficiency. Melting curve analysis was used to confirm the production of a specific single product from each primer pair. qRT-PCR was performed using a CFX96 Touch Deep Well™ Real-Time PCR Detection System (BioRad) instrument using Hard-Shell® 96-Well White PCR Plates (BioRad), sealed with thermostable film covers (ThermoFisher Scientific, Waltham, USA). The SensiFAST™ SYBR® No-ROX Kit (Meridian Bioscience, Cincinnati, OH, USA) was used to amplify PCR products using the following programme: an initial denaturation phase (95°C for 3 min), then 45 cycles of denaturation (95°C for 5 s), annealing (63°C for 10 s) and extension (72°C for 7 s). Melting curves were generated at 65°C to 95°C with 0.5°C increments. For the absolute quantification of target gene transcription, Cq (quantification cycle) values were calibrated using the genomic DNA standard curve for each primer pair, yielding the SQ (starting quantity) values for each sample. The *iosA* SQ values were divided by the mean *hrdB* SQ values for the corresponding samples, resulting in relative expression values. The mean relative expression values were normalised against the mean relative expression value of the WT, which was set to 1.

RNA-Seq Analysis

Total RNA from three biological replicates per time point was isolated as decribed above. RNA library preparation and sequencing were performed by Genewiz (NJ, USA). rRNA depletion was conducted using the Illumina Ribo-Zero rRNA removal kit and paired-end sequencing conducted by Illumina Hiseq (2x150bp configuration).

I conducted all RNA-seq analysis under supervision from Dr Govind Chandra. The reads in the fastq files received from the sequencing contractor were aligned to the *S. venezuelae* genome (GenBank: CP018074) using the most current version of the bowtie2 software (Langmead and Salzberg, 2012), which resulted in one SAM (.sam) file for each pair of fastq files (paired-end sequencing). The featureCounts() function of the Bioconductor package Rsubread was used to count the number of reads mapping to each gene on the chromosome (Liao, Smyth and Shi, 2013). Quasi-likelihood F test implemented in the function glmQLFTest() of the Bioconductor package edgeR was used for differential expression analysis as described in the edgeR user's guide (Lun, Chen and Smyth, 2016).

Microbiological Methods

Preparation and Transformation of Electrocompetent *E. coli*

Overnight cultures were diluted 1:100 in 50 mL LB containing an appropriate concentration of antibiotics. The flasks were incubated at 37°C, shaking at 250 rpm until the cultures reached an OD_{600} of 0.4. The cultures were transferred to 50 mL centrifuge tubes and centrifuged at 4,000 rpm for 5 min at 4°C in a Sorvall GS3 rotor. The supernatant was discarded, and the pelleted cells were resuspended in 50 mL ice-cold 10% (v/v) glycerol. The cells were washed twice more with 10% glycerol to remove the antibiotics and salt from the culture medium. Finally, the pellets were resuspended in 100 µL 10% glycerol, cells aliquoted into sterile Eppendorf tubes and stored at -80°C.

For each transformation, a maximum volume of 5 µL of DNA (100-200 ng) was added to 50 µL of competent cells. Electroporation was carried out in 0.2 cm electroporation cuvettes in a BioRad GenePulser II with the following settings: 200 Ω, 25 µF, 2.5 kV, with an expected time constant of 4.5 – 4.9 ms. After the immediate addition of 1 mL room temperature SOC medium, the electroporated cells were transferred to sterile Eppendorf tubes, and incubated at 37°C for 1 hour, shaking at 250 rpm. The cells were then centrifuged, the superfluous medium discarded, and the concentrated cells plated on appropriate selective media. Plates were incubated overnight at 30 - 37°C.

Preparation and Transformation of Chemically Competent *E. coli*

Overnight cultures were diluted 1:100 in 100 mL LB. The flasks were incubated at 37°C, shaking at 250 rpm until the cultures reached an OD_{600} of 0.4. The cultures were transferred to 50 mL centrifuge tubes and centrifuged at 4,000 rpm for 10 min at 4°C in a Sorvall GS3 rotor. The cell pellets were gently resuspended in 12.5 mL ice-cold 100 mM $MgCl_2$ and were again centrifuged at 4,000 rpm for 10 minutes at 4°C. The resulting cell pellet was then resuspended in 25 mL ice-cold 100 mM $CaCl_2$ and incubated on ice for 20 minutes. After this, the cell suspension was centrifuged under the same conditions. The pellet was then carefully resuspended in 1 mL ice-cold storage buffer (100 mM $CaCl_2$ in 20% glycerol). The competent cells were then stored in 100 - 200 µL aliquots at -80°C.

For each transformation, ~5 µL (approximately 100 ng) of DNA was added to 50 µL of competent cells in sterile Eppendorf tubes. The tubes were incubated for 30 minutes on ice, then the cells were heat-shocked at 42°C for 90 seconds. Following this, 1 mL room-temperature SOC medium was immediately added to recover the cells.

The Eppendorf tubes were incubated, shaking at 37°C for 1 hour. After recovery, the tubes were centrifuged in a table-top centrifuge at top speed, the supernatant was discarded, and the cells were plated on appropriate selective media. Plates were incubated overnight at 37°C.

Interspecies Conjugation from *E. coli* to *S. venezuelae*

Conjugation was performed according to established protocols, modified for the use of *S. venezuelae* (Kieser *et al.*, 2000). The plasmids or cosmids of interest were assembled and transformed into the methylation-deficient *E. coli* strain ET12567 containing the helper plasmid pUZ8002 (MacNeil *et al.*, 1992; Paget *et al.*, 1999). The resulting strains were later used for conjugation into *Streptomyces.* This is a necessary step, particularly for conjugation of plasmids into *S. coelicolor*, as this species has a methylation restriction system, which prevents its uptake of methylated DNA (González-Cerón, Miranda-Olivares and Servín-González, 2009). Using the ET12567/pUZ8002 strain for conjugation circumvents the issue, as its plasmids are not methylated, and thus, more efficiently taken up by *Streptomyces*. Notably, *S. venezuelae* does not restrict methylated DNA, so conjugation from methylating *E. coli* strains is possible.

Freshly transformed ET12567/pUZ8002 colonies were inoculated in LB containing appropriate antibiotics to select for the incoming plasmid or cosmid. The overnight cultures were diluted 1:100 with fresh LB supplemented with the same antibiotics and grown shaking at 37°C to an OD_{600} of 0.4. The cells were then centrifuged, pellets were washed with fresh LB twice to remove the antibiotics, and resuspended in 100 µL LB. For each conjugation, approximately 10^8 *S. venezuelae* spores were added to the ET12567/pUZ8002 cells. In the case of the non-sporulating strains, 100 µL freshly grown mycelium was added instead.

The cell suspensions were mixed and spread on SFM plates, which were incubated overnight at room temperature. On the following day, the plates were flooded with 1 mL dH_2O containing 0.5 mg nalidixic acid and an appropriate antibiotic to select for the incoming plasmid or cosmid. Once dry, the plates were incubated at 28°C for 3 - 5 days. Ex-conjugants were picked from the plates and streaked out consecutively on DNA and MYM solid media supplemented with appropriate antibiotics to screen for the desired genotype.

Construction of *S. venezuelae* Mutants via Redirect

The PCR-targeting method Redirect was used to generate *S. venezuelae* mutants (Gust *et al.*, 2003), making use of a cosmid library that covers >98% of the *S. venezuelae* genome (M.J. Bibb and M.J. Buttner, unpublished) and is fully documented at http://strepdb.streptomyces.org.uk/. To generate the mutation, the wild-type gene in the cosmid of interest was exchanged for an apramycin resistance cassette containing an *oriT*, which was isolated from pIJ773. These cosmids were transformed into ET12567/pUZ8002, and the transformed strains were then used for conjugation into *S. venezuelae*. The ex-conjugants were streaked out on selective media. Ex-conjugants, which had undergone double crossovers, were sensitive to kanamycin, but resistant to apramycin. Colony PCR was then used to confirm the insertion of the apramycin resistance cassette in place of the gene of interest.

Phage Transduction

SV1-mediated generalised transduction was used to move the *ΔbldB* deletion into a clean background and as a final step towards the generation of the *ΔwhiJ9 ΔbldB* double mutant and the *ΔabaA6 ΔiosA ΔbldB* triple mutant. High-titre SV1 lysate was used to infect two Redirect *ΔbldB* mutant strains. Different phage dilutions (20 µL of 10^{-5}-10^{-12} in DNB) were used to infect 15 µL of *ΔbldB* mycelial fragments, as previously described. On the following day, the mutant phage lysate was collected, and used to infect wild-type *S. venezuelae*. 100 µL mutant lysate was mixed with 10 µL wild-type spores and spread onto MYM plates, which were incubated at room temperature overnight.

On the following morning, the plates were overlaid with 1 mL dH_2O containing a final concentration of 50 µg/ml apramycin. The plates were incubated at 28°C until apramycin-resistant transductants formed. The resulting transductants were first streaked onto MYM plates containing apramycin, then on MYM plates without antibiotics added. Colony PCR was used to confirm the presence of the apramycin resistance cassette in place of the *bldB* gene in the transductants.

Construction of *S. venezuelae* Mutants via CRISPR/Cas9

CRISPR/Cas9 was used for the generation of *S. venezuelae* mutants whenever it was necessary to obtain clean deletions, such as in the creation of double and triple mutants. The well-established pCRISPomyces-2 system was used (Cobb, Wang and Zhao, 2015).

From the sequence of each gene to be deleted, a 20 bp protospacer was chosen with the following characteristics: protospacer ending in NGG (where N is any nucleotide), the 4 base pairs preceding the NGG being purine-rich, and the last 15 base pairs of the protospacer sequence being unique (to lower the chance of unintended deletions). The dsDNA protospacer was cloned into the BbsI site of pCRISPomyces-2 using Golden Gate Assembly. This resulting vector was then digested with XbaI, and 1-2 kb repair flanking sequences from each side of the target gene were cloned via Gibson Assembly. The resulting vector was transformed into *E. coli*, isolated, and sequenced to confirm correct assembly.

The final vector was transformed into ET12567/pUZ8002, and the resulting strain was used for conjugation into *S. venezuelae*. Ex-conjugants (Apr^R) were re-streaked on DNA medium containing apramycin, and colony PCRs with external and internal primers were performed to screen for the deletion. Mutant candidates with the confirmed deletion were grown at 37°C to promote loss of the temperature-sensitive pCRISPomyces-2 vector. The final double and triple mutants were subjected to whole-genome resequencing to validate the strains.

Complementation of *S. venezuelae* Mutants

The full-length genes were introduced back into the respective mutants *in trans* via the integrative vectors pSS170 or pIJ10257. To express the genes under their native promoters, the coding sequences as well as the promoter regions were cloned into pSS170. To express the genes under the *ermE** promoter, only the coding sequences were cloned into pIJ10257. The assembled plasmids were then conjugated into the relevant mutants. Hygromycin-resistant ex-conjugants were re-streaked onto MYM agar containing hygromycin. All strains were validated using colony PCR.

Generation of 3xFLAG Alleles

For the ChIP-seq experiments on BldB, WhiJ6 and WhiJ9, fusions with N- or C-terminal 3xFLAG tags were generated. To express the 3xFLAG alleles under their native promoters, they were cloned into the integrative vector pSS170.

To achieve an N-terminal 3xFLAG fusion, a two-step PCR approach was used. First, two overlapping products were amplified - the first one including the native promoter and a sequence of the 3xFLAG tag, the second one including an overlapping sequence of the 3xFLAG tag and the coding region. The two overlapping products were then joined via a second PCR using the external primers. The resulting product was cloned into pSS170.

To achieve a C-terminal 3xFLAG fusion, a similar approach was used to insert the 3xFLAG sequence before the stop codon. Two overlapping products were amplified - the first one containing the native promoter, coding sequence and a sequence of the 3xFLAG tag, the second one including an overlapping sequence of the 3xFLAG tag, the stop codon, and some downstream sequence. The two overlapping products were joined via a second PCR with the external primers. The resulting product was cloned into pSS170. A special case was the C-terminally 3xFLAG-tagged *bldB* - the gene with its native promoter and without a stop codon was cloned into pIJ10500 instead.

To express the 3xFLAG-WhiJ9 alleles under the *ermE** promoter, they were cloned into the integrative vector pIJ10257 by directly amplifying the fully assembled 3xFLAG-WhiJ9 fusion constructs described above. To check whether all 3xFLAG alleles were functional, the pSS170-derived plasmids were conugated into the relevant *S. venezuelae* mutant strains, and the pIJ10257-derived plasmids into wild-type. Hygromycin-resistant ex-conjugants were re-streaked onto MYM agar containing hygromycin. All strains were validated using colony PCR. The phenotypes of the resulting strains were inspected to see if the alleles were functional.

Gene Overexpression in *S. venezuelae*

To overexpress target genes in *S. venezuelae*, they were placed under the control of the constitutive *ermE** promoter (Bibb, Janssen and Ward, 1985). The coding sequences were amplified by PCR and cloned into the integrative vector pIJ10257. The assembled plasmids were then conjugated into wild-type *S. venezuelae*. Hygromycin-resistant ex-conjugants were re-streaked onto MYM agar containing hygromycin. All strains were validated using colony PCR.

Bacterial-Two-Hybrid Library Screens

A bacterial-two-hybrid screen was conducted as outlined in previous studies (Karimova *et al.*, 1998; Karimova, Ullmann and Ladant, 2000). Briefly, the experiment relies on the ability to split the enzyme adenylate cyclase into two peptides - T18 and T25. When physically apart, T18 and T25 do not have any adenylate cyclase activity, but when fused to interacting proteins, T18 and T25 are brought together, leading to the reconstitution and activation of adenylate cyclase activity. When adenylate cyclase is active, cAMP is produced, and the expression of reporter genes is activated. β-galactosidase activity can be measured, in order to quantify the strength of interaction between the two proteins fused to T18 and T25.

The proteins of interest were fused to the T18 and T25 peptides via amplifying and cloning the target coding regions into the bacterial-two-hybrid vectors pUT18, pUT18C, pKT25, pKNT25. These constructs were then used as bait against bacterial-two-hybrid shotgun genomic libraries, prepared by Dr Matt Bush (Bio S&T, Montréal, Canada). To construct these libraries, genomic DNA from *S. venezuelae* was sheared by sonication, then end-repaired and cloned into SmaI-digested pUT18C or pKT25. The ligation mix was transformed into competent DH10B *E. coli* cells and spread onto large agar plates, resulting in >329,200 colonies (40X coverage, assuming an insert size of 1 kb) for each library. Colonies on each plate were washed into tubes, pooled, and plasmids purified by maxi-prep. For quality control, 8-12 clones were randomly selected from each library. All clones selected were found to contain inserts, and the average size of each insert was 2.6 kb in the pUT18C library and 2.2 kb in the pKT25 library. The random nature of the genomic DNA sonication makes the libraries representative and unbiased.

The bait vectors were co-electroporated with 0.25 µL of a working stock (0.1-0.5 µg/µL) of the appropriate corresponding genomic library into electrocompetent *E. coli* strain BTH101. Prior to plating, transformants were washed twice in M63 minimal medium, followed by resuspension in 1 mL of M63. To ensure that the transformation efficiency was sufficient for the screening of all possible interactions, the total number of transformants was measured by plating 1 µL onto an LB agar plate containing appropriate antibiotics. Transformation efficiency was calculated based on the number of arising colonies.

The remaining transformation mixture was then plated onto M63 agar containing 0.3% lactose, 0.5 mM IPTG, 40 µg/mL X-gal, and appropriate antibiotics. Positive clones were streaked on MacConkey agar containing 1% maltose and appropriate antibiotics.

Red bacterial growth on MacConkey agar was used as a first indicator for strong protein-protein interactions. Plasmid DNA was then isolated from positive clones and library inserts were sequenced. Out-of-frame clones and common false positives (*e.g.* adenylate cyclase) were excluded from further analysis.

β-Galactosidase Assays

β-galactosidase assays were performed in 96-well plates as a follow-up to the bacterial-two-hybrid library screens, in order to validate and assess the strength of the identified protein-protein interactions. β-galactosidase is produced following the reconstitution of adenylate cyclase activity via the interaction of 2 proteins of interest fused to the T18 and T25 peptides in the bacterial-two-hybrid system. β-galactosidase hydrolyses the substrate o-nitrophenyl-β-D-galactopyranoside (ONPG), resulting in the release of o-nitrophenol, which leads to the formation of a yellow colour detectable at OD_{420}.

BTH101 chemically competent cells were transformed with the relevant T18 and T25 fusions. 3 individual colonies per strain were picked and inoculated into 1 mL LB (containing kanamycin and carbenicillin) and incubated in 2.2 mL 96-well polypropylene blocks (ThermoFisher Scientific, Waltham, USA), shaking at 28˚C for 6 - 8 hours. After this, 10 µL of these cultures were inoculated into 1 mL LB (containing kanamycin and carbenicillin and IPTG) in fresh polypropylene blocks in duplicate. These were incubated overnight at 28˚C, shaking at 250 rpm. 50 µL of each overnight culture was added to 150 µL LB in microtitre plates, and the OD_{600} was determined using a plate reader. LB was used as a blank.

40 µL chloroform was added to 1 mL lysis buffer in the wells of a new 96-well polypropylene block. 100 µL of overnight culture was added and resuspended in each well. After the chloroform settled in the bottom of the wells, 100 µL of this mixture was transferred to duplicate microtitre plates. 50 µL of ONPG was mixed in each well, and the start time of each reaction was recorded. Upon the development of a yellow colour, 50 µL of 1M Na_2CO_3 was added to stop the reactions, and their stop time was noted. The OD_{420} and OD_{550} of the samples were measured using a plate reader. β-galactosidase activity (measured in Miller units) was calculated using the equation:
$(1000*(OD_{420} – 1.75*OD_{550})) / (t*V*OD_{600})$; where t is the time in minutes, and V is the volume of cell sample added to the reaction in mL.

Protein Methods

Protein Overexpression

The 6xHis-BldB, 6xHis-BldB9, 6xHis-WhiJ6 and 6xHis-WhiJ9 proteins were overexpressed and purified from *E. coli*. The purification of BldB in particular was conducted following a previously established protocol (Eccleston *et al.*, 2002). The full-length genes were amplified via PCR, the resulting inserts were digested and cloned into pET15B. Genes were expressed under the control of the T7 promoter to yield proteins with an N-terminal hexahistidine (6xHis) tag. The assembled plasmids with the 6xHis constructs were transformed into BL21 DE3 pLysS Rosetta or BL21 DE3 NiCo competent cells. Colonies were inoculated into 50 mL LB starter cultures containing appropriate antibiotics and incubated overnight at 37˚C shaking at 250 rpm.

On the following day, 4 – 8x 1L volumes of LB supplemented with appropriate antibiotics in 2L flasks were inoculated with a 1% final concentration of the mixed overnight starter cultures. These cultures were incubated at 37˚C, shaking at 200 rpm until they reached an OD_{600} of 0.6. For purifying BldB, the cultures were induced by adding IPTG to a final concentration of 1 mM and were then further incubated at 37˚C for 3 more hours. For purifying BldB9, WhiJ6 and WhiJ9, the cultures were left at 4˚C for 30 min to cool down with occasional shaking, after which they were induced with IPTG (at 1 mM final concentration) and incubated at 16-18˚C overnight, shaking at 200 rpm.

Pellets were harvested by centrifuging at 5,000 rpm for 10 minutes, after which they were resuspended in a total volume of 40 mL Buffer A, with added EDTA-free protease inhibitor (Roche, Basel, Switzerland). For the purification of BldB, Buffer A containing 50 mM Tris-HCl, 500 mM NaCl and 50 mM imidazole at pH 7.5 was used. For the purification of BldB9, WhiJ6 and WhiJ9, Buffer A containing 10 mM HEPES, 250 mM NaCl and 50 mM imidazole at pH 8 was used.

Pre- and post-induction samples were taken from the growing cultures to check for the successful overexpression of the proteins. 1 mL of pre- or post-induction culture was centrifuged at 13,000 rpm for 1 min. The supernatant was discarded, and pellets were resuspended in 200 µL buffer containing 20mM Tris pH 8, 10mM $MgCl_2$. Samples were mixed with 4X SDS-PAGE loading dye to a 1X final concentration, boiled at 95˚C for 3 minutes and then loaded on a SDS polyacrylamide gel.

Protein Purification

The harvested post-induction cells resuspended in Buffer A were sonicated on ice (8 cycles 30 sec on/1 min off). The lysate was then centrifuged at 15,000 rpm for 45-60 min and the resulting supernatant was passed through Minisart® 0.22 µm syringe filters (Sartorius, Göttingen, Germany) to remove the insoluble material. All protein purification was conducted on an ÄKTA Pure Protein Purification System (Cytiva, Marlborough, MA, USA). The filtered supernatant was loaded onto a HisTrap™ HP or Excel 1 mL nickel column (Sigma-Aldrich, Gillingham, UK), after the column and the whole system were equilibrated with Buffer A. After washes with Buffer A, the bound 6xHis protein was eluted from the column with Buffer B (the appropriate Buffer A with the addition of 500 mM imidazole). Fractions were collected and aliquots taken for SDS-PAGE to determine which fractions contained the eluted protein. The relevant fractions were collected and were either frozen for future use at -80°C, or further purified via size-exclusion chromatography.

For size-exclusion chromatography, up to 5 mL of the relevant nickel column fractions were loaded onto a HiLoad™ 16/600 Superdex™ 200 pg column (Sigma-Aldrich, Gillingham, UK), pre-equilibrated with gel filtration buffer, with the flow rate set to 1 mL/min. For BldB purification, the gel filtration buffer contained 50 mM HEPES, 200 mM NaCl and 1 mM DTT at pH 7.5. For BldB9 and WhiJ9 purification, the gel filtration buffer contained 10 mM HEPES and 250 mM NaCl at pH 8. SDS-PAGE was used to identify the fractions containing the protein of interest. These fractions were pooled and concentrated using an Amicon Ultra-15 Centrifugal Filter Unit (Merck, Gillingham, UK) with 10 kDa cut-off for BldB and WhiJ9, and with 3 kDa cut-off for BldB9. The protein samples were flash-frozen in liquid nitrogen and stored at -80°C.

Protein Co-expression

To co-express 6xHis-BldB9 and untagged WhiJ9, the *bldB9* and *whiJ9* genes were codon-optimised for expression in *E. coli*, synthesised and cloned into pCOLA-Duet1 by GenScript (Piscataway, NJ, USA). The assembled plasmid was verified by sequencing and transformed into BL21(DE3) NiCo for protein expression. Protein purification was performed from 8 L of culture, as described above. Filtered supernatant was loaded onto a HisTrap™ HP 1 mL nickel column (Sigma-Aldrich, Gillingham, UK), washed with 10 mL Buffer A containing no imidazole, followed by a 30 mL Buffer A with 30 mM imidazole. Proteins were eluted using Buffer B with 500 mM imidazole and analysed by SDS-PAGE.

Gel bands corresponding to the predicted molecular weights of 6xHis-BldB9 and WhiJ9 were cut and processed for trypsin digestion. Mass spectrometry on the samples was performed by Dr Carlo de Oliveira Martins and Dr Gerhard Saalbach.

SDS-PAGE

SDS polyacrylamide gel electrophoresis was conducted using pre-cast Novex Tris-Glycine SDS Gels 4-20% (ThermoFisher Scientific, Waltham, USA). Protein samples were mixed with 4X SDS-PAGE loading dye [0.2 M Tris-HCl pH 6.8, 25% glycerol, 8% SDS (w/v), 0.4% β-mercaptoethanol (w/v), 6 mM bromophenol blue, topped up with dH_2O] to a 1X final concentration and heated to 95˚C for 3 minutes. Samples, along with a protein ladder [Color Prestained Protein Standard, Broad Range (10–250 kDa), NEB] were loaded on the gels, which were run in 1X Novex Tris-Glycine SDS Running Buffer (ThermoFisher Scientific, Waltham, USA). The gels were run at 100 V until all samples entered the gel, and then at 180 V and 20 mA for approximately 1 hour. To visualise protein bands, the gels were stained with InstantBlue Coomassie Protein Stain (Abcam, Cambridge, UK) shaking at room temperature overnight. On the following day the gels were de-stained in dH_2O and imaged.

Protein Concentration Quantification

Bradford assays were used to determine protein concentrations (Bradford, 1976). The assays were performed using Bradford Reagent (Bio-Rad) according to the manufacturer's instructions. Known concentrations of bovine serum albumin (BSA) were used to generate a standard curve. Protein concentrations were calculated using this standard curve and the measured OD_{595} absorbances of 3 different protein dilutions.

Western Blotting

S. venezuelae cultures were grown in liquid MYM medium, and samples for time courses were taken every 2 hours, from 8 hours post-inoculation onwards. For the earliest time points (8- and 10-hours post-inoculation), 5 mL of culture was pelleted to gain enough biomass, whereas for the later time points 2 mL of culture was pelleted and the supernatant was discarded. Pellets were washed and resuspended in 0.4 mL ice-cold sonication buffer [20 mM Tris pH 8.0, 5 mM EDTA, 1 x EDTA-free protease inhibitor tablet (Roche, Basel, Switzerland)]. Samples were sonicated at a 4.5-micron amplitude (5 cycles: 15 sec on/ 15 sec off) on ice. Lysates were then centrifuged at 13,000 rpm for 15 min at 4˚C to remove any unlysed cells or debris. Total protein concentration was determined using Bradford assays. The automated Wes™ system (ProteinSimple, San Jose, CA) was used to detect proteins of interest in the *S.venezuelae* crude lysates using an anti-FLAG antibody, or in the case of untagged BldB - an anti-BldB polyclonal antibody. The experiment was conducted according to the manufacturer's instructions and results were analysed using the CompassSW software.

For detection of untagged BldB in a time course, and for the validation of the *bldB* overexpression strain, the dilution of the anti-BldB polyclonal antibody used in the assays was 1:500. 1.5 µg of total protein from each time point was loaded in duplicate, except for the 8-hour time course sample, where 0.3 µg of total protein was loaded, due to low protein concentration of the whole cell lysate.

For detection of 3xFLAG-BldB in a time course, the dilution of the anti-FLAG antibody used in the assay was 1:100. 0.9 µg of total protein from each time point was loaded in duplicate.

For detection of 3xFLAG-WhiJ6 and 3xFLAG-WhiJ9 produced from their native promoters and 3xFLAG-WhiJ9 produced from the *ermE** promoter, the dilution of the anti-FLAG antibody used in the assay was 1:100. 1.5 µg of total protein from each time point was loaded in duplicate.

Biochemical and Biophysical Methods

Surface Plasmon Resonance

To test protein-DNA interactions *in vitro*, surface plasmon resonance (SPR) was performed using the ReDCaT method (Stevenson *et al.*, 2013; Stevenson and Lawson, 2021). Experiments were performed in collaboration with Dr Clare Stevenson. Single-stranded DNA oligos from target promoter regions were designed, ordered, and dissolved to a concentration of 100 µM in dH_2O. Complementary oligos were annealed to form ≤40 bp dsDNA molecules with a 20 bp ssDNA overhang (cctaccctacgtcctcctgc) complementary to the biotinylated ReDCaT linker. The annealed oligos were diluted to a concentration of 1 µM in running buffer (0.01 M HEPES, 0.25 M NaCl, 3 mM EDTA, 0.05% v/v Tween 20, pH 7.4). A full list of oligos used for SPR is included in **Table 2.9.**

A streptavidin Sensor Chip SA (Cytiva, Marlborough, MA, USA) was docked to a Biacore 8K System (Cytiva, Marlborough, MA, USA). Prior to the experiment, all samples were kept at 4°C. The 20 bp biotinylated linker DNA was immobilised to one of the flow cells of the chip and the other one was left blank as a reference. The DNA to be tested was then flowed over this flow cell at a rate of 10 µL/min and thus annealed to the single-stranded linker. The protein of interest (6xHis-BldB, 6xHis-BldB9, 6xHis-WhiJ6 or 6xHis-WhiJ9) diluted to a desired concentration in running buffer was then flowed over both the reference control cell and the cell with immobilised DNA. The protein and test DNA were then washed away with 1 M NaCl, 50 mM NaOH, regenerating the chip for the loading of new test DNA to the immobilised linker. For the experiments testing if BldB or BldB9 bind to WhiJ9 immobilised on DNA, each of the two protein was flowed over both the reference and testing flow cell after the injection of WhiJ9. SPR response was monitored throughout all experiments, which were undertaken at a constant temperature of 25°C.

Sensorgrams were generated for each ReDCaT experiment using the Biacore T200 Evaluation software (Cytiva). To normalise the results for different proteins and DNA molecules used, %Rmax was calculated as referenced in Stevenson and Lawson (2021).

X-ray Crystallography Screens

For crystallisation of 6xHis-WhiJ9, purified protein was concentrated to 8 mg/mL (which led to its precipitation) and was either used immediately, or it was flash-frozen in liquid nitrogen and stored in aliquots at -80°C. Sitting drop vapour diffusion explorative screens were performed in 96-well MRC 2 Well Crystallisation Plates (SWISSCI, High Wycombe, UK) using an Oryx or OryxNano robot (Douglas Instruments, Berkshire, UK). Three commercial crystallisation screens were used in this study - PEGs suite (QIAGEN, Manchester, UK), Morpheus® (Molecular Dimensions) and ProPlex™ (Molecular Dimensions). Initial screens were performed with WhiJ9 alone, and with WhiJ9 mixed with 22 bp blunt-ended dsDNA containing the two direct repeats DR2 and DR3 from the *iosA-whiJ9* intergenic region. Upon addition of the dsDNA that was confirmed to be bound by WhiJ9 via ReDCaT, the precipitated WhiJ9 protein immediately went back into solution. Crystallisation plates were sealed with transparent plastic films, and were incubated at 20°C. The plates were imaged regularly under visible and UV light to monitor for any crystal formation.

The PEGs suite screen yielded protein-DNA spherulites - small, soft crystal-like moieties, the formation of which indicated that the particular conditions resulted in precipitation patterns close to the optimal crystallisation conditions (Heijna *et al.*, 2007). Thus, further optimisation screens were performed based on the PEGs screen using 48-Well MRC Maxi Optimization Plates (SWISSCI, High Wycombe, UK), with variations including the size and concentration of the PEGs precipitants, the drop size, and the use of seed from previous promising wells. Additionally, a range of dsDNA molecules were designed for use in the optimisation screens, with lengths ranging from 18 to 32 bp and the addition of sticky (A/T) ends to the DNA to promote the formation of DNA pseudo filaments and thus crystal formation and nucleation (**Table 2.9**). For all crystallisation screens, in which WhiJ9 was premixed with dsDNA, the ratio of protein to DNA was 1:1.2.

The optimisation screens resulted in small, unstable WhiJ9-DNA crystals under the following specific conditions: buffer-precipitant mix composed of 0.1M Tris-HCl pH 8.5, 36.25% PEG 2000, 22 bp sticky-ended DNA; drops were dispensed manually with a 2:1 ratio of buffer-precipitant mix to protein-DNA mix. Crystals were isolated, cryoprotected and flash-frozen in liquid nitrogen by Dr Clare Stevenson. The frozen crystals were sent to the Diamond Light Source synchrotron and tested for diffraction using x-rays. Assistance was provided by Prof Dave Lawson, Dr Clare Stevenson and Julia Mundy. Data were not collected as the diffraction was at a very low resolution.

Bioinformatic Methods

Overall Data Analysis

Data analysis for specific experiments was performed as described above. GraphPad Prism was used to generate graphs and perform statistical analysis. Graphs were further formatted using Adobe Illustrator. Commonly used bioinformatic software included Integrated Genome Browser (for viewing genome alignments), SnapGene (for viewing and constructing plasmid maps), Scaffold 4 (for analysing mass spectrometry results), as well as software already listed above.

For the analysis of RNA-seq data (done with guidance from Dr Govind Chandra), I used the Linux command line, as well as RStudio for programming in R. Whenever computationally heavy tasks needed to be performed, I used the High Performance Computing (HPC) cluster supported by the Norwich Bioscience Institutes.

Bacterial Genome Collection

A collection of 30,772 bacterial genomes was assembled on 21/09/2021 by Dr Govind Chandra using the available bacterial genome assemblies in GenBank. The collection includes all available actinobacterial genomes, as well as reference or representative genomes from all other bacterial phyla. Unannotated genomes were excluded from the collection. Further bioinformatic analysis based on this genome collection was performed by Dr Govind Chandra using Perl and R, and by myself using R. The presence or absence of BldB homologues in the collected genomes was performed using NCBI Blast, accessed via Perl scripts.

Phylogenetic Analysis

Amino acid sequences of BldB and its 10 homologues in *S. venezuelae* were obtained from StrepDB (http://strepdb.streptomyces.org.uk/). The sequences were aligned with T-Coffee (Notredame, Higgins and Heringa, 2000), and maximum likelihood phylogeny analysis was conducted using PhyML 3.0 (Guindon *et al.*, 2010) with the default settings, and 100 bootstraps were performed. The WAG + G substitution model was selected automatically using Akaike Information Criterion (AIC). The phylogenetic tree was visualised using iTOL (Letunic and Bork, 2019).

Microscopy Methods

Scanning Electron Microscopy

All scanning electron microscopy was performed by Kim Findlay. *S. venezuelae* colonies (incubated for 3 to 5 days) were mounted on the surface of an aluminum stub with optimal cutting temperature compound (Agar Scientific Ltd, Essex, UK), plunged into liquid nitrogen slush at approximately -210°C to cryopreserve the material, and transferred to the cryostage of an Alto 2500 cryotransfer system (Gatan, Oxford, UK) attached to a FEI Nova NanoSEM 450 (ThermoFisher Scientific, Eindhoven, The Netherlands). The surface frost was sublimated at -95°C for 3.5 min before the sample was sputter coated with platinum for 2 min at 10 mA at below -110°C. Finally, the sample was moved onto the cryostage in the main chamber of the microscope, held at approximately -125°C, and viewed at 3 kV.

3. BldB and Two BldB Homologues are Necessary for Sporulation in *Streptomyces venezuelae*

Introduction

The BldB Homologues and Their Role in *Streptomyces* Development

The first four *bld* genes, *bldA-D*, were described in 1976 (Merrick, 1976). Unlike *bldA*, *bldC* and *bldD*, *bldB* has remained somewhat of a mystery. The *S. coelicolor ΔbldB* mutant was first described as a class II *bld* mutant with a non-fragmenting, smooth surface (Merrick, 1976). Due to the lack of more sophisticated research techniques at that time, the early studies of the newly isolated *bld* mutants were focused on their growth on different carbon sources. It was discovered that when different *bld* mutants were grown on minimal media containing mannitol, the bald phenotype was at least partially rescued - however this was not true for the *ΔbldB* mutant, which retained its developmental phenotype (Merrick, 1976). Despite having this pleiotropic bald phenotype, one study reported that the *ΔbldB* mutant was "leaky" and started sporulating and producing actinorhodin upon prolonged incubation (Passantino, Puglia and Chater, 1991). The overexpression of *bldB* in *S. coelicolor* (expressed under the control of its own promoter, on a high-copy plasmid), resulted in a phenotype resembling that of the *whi* mutants, with the overexpression strain being unable to complete sporulation, but able to raise an aerial mycelium (Eccleston *et al.*, 2006).

The *S. coelicolor ΔbldB* mutant has been shown to have an abnormal carbon metabolism, in that genes normally repressed by glucose were found to be expressed in the *ΔbldB* mutant in the presence of glucose in the media (Pope, Green and Westpheling, 1996). Thus, a lot of literature briefly discusses BldB as a regulator of carbon catabolite repression, and some authors specifically suggest a connection between BldB and the glucose kinase GlkA (Gubbens *et al.*, 2017). The *ΔbldB* mutant (as well as the *ΔbldA*, *ΔbldG*, *ΔbldH* and *ΔbldJ* mutants) was reported to acidify the R2YE medium through accumulation of pyruvate and succinate (Viollier *et al.*, 2001). Looking at secondary metabolite biosynthesis, the *S. coelicolor ΔbldB* mutant was found to be unable to produce actinorhodin, methylenomycin, and the calcium-dependent antibiotic CDA (Merrick, 1976; Hopwood and Wright, 1983).

The *S. coelicolor bldB* gene was recently found among the regulon of the principal sigma factor HrdB (Šmídová *et al.*, 2019). The *bldB* gene encodes a small ~11 kDa acidic protein with an unknown function (Eccleston *et al.*, 2002, 2006). BldB has been proposed to be a transcription factor, based on a bioinformatic prediction of the potential presence of a helix-turn-helix Xre domain (Pope, Green and Westpheling, 1998), however its DNA-binding ability has been a subject of controversy in the field. The only evidence for any DNA binding was an early speculation that BldB self-regulates its expression (Pope, Green and Westpheling, 1998), and EMSA results in *Streptomyces lividans*, which stated that BldB binds and represses its own promoter (Mishig-Ochiriin *et al.*, 2003). This result has not been replicated in other studies (Eccleston *et al.*, 2002).

In a *S. coelicolor* quantitative proteomics study, BldB was found to be differentially abundant during the later stages of development (Rioseras *et al.*, 2018), consistent with the same authors' earlier gene expression study, in which they found that *bldB* was upregulated in late development (Yagüe *et al.*, 2014). The *ram* developmental regulators: *ramR* and *ramCSAB* cluster were found not to be expressed in the *S. coelicolor ΔbldB* mutant (Keijser *et al.*, 2002). Since *ramS* codes for the precursor peptide of SapB, the *ΔbldB* mutant was indeed found to be unable to produce this spore-associated peptide (Willey *et al.*, 1991). When conditional *bld* mutants are grown on SFM medium, they regain the ability to form aerial hyphae, and produce the spore surface chaplins. The *S. coelicolor ΔbldB* mutant was an exception - it did not produce aerial hyphae or the chaplins on SFM media (Capstick *et al.*, 2007). The *bldB* gene was found to be upregulated in the *ΔssgA* mutant (Noens *et al.*, 2007), and downregulated in the *ΔohkA* mutant – the *ohkA* gene encodes an antibiotic production regulator kinase (Lu *et al.*, 2011).

In terms of protein structure, several residues have been proposed to influence BldB function. The tyrosine at position 21 in *S. coelicolor* BldB has been a subject of speculation, with authors proposing that this tyrosine is important for protein-protein interactions and multimerisation, or that the tyrosine is phosphorylated, thus activating BldB function (Kelemen and Buttner, 1998; Pope, Green and Westpheling, 1998). More comprehensive biochemical studies suggested that BldB forms asymmetric dimers *in vitro* (Eccleston *et al.*, 2002). The same authors performed a bacterial-two-hybrid assay and confirmed that the *S. coelicolor* 6xHis-BldB is able to self-interact. Using the same approach, they showed that residues 20 to 78 of the *S. coelicolor* BldB are responsible for homodimerisation. However, tyrosine 21 was not required for dimerisation, as a BldB protein with its Y21 swapped for either leucine or cysteine was able to dimerise with itself and with wild-type BldB (Eccleston *et al.*, 2002).

BldB has been found to have numerous homologues in different bacterial species, usually with multiple *bldB* homologues found per genome. These homologues all contain a DUF397 domain, which is a characteristic feature of the BldB family of proteins. Notably, all BldB homologues that have been identified up to this day have been found in filamentous actinomycetes (Eccleston *et al.*, 2006). After an alignment of the protein sequences of all *S. coelicolor* BldB homologues, several conserved residues were identified, and mutated to alanine in the canonical BldB to figure out their importance for BldB function. Out of those conserved residues, 5 (Y21 - already discussed above, W30, R56, W72 and F75) were found to be important for BldB function, as the single alanine substitutions in each amino acid resulted in *ΔbldB*-like mutant strains with defective antibiotic production, and no aerial mycelium formation. It was proposed that W30, R56 and W72 are residues essential for homodimerisation, while Y21 and F75 are important for interactions of BldB with other proteins (Eccleston *et al.*, 2006). So far, only one potential protein partner for BldB has been reported - PkaI, a PknB-like serine-threonine kinase, which is a part of the Streptomyces Spore Wall Synthesising Complex (Vollmer *et al.*, 2019).

In bacteria, the position of a given gene in the genome, and its surrounding genes can provide clues as to possible functional interactions between the proteins encoded by the neighbouring genes. Such genes are often found in operons, under the control of a single promoter. In the case of canonical *S. coelicolor bldB* (*sco5723*), the gene is not found in an operon, and no genes are found immediately surrounding it on the same DNA strand (the closest upstream and downstream genes on the same strand are more than 2 kB away from *bldB*). Its neighbouring genes (*sco5720*, *sco5721*, *sco5722*, *sco5724*, *sco5725*, *sco5731*, *sco5734*, *sco5735*), however, encode proteins that are involved in a type VII secretion system (Akpe San Roman *et al.*, 2010). This is true for other *Streptomyces* species as well - the *bldB* gene was found to be encoded near type VII secretion system genes in *S. griseus*, *S. avermitilis*, *S. pristinaespiralis* and *S. ghanaensis* (**Fig. 3.1**). Two of the aforementioned genes, which are found in an operon - *sco5724* and *sco5725* (*esxB* and *esxA*, respectively), were knocked out - this resulted in delayed sporulation, and irregular aerial hyphae formation of the double mutant (Akpe San Roman *et al.*, 2010). In Δ*bldB*, the expression of *esxBA* was upregulated four-fold at 36 hours post-incubation, compared to wild-type, suggesting that BldB represses *esxBA* expression. In the Δ*esxBA* mutant, the expression of *bldB* was not affected (Akpe San Roman *et al.*, 2010). Interestingly, in *Streptomyces scabies*, the *bldB* gene is not found encoded next to type VII secretion encoding genes - it is encoded elsewhere in the genome (Fyans *et al.*, 2013).

The *bldB* and *whiJ* genes were reported to be missing from *Kitasatospora* - as the rest of the type VII secretion system genes remain, the authors stated that the *bldB* gene "appears to be deleted with surgical precision from the *Kitasatospora* genomes" (Girard *et al.*, 2014; Labeda *et al.*, 2017).

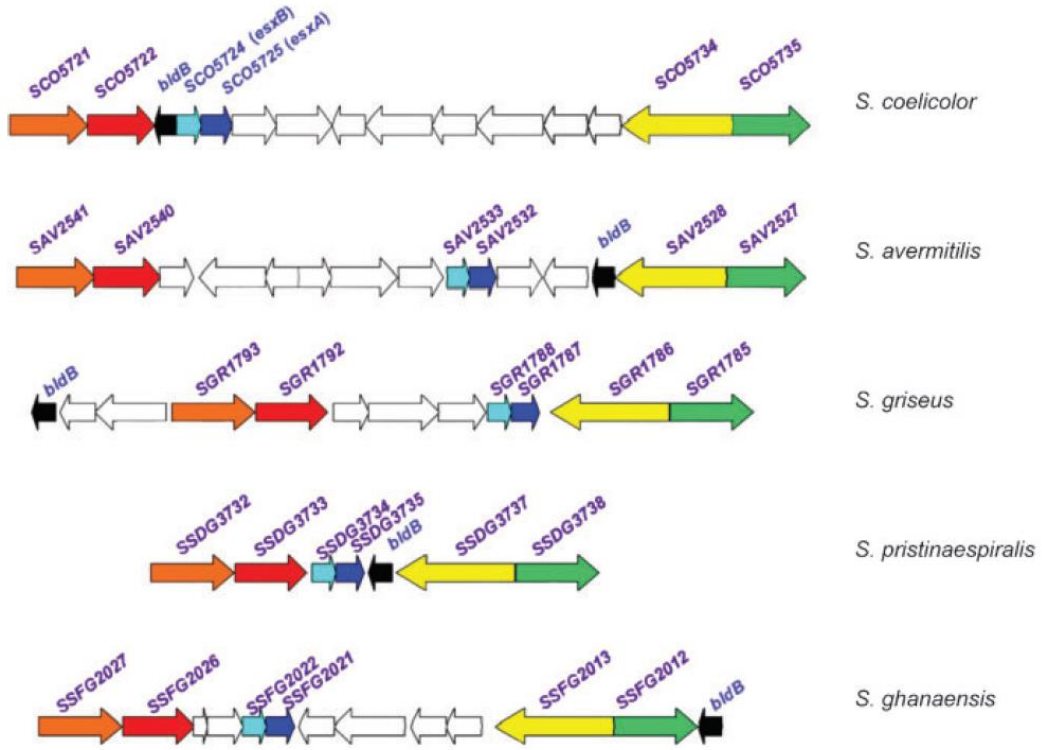

Figure 3.1. Type VII Secretion Clusters in *Streptomyces* Species.

The canonical *bldB* gene is found nestled between type VII secretion genes in different *Streptomyces* species. Figure reproduced with permission from Akpe San Roman *et al*., (2010).

Strikingly, most other “non-canonical” *bldB* homologues across different *Streptomyces* species are found encoded next to homologues of *abaA orfA* (encoding predicted anti-sigma factors with HATPase_c domains), and/ or homologues of *whiJ* - encoding predicted DNA-binding proteins with N-terminal HTH-Xre domains (Chater and Chandra, 2006; Chandra and Chater, 2014). The genomic context of the *S. coelicolor bldB* homologues is represented in **Figure 3.2**. Several studies have described aspects of this syntenic relationship between the homologues of *bldB*, *whiJ* and *abaA orfA*, as detailed below.

abaA was first described in a study in which the overexpression of a 5-gene locus in *S. coelicolor* and *S. lividans* resulted in an increased production of actinorhodin - for this reason the whole locus was called *abaA* (standing for **a**ntibiotic **b**iosynthesis **a**ctivator **A**), and the genes within the locus were designated *orfA* to *orfE* (Fernández-Moreno *et al.*, 1992). One of the genes in this locus - *abaA orfD* - is a homologue of *bldB* as it encodes a protein with a DUF397 domain. Found immediately downstream, *abaA orfE* encodes a homologue of WhiJ, and *abaA orfA* encodes a predicted anti-sigma factor. The BldB homologue in this locus (SCO0703, AbaA OrfD) was reported to homodimerise, in a similar fashion to the canonical *S. coelicolor* BldB (Eccleston *et al.*, 2006).

In a study of transposon insertion mutants in *S. coelicolor,* one of the mutants exhibited a classical white phenotype, with observed production of undifferentiated aerial hyphae (Gehring *et al.*, 2000). The authors struggled to map the insertion precisely, as the Sanger sequence of *S. coelicolor* genome had not been finalised yet at the time, but they were able to discern that the insertion had occurred in a region that contained a *bldB*, a *whiJ* and an *abaA orfA* homologue (or as they refer to them, the 63 codon ORF, the 283 codon ORF, and the 141 codon ORF, respectively). They noted the existence of at least 21 *whiJ* homologues in *S. coelicolor*, with 16 of them having a *bldB* homologue encoded immediately downstream, and 8 of those 16 also having an *abaA orfA* homologue encoded upstream of the *whiJ* homologue on the opposite strand (Gehring *et al.*, 2000). From the provided sequences, I was able to deduce that the transposon insertion discussed in this paper covered *sco4542* (*bldB* homologue), *sco4543* (canonical *whiJ*), and *sco4544* (*abaA orfA* homologue).

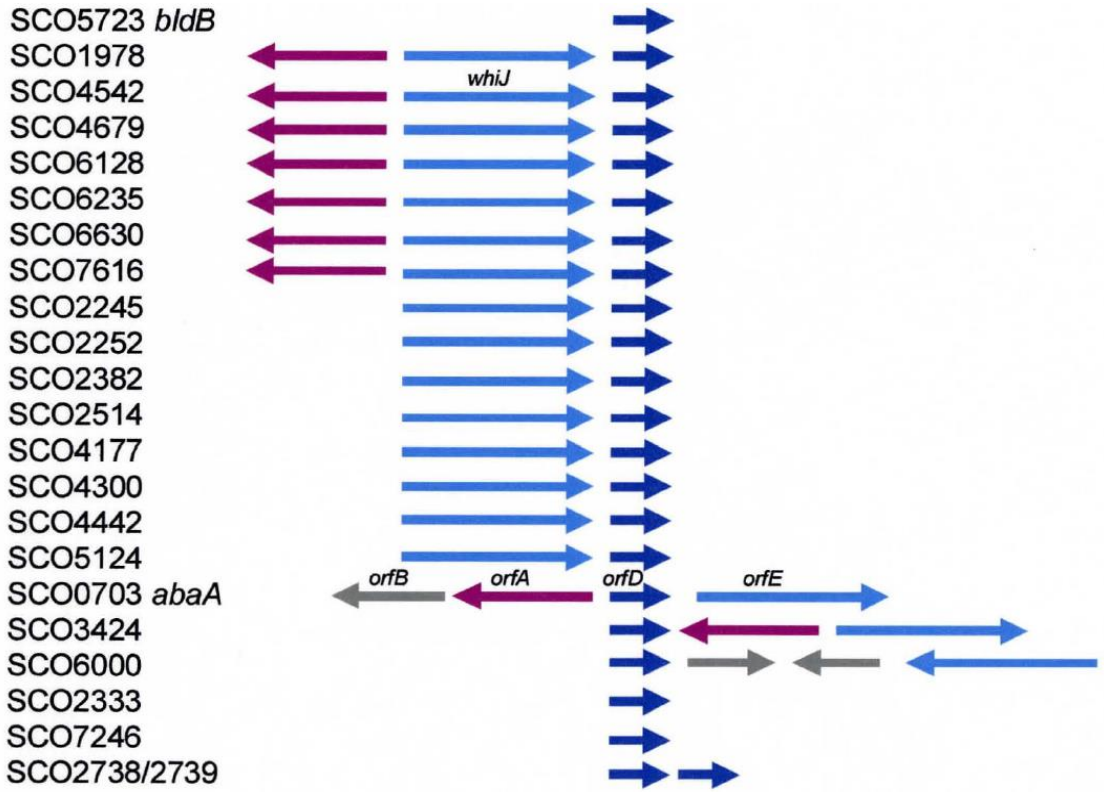

Figure 3.2. The *bldB*, *whiJ* and *abaA orfA* Homologues in *Streptomyces coelicolor*.

Homologues of *bldB* (dark blue) in *S. coelicolor* are often found encoded next to homologues of *whiJ* (light blue) and *abaA orfA* (purple). Figure reproduced with permission from Marton (2008).

Another BldB - WhiJ pair (SCO4441 and SCO4442) was designated Scr1 and Scr2 respectively (standing for ***S**treptomyces **c**oelicolor* **r**egulator) (Santamaría *et al.*, 2018). The Δ*scr1*Δ*scr2* double mutant had a wild-type phenotype; while the *scr1* and *scr2* double overexpression strain had a slight developmental delay. In both *S. coelicolor* and *S. lividans*, the overexpression of *scr1* alone led to increased actinorhodin and prodiginine production. This did not occur when it was overexpressed in the Δ*scr2* mutant, which suggests that Scr1 (the WhiJ homologue) is an activator of antibiotic biosynthesis, and that it only acts as one in the presence of Scr2 (the BldB homologue). When the authors overexpressed *scr1* and *scr2* in several *Streptomyces* species, they observed production of previously unobserved metabolites, so they concluded that the *scr1 scr2* double overexpression construct could be used as a biotechnological tool to awaken cryptic natural product clusters (Santamaría *et al.*, 2018).

There is at least one instance in which a pair of *bldB* and *whiJ* homologues is found in a biosynthetic gene cluster - designated *sky9* and *sky8* respectively in the skyllamycin gene cluster in *Streptomyces* sp. Acta 2897 (Pohle *et al.*, 2011). The authors suggested that the WhiJ homologue (and potentially the BldB homologue) is one of the transcriptional regulators for the skyllamycin cluster.

In a more comprehensive study of transcriptional regulation in *Streptomyces clavuligerus*, the authors also remarked on the abundance of transcriptional unit clusters containing *bldB* and *whiJ* homologues - 24 in total in *S. clavuligerus* (Hwang *et al.*, 2021). When they compared the protein sequences of BldB and WhiJ homologues encoded next to each other versus the sequences of unpaired homologues, they found that the pairwise distances of the paired BldB or WhiJ homologues was lower than that of the unpaired ones. The authors suggest that this points to distinct biological functions between the respective paired homologues, as opposed to the unpaired ones.

For the *S. coelicolor* locus containing the canonical *whiJ* (*sco4543*), as well as a *bldB* homologue (*sco4542*) and an *abaA orfA* homologue (*sco4544*), a partial *whiJ* deletion mutant (with codons 1 to 93 intact to form a truncated protein) was constructed (Aínsa *et al.*, 2010). It exhibited the classical white phenotype - its aerial mycelium was composed of straight unbranched hyphae, which could not go on to sporulate. This phenotype could be complemented by re-introducing the full-length *whiJ* gene. When the entire *whiJ* gene was deleted, however, the resulting mutant had no developmental phenotype. The same authors did some further mutation analyses (Aínsa *et al.*, 2010). When they knocked out *sco4542* (*bldB* homologue), the resulting ex-conjugants were bald when grown on SFM medium, but able to form an aerial mycelium (though still unable to sporulate) when grown on R2YE medium. Finally, they knocked out both *sco4542* and *sco4543* (canonical *whiJ*), which resulted in a double mutant with a wild-type phenotype, which suggests that canonical WhiJ and its neighbouring BldB homologue SCO4542 function together in the same pathway.

In a bioinformatic study of genome evolution through recombination in different *Streptomyces pratensis* isolates, it was found that WhiJ and BldB homologues co-evolve in a paired fashion (Doroghazi and Buckley, 2014). This conservation of pairing has led to the hypothesis that WhiJ and BldB homologues are an example of a novel toxin-antitoxin-like system in *Streptomyces* (Makarova, Wolf and Koonin, 2009). Chater and Chandra (2014) speculate that canonical BldB interacts promiscuously with multiple WhiJ homologues, which leads to the more severe developmental phenotype of the Δ*bldB* mutant.

Results

BldB Has 10 Homologues in *Streptomyces venezuelae*

Before delving into experimental work, I undertook a bioinformatic study on the *bldB* homologues, with significant help from Dr Govind Chandra. First, a collection of 30,772 bacterial genomes was assembled - this collection is current as of 21/09/2021. All bioinformatic work described in **Figures 3.3**, **3.4**, **3.5**, **3.6** and **Table 3.1** is based on this collection of genomes. As BldB homologues have thus far only been reported in filamentous actinomycetes (Eccleston *et al.*, 2006), our collection of genomes is intentionally heavily biased in favour of Actinobacteria genomes. All available Actinobacteria genomes were included in this collection, whereas only reference or representative genomes were included for all other bacteria, which is why the number of "Other Bacteria" genomes is so low in comparison (**Fig. 3.3**). Out of the 22,541 actinobacterial genomes, *bldB* homologues can only be found in 14.9%, or 3,358 genomes. No *bldB* homologues were found in the 8,231 "Other Bacteria" genomes. Out of the 3,358 *bldB*-containing Actinobacteria genomes, 1,825 (or 54.3%) were *Streptomyces* genomes. Only 7 *Streptomyces* genomes were found to not have any *bldB* homologues (**Fig. 3.3**).

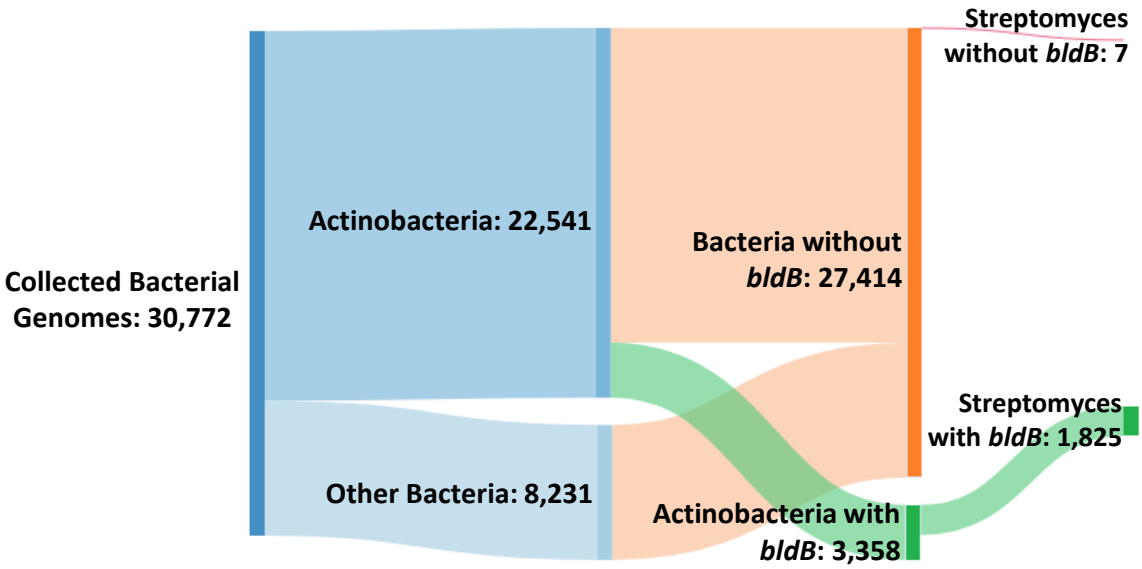

Figure 3.3. Presence or Absence of *bldB* Homologues in the 21/09/2021 Collection of Genomes.

Sankey diagram illustrating the macro-level phylogeny and number of genomes with and without homologues of *bldB*.

In some preliminary BLAST searches, I found that while most BldB homologues appear to be small proteins, mainly consisting of the DUF397 domain, there are a few that are longer and may contain alternative domains. Any alternative domains that have already been characterised for these “long” BldB' homologues could point towards a function for the canonical BldB itself.

From the 21/09/2021 genome collection, the protein lengths of 64,651 BldB homologues were collected and represented in **Fig. 3.4**. As literature and my preliminary studies suggested, the bulk of BldB homologues have a protein length of under 100 amino acids (**Fig. 3.4A**). This suggests that indeed, most BldB homologues are quite small proteins, compared to the average bacterial protein length - reported as ranging from 312 - 320 amino acids (Tiessen, Pérez-Rodríguez and Delaye-Arredondo, 2012; Kozlowski, 2017). Protein size can have implications for the potential function of BldB - small proteins with single domains must have a more limited functionality than larger multidomain proteins. This put protein-protein interaction experiments on the agenda - BldB might have protein partner(s), which allow it to perform a larger range of functions in tandem.

Looking more closely at the distribution of BldB protein lengths (**Fig. 3.4B**), I could see that while most BldB homologues are ≤100 amino acids long, there are still quite a few “long” BldB homologues. A conserved domain (CD) search was run on these long homologues, to find any domains additional to the DUF397 motif. Results are summarised in **Table 3.1**.

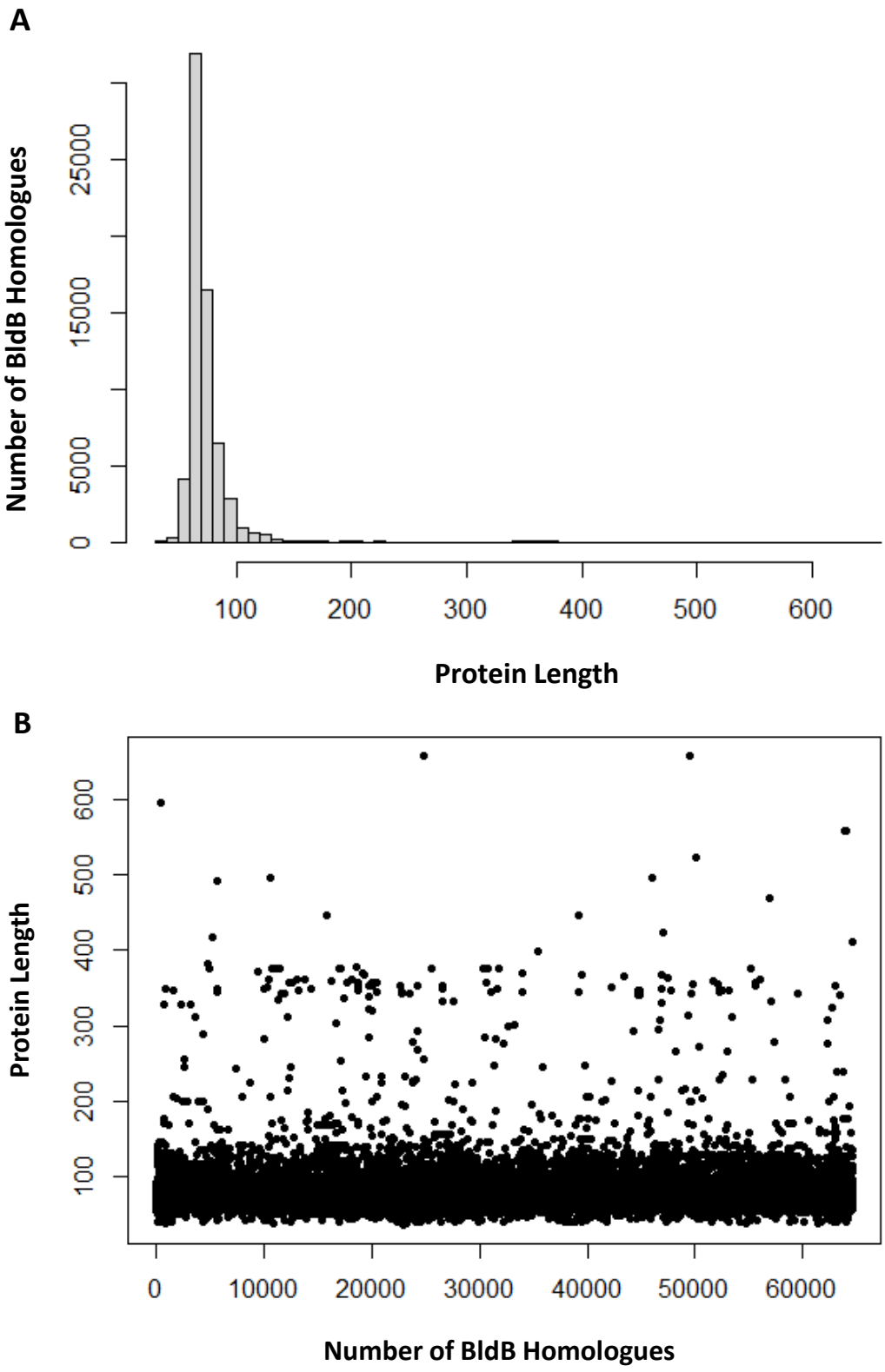

Figure 3.4. Distribution of BldB Homologue Protein Length.

(A) Histogram representing the protein lengths of 64,651 BldB homologues collected from the 3,358 bacterial genomes. **(B)** Dot plot representing the distribution of protein lengths from the same set of BldB homologues.

Table 3.1. “Long” BldB Homologues with Alternative Domains.

Domain	Number of BldB Homologues
HTH	129
2x DUF397	53
3x DUF397	6
DUF4185	5
TIR domain	3
Acetyltransferase	2
Methyltransferase	2
Hydrolase	2
Peptide deformylase	2
DNA Polymerase subunits gamma and tau	2
Tegument	2
UTRA Ligand Binding	2
Aminotransferase	1
Rho transcription termination factor	1
ATPase - ParA, MinD like	1
Carboxylate reductase	1
Cytochrome oxidase	1
DUF427	1
DUF772 transposase	1
MFS transporter	1
NIMA kinase	1
Outer membrane porin	1
Phosphotransferase	1

59 of the “long” BldB homologues have multiple DUF397 domains - it would be interesting to find out what the implications of having 2 or 3 DUF397 domains might be for these proteins (**Table 3.1**). 129 homologues have a helix-turn-helix domain with significant homology to the HTH-Xre motif found in WhiJ homologues. This means that these proteins represent fusions of BldB and WhiJ, which could suggest that the separate BldB and WhiJ proteins might bind and have a collaborative function, be it DNA binding or something else. 5 BldB homologues have a DUF4185 domain, and 3 have a TIR domain (**Table 3.1**). There is not much information about the DUF4185 domain, but proteins with this domain are described as sharing homology with sialidases - enzymes that cleave the terminal sialic acid off carbohydrate moieties (Ramakrishnan *et al.*, 2015). TIR (Toll/interleukin-1 receptor) domains in bacteria have been associated with virulence (Cirl *et al.*, 2008), and have more recently been found to have NADase activity (Essuman *et al.*, 2018). Furthermore, 2 BldB homologues have methyltransferase domains (**Table 3.1**). Proteins with methyltransferase domains are sometimes found encoded in the vicinity of *bldB-whiJ-abaA orfA* containing loci, so this finding might be biologically relevant.

Another question I wanted to answer concerned the number of *bldB* homologues found per bacterial genome. Once again, sourcing the initial genome collection, I plotted the number of *bldB* homologues against the number of genomes, in which they were found (**Fig. 3.5**). The minimum number of *bldB* homologues was a single homologue found in 71 genomes; the maximum number was 94 homologues, found in one genome (*Actinomadura craniellae*). The median number of *bldB* homologues per genome was 19, so *S. coelicolor* goes over the median with 24 homologues, and *S. venezuelae* goes under with 11 homologues.

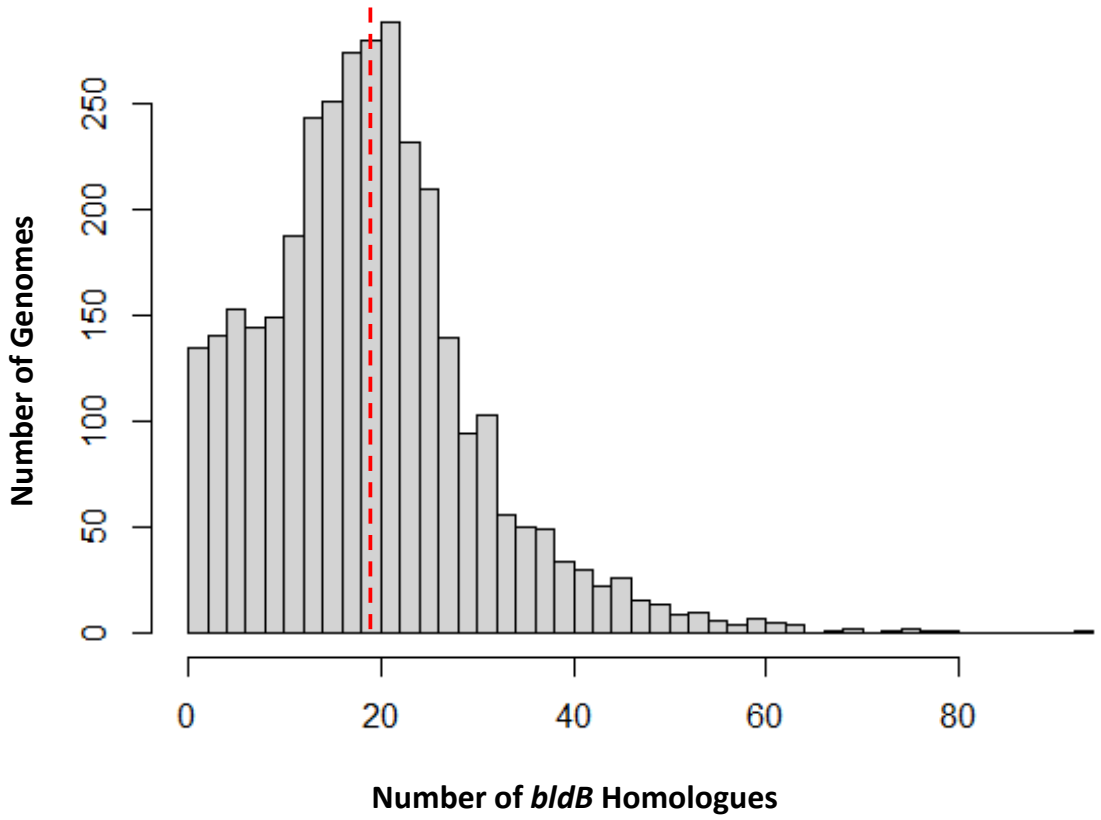

Figure 3.5. Distribution of *bldB* Homologues per Genome.

Histogram representing the number of *bldB* homologues found per bacterial genome. Red dashed line indicates the median.

In addition to the "canonical" *bldB* (the direct orthologue of *S. coelicolor bldB*), the model species of this study - *S. venezuelae* has 10 other *bldB* homologues, which I designated *bldB2* to *bldB11* (**Fig. 3.6**). Each one of these 10 homologues is encoded next to a *whiJ* homologue, and 5 of them also have a homologue of *abaA orfA* (referred to as *abaA* from here onwards) encoded in the vicinity. I designated numbers for these *whiJ* and *abaA* homologues that connect to my nomenclature for the *bldB* homologues, so I refer to the 10 *whiJ* homologues as *whiJ2* to *whiJ11*, and the 5 *abaA* homologues as *abaA3, abaA4, abaA6, abaA7* and *abaA10* (**Fig. 3.6**).

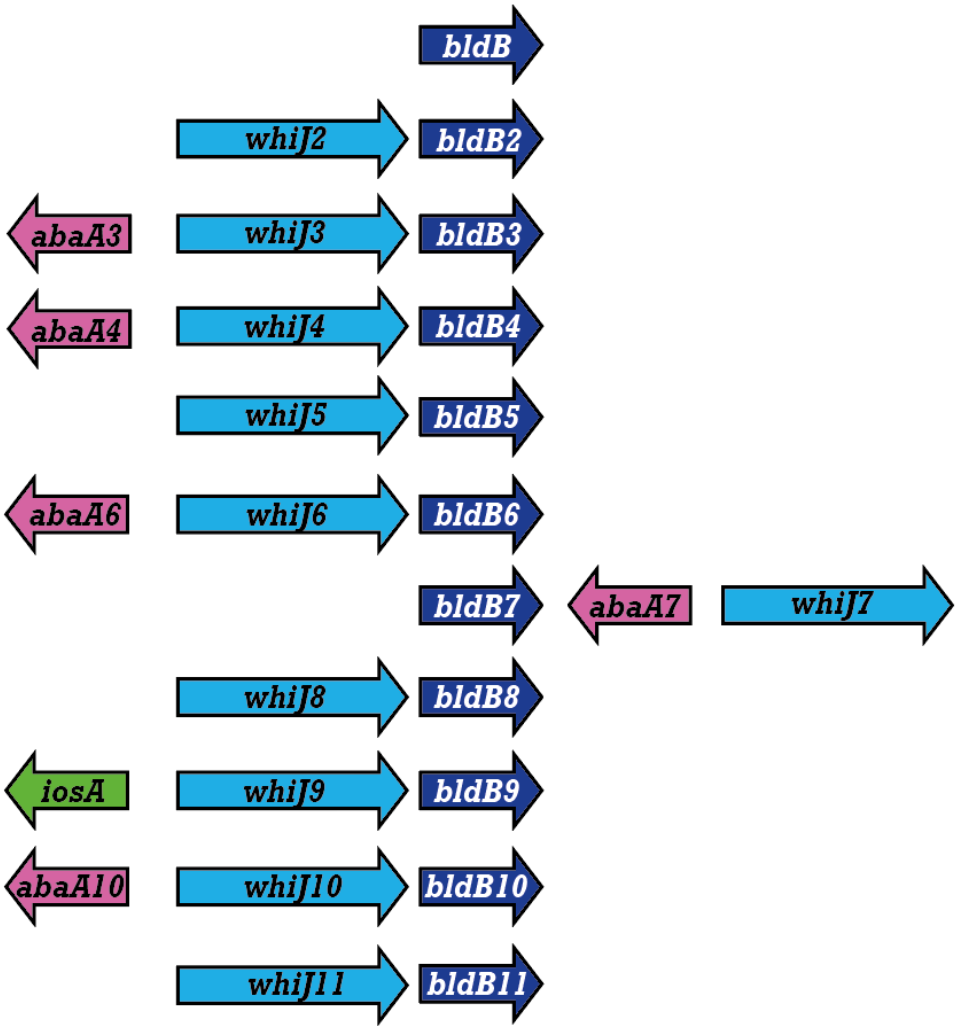

Figure 3.6. Genomic Arrangement of the *bldB*, *whiJ* and *abaA* Homologues in *S. venezuelae*.

Arrow chart representing the genomic arrangement of the canonical *bldB* gene, its homologues (*bldB2* to *bldB11*), and the *whiJ* and *abaA* homologues encoded near the *bldB* homologues. Vnz identifiers for the genes are as follows: *bldB – vnz26620, bldB2 – vnz15145, bldB3 – vnz29075, bldB4 – vnz25555, bldB5 – vnz20565, bldB6 – vnz09895, bldB7 – vnz16140, bldB8 – vnz28285, bldB9 – vnz16680, bldB10 – vnz31505, bldB11 – vnz28375, whiJ2 – vnz15140, whiJ3 – vnz29080, whiJ4 – vnz25560, whiJ5 – vnz20560, whiJ6 – vnz09900, whiJ7 – vnz16130, whiJ8 – vnz28280, whiJ9 – vnz16675, whiJ10 – vnz31500, whiJ11 – vnz28370, abaA3 – vnz29085, abaA4 – vnz25565, abaA6 – vnz09905, abaA7 – vnz16135, abaA10 – vnz31495, iosA – vnz16670.*

BldB is Necessary for Aerial Mycelium Formation and Sporulation in *S. venezuelae*

In order to establish whether BldB is necessary for normal development in *Streptomyces venezuelae*, as it is in *S. coelicolor*, I constructed a Δ*bldB* mutant using the Redirect approach (Gust *et al.*, 2003). I isolated apramycin-resistant, kanamycin-sensitive ex-conjugants, and verified the presence of the apramycin resistance cassette in place of the native gene by PCR. All verified Δ*bldB* ex-conjugants exhibited a bald phenotype on SFM and DNA, however, slight differences in phenotype became apparent when I grew the mutant candidates on MYM agar. The ex-conjugants exhibited varying levels of melanin production, and more concerningly - inconsistent bald “sub-phenotypes”. Under a stereo microscope, the mutant candidates with a high production of melanin had what is considered a “classical" bald phenotype - consisting largely of tight clumps of vegetative mycelium, reminiscent of the phenotype of the *S. venezuelae* Δ*bldM* mutant (Al-Bassam *et al.*, 2014). The candidates with low melanin production had a Δ*bldC*-like phenotype (Bush *et al.*, 2019), where precocious hypersporulation without the formation of aerial hyphae had occurred.

The inconsistency in phenotypes in these confirmed Δ*bldB* ex-conjugants was most likely caused by secondary suppressor mutation(s) in some isolates. To address this inconsistency in phenotypes, I complemented the mutant candidates with a wild-type copy of the *bldB* gene *in trans*, using the pSS170 vector. I expected that only one of the two Δ*bldB* sub-phenotypes (the ‘true’ Δ*bldB* phenotype) would be successfully complemented and result in a restoration of the wild-type phenotype. Surprisingly, sporulation was restored to both sub-phenotypes. To resolve this issue and obtain a clean *ΔbldB* strain free of potential suppressor mutations, I used two approaches.

Firstly, I used the Redirect method once again to generate a second set of *ΔbldB* mutants. This time, I streaked out the resulting ex-conjugates to single colonies on MYM medium only, in order to monitor the phenotype of the mutants between streak-outs. I only obtained 7 apramycin-resistant ex-conjugates this time, and interestingly, in the initial SFM conjugation plates, 2 of the 7 ex-conjugant colonies were mostly bald, but with a white, fuzzy quarter-section of the colony. This is indicative of potential genetic instability of the *ΔbldB* mutant strains.

Secondly, I did phage transduction using the *S. venezuelae* generalised transducing phage SV1 (Stuttard, 1979). In this approach, I used the SV1 phage to infect two *ΔbldB* candidate strains from the first round of Redirect mutagenesis - a precociously sporulating one, and a clumping vegetative growth one. I isolated the mutant phage lysates and then used them to infect wild-type *S. venezuelae*, resulting in apramycin-resistant *ΔbldB* transductants. Since the SV1 phage is only able to package approximately 40 kilobases of host DNA, only the 40 kB stretch of DNA surrounding the apramycin resistance marker in the *ΔbldB* mutant was transduced into the new wild-type host, yielding apramycin-resistant *ΔbldB* strains in a clean background. The assumption here was that the suppressor mutation(s) did not occur in such close proximity to the original *bldB* gene - otherwise this approach would be ineffective in producing a “clean” *ΔbldB* mutant.

Indeed, when I infected wild-type *S. venezuelae* with either phage lysate from the infection of a hypersporulating bald mutant, or phage lysate from a “classical” bald mutant, all resulting *ΔbldB* transductants had “classical” bald phenotypes with clumping growth. This showed that the true *ΔbldB* phenotype was caused by the inability to produce aerial hyphae, rather than by precocious sporulation.

I complemented four *ΔbldB* transductants and five *ΔbldB* ex-conjugates from the second round of Redirect mutagenesis with a wild-type copy of the *bldB* gene *in trans* - in all of them sporulation was restored to wild-type levels. When I introduced a pSS170 empty vector into these mutants as a negative control, the resulting colonies remained bald. Thus, I chose a representative transductant as the *ΔbldB* mutant (designated SV100), which I used in all subsequent experiments in this thesis. Suppressor mutations remained a potential problem, and something I watched out for before every experiment using the *ΔbldB* mutant.

While the 2-day-old *ΔbldB* strain appears completely bald on MYM agar, upon longer incubation the edges of the *ΔbldB* colonies become white and fuzzy, while the centre sections remain bald (**Fig. 3.7**). This is indicative of sparse aerial hyphae formation at the periphery of the colonies. I noted, however, that when grown in liquid MYM, the Δ*bldB* mutant is able to sporulate at a rate comparable to that of WT *S. venezuelae*.

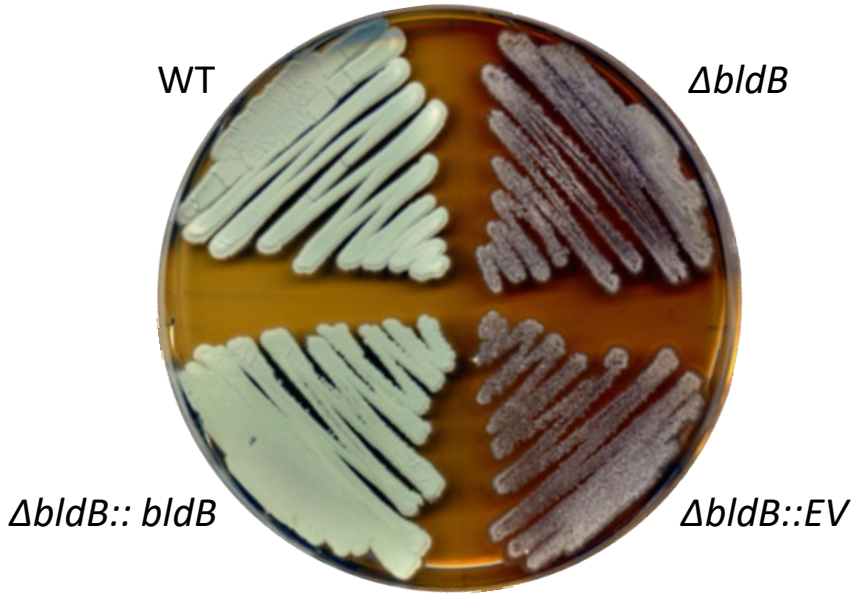

Figure 3.7. The Bald Phenotype of the *S. venezuelae ΔbldB* Mutant.

Plate depicting the growth of the *ΔbldB* mutant and its complementation strain on MYM agar. EV stands for empty pSS170 vector control. Plate image was taken after a 4-day incubation at 28˚C.

To better characterise the phenotype of the *ΔbldB* mutant, scanning electron microscopy was performed by Kim Findlay from JIC Bioimaging. The centre section of the *ΔbldB* colony was indeed bald - the vegetative mycelium could be observed, but there was no visible aerial mycelium (**Fig. 3.8B**). The periphery of the *ΔbldB* colony exhibited aerial hyphae growth with some sporadic sporulation (**Fig. 3.8C**). However, these mostly undifferentiated hyphae looked unhealthy, some were lysed, and the growth pattern was not comparable to that of the sporulating wild-type *S.venezuelae* colony (**Fig. 3.8A**). The complemented *ΔbldB* strain exhibited restored sporulation (**Fig. 3.8D**).

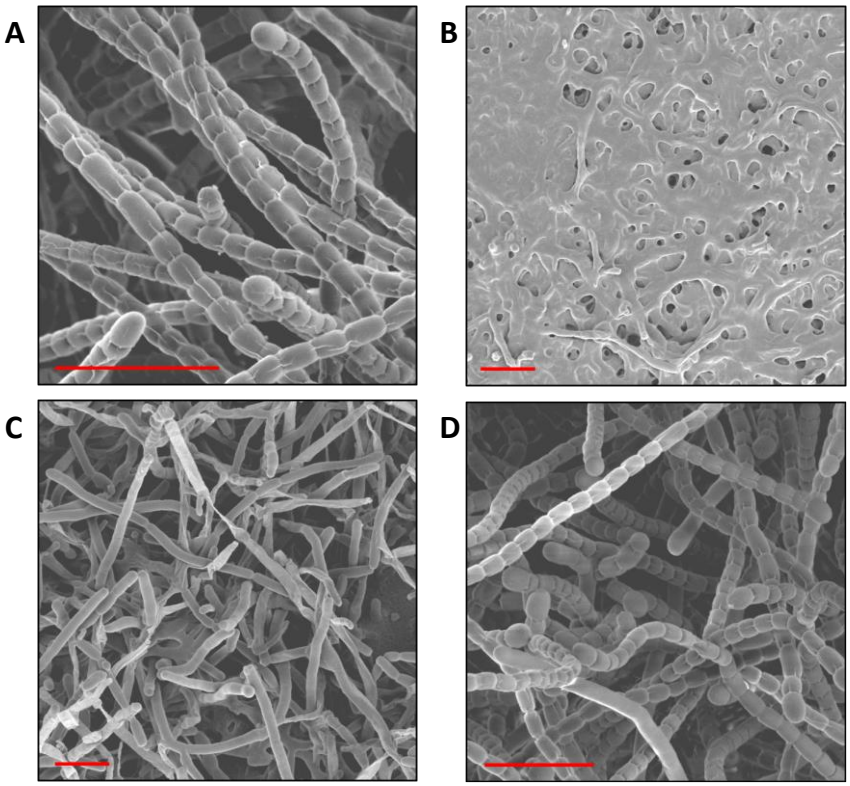

Figure 3.8. Phenotype Characterisation of the *S. venezuelae ΔbldB* Mutant.

Scanning electron micrographs comparing the phenotypes of wild-type *S. venezuelae* **(A),** the bald colony centre of the *ΔbldB* mutant **(B)** the aerial hyphae-rich colony periphery of the *ΔbldB* mutant **(C)**, and the complemented *ΔbldB* strain **(D).** Scale bars in red indicate 5 µm.

The Overexpression of *bldB* Has No Impact on *Streptomyces* Development

To overexpress *bldB* in *S. venezuelae*, I cloned the *bldB* gene into pIJ10257, so that it would be placed under the control of the constitutive *ermE** promoter (Bibb, Janssen and Ward, 1985), and conjugated the assembled construct into wild-type *S. venezuelae*. I then performed an automated Western blot (using the anti-BldB polyclonal antibody I generated) to confirm the enhanced production of BldB in this overexpression strain compared to wild-type *S. venezuelae* (**Fig. 3.9**). This result also served to validate the *ΔbldB* strain, in which I saw no production of BldB.

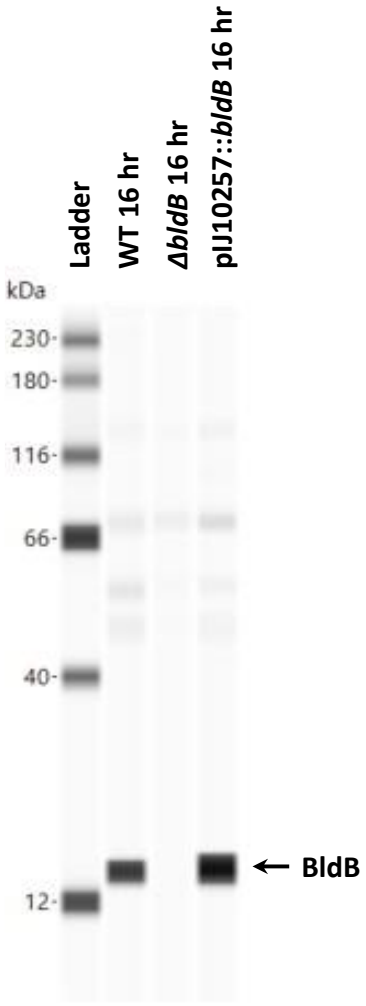

Figure 3.9. Validation of BldB Overexpression via Western Blot.

The levels of BldB were measured using an automated quantitative Western blot using a polyclonal anti-BldB antibody. Samples were taken at 16 hours post-inoculation from wild-type *S. venezuelae*, the *ΔbldB* mutant and the pIJ10257::*bldB* overexpression strain. All samples were diluted to the same total protein concentration, as determined by Bradford assays. A single replicate is shown for each sample. Arrow indicates the BldB bands at ~17 kDa.

On MYM agar, the *bldB* overexpression strain was able to sporulate to wild-type-like levels (**Fig. 3.10**). I validated this using SEM - the *bldB* overexpression strain looked indistinguishable from wild type *S. venezuelae* or the empty vector control in its ability to produce spores (**Fig. 3.11**).

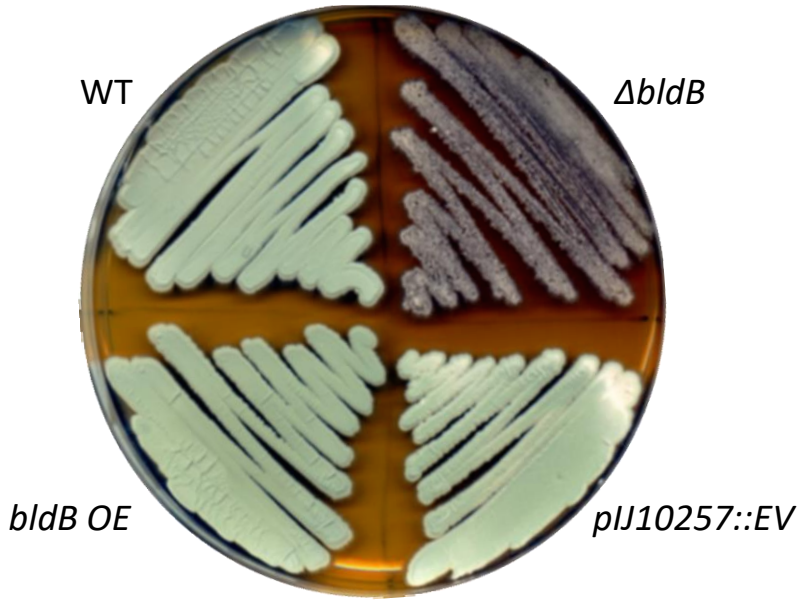

Figure 3.10. Overexpression of *bldB* in *S. venezuelae*.

Plate depicting the growth of the *bldB* overexpression strain on MYM agar. EV stands for empty pIJ10257 vector control. Plate image was taken after a 4-day incubation at 28˚C.

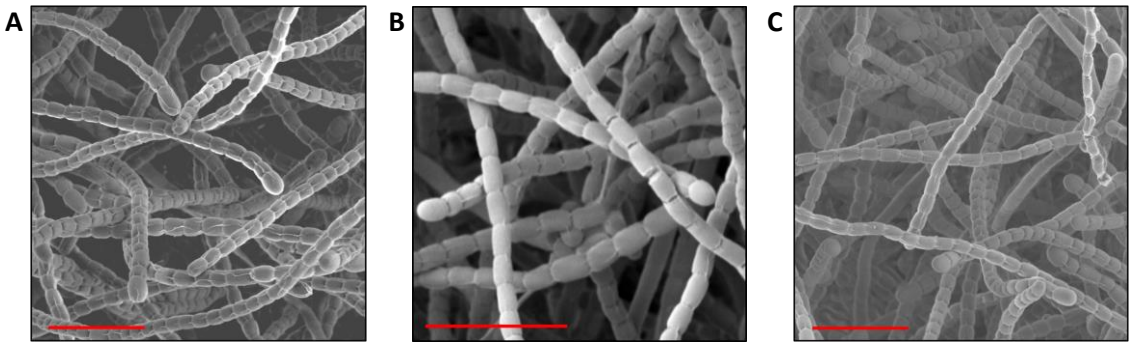

Figure 3.11. Phenotypic Characterisation of the *S. venezuelae bldB* Overexpression Strain.

Scanning electron micrographs comparing the phenotypes of wild-type *S. venezuelae* **(A)**, the pIJ10257 empty vector control **(B)**, and the *bldB* overexpression strain **(C).** Scale bars in red indicate 5 µm.

A Bacterial-Two-Hybrid Library Screen Identified Possible Protein Partners for BldB

Identifying interacting proteins might give insight into the function of BldB in the *Streptomyces* developmental cascade. To help identify proteins that BldB might interact with, I undertook a bacterial-two-hybrid experiment (Karimova *et al.*, 1998; Karimova, Ullmann and Ladant, 2000). Here, I took advantage of the already constructed *S. venezuelae* bacterial-two-hybrid shotgun libraries available in the Buttner lab, as cited previously (Gallagher *et al.*, 2020; Stewart *et al.*, 2020). To build the libraries, *S. venezuelae* genomic DNA was sonicated, and the resulting DNA fragments cloned into the pUT18C and pKT25 vectors to produce fusions with the adenylate cyclase peptides. A great advantage of using these libraries is that the resulting clones are truly random - due to the use of sonicated genomic DNA instead of DNA digested with restriction enzymes. This eliminates the chance of any restriction digest-related bias and makes sampling the libraries truly representative, with the *S. venezuelae* genome covered in each library an estimated 40 times, to aid a thorough screen for protein-protein interactions.

I performed two independent bacterial-two-hybrid screens of both libraries with 4 “bait” constructs, where I fused the full-length BldB to either the N- or C-terminus of the T18 and T25 peptides. After growth on MacConkey agar to assess strength of interaction, I isolated and sequenced a total of 267 library-derived positive clones. After removing common false positive hits (*e.g.* adenylate cyclase), I ended up with 123 in-frame, good quality hits, representing 106 *Streptomyces* proteins. **Table 3.2** contains a selection of the hits that might be of particular interest for this study.

Most library screen hits were isolated only once, which could indicate that they are false positives. Among the hits, however, some patterns can be found - there are 13 proteins annotated as “transcriptional regulator”, 11 proteins annotated as some kind of transporter, and several proteins, which have a role in development, such as CRP, FtsI, SigT, and DisA (Derouaux *et al.*, 2004; Bennett *et al.*, 2009; Mao *et al.*, 2009; Latoscha *et al.*, 2020).

The hits that seemed most promising to me, as they came up in the screen more than once, were four of the non-canonical BldB homologues (BldB3, BldB4, BldB5 and BldB9). In addition to this, other hits of particular interest were two WhiJ-like proteins (Vnz20185 and Vnz28290), and the multidomain protein OsaC (Vnz26705), which has the HATPase_c domain characteristic of the AbaA homologues.

Each BldB homologue that came up in the screens is encoded next to a WhiJ homologue, which did not appear in the screens (but interaction cannot be ruled out). The WhiJ-like proteins that did come up in the screens do not have BldB homologues encoded nearby.

Table 3.2. BldB Bacterial-Two-Hybrid Library Screen Results.

Protein	Number of Hits	Predicted Function and Domains of Interest
Vnz21035	3	Drug:proton antiporter
Vnz16680	3	BldB9
Vnz07430	3	AraC family transcriptional regulator
Vnz36375	2	MFS transporter
Vnz30925	2	Cytochrome
Vnz29075	2	BldB3
Vnz25750	2	Citramalate synthase
Vnz25555	2	BldB4
Vnz23620	2	TetR family transcriptional regulator
Vnz20565	2	BldB5
Vnz20185	2	Transcriptional regulator, HTH-Xre domain
Vnz16460	2	Crp/Fnr family transcriptional regulator
Vnz08765	2	Arsenical pump-driving ATPase
Vnz35365	1	DNA-binding response regulator
Vnz33135	1	Sugar ABC transporter ATP-binding protein
Vnz32830	1	Xylose isomerase
Vnz32160	1	Pirin
Vnz28920	1	Phage tail protein, eCIS component
Vnz28460	1	Two-component sensor histidine kinase
Vnz28355	1	Helicase
Vnz28290	1	Transcriptional regulator, HTH-Xre domain

Protein	Number of Hits	Predicted Function and Domains of Interest
Vnz27110	1	ATP-dependent helicase
Vnz26835	1	Hypothetical protein, zinc finger domain
Vnz26705	1	PAS domain S-box protein – **OsaC**
Vnz26075	1	Chromosome partition protein SMC
Vnz25780	1	DNA polymerase III subunit beta
Vnz25185	1	Maltokinase
Vnz24575	1	Hypothetical protein, DNA polymerase III subunits
Vnz24535	1	Tetratricopeptide repeat protein, ATPase domain
Vnz24380	1	Aminoglycoside phosphotransferase
Vnz24335	1	LysR family transcriptional regulator
Vnz23555	1	Peptide ABC transporter substrate-binding protein
Vnz22040	1	Hypothetical protein, kinase domains
Vnz20095	1	MFS transporter
Vnz20070	1	CmlR1 chloramphenicol resistance protein
Vnz18710	1	MFS transporter
Vnz18040	1	RNA polymerase sigma factor SigT
Vnz17735	1	AsnC family transcriptional regulator
Vnz17395	1	ABC transporter
Vnz17225	1	LuxR family transcriptional regulator
Vnz15820	1	DNA integrity scanning protein DisA
Vnz13350	1	LysR family transcriptional regulator
Vnz12995	1	MFS transporter
Vnz12710	1	Transcriptional regulator
Vnz12595	1	DesD, desferrioxamine biosynthesis protein
Vnz12315	1	Transcriptional regulator, GAF domain
Vnz11450	1	LepA, elongation factor 4, GTP-binding domain

Protein	Number of Hits	Predicted Function and Domains of Interest
Vnz09520	1	AfsR family transcriptional regulator
Vnz08560	1	Cell division protein FtsI
Vnz07125	1	Hypothetical protein, ATPase domain
Vnz06745	1	DNA-binding transcriptional regulator
Vnz05975	1	Cytochrome P450
Vnz02580	1	MFS transporter
Vnz01295	1	Hypothetical protein, ATPase domain

BldB Interacts Strongly with 7 of the Non-Canonical BldB Homologues

Because sonication generated random genomic DNA fragments in the construction of the bacterial-two-hybrid libraries, any library clones that exhibited strong protein-protein interactions with the 'bait' BldB protein only represent truncated peptides, as opposed to full-length proteins. As a consequence, I followed up these initial library screens with one-on-one bacterial-two-hybrid β-galactosidase assays using full-length proteins.

I decided to examine the strength of interaction between canonical BldB and all 10 of its *S. venezuelae* homologues, anticipating that there would be varying degrees of interaction, as only 4 homologues came up in the library screen (**Table 3.2**). To ensure that none of the assayed proteins interact with the T18 or T25 peptides, I performed empty vector negative controls. None of the negative controls showed any interaction. For clarity, only one representative negative control is shown in **Figure 3.12**.

BldB did not appear to self-interact (*i.e.* homodimerise) strongly in this experiment (**Fig. 3.12**). However, it interacted strongly (strength of interaction comparable to the T18C-zip-T25-zip positive control) with 7 of its homologues - BldB3, BldB4, BldB5, BldB6, BldB8, BldB9, and BldB11 (**Fig. 3.12**). Self-interaction assays with these 7 homologues showed weak to background interaction in comparison. Two of the homologues - BldB7 and BldB10 did not interact with BldB - instead, their self-interactions were stronger. BldB2 did not interact with BldB or with itself (**Fig. 3.12**). Overall, this suggested that the homologues favour either an interaction with BldB or self-interaction, but not both.

While two-hybrid assays are a powerful *in vivo* tool for measuring protein-protein interaction strength, they also have their weaknesses. Bacterial-two-hybrid experiments are performed using *E. coli*, with the tested proteins overexpressed at the same time. This is not necessarily indicative of interactions in *Streptomyces*, where the proteins of interest might be expressed in a different time or place during the life cycle. In the case of BldB itself, from timecourse Western blots I performed (**Fig. 4.1**) I knew that the protein was detected throughout the entire developmental cycle of *Streptomyces*. In theory, that means that BldB should be available to interact with its homologues depending on when they are expressed.

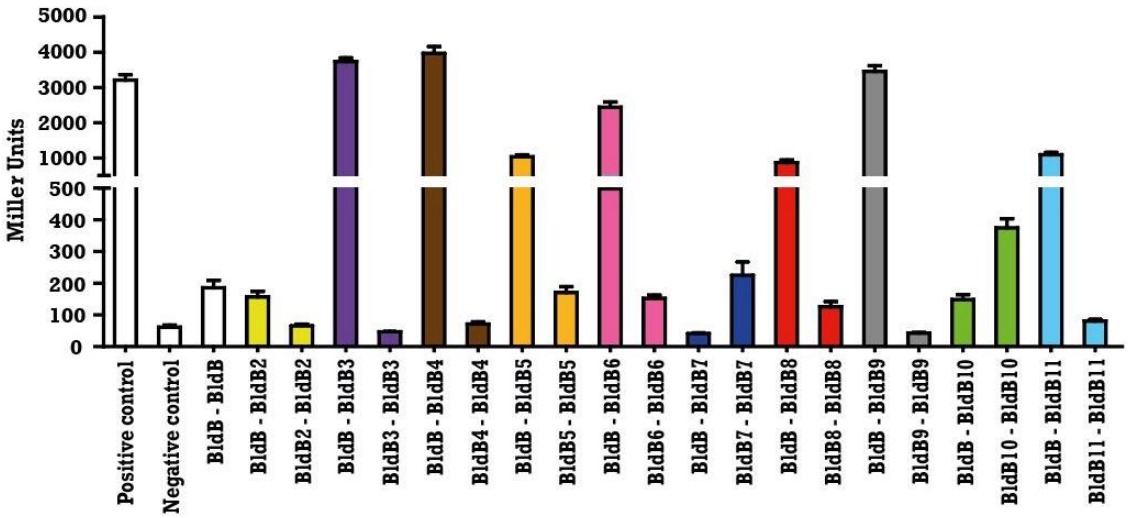

Figure 3.12. Interactions Between BldB and its 10 BldB Homologues.

β-galactosidase assays were performed to measure strength of protein-protein interactions (in Miller units). The strong interaction between the leucine zipper domains of leucine zipper of GCN4 (T18C-zip and T25-zip) was used as a positive control. Empty vector negative controls were performed for every interaction displayed here, but for the sake of clarity, only one representative negative control is displayed. Results are the average of three independent experiments, with two technical replicates per experiment. Error bars indicate the SEM.

Two Non-Canonical BldB Homologues are Necessary for Sporulation

To establish if any of the BldB homologues play a role in the development of *Streptomyces*, I generated mutants for all 10 non-canonical *bldB* homologues using the Redirect method. When plated on solid MYM medium, 2 of these 10 mutants appeared white - *ΔbldB6* and *ΔbldB9* (**Fig. 3.13**). This suggested that these strains were impaired in the production of mature, pigmented spores. When I complemented the *ΔbldB6* and *ΔbldB9* mutants with pIJ10257::*bldB6* and pIJ10257::*bldB9* respectively, the phenotypes of the resulting strains resembled that of the wild type, proving that the white mutant phenotypes were indeed due to the loss of *bldB6* and *bldB9* (**Fig. 3.14**). Overexpression of *bldB6* or *bldB9* in wild-type *S. venezuelae* using pIJ10257 had no obvious phenotypic consequences (**Fig. 3.14**).

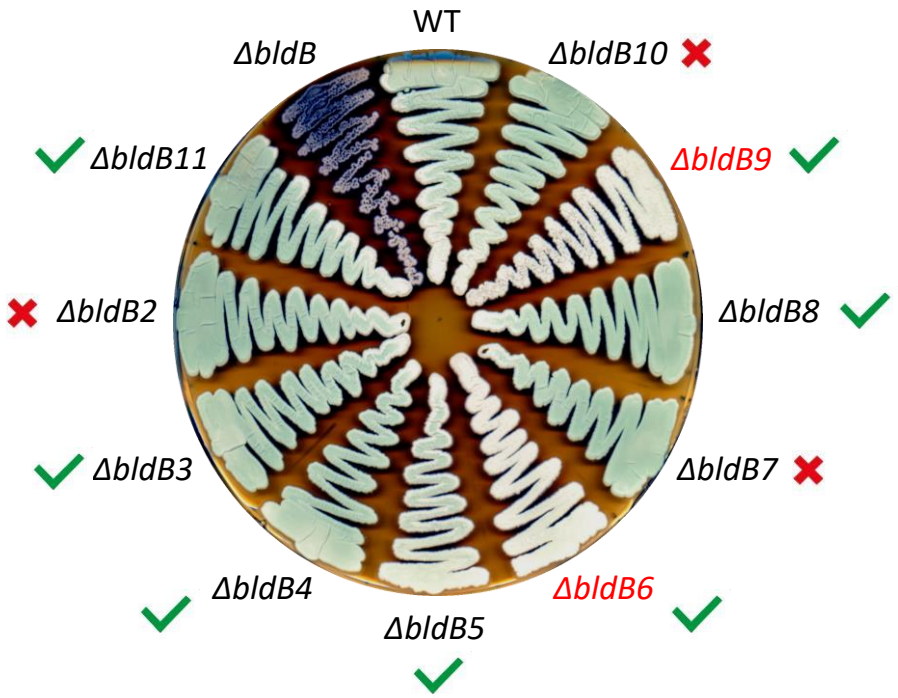

Figure 3.13. The Mutant Phenotypes of the *S. venezuelae bldB* Homologues.

Plate depicting the growth of the mutants for all 11 *S. venezuelae bldB* homologues on MYM agar. Green ticks denote a strong interaction between the deleted homologue and canonical BldB, and red crosses indicate weak/no interaction with BldB - as observed in the bacterial-two-hybrid experiments. Red labels indicate a white mutant phenotype. Plate image was taken after a 4-day incubation at 28˚C.

Figure 3.14. The Phenotypes of BldB6- and BldB9-related Strains.

Plates depicting the growth of the mutant, complemented mutant and overexpression strains for *bldB6* and *bldB9* on MYM agar. EV stands for empty pIJ10257 vector control. OE stands for overexpression. Plate images were taken after a 4-day incubation at 28˚C.

Scanning electron microscopy confirmed the phenotypes I observed on plates - both the *ΔbldB6* (**Fig. 3.15**) and the *ΔbldB9* (**Fig. 3.16**) mutants produce mostly undifferentiated aerial hyphae with very few sporulation septa placed, resulting in irregularly sized compartments. Complementing these mutants or overexpressing them in the wild-type background with the native genes under the control of the *ermE** promoter resulted in wild-type like phenotypes (**Fig. 3.15, Fig. 3.16**).

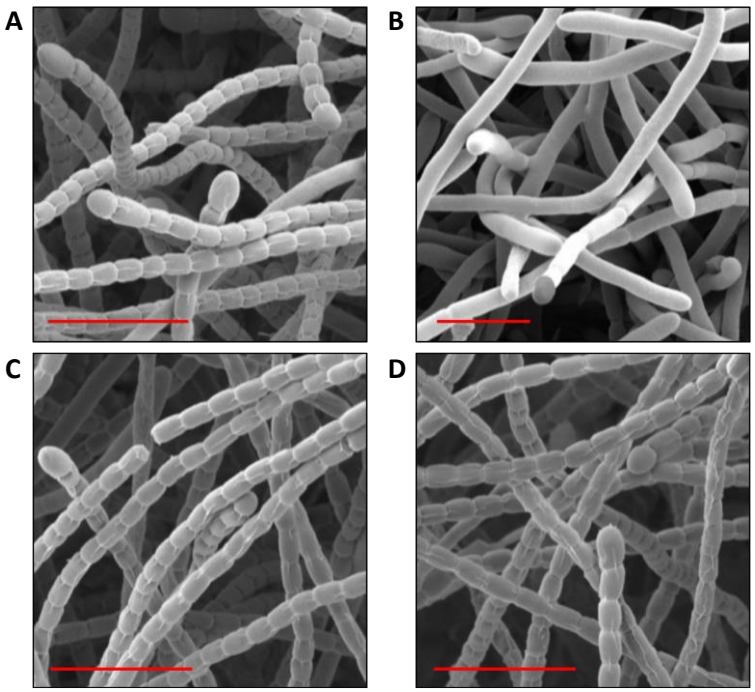

Figure 3.15. Phenotypic Characterisation of BldB6-derived Strains.

Scanning electron micrographs comparing the phenotypes of wild-type *S. venezuelae* **(A)**, the *ΔbldB6* mutant **(B)**, the *ΔbldB6* pIJ10257::*bldB6* complementation strain **(C)** and the pIJ10257::*bldB6* overexpression strain **(D).** Scale bars in red indicate 5 µm.

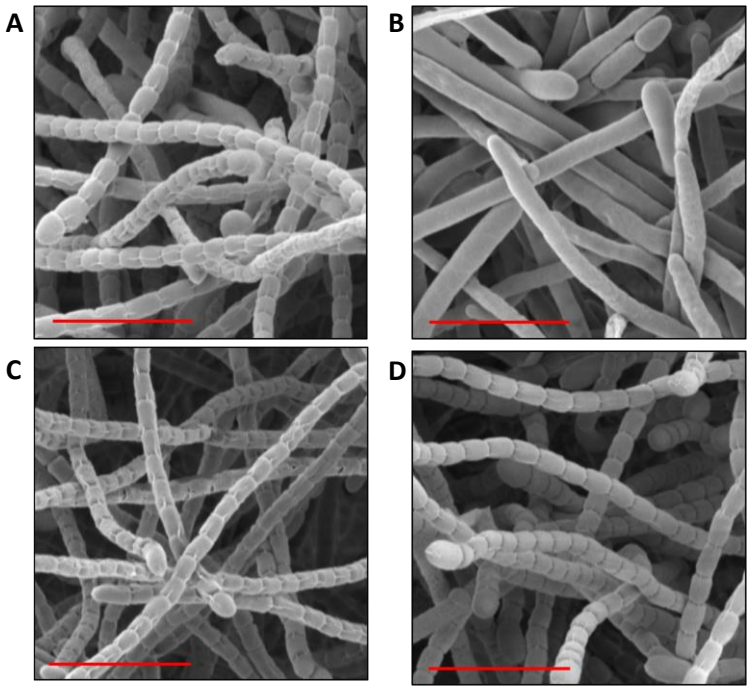

Figure 3.16. Phenotypic Characterisation of BldB9-derived Strains.

Scanning electron micrographs comparing the phenotypes of wild-type *S. venezuelae* **(A)**, the *ΔbldB9* mutant **(B)**, the *ΔbldB9* pIJ10257::*bldB9* complementation strain **(C)** and the pIJ10257::*bldB9* overexpression strain **(D).** Scale bars in red indicate 5 µm.

The expression profiles of *bldB6* and *bldB9* throughout the *S. venezuelae* life cycle [dataset described by Bibb et al. (2012) and deposited in ArrayExpress under the accession number E-MEXP-3612] revealed that both genes are highly expressed in mid- to late development (**Fig. 3.17**). This would be consistent with the *ΔbldB6* and *ΔbldB9* mutants having a 'late' developmental defect, rather than being bald like the *ΔbldB* mutant.

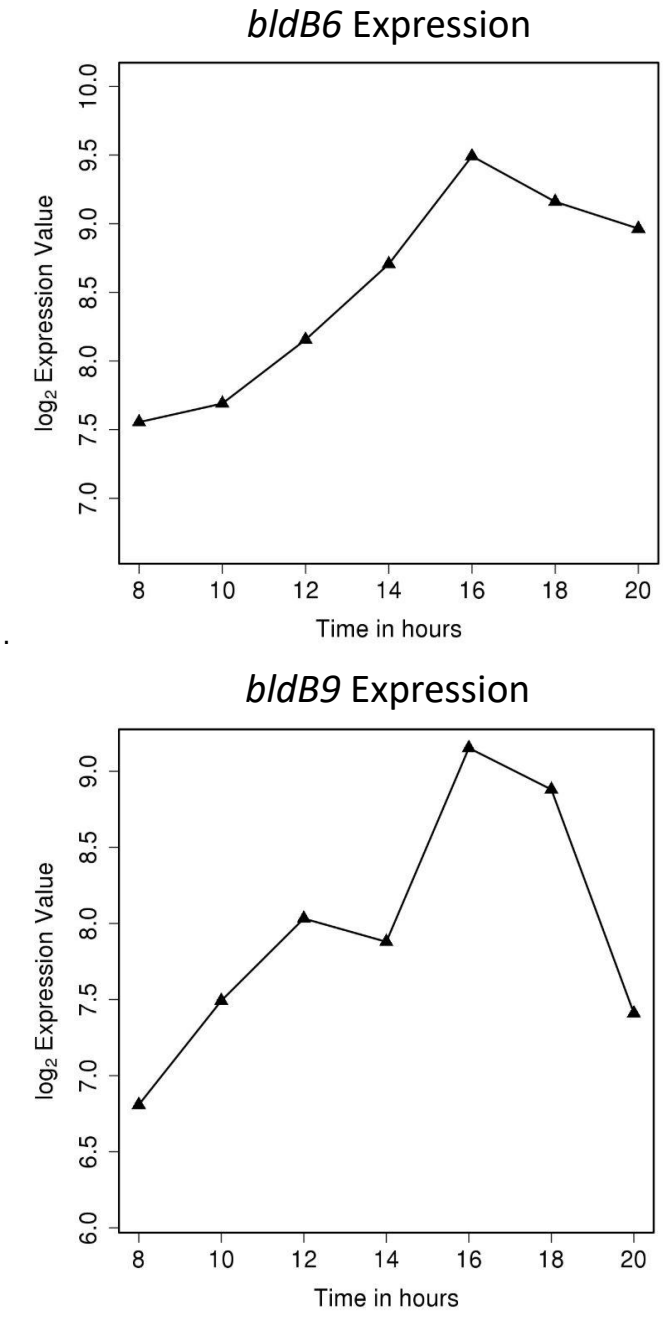

Figure 3.17. Expression of *bldB6* and *bldB9* Throughout *S. venezuelae* Development.

Transcriptional expression profiles of *bldB6* (upper panel) and *bldB9* (lower panel) in wild-type *S. venezuelae* grown in liquid MYM culture. The x-axes represent the age of the culture post-inoculation (hr), and the y-axes represent the normalized abundance of transcripts (log_2).

Phylogenetic Analysis of the BldB Homologues

The bacterial-two-hybrid screen assays revealed that BldB preferentially interacts with 7 out of 10 non-canonical BldB homologues (**Fig. 3.12**), suggesting that there are key differences between the protein sequences and three-dimensional structures of the BldB homologues. To look more closely into those differences on a sequence level, I did preliminary alignments of the amino acid sequences of all 11 BldB homologues. What became apparent was that the sequence of canonical BldB is longer and that it aligns poorly with the sequences of the non-canonical homologues. For this reason I did a separate alignment of the non-canonical homologues BldB2-BldB11, and then aligned the sequence of BldB to this already established alignment profile. This resulted in a higher quality alignment, as represented in **Figure 3.18**.

The conserved regions in this alignment (KSSYSG, CVEVA, VAVRDSKXP) are characteristic for the DUF397 domain shared by the BldB homologues. Canonical BldB, however, is a poor match for this domain (**Fig. 3.18**). BldB only contains a few of the conserved residues in the DUF397 domain and notably, it has an extended N-terminal region.

To further look into the sequence similarity between the BldB homologues, I constructed a phylogenetic tree based on the presented protein alignment (**Fig. 3.19**). In this tree, the BldB sequence was used as a root, as it was a clear outlier compared to the sequences of BldB2-BldB11. Interestingly, the BldB homologues closest in sequence to canonical BldB are BldB7, BldB10 and BldB2 – the 3 homologues that did not interact strongly with BldB in the bacterial-two-hybrid assays (**Fig. 3.12**). The relatively high bootstrap values at the branching points for these 3 homologues in particular indicates a higher degree of confidence in the placement of these branches.

What is also notable is that BldB6 and BldB9 - the two homologues whose deletion resulted in white phenotypes (**Fig. 3.13, 3.14, 3.15**) are not especially similar to each other in terms of amino acid sequence, evidenced by their positions in the tree (**Fig. 3.19**). BldB6 appears to be more similar to BldB5, whereas the “evolutionarily newest” branch contains BldB9 and BldB3, which are more similar to each other (**Fig. 3.19**).

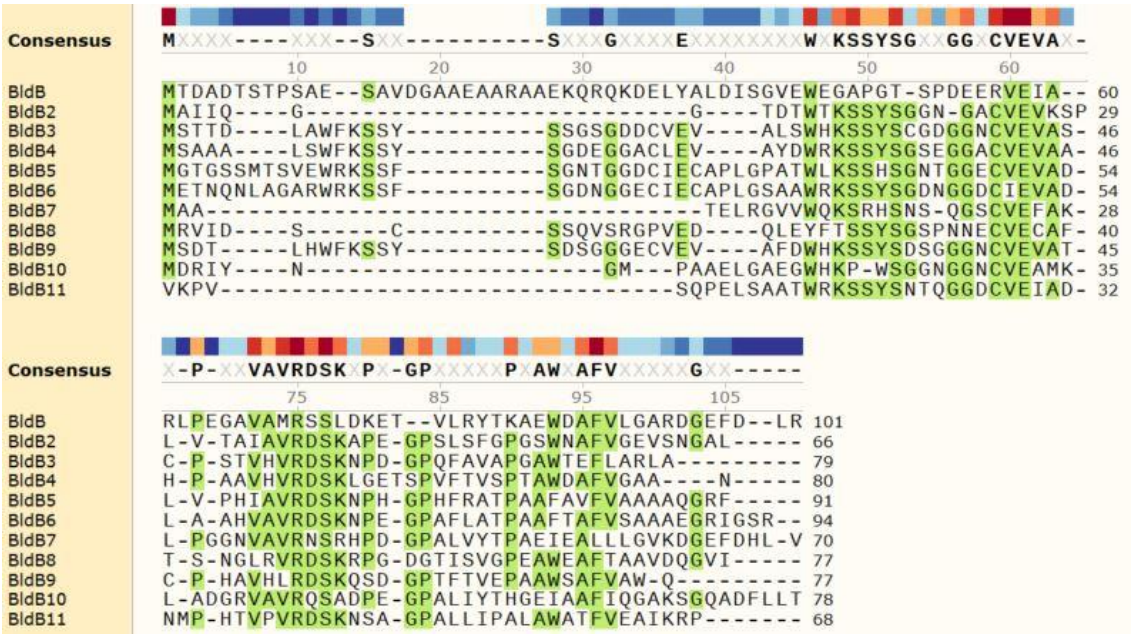

Figure 3.18. Protein Sequence Alignment for the BldB Homologues.

The amino acid sequences of the non-canonical BldB homologues were aligned using T-Coffee. The sequence of canonical BldB was then aligned to this existing profile. The consensus sequence is displayed above, with high sequence identity regions marked in green.

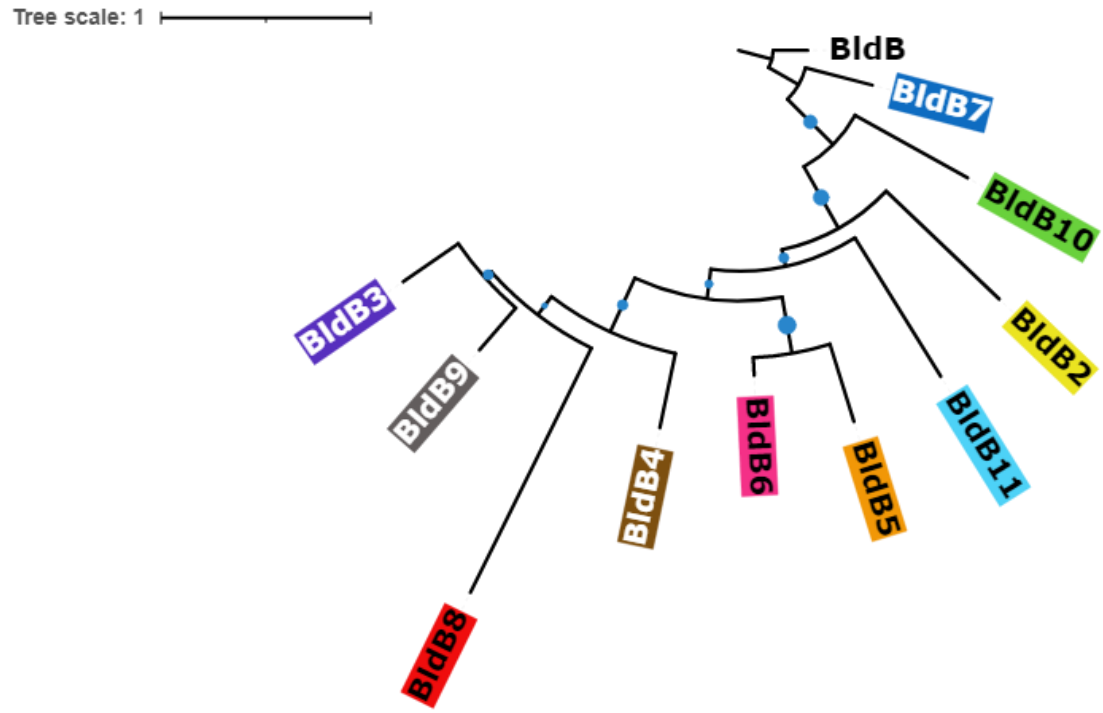

Figure 3.19. BldB Homologue Phylogenetic Tree.

A maximum-likelihood phylogeny of the *S. venezuelae* BldB homologues. The sequence of canonical BldB was used to root the tree. Scale bar indicates the number of substitutions per site. The size of the circles on the branches indicates the number of bootstraps.

Discussion

From Dr Govind Chandra's collection of 30,772 bacterial reference genomes, the 64,651 *bldB* homologues we identified are only found in Actinobacteria (**Fig. 3.3**). This is not surprising - it is consistent with some previous reports (Eccleston *et al.*, 2006), and expands on others, which state that *bldB* is restricted to streptomycetes (Chandra and Chater, 2014). The analysis of Chandra and Chater (2014) centered on just over 100 well-annotated Actinobacterial genomes, and presumably used only the canonical *bldB* sequence for their searches, which could explain why they found no BldB homologues outside of the sampled *Streptomyces* genomes. The dramatic rise in whole-genome sequencing has resulted in a significantly larger database of bacterial genomes, from which we could sample and map out the phylogenetic distribution of *bldB* homologues.

The majority of species with *bldB* homologues indeed come from *Streptomyces* - out of the 3,358 Actinobacterial species that have *bldB*, 54.3% are *Streptomyces* species (**Fig. 3.3**). The remaining 1,533 non-streptomycete Actinobacterial species that have *bldB* homologues comprise only 6.8% of the total sampled Actinobacteria genomes, so it is perhaps understandable that some earlier studies claimed *bldB* homologues were found exclusively in *Streptomyces*. Notably, *bldB* homologues were found to be present in *Kitasatospora* species, contrary to earlier reports (Girard *et al.*, 2014; Labeda *et al.*, 2017). 7 *Streptomyces* genomes were found not to possess *bldB* homologues, but it is possible that these genomes are not fully assembled and may therefore represent false negatives (**Fig. 3.3**).

When we investigated the protein length of the 64,651 BldB homologues, we found that most of them were 100 amino acids or smaller, which is consistent with the length of the BldB homologues in *S. venezuelae* (**Fig. 3.4**). Interestingly, we also identified BldB homologues longer than 100 amino acids (**Fig. 3.4**). These "long" BldB homologues contained extra domains, the most common one being the N-terminal HTH-Xre domain characteristic of the WhiJ homologues (**Table 3.1**). This leads to the tempting idea that the adjacently encoded BldB and WhiJ homologues may be able to interact with one another and fulfil the same function(s) as the fusion proteins do. If WhiJ is a DNA-binding protein and BldB is its interaction partner, perhaps BldB can bind WhiJ only after reception of a signal and help it bind or unbind DNA. The interaction between domains of the long BldBs could be controlled in the same way, even though they form part of the same protein.

The conserved domain search also revealed that there are multiple BldB homologues with more than one DUF397 domain (**Table 3.1**). This poses another interesting question - what is the advantage (or disadvantage) of having multiple DUF397 domains? Since I already know that the canonical BldB is able to interact *in vivo* with 7 of its homologues in *S. venezuelae* (**Fig. 3.12**), and they all have single DUF397 domains, this might suggest that the multi-DUF397 BldB homologues are not able to bind to other BldB homologues. More work would need to be done to test this, as well as to establish the level of binding promiscuity between the non-canonical BldB homologues.

One more alternative domain of potential interest is the methyltransferase domain found in 2 BldB homologues (**Table 3.1**). Proteins encoding methyltransferases are sometimes found encoded in the vicinity of the *bldB-whiJ-abaA* loci. The possibility therefore exists that a methyltransferase could also be involved in this already complex system of proteins.

Again, drawing on the 21/09/2021 collection of genomes, we collected the number of *bldB* homologues found per Actinobacterial genome, the median number being 19 (**Fig. 3.5**). 71 genomes only had 1 *bldB* homologue, but a few had 60+ homologues, with the top hit *Actinomadura craniellae* having a striking 94 *bldB* homologues. It would be very interesting to investigate the species with just 1 *bldB* homologue and see if they represent orthologues of the canonical *bldB*. It would also be fascinating to look at the species with most *bldB* homologues and try to find out the reason why they would need so many *bldB* homologues. One possibility is that these species inhabit a complex or challenging environment. For example, *Actinomadura craniellae*, the species with the most *bldB* homologues, was first isolated from a marine sponge of the *Craniella* genus (Li *et al.*, 2019). It would be interesting to know if the other species with high numbers of *bldB* homologues come from a marine environment, and/ or have a symbiotic relationship with another organism. It should be noted that the current genome assembly of *Actinomadura craniellae* contains over 40 contigs, which might mean that the documented number of BldB homologues present will need to be adjusted in the future.

Focusing on the *S. venezuelae* BldB homologues - there are 10 BldB homologues in addition to the canonical BldB, which is the main focus of this study (**Fig. 3.6**). While the canonical *bldB* gene is encoded in the middle of a type VII secretion cluster, each of the other 10 *bldB* homologues has a homologue of *whiJ* encoded next to it (usually upstream, on the same strand). In half of these cases, there is also an *abaA* homologue encoded nearby (usually upstream of the *whiJ* homologue, on the opposite strand).

This genomic arrangement was the first obvious difference between the canonical BldB and its 10 homologues. The second difference is the difference in mutant phenotypes. The canonical Δ*bldB* mutant in *S. venezuelae* has a classical bald, albeit leaky phenotype: the colony mainly consisted of a vegetative mycelium, with some formation of undifferentiated aerial hyphae around the edges of the colony (**Fig. 3.7, Fig. 3.8**). This is consistent with the observation that the *S. coelicolor ΔbldB* mutant starts sporulating upon prolonged incubation (Passantino, Puglia and Chater, 1991). In contrast, when I knocked out the 10 non-canonical Δ*bldB* genes, 8 of the resulting mutants had no developmental phenotype, and 2 (*ΔbldB6* and *ΔbldB9*) had a white phenotype (**Fig. 3.13, Fig. 3.14, Fig. 3.15, Fig. 3.16**). Since the earliest and most severe developmental phenotype can only be observed in the canonical *ΔbldB* mutant, this suggests that there is no functional redundancy between the canonical BldB and any of its homologues.

Indeed, the amino acid sequence of the canonical BldB differs from the sequences of its homologues. The non-canonical homologues have well-defined DUF397 domains, whereas canonical BldB is a weaker match for this domain – as exemplified by the protein sequence alignment of the BldB homologues (**Fig. 3.18**). In a BLAST search of the canonical BldB protein sequence against the *S. venezuelae* proteome, the best matches are BldB7 and BldB10, with 42% and 40% identity, respectively. My phylogenetic analysis also strengthens this finding – the proteins closest in sequence to canonical BldB were BldB7, BldB10 and BldB2 (**Fig. 3.19**).

Interestingly, BldB2, BldB7 and BldB10 are the three homologues that canonical BldB did not interact with in the bacterial-two-hybrid assays (**Fig. 3.12**). In the same experiment, BldB7 and BldB10 exhibited a low level of self-interaction, whereas BldB2 did not (**Fig. 3.12**). This could indicate an evolutionary trajectory, in which the proteins closest in sequence to BldB – BldB7 and BldB10 do not interact with BldB, but instead form homodimers. The next one, BldB2 has lost the ability to self-interact, whereas the following homologues have gained the ability to interact with canonical BldB.

This would suggest that for the BldB homologues there is a trade-off between self-interaction and interaction with BldB. It would also suggest that there are specific residues in the DUF397 domain that promote binding to canonical BldB - further work could focus on unravelling those specific interactions.

My initial bacterial-two-hybrid library screen with BldB as bait revealed numerous potential interacting proteins (**Table 3.2**), but I did not test the majority of them in one-on-one β-galactosidase assays using the full-length proteins. It is possible that BldB is an enzyme that adds or removes a post-translational modification to or from proteins, which would explain the multitude of two-hybrid screen hits. It is also possible that BldB is simply a sticky protein that produced a lot of weak interactions in this library screen that are not physiologically relevant. The kinase PkaI, which has a role in spore wall synthesis, was proposed to interact with BldB in *S. coelicolor* (Vollmer *et al.*, 2019). PkaI was not identified in the library screen - upon inspection there is no obvious orthologue *of S. coelicolor* PkaI in *S. venezuelae*.

What I found was that BldB is able to bind strongly to 7 of its *S. venezuelae* homologues *in vivo* (**Fig. 3.12**), with two of these interacting homologues - BldB6 and BldB9 - being important for *S. venezuelae* development, as their individual deletions resulted in white phenotypes (**Fig. 3.13, 3.14, 3.15, 3.16**). The expression patterns of the *bldB6* and *bldB9* genes fit with the white phenotypes of the mutants, as both genes are more highly expressed later in development (**Fig. 3.17**). Aside from this, the *S. venezuelae* BldB homologues have not been characterised at all so far, except for the *bldB2* gene, whose expression was found to be under the control of the response regulator BldM (Al-Bassam *et al.*, 2014).

In the β-galactosidase assays, I observed a very low level of self-interaction for BldB (**Fig. 3.12**). This is not consistent with what Eccleston *et al*. (2002, 2006) observed for *S. coelicolor*, where BldB was reported to form homodimers. These results are not directly comparable - after their two-hybrid assays, Eccleston *et al.* did not do β-galactosidase assays to measure the strength of self-interaction for BldB, though they did follow it up with analytical gel filtration, which led them to state that BldB forms asymmetric dimers.

In a future experiment, I could also use analytical gel filtration, or other biochemical approaches to see whether *S. venezuelae* BldB forms multimers *in vitro*. However, it is possible that the canonical *S. venezuelae* and *S. coelicolor* homologues have slightly different functions in their respective species. Indeed, when comparing their protein sequences, the two BldB proteins share 82% identity, suggesting they are different enough to have evolved differences in function.

These possible differences in function could also explain the differences in *bldB* overexpression phenotypes between *S. venezuelae* and *S. coelicolor* (Eccleston *et al.*, 2006). When I overexpressed *bldB* in *S. venezuelae*, the resulting strain sporulated normally (**Fig. 3.10, Fig. 3.11**). In contrast, the *S. coelicolor bldB* overexpression strain was reported to exhibit a phenotype reminiscent of a *whi* mutant (Eccleston *et al.*, 2006). These differences in phenotype might also be due to the different methods used to overexpress *bldB*. I overexpressed *bldB* in *S. venezuelae* by placing it under the control of the constitutive promoter *ermE** on the integrative vector pIJ10257, whereas Eccleston *et al.* (2006) cloned *bldB* under the control of its own promoter in the high-copy vector pIJ486. The levels of BldB production in these two strains might therefore differ, and for this reason, the phenotype of my *S. venezuelae bldB* overexpression strain might not be directly comparable to that of the *S. coelicolor* overexpression strain.

In this chapter I described my work towards the characterisation of the mutant and overexpression phenotypes related to *bldB*. I also found that a subset of the non-canonical BldB homologues interact strongly with BldB, out of which 2 are important for *Streptomyces* sporulation. In the next chapter, I focus on verifying whether BldB is a direct regulator of transcription – something that has been proven for most of the other Bld regulators, and something that has been suggested in literature.

4. The Δ*bldB* Mutant Phenotype Is Recapitulated by Co-overexpression of *abaA6* and *iosA*

Introduction

Phosphorylation-dependent Regulation of Sigma Factor Activity in *Bacillus*

The two best-characterised alternative sigma factor systems, whose regulation is dependent on partner-switching mechanisms influenced by the phosphorylation state of the partners, are the systems involving the sporulation sigma factor SigF and the stress response sigma factor SigB in *Bacillus*.

SigF (also referred to as SpoIIAC) is a forespore-specific sigma factor, which is necessary for *Bacillus* sporulation (Schmidt *et al.*, 1990). The *sigF* gene is found in an operon with the genes encoding SpoIIAB and SpoIIAA. The anti-sigma factor SpoIIAB has a histidine kinase-like HATPase_c domain, and in its homodimeric form binds SigF to prevent it from associating with core RNA polymerase (Duncan and Losick, 1993; Decatur and Losick, 1996; Campbell *et al.*, 2002). SpoIIAA is a STAS domain-containing anti-sigma antagonist, which is phosphorylated by the kinase domain of SpoIIAB prior to sporulation, and is thus prevented from fulfilling its anti-sigma antagonist function (Min *et al.*, 1993; Magnin *et al.*, 1996). Once asymmetric septum formation is completed and spore formation is initiated, the membrane-bound phosphatase SpoIIE dephosphorylates SpoIIAA, which frees it to bind the anti-sigma factor SpoIIAB, thus allowing the release of SigF, its association with core RNA polymerase and the subsequent expression of sporulation-related genes (Diederich *et al.*, 1994; Arigoni *et al.*, 1996). SpoIIE is also part of the division machinery in *Bacillus*, as it was found to localise on the forespore side of the sporulation septum and to interact directly with FtsZ, linking cell division with SigF activation (Arigoni *et al.*, 1995; Wu, Feucht and Errington, 1998; Lucet *et al.*, 2000).

Another well-characterised example of phosphorylation-dependent control of sigma factor function in *Bacillus* is the network involving the stress-response sigma factor SigB. SigB was the first alternative sigma factor identified in bacteria (Haldenwang and Losick, 1979). The regulation of SigB is reminiscent of that of SigF, though it is a lot more complex and involves two partner-switching mechanisms that feed into one another.

The core partner-switching mechanism involves SigB directly, as well as the anti-sigma factor RsbW, the anti-sigma antagonist RsbV and the two sensor phosphatases RsbU and RsbP. Under non-stress conditions, SigB is bound by its anti-sigma factor RsbW and is unable to associate with the core RNA polymerase (Benson and Haldenwang, 1993). RsbW is also able to phosphorylate its antagonist RsbV via its HATPase_c kinase domain, thus keeping it inactive (Dufour and Haldenwang, 1994). Once a stress signal has been perceived by either RsbU or RsbP, that phosphatase goes on to remove the phosphate from serine 56 of the anti-sigma antagonist RsbV, which is then free to bind the anti-sigma factor RsbW (Yang *et al.*, 1996). This releases SigB, which is able to form the RNA polymerase holoenzyme and go on to transcribe more than 150 stress response-related target genes (Hecker, Pané-Farré and Uwe, 2007).

The two sensor phosphatases - RsbP and RsbU are able to respond to different sets of signals. RsbP contains a PP2C phosphatase domain, as well as a PAS domain, and is suggested to be important for sensing “energy stress”, such as oxygen, phosphate and carbon stress (Vijay *et al.*, 2000). RsbU contains the same phosphatase domain, and responds to environmental stresses in a way that is further controlled by the second SigB-related partner-switching mechanism - one involving the phosphatase RsbX and the stressosome components, which include the antagonists RsbR/RsbS and the RsbW-like kinase RsbT (Yang *et al.*, 1996).

Under non-stress conditions, the stressosome is a multi-protein structure composed of 40 units of RsbR (or its homologues) and 20 units of RsbS, which collectively bind 20 units of the RsbW-like kinase RsbT (Chen *et al.*, 2003; Marles-Wright *et al.*, 2008). Under stress conditions, the RsbR and RsbS subunits of the stressosome are phosphorylated, which leads to the release of RsbT from the macromolecular structure (Kim, Gaidenko and Price., 2004; Liebal *et al.*, 2013). RsbT is then able to bind the RsbU phosphatase and activate its function, ultimately resulting in SigB activity (Yang *et al.*, 1996; Kang, Vijay and Price, 1998).

Upon returning to non-stress conditions, the RsbX phosphatase returns the stressosome to its base state by dephosphorylating RsbS and RsbR, which leads to an increased binding affinity between them and RsbT, meaning that RsbT can be bound by the stressosome once again (Voelker *et al.*, 1997; Chen, Yudkin and Delumeau, 2004).

Overall, these partner-switching mechanisms allow for a fine-tuned transcriptional response to a given signal. In both the SigF and SigB partner-switching modules, the phosphorylation state of the SpoIIAA and RsbV anti-sigma antagonists ultimately determines the activation state of their respective target sigma factors. SpoIIAA and RsbV, as well as the stressosome components RsbR and RsbS all share a conserved domain with sulfate transporters - this domain was designated STAS, standing for **S**ulfate **T**ransporter and **A**nti-**S**igma factor antagonist (Aravind and Koonin, 2000). After the identification of the SigB and SigF partner-switching systems in *Bacillus*, multiple similar systems have been identified in other bacteria. As a core module, these systems have a HATPase_c domain-containing anti-sigma factor, a STAS domain-containing anti-sigma antagonist, and a PP2C phosphatase, which control the activity of a SigB-like sigma factor generally associated with development or stress responses.

Bacillus SigB-like Systems in *Streptomyces* and Their Involvement in Development

In *S. coelicolor*, there are reported to be 9 SigB-like sigma factors - SigB, SigF, SigG, SigH, SigI, SigK, SigL, SigM and SigN.

The *S. coelicolor* SigB (sometimes referred to in literature as SigJ) has been reported to be involved in response to hyperosmotic stress, acidic pH and heat shock (Viollier, Kelemen, *et al.*, 2003; Kim *et al.*, 2008; Bucca *et al.*, 2009). The *S. coelicolor ΔsigB* mutant displayed a bald phenotype, an overproduction of actinorhodin and a reduced ability to grow on osmolyte-supplemented media (Cho *et al.*, 2001). In comparison, the *Streptomyces avermitilis ΔsigB* mutant exhibited no changes in development, but an enhanced production of avermectin and a slight reduction in growth after hyperosmotic, oxidative or heat shock (Sun *et al.*, 2017). In *S. coelicolor*, the anti-sigma RsbA (whose gene is encoded upstream from *sigB*) was demonstrated to prevent expression of SigB targets by binding to SigB (Lee *et al.*, 2004). The *ΔrsbA* mutant displayed accelerated development and no actinorhodin production, in contrast to the *ΔsigB* mutant.

Interestingly, the anti-sigma antagonist for RsbA was not the STAS-domain containing RsbB encoded next to *rsbA* – it was another homologue, which was designated RsbV after its *B. subtilis* counterpart. Similarly to the system in *Bacillus*, RsbA phosphorylated RsbV, thus releasing itself in order to bind SigB (Lee *et al.*, 2004).

Control of SigB activity by RsbA and RsbV in *S. coelicolor* has been suggested to occur during general stress conditions, whereas control by OsaC (to be discussed in more detail in the next chapter) was proposed to occur during osmotic stress only (Fernández Martínez *et al.*, 2009). SigB was found to control the expression of two other SigB-like sigma factors - SigL and SigM (Lee *et al.*, 2005).

Not much is known about SigL except that its expression was induced by heat shock in *S. coelicolor* (Bucca *et al.*, 2009). The *S. coelicolor ΔsigL* mutant displayed a white phenotype and no antibiotic production (Lee *et al.*, 2005).

The regulation of SigM in *S. coelicolor* follows a similar theme to that of SigB, but with an interesting variation - its anti-sigma factor RsmA has the characteristic HATPase_c domain, but also has a [2Fe-2S] iron-sulfur cluster (Gaskell *et al.*, 2007). An anti-sigma antagonist has not yet been discovered for RsmA, which means that its specific kinase activity cannot be examined. Nevertheless, RsmA was shown to be able to bind ATP *in vitro* in a manner that was not dependent on the presence of the iron-sulfur cluster. The [2Fe-2S] cluster was found to be necessary for the binding of RsmA to SigM instead (Gaskell *et al.*, 2007). The *S. coelicolor ΔsigM* mutant was able to sporulate, but with an overall reduced biomass (Lee *et al.*, 2005).

SigI was found to be produced after hyperosmotic shock specifically (Viollier, Kelemen, *et al.*, 2003; Karoonuthaisiri *et al.*, 2005; Homerova *et al.*, 2012). However, the *ΔsigI* mutant was found to have a wild-type-like phenotype under normal and hyperosmotic stress conditions (Homerova *et al.*, 2012). Encoded next to the *sigI* gene were found the genes for its anti-sigma factor PrsI and the anti-sigma antagonist ArsI. PrsI was demonstrated to bind both SigI and ArsI, and to phosphorylate ArsI via its histidine kinase-like domain (Homerova *et al.*, 2012).

The *sigF* and *sigN* genes are found next to each other, so it was thought that the two sigma factors somehow function together. *S. coelicolor* SigN has been described as being involved in development, stress responses and secondary metabolism, as suggested by the characterisation of the differential protein abundance in the *ΔsigN* mutant (Wang *et al.*, 2010). When SigN was deleted from *S. coelicolor*, the resulting strain only exhibited a developmental phenotype when grown on media containing glucose - otherwise it completed sporulation as expected (Dalton *et al.*, 2007). The same authors proposed that SigN functions in a specific compartment of the aerial hyphae – the so-called ‘subapical stem’.

SigF has been referred to as a sporulation sigma factor, as it was found to localise in spores (Sun *et al.*, 1999), and its own expression and that of its target genes was detected at the later stages of development in *S. coelicolor* (Kelemen *et al.*, 1996). Furthermore, the expression of *sigF* was found to be independently regulated in each pre-spore compartment, as loss of *sigF* expression was observed for some, but not all pre-spore compartments in a *ΔftsK* mutant (Wang *et al.*, 2007). Disruption of *sigF* in *S. coelicolor* J1508 resulted in a strain with a white phenotype (Potúcková *et al.*, 1995). However, when *sigF* was deleted in the M145 background, the resulting strain produced spores with a green pigment instead of the typical grey one (Kelemen *et al.*, 1998). This green spore phenotype of the M145 *ΔsigF* mutant was attributed to the loss of production of WhiE OrfVIII, which is responsible for the final steps of production of the spore pigment (Kelemen *et al.*, 1998). The same green spore pigment phenotype was also observed in the *Streptomyces aureofaciens ΔsigF* mutant (Rezuchová, Barák and Kormanec, 1997). A *ΔsigF ΔsigN* double mutant in *S. coelicolor* exhibited features of the respective single mutant phenotypes - on media without glucose it looked like the *ΔsigF* single mutant, whereas on glucose-supplemented media it resembled the phenotype of the *ΔsigN* single mutant (Dalton *et al.*, 2007). One target of *S. coelicolor* SigF - SspA was found to affect spore formation, and septum placement in particular (Tzanis *et al.*, 2014).

No strong link between the functions of SigF and SigN has been uncovered yet, but such a link does exist between SigF and SigH - in the shape of the anti-sigma antagonist BldG, which has the characteristic STAS domain (Parashar *et al.*, 2009). The activity of the sporulation sigma factor SigF is regulated by the anti-sigma factor RsfA (SCO4677). The *ΔrsfA* mutant exhibited accelerated development and enhanced production of actinorhodin (Kim *et al.*, 2008; Hindra *et al.*, 2014). In a series of yeast-two-hybrid experiments, RsfA was shown to interact with SigF, and also with the predicted anti-sigma antagonists SCO0781 and SCO0869 (Kim *et al.*, 2008).

In an analogous way to the SpoIIAB - SpoIIAA interaction, the anti-sigma antagonist BldG was found to bind RsfA, relieving the repression on SigF, while RsfA was able to phosphorylate and inactivate BldG via its kinase activity (Mingyar *et al.*, 2014). However, *in vivo* interactions between the kinase anti-sigma factors and the STAS domain anti-sigma antagonists might not necessarily lead to phosphorylation events, because RsfA was found to be unable to phosphorylate SCO0869 *in vitro* (Mingyar *et al.*, 2014). If that is also true *in vivo*, this might represent another layer of regulation, in which the anti-sigma antagonist can bind and repress the activity of an anti-sigma factor, but that repression can only be reversed by phosphorylation by another anti-sigma factor, and not the one locked in an interaction.

The histidine kinase-like anti-sigma factor RsfA is one of the strongest targets of the master regulator BldD, as identified via ChIP-chip analysis (den Hengst *et al.*, 2010). Interestingly, *S. coelicolor rsfA* is found encoded next to the *whiJ* homologue *sco4678* and the *bldB* homologue *sco4679*, which have not been studied before. A small RNA *scr4677* was found encoded in the intergenic region between *sco4676* and *rsfA* (Hindra *et al.*, 2014). In other *Streptomyces* genomes, the position of *scr4677* equivalents next to the *rsfA* gene was not always conserved. The small RNA was found to stabilise the *sco4676-rsfA* polycistronic transcript, and to be developmentally regulated by an unknown protein binding upstream of the *scr4677* transcriptional start site (Hindra *et al.*, 2014).

BldG also has a role in the regulation of SigH. The expression of *sigH* was reported to be greatly induced after heat, osmotic, or acidic pH stress (Kormanec *et al.*, 2000; Kim *et al.*, 2008), and to be developmentally controlled by BldD in *S. coelicolor* (Kelemen *et al.*, 2001). The *ΔsigH* mutant was found to form aerial hyphae, but was defective in the formation of mature, pigmented spores (Sevciková *et al.*, 2001). In contrast, the *ΔsigH* mutant constructed by Viollier, Kelemen, *et al.* (2003) exhibited normal sporulation. The expression of the genes encoding the cell division protein SsgB and the ECF sigma factor SigJ (not to be confused with previous SigB nomenclature) was found to be under SigH control (Kormanec and Sevcikova, 2002; Mazurakova *et al.*, 2006).

SigH was found to be post-translationally controlled by proteolytic cleavage, as well as by the anti-sigma factor PrsH (also referred to as UshX and RshA in other literature) (Viollier, Weihofen, *et al.*, 2003). The *prsH* gene is found encoded immediately upstream of *sigH*, and when disrupted was found to cause developmental phenotypes in both *S. coelicolor* and *S. griseus* (Takano *et al.*, 2003; Viollier, Kelemen, *et al.*, 2003). The gene was also reported to have a conditional bald phenotype on glucose-containing media when overexpressed (Takano *et al.*, 2003). In a similar way to listed examples so far, the anti-sigma factor PrsH binds and represses SigH (Kormanec *et al.*, 2000; Sevcikova and Kormanec, 2002). The anti-sigma antagonist BldG, in turn represses PrsH, allowing SigH to associate with core RNA polymerase (Sevcikova *et al.*, 2010). In *S. griseus*, PrsH was shown to be also able to interact with the SigN (referred to as SigL in *S. griseus*) and SigF orthologues, as well as with SigH (Takano *et al.*, 2003). A triple *ΔsigHNF* mutant exhibited irregularities in spore sizes, but did not recapitulate the conditional bald phenotype of the *prsH* overexpression strain, which led the authors to believe that PrsH might bind yet another missing protein partner (Takano *et al.*, 2007).

The anti-sigma antagonist BldG has also been shown to interact with SCO3548 (ApgA), another predicted anti-sigma factor encoded downstream of *bldG*, however, no sigma factor interacting with ApgA has been identified as of yet (Parashar *et al.*, 2009; Sevcikova *et al.*, 2010).

SigG has not been extensively studied, but the *S. coelicolor ΔsigG* mutant does not appear to have any defects in development or antibiotic production (Kormanec *et al.*, 1999; Ševčíková, Mazuráková and Kormanec, 2005). The deletion of *sigK* in *S. coelicolor* resulted in an enhanced production of antibiotics and accelerated development, with no particular response to osmotic or temperature stress (Mao *et al.*, 2009). No anti-sigma factors or anti-sigma antagonists have been experimentally validated for SigG, SigK, SigL and SigN, and there are no candidates encoded next to the sigma genes, except for SigL, where the upstream gene encodes a protein with an HATPase_c domain, and the downstream gene encodes the WhiJ-like transcriptional regulator PopR.

The *abaA* Locus in *S. coelicolor*

The *abaA* locus was first discovered in a study of antibiotic production in *Streptomyces coelicolor* (Fernández-Moreno *et al.*, 1992). This locus was identified to have 5 open reading frames, designated *orfA*, *orfB*, *orfC*, *orfD*, and *orfE* (*sco0700* to *sco0704*). When the *abaA* locus was overexpressed in *S. coelicolor* and *S. lividans*, the authors observed a higher level of actinorhodin production. This effect was largely attributed to AbaA OrfB, as the *S. coelicolor* mutant for *orfB* showed a reduced production of CDA and undecylprodigiosin, and no production of actinorhodin, though the authors speculated that AbaA OrfA might also be responsible for these phenotypes.

abaA orfD (*sco0703*) is one of the homologues of *bldB* in *S. coelicolor*, while its neighbouring *abaA orfE* (*sco0704*) is a homologue of *whiJ*. Homologues of *abaA orfA* (*sco0702*), henceforth simply referred to as *abaA* homologues, which are encoded in the vicinity of *bldB* homologues, are of particular interest for this study, as detailed later in this chapter. The AbaA homologues in *Streptomyces* share the same histidine kinase-like HATPase_c domain that is found in all anti-sigma factors for the aforementioned SigB-like homologues. This domain is a part of the GHKL superfamily, and can also be found in DNA gyrase B, topoisomerase IV, heat-shock protein HSP90, and the DNA mismatch repair protein MutL, with the outstanding feature of an unconventional Bergerat ATP-binding fold (Dutta and Inouye, 2000). In this chapter, I examine the connection between the developmental phenotype of the *S. venezuelae* Δ*bldB* mutant and the expression patterns of the *abaA* homologues.

Results

BldB is Abundant Throughout the *Streptomyces* Life Cycle

Some previous studies had suggested BldB to be a DNA-binding protein (Pope, Green and Westpheling, 1998; Mishig-Ochiriin *et al.*, 2003), so I decided to test this hypothesis in *S. venezuelae* using ChIP-seq. As I planned to sample from 3 different timepoints, I wished to see what the levels of BldB protein were like throughout the *Streptomyces* life cycle. For this reason, I took time course samples and used them to perform automated Western blots, which allowed me to quantify relative protein levels (**Fig. 4.1**).

For ChIP-seq, I planned to do two separate experiments. In the first one, I planned to use the validated polyclonal anti-BldB antibody to extract BldB bound to DNA from wild-type *S. venezuelae*. In the second one, I planned to use an anti-FLAG antibody to isolate 3xFLAG-BldB bound to any DNA from the Δ*bldB* mutant that I successfully complemented with a 3xFLAG-BldB allele *in trans*. The control strains would be the Δ*bldB* mutant for the first experiment using the anti-BldB antibody, and wild-type *S. venezuelae* for the second experiment using the anti-FLAG antibody. Therefore, I used these same strains to observe levels of BldB or 3xFLAG-BldB in Western blots throughout the *S. venezuelae* life cycle.

I took samples from liquid MYM cultures of wild-type *S. venezuelae,* the Δ*bldB* mutant and the Δ*bldB::*3xFLAG-BldB strain at 2-hour intervals, starting at 8 hours. Both of my automated Western blots revealed similar patterns - BldB was present throughout every stage of development with a higher abundance in mid- to late development (**Fig. 4.1**). For the first experiment, where I used the anti-BldB antibody on the wild-type samples, there was no BldB detected in the 8-hour sample (**Fig. 4.1A, 4.1C**). This is likely due to the lower quantity of total protein loaded, which was 5 times lower for the 8-hour sample than for the rest of the samples – as described in the Materials and Methods. This occurred because at 8 hours the wild-type culture was lagging behind in growth compared to the Δ*bldB::*3xFLAG-BldB strain, resulting in less biomass in the wild-type 8-hour sample specifically. Therefore, that 8-hour sample does not necessarily reflect a complete absence of BldB in the earliest stages of development.

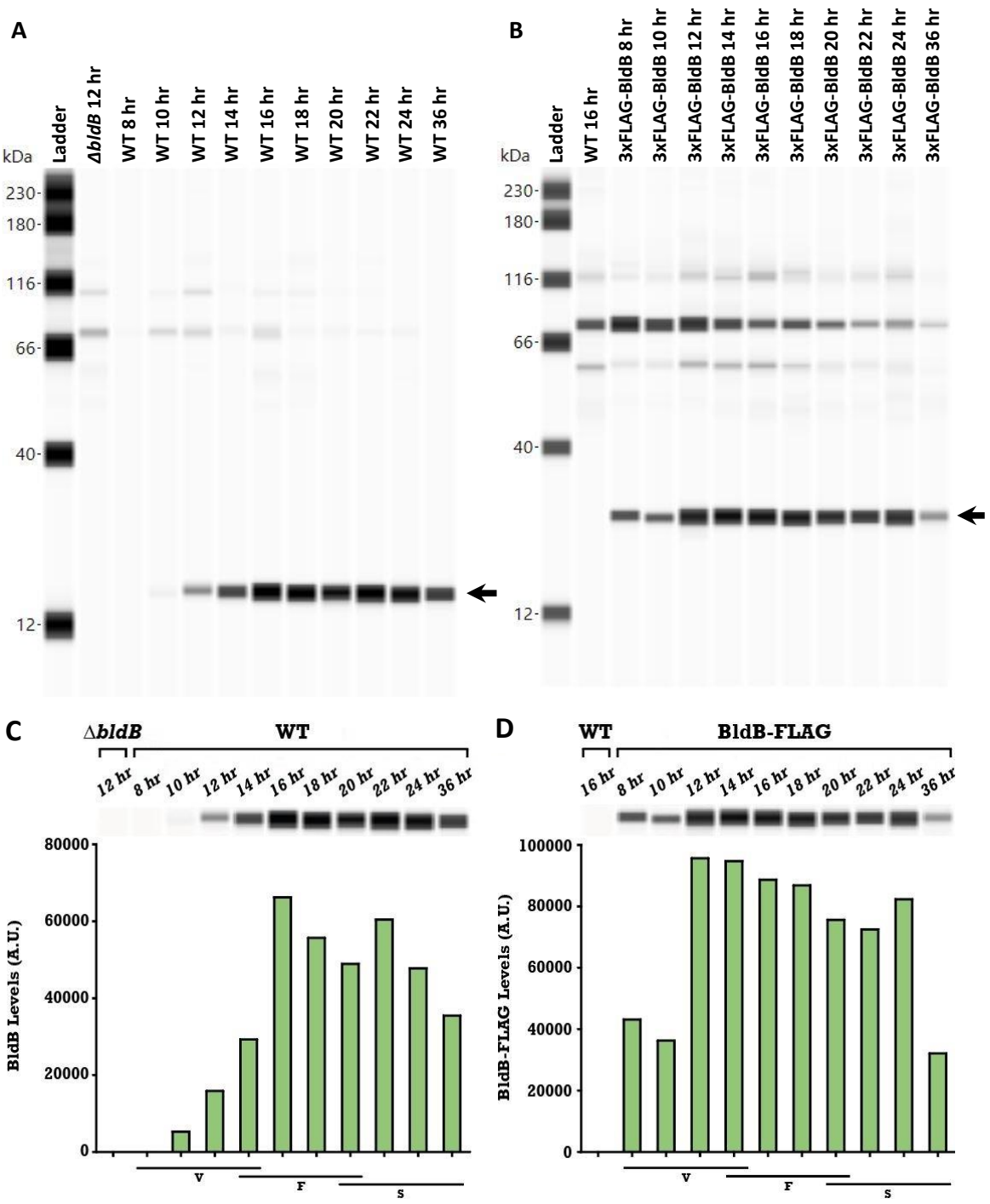

Figure 4.1. BldB Abundance Throughout *Streptomyces* Development.

The levels of BldB (**A**) and 3xFLAG-BldB (**B**) were measured using automated Western blots. Samples were taken every 2 hours from wild-type *S. venezuelae* and the Δ*bldB::*3xFLAG-BldB strain during the vegetative (V), filamentous (F) and sporulation (S) growth stages. Samples from the Δ*bldB* mutant at 12 hours (**A**) and from wild-type *S. venezuelae* at 16 hours (**B**) were used as negative controls for the respective experiments. All samples (except for the WT 8 hr sample in **A)** and **C)**, see Materials and Methods) were diluted to the same total protein concentration, as determined by Bradford assays. A single replicate is shown for each timepoint. Arrows indicate the BldB (**A**) and 3xFLAG-BldB (**B**) bands. BldB (**C**) and 3xFLAG-BldB (**D**) protein levels were quantified and measured in arbitrary units (A.U). Bars represent the average of two duplicates.

In comparison, timecourse microarray data for *S. venezuelae* [dataset described by Bibb *et al*. (2012) and deposited in ArrayExpress under the accession number E-MEXP-3612] suggested that *bldB* is highly expressed during early development, followed by a drop in expression during mid- and late development (**Fig. 4.2**).

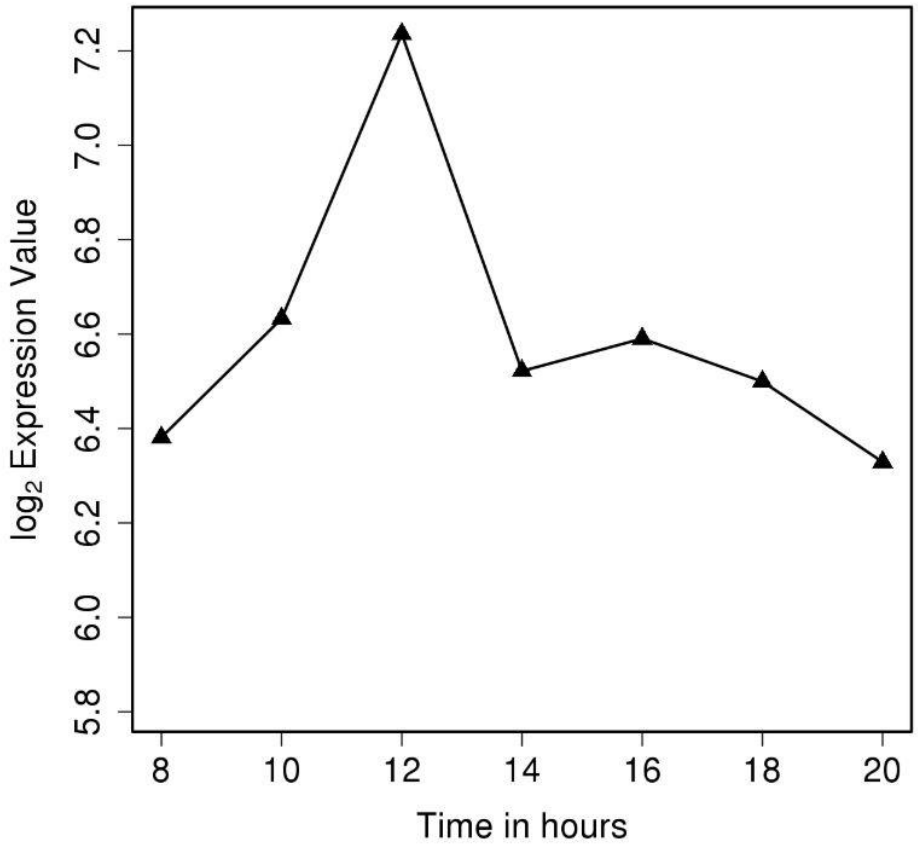

Figure 4.2. Expression of *bldB* Throughout Development.

Transcriptional expression profile of the *bldB* gene in wild-type *S. venezuelae* grown in liquid MYM culture. The x-axis represents the age of the culture post-inoculation (hr), and the y-axis represents the normalized abundance of *bldB* transcripts (log_2).

BldB Is Not a DNA-binding Protein

Based on the results from the automated Western blots, I chose 3 time points to sample from for my ChIP-seq experiments – 10-, 14- and 22 hours post-inoculation, in order to represent early, mid- and late development. The control samples for both experiments were taken at 14 hours only. All ChIP-seq analysis was done by Dr. Govind Chandra.

In the polyclonal anti-BldB antibody experiment there were a lot of enrichment peaks but most of these were also present in the control experiment, suggesting that the anti-BldB antibody non-specifically bound to DNA-binding protein(s) other than BldB. When we subtracted the wild-type control enrichment from each sample enrichment, there were several significant peaks of differential enrichment remaining, potentially representing BldB binding to DNA (**Fig. 4.3**). However, further examination showed that these peaks were positioned next to stable RNA genes, an artefact commonly observed in ChIP-seq experiments.

In the anti-FLAG ChIP-seq experiment, there were a number of peaks in the 3xFLAG-BldB samples, which were absent in the wild-type control, as the control subtracted enrichment across the 3 samples indicated (**Fig. 4.4**). One of the highest peaks mapped to the *bldB* promoter, as indicated in **Figure 4.4**. The 10-hour sample in particular exhibited a lot of differential enrichment, but most of the high peaks across all samples again corresponded to genes encoding stable RNAs, so those peaks were unlikely to represent BldB binding (**Fig. 4.4**). Although there were statistically significant peaks flanked by protein-coding genes, some of these peaks were also present (albeit at lower levels) in the negative control, which led me to think that they might be false positives as well. In the light of subsequent RNA-seq experiments (described in the next section), it should be noted that no peaks were found in the promoters of any of the genes that I later found to be dramatically upregulated in the *ΔbldB* mutant, or in the promoters of other genes that might be relevant to this project, including the *bldB* and *whiJ* homologues, and genes encoding type VII secretion system components.

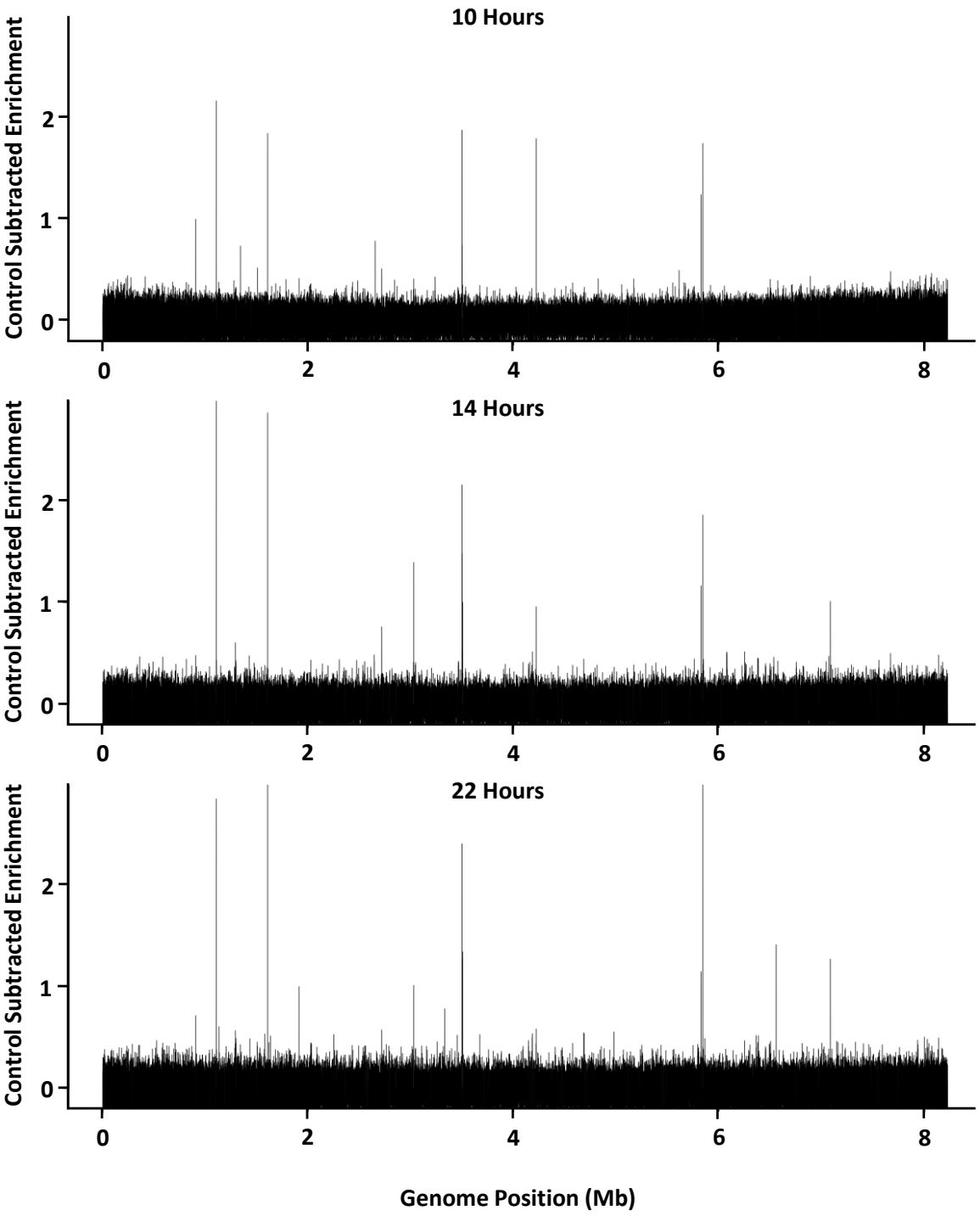

Figure 4.3. Polyclonal Anti-BldB ChIP-Seq Whole Genome Enrichment.

ChIP-seq results representing levels of BldB binding to DNA across the whole genome, with protein-DNA complexes captured from wild-type *S. venezuelae* using the anti-BldB polyclonal antibody. The *ΔbldB* mutant was used as a negative control. The x-axes indicate the genome position in megabases, and the y-axes represent the control subtracted enrichment for each time point.

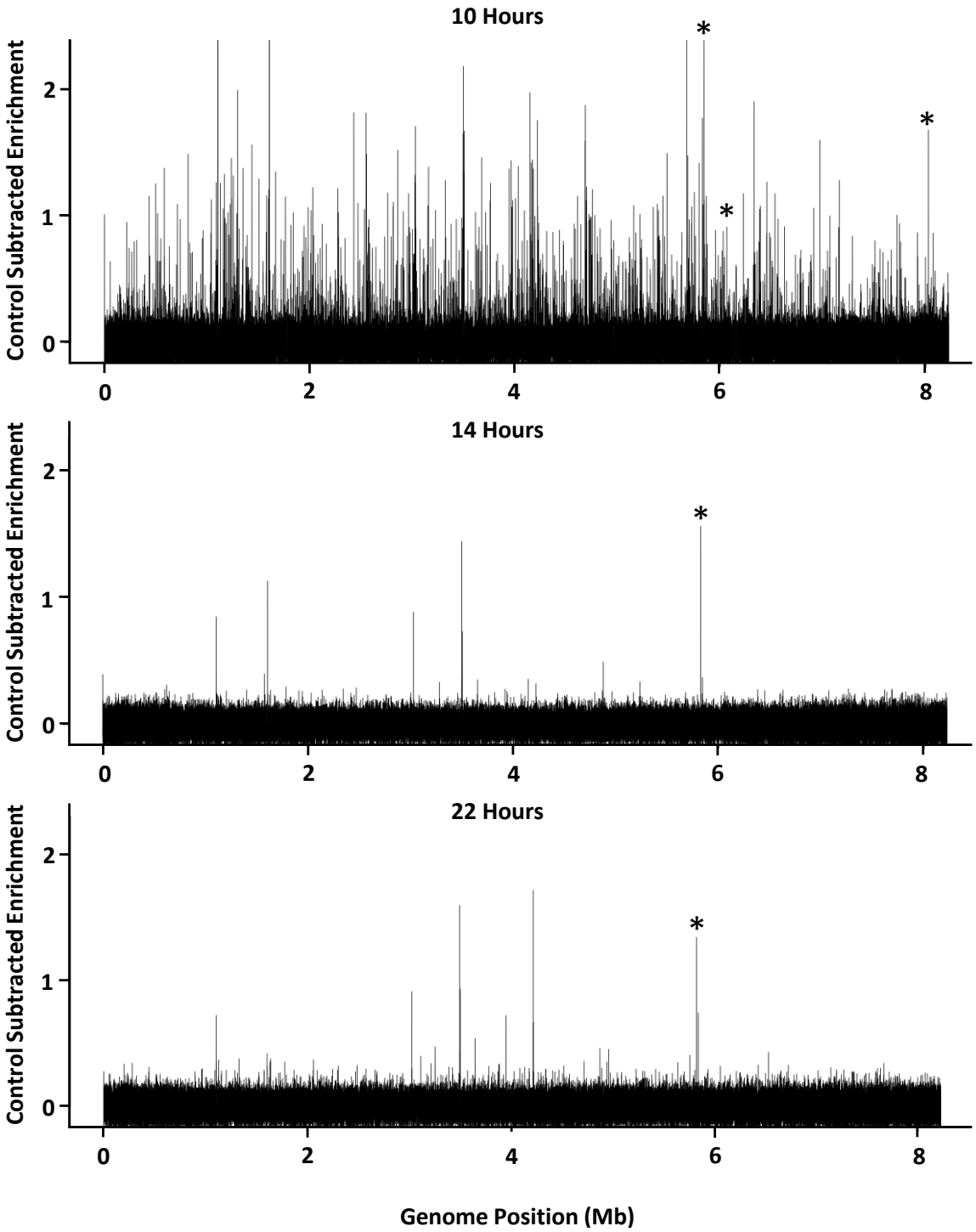

Figure 4.4. Anti-FLAG ChIP-Seq Whole Genome Enrichment.

ChIP-seq results representing levels of 3xFLAG-BldB binding to DNA across the whole genome, with protein-DNA complexes captured from the Δ*bldB::*3xFLAG-BldB strain using an anti-FLAG antibody. Wild-type *S. venezuelae* was used as a negative control. The x-axes indicate the genome position in megabases, and the y-axes represent the control subtracted enrichment for each time point. Asterisks in the 10-hour sample indicate the significant enrichment at the *bldB-vnz26625*, *lexA-nrdR* and *vnz35960-vnz35965* intergenic regions, in this sequence. Asterisks in the 14- and 22-hour samples indicate the significant enrichment at the *bldB-vnz26625* intergenic region.

While the 3xFLAG-BldB ChIP-seq results suggested that BldB is not able to bind DNA, there were a few statistically significant peaks with a low level of enrichment in the dataset, including one in the *bldB* promoter. I decided to use the SPR-dependent ReDCaT method (Stevenson *et al.*, 2013; Stevenson and Lawson, 2021) to see if purified 6xHis-BldB was able to bind its own promoter *in vitro.* I split the sequences of the *bldB* promoter into 40 bp long overlapping oligos and bound them to a streptavidin SPR chip via a biotinylated DNA linker to test for any 6xHis-BldB binding. 6xHis-BldB did not bind to any of the assayed oligos, which strengthened the evidence that BldB is not a transcription factor (**Fig. 4.5**).

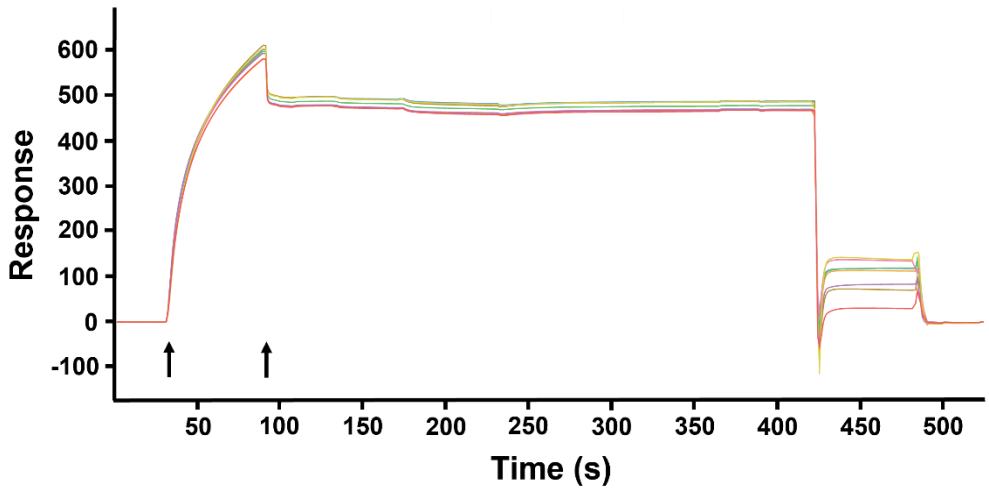

Figure 4.5. 6xHis-BldB Does Not Bind Its Own Promoter.

Surface Plasmon Resonance (SPR) was used to measure the level of binding of 6xHis-BldB to 40 bp overlapping dsDNA oligos from the *bldB* promoter region. SPR sensorgram measuring binding response (y-axis) over time (x-axis). Arrows indicate the subsequent injections of DNA and 6xHis-BldB.

BldB Indirectly Represses the Expression of the *abaA* Homologues and *iosA*

Despite not being a transcription factor itself, BldB still has an important developmental role in *S. venezuelae*. I used RNA-seq to determine which genes are differentially expressed in the *ΔbldB* mutant compared to wild-type *S. venezuelae* and might therefore contribute to the bald phenotype of the mutant. For consistency, I took samples from the same 3 time points as I did in the ChIP-seq experiments: 10, 14 and 22 hours. The most striking finding from this experiment was the extremely high upregulation of the 5 *abaA* homologues in the *ΔbldB* samples across the 3 time points (**Fig. 4.6**). One additional gene, *vnz16670*, which I have named *iosA* (for **i**nhibitor **o**f **s**porulation **A**), was the most highly upregulated gene at the 14- and 22-hour time points across the whole dataset, with the highest $\log_2$ fold change being 9.56 (expression in the *ΔbldB* mutant ~750 times higher than in wild type). Interestingly, *iosA* is encoded immediately upstream of *whiJ9* and *bldB9* on the opposite strand, which is the same genomic arrangement as that of the *abaA* homologues (**Fig. 3.6**). Despite its genomic context however, IosA is not an AbaA homologue, as it lacks the characteristic anti-sigma factor HATPase_c domain. In terms of function, IosA has no bioinformatically predicted domains, and there is no prior literature to suggest what its cellular function might be.

To expand on the BldB RNA-seq dataset, I have summarised the expression patterns of selected genes of interest in **Table 4.1**.

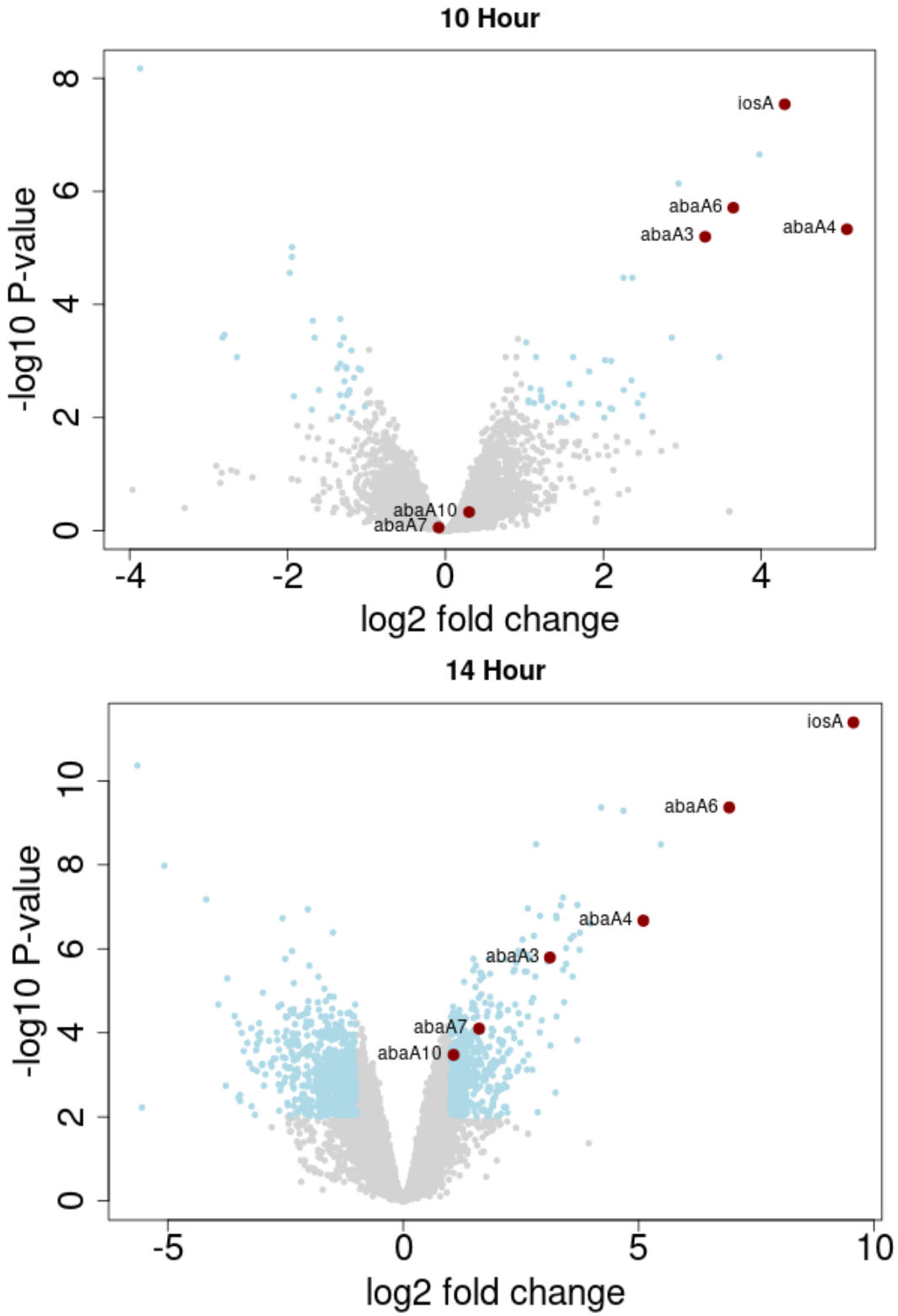

(Figure continued on next page.)

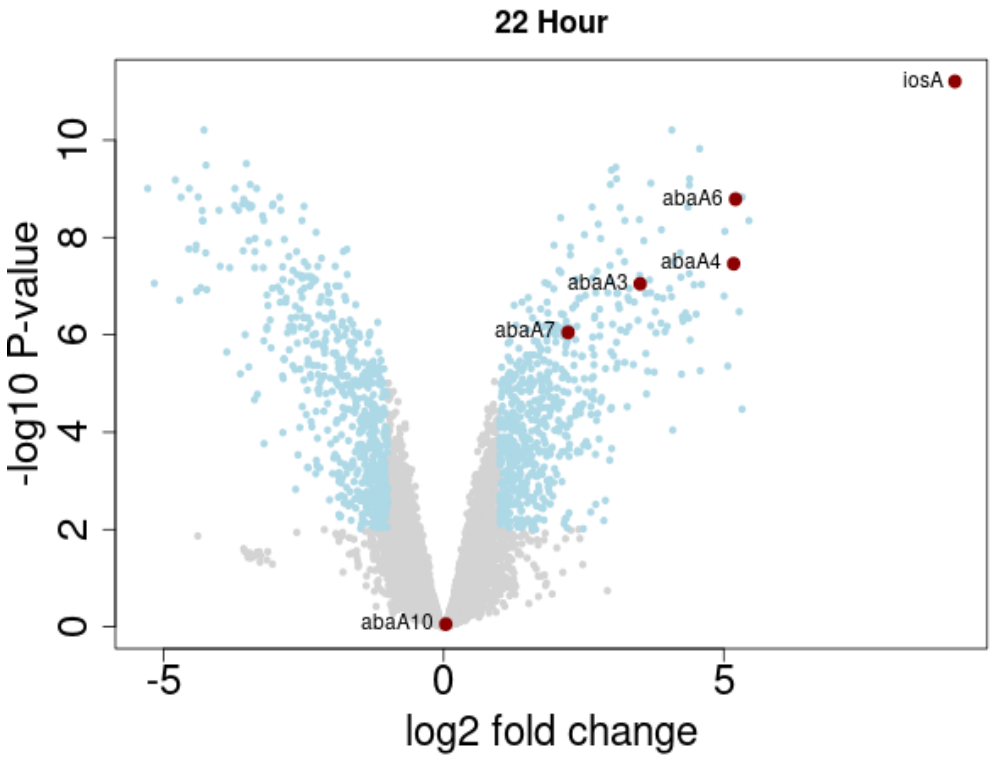

Figure 4.6. Differential Gene Expression in the *ΔbldB* mutant from an RNA-seq Experiment.

Volcano plots were generated to illustrate the differential gene expression in the *ΔbldB* mutant compared to wild-type *S. venezuelae* as assayed by RNA-seq using three biological replicates per time point. The x-axes represent the $\log_2$ fold change of gene expression in the *ΔbldB* mutant, compared to wild type. The y-axes represent the $-\log_{10}$ P value. Represented by blue dots are all significantly down- or up-regulated genes with a $\log_2$ fold change less than -1 or above 1 respectively, and P value ≤ 0.01. The *abaA* homologues and *iosA* are highlighted in red.

The seeming downregulation of expression of *bldB* itself in the *ΔbldB* mutant is an artefact arising from the deletion of the gene (**Table 4.1**). For most of the other *bldB* homologues there was no significant change in expression, except for *bldB2* and *bldB6*, which were both downregulated at 22 hours, and *bldB7*, which was upregulated at 14 and 22 hours. Looking at their neighbouring *whiJ* homologues, the expression of *whiJ2*, *whiJ5* and *whiJ6* was downregulated at 22 hours, whereas *whiJ10* was upregulated at 14 hours. None of the other *whiJ* homologues exhibited any change in expression, and neither did the other genes I will be discussing in this thesis, namely: *asfA1*, *asfA2*, *osaC*, and *osaC2*. The expression of *sigB*, *sigB2* and *sigB3* was significantly reduced at 14 hours (and at 22 hours for *sigB2*).

Looking at the expression of the genes associated with the *Streptomyces* type VII secretion system, there was an upregulation for *eccC*, *eccD* and *eccE* in the middle and late time point, and no change in expression for the rest of the genes.

Out of all other *bld* genes only the expression of *bldM* and *bldN* was downregulated at the later time point. The expression of *whiB*, *whiG*, *whiH* and *whiI* was downregulated at the mid- to late development time points. All of the chaplins and rodlins, as well as the *ram* genes were downregulated during mid- and late development, which is logical for a strain that exhibits impaired formation of aerial hyphae. The expression of the polarisome genes *divIVA*, *scy*, and *filP* was unchanged, as expected. Other regulators of cell division and development, such as *rsbN*, *rsiG*, *ssgA*, *ssgB*, *ssgG*, *sffA* and *smeA* were downregulated in the 22-hour time point as well (**Table 4.1**).

Table 4.1. BldB RNA-seq Results.

S. venezuelae **Gene**	***S. coelicolor*** **Homologue**	**Product**	**LFC 10 Hours**	**FDR 10 Hours**	**LFC 14 Hours**	**FDR 14 Hours**	**LFC 22 Hours**	**FDR 22 Hours**
vnz29085	*sco6237*	AbaA3	3.29	6.34E-06	3.12	1.61E-06	3.51	8.97E-08
vnz25565	*sco6130*	AbaA4	5.08	4.67E-06	5.1	2.13E-07	5.18	3.46E-08
vnz09905	*scp1.59, scp1.294*	AbaA6	3.64	1.95E-06	6.92	4.31E-10	5.21	1.63E-09
vnz16135	*sco3423*	AbaA7	n.s.	n.s.	1.61	7.91E-05	2.22	8.92E-07
vnz31495	*sco1980*	AbaA10	n.s.	n.s.	1.07	0.000334	n.s.	n.s.
vnz16670	-	IosA	4.3	2.89E-08	9.56	4.08E-12	9.12	6.21E-12
vnz26620	-	BldB	-3.87	6.74E-09	-5.64	4.32E-11	-4.24	3.27E-10
vnz15145	*sco4442*	BldB2	n.s.	n.s.	n.s.	n.s.	-1.7	3.39E-05
vnz29075	*sco6235*	BldB3	n.s.	n.s.	n.s.	n.s.	n.s.	n.s.
vnz25555	*sco6128*	BldB4	n.s.	n.s.	n.s.	n.s.	n.s.	n.s.
vnz20565	-	BldB5	n.s.	n.s.	n.s.	n.s.	n.s.	n.s.
vnz09895	-	BldB6	n.s.	n.s.	n.s.	n.s.	-2.18	2.67E-08
vnz16140	*sco3424*	BldB7	n.s.	n.s.	2.9	1.64E-07	2.67	6.74E-08

S. venezuelae **Gene**	***S. coelicolor*** **Homologue**	**Product**	**LFC 10 Hours**	**FDR 10 Hours**	**LFC 14 Hours**	**FDR 14 Hours**	**LFC 22 Hours**	**FDR 22 Hours**
vnz28285	-	BldB8	n.s.	n.s.	n.s.	n.s.	n.s.	n.s.
vnz16680	-	BldB9	n.s.	n.s.	n.s.	n.s.	n.s.	n.s.
vnz31505	*sco1978*	BldB10	n.s.	n.s.	n.s.	n.s.	n.s.	n.s.
vnz28375	*sco2382*	BldB11	n.s.	n.s.	n.s.	n.s.	n.s.	n.s.
vnz15140	*sco4441*	WhiJ2	n.s.	n.s.	n.s.	n.s.	-2.02	2.17E-07
vnz29080	*sco6236*	WhiJ3	n.s.	n.s.	n.s.	n.s.	n.s.	n.s.
vnz25560	*sco6129*	WhiJ4	n.s.	n.s.	n.s.	n.s.	n.s.	n.s.
vnz20560	*sco3365*	WhiJ5	n.s.	n.s.	n.s.	n.s.	-1.92	2.37E-06
vnz09900	-	WhiJ6	n.s.	n.s.	n.s.	n.s.	-3.43	2.22E-09
vnz16130	*sco3421*	WhiJ7	n.s.	n.s.	n.s.	n.s.	n.s.	n.s.
vnz28280	*sco2865*	WhiJ8	n.s.	n.s.	n.s.	n.s.	n.s.	n.s.
vnz16675	-	WhiJ9	n.s.	n.s.	n.s.	n.s.	n.s.	n.s.
vnz31500	*sco1979*	WhiJ10	n.s.	n.s.	1.12	0.000162	n.s.	n.s.
vnz28370	-	WhiJ11	n.s.	n.s.	n.s.	n.s.	n.s.	n.s.
vnz03680	-	AsfA1	n.s.	n.s.	n.s.	n.s.	n.s.	n.s.

S. venezuelae **Gene**	***S. coelicolor*** **Homologue**	**Product**	**LFC 10 Hours**	**FDR 10 Hours**	**LFC 14 Hours**	**FDR 14 Hours**	**LFC 22 Hours**	**FDR 22 Hours**
vnz10850	*sco7754*	AsfA2	n.s.	n.s.	n.s.	n.s.	n.s.	n.s.
vnz17535	*sco3796*	OsaC2	n.s.	n.s.	n.s.	n.s.	n.s.	n.s.
vnz26710	*sco5748*	OsaA	n.s.	n.s.	n.s.	n.s.	n.s.	n.s.
vnz26715	*sco5749*	OsaB	n.s.	n.s.	n.s.	n.s.	n.s.	n.s.
vnz26705	*sco5747*	OsaC	n.s.	n.s.	n.s.	n.s.	n.s.	n.s.
vnz01755	*sco7327*	OsaD	n.s.	n.s.	n.s.	n.s.	n.s.	n.s.
vnz01715	*sco0600*	SigB	n.s.	n.s.	-1.01	0.015035	n.s.	n.s.
vnz01090	-	SigB2	n.s.	n.s.	-2.69	9.78E-05	-1.83	0.001112
vnz02255	-	SigB3	n.s.	n.s.	-1.06	0.001691	n.s.	n.s.
vnz13800	*sco3068*	SigI	n.s.	n.s.	n.s.	n.s.	n.s.	n.s.
vnz18615	*sco4034*	SigN	n.s.	n.s.	n.s.	n.s.	n.s.	n.s.
vnz18620	*sco4035*	SigF	n.s.	n.s.	n.s.	n.s.	n.s.	n.s.
vnz24270	*sco5243*	SigH	n.s.	n.s.	n.s.	n.s.	n.s.	n.s.
vnz05860	*sco1607*	T7SS-associated serine protease mycosin	n.s.	n.s.	n.s.	n.s.	n.s.	n.s.

S. venezuelae **Gene**	***S. coelicolor*** **Homologue**	**Product**	**LFC 10 Hours**	**FDR 10 Hours**	**LFC 14 Hours**	**FDR 14 Hours**	**LFC 22 Hours**	**FDR 22 Hours**
vnz13260	*sco5731*	T7SS-associated serine protease mycosin	n.s.	n.s.	n.s.	n.s.	n.s.	n.s.
vnz26595	*sco5720*	T7SS secretion protein EccE	n.s.	n.s.	n.s.	n.s.	1.38	0.004097
vnz26600	*sco5721*	T7SS secretion protein EccB	n.s.	n.s.	n.s.	n.s.	n.s.	n.s.
vnz26605	*sco5722*	T7SS-associated serine protease mycosin	n.s.	n.s.	n.s.	n.s.	n.s.	n.s.
vnz26610	*sco5724*	T7SS-associated protein EsxB	n.s.	n.s.	n.s.	n.s.	n.s.	n.s.
vnz26615	*sco5725*	T7SS-associated protein EsxA	n.s.	n.s.	n.s.	n.s.	n.s.	n.s.
vnz26625	*sco5734*	T7SS secretion protein EccC	n.s.	n.s.	n.s.	n.s.	1.61	0.00048
vnz26630	*sco5735*	T7SS integral membrane protein EccD	n.s.	n.s.	1.19	0.005999	1.47	0.001074
vnz18945	*sco4091*	BldC	n.s.	n.s.	n.s.	n.s.	n.s.	n.s.
vnz05285	*sco1489*	BldD	n.s.	n.s.	n.s.	n.s.	n.s.	n.s.
vnz16350	*sco3549*	BldG	n.s.	n.s.	n.s.	n.s.	n.s.	n.s.
vnz12630	*sco2792*	BldH	n.s.	n.s.	n.s.	n.s.	n.s.	n.s.
vnz22005	*sco4768*	BldM	n.s.	n.s.	n.s.	n.s.	-1.57	1.01E-05

S. venezuelae **Gene**	***S. coelicolor*** **Homologue**	**Product**	**LFC 10 Hours**	**FDR 10 Hours**	**LFC 14 Hours**	**FDR 14 Hours**	**LFC 22 Hours**	**FDR 22 Hours**
vnz15655	*sco3323*	BldN	n.s.	n.s.	n.s.	n.s.	-2.92	1.49E-09
vnz04660	*sco1381*	BldO	n.s.	n.s.	n.s.	n.s.	n.s.	n.s.
vnz07750	*sco1950*	WhiA	n.s.	n.s.	n.s.	n.s.	n.s.	n.s.
vnz13645	*sco3034*	WhiB	n.s.	n.s.	-1.15	0.0079	n.s.	n.s.
vnz22000	*sco4767*	WhiD	n.s.	n.s.	n.s.	n.s.	n.s.	n.s.
vnz33520	*sco5320*	WhiE ORFI	n.s.	n.s.	n.s.	n.s.	n.s.	n.s.
vnz33515	*sco5319*	WhiE ORFII	n.s.	n.s.	n.s.	n.s.	n.s.	n.s.
vnz33510	*sco5318*	WhiE ORFIII	n.s.	n.s.	n.s.	n.s.	n.s.	n.s.
vnz33505	*sco5317*	WhiE ORFIV	n.s.	n.s.	n.s.	n.s.	n.s.	n.s.
vnz33500	*sco5316*	WhiE ORFV	n.s.	n.s.	n.s.	n.s.	n.s.	n.s.
vnz33495	*sco5315*	WhiE ORFVI	n.s.	n.s.	n.s.	n.s.	n.s.	n.s.
vnz33490	*sco5314*	WhiE ORFVII	n.s.	n.s.	n.s.	n.s.	n.s.	n.s.
vnz33525	*sco5321*	WhiE ORFVIII	n.s.	n.s.	n.s.	n.s.	n.s.	n.s.
vnz26215	*sco5621*	WhiG	n.s.	n.s.	n.s.	n.s.	-1.28	5.75E-05
vnz27205	*sco5819*	WhiH	n.s.	n.s.	-1.11	0.005	-2.22	1.24E-05

***S. venezuelae* Gene**	***S. coelicolor* Homologue**	**Product**	**LFC 10 Hours**	**FDR 10 Hours**	**LFC 14 Hours**	**FDR 14 Hours**	**LFC 22 Hours**	**FDR 22 Hours**
vnz28820	*sco6029*	WhiI	n.s.	n.s.	-1.32	0.013	-1.25	0.017136
vnz15660	*sco3324*	RsbN	n.s.	n.s.	n.s.	n.s.	-1.33	5.03E-05
vnz19430	*sco4184*	RsiG	n.s.	n.s.	n.s.	n.s.	-1.37	8.65E-06
vnz06205	*sco1674*	ChpC	n.s.	n.s.	n.s.	n.s.	-2.82	2.14E-07
vnz22895	*sco2717*	ChpD	n.s.	n.s.	n.s.	n.s.	-2.25	0.0001
vnz07055	*sco1800*	ChpE	n.s.	n.s.	n.s.	n.s.	-3.32	1.66E-05
vnz22960	*sco2705*	ChpF	n.s.	n.s.	n.s.	n.s.	-3.63	6.34E-06
vnz22985	*sco2699*	ChpG	1.16	0.04	n.s.	n.s.	-3.15	7.76E-07
vnz06210	*sco1675*	ChpH	n.s.	n.s.	n.s.	n.s.	-4.55	1.72E-08
vnz22870	*sco2719*	RdlAB-like	n.s.	n.s.	n.s.	n.s.	-3.15	6.94E-07
vnz22885	-	RdlAB-like	n.s.	n.s.	n.s.	n.s.	-2.85	3.12E-06
vnz22890	-	RdlAB-like	n.s.	n.s.	n.s.	n.s.	-1.94	0.0003
vnz31965	*sco6683*	RamA	n.s.	n.s.	-2.45	4.09E-05	-1.32	0.002
vnz31960	*sco6684*	RamB	n.s.	n.s.	-2.32	6.55E-06	-1.87	1.1E-05
vnz31975	*sco6681*	RamC	n.s.	n.s.	-2.02	0.0011	n.s.	n.s.

S. venezuelae **Gene**	***S. coelicolor*** **Homologue**	**Product**	**LFC 10 Hours**	**FDR 10 Hours**	**LFC 14 Hours**	**FDR 14 Hours**	**LFC 22 Hours**	**FDR 22 Hours**
vnz31955	*sco6685*	RamR	n.s.	n.s.	-2.34	3.41E-05	-1.41	0.001
vnz31970	*sco6682*	RamS	n.s.	n.s.	-1.38	0.015	-1.26	0.033
vnz08495	*sco2077*	DivIVA	n.s.	n.s.	n.s.	n.s.	n.s.	n.s.
vnz24950	*sco5396*	FilP	n.s.	n.s.	n.s.	n.s.	n.s.	n.s.
vnz24955	*sco5397*	Scy	n.s.	n.s.	n.s.	n.s.	n.s.	n.s.
vnz08520	*sco2082*	FtsZ	n.s.	n.s.	n.s.	n.s.	n.s.	n.s.
vnz01280	*sco6073*	GeoA	n.s.	n.s.	-1.07	0.00018	-3.45	8.18E-10
vnz27115	*sco5803*	LexA	n.s.	n.s.	n.s.	n.s.	-1.29	0.0007
vnz27120	*sco5804*	NrdR	n.s.	n.s.	n.s.	n.s.	n.s.	n.s.
vnz06980	*sco1789*	ParA	n.s.	n.s.	1.63	0.0019	n.s.	n.s.
vnz18015	*sco3887*	ParB	n.s.	n.s.	n.s.	n.s.	n.s.	n.s.
vnz26075	*sco5577*	Smc	n.s.	n.s.	n.s.	n.s.	n.s.	n.s.
vnz04890	*sco1416*	SffA	n.s.	n.s.	n.s.	n.s.	-1.15	0.0037
vnz04885	*sco1415*	SmeA	n.s.	n.s.	n.s.	n.s.	-1.26	0.00265
vnz18205	*sco3926*	SsgA	n.s.	n.s.	n.s.	n.s.	-2.55	6.94E-07

S. venezuelae **Gene**	***S. coelicolor*** **Homologue**	**Product**	**LFC 10 Hours**	**FDR 10 Hours**	**LFC 14 Hours**	**FDR 14 Hours**	**LFC 22 Hours**	**FDR 22 Hours**
vnz05545	*sco1541*	SsgB	n.s.	n.s.	n.s.	n.s.	-1.36	0.0016
vnz31585	*sco6722*	SsgD	n.s.	n.s.	1.56	0.002251	n.s.	n.s.
vnz13140	*sco2924*	SsgG	n.s.	n.s.	n.s.	n.s.	-1.71	6.94E-06

Overexpression of *abaA6* or *iosA* Results in Sporulation-Deficient Phenotypes

Because the 5 *abaA* homologues and *iosA* were among the most highly upregulated genes in the *ΔbldB* mutant (**Fig. 4.6**, **Table 4.1**), and given their genomic context next to *bldB* homologues, it seemed likely that they might contribute significantly to BldB function. To further investigate their roles in *Streptomyces* development, and in particular, their contribution to the *ΔbldB* phenotype, I generated mutant and overexpression strains for all 6 genes.

None of the single mutants for the six genes appeared to have any developmental defects - all 6 strains were able to sporulate on MYM solid medium (**Fig. 4.7**).

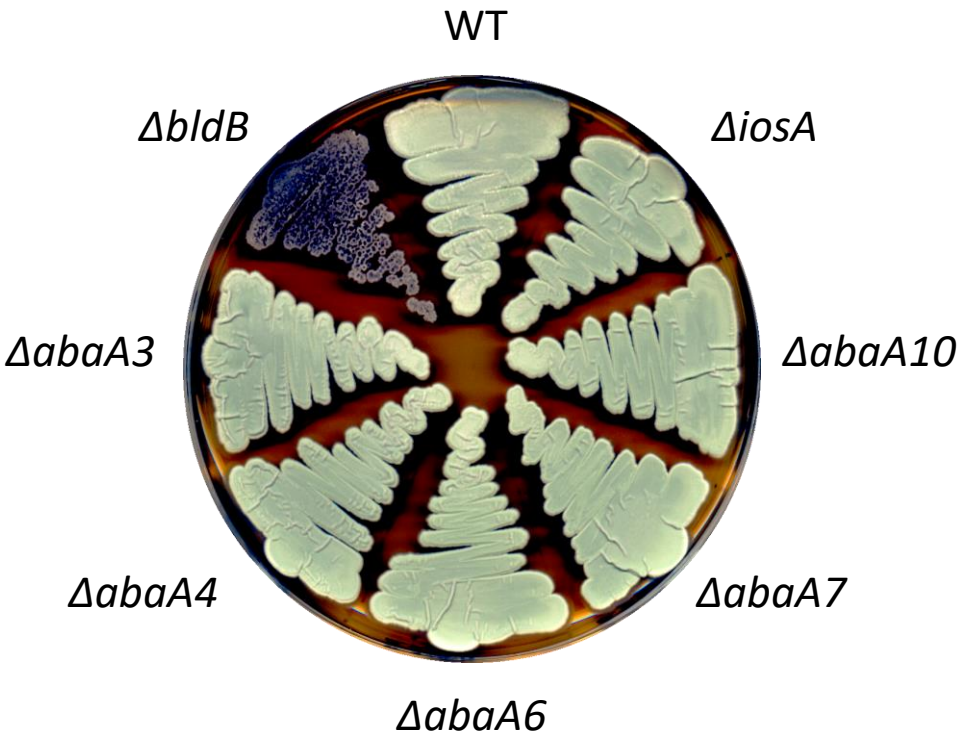

Figure 4.7. Mutant Phenotypes for the *abaA* Homologues and *iosA*.
Plate depicting the growth of the mutant strains for the 5 *abaA* homologues and *iosA* on MYM agar. Plate image was taken after a 4-day incubation at 28˚C.

Next, I placed each of the *abaA* homologues as well as *iosA* under the control of the strong constitutive *ermE** promoter in *S. venezuelae*, in order to establish whether the overexpression of any of these genes causes a developmental phenotype. While the overexpression of *abaA3*, *abaA4*, *abaA7* and *abaA10* did not impact the development of *S. venezuelae*, overexpressing *abaA6* or *iosA* resulted in strains that have white phenotypes when plated on MYM agar (**Fig. 4.8**).

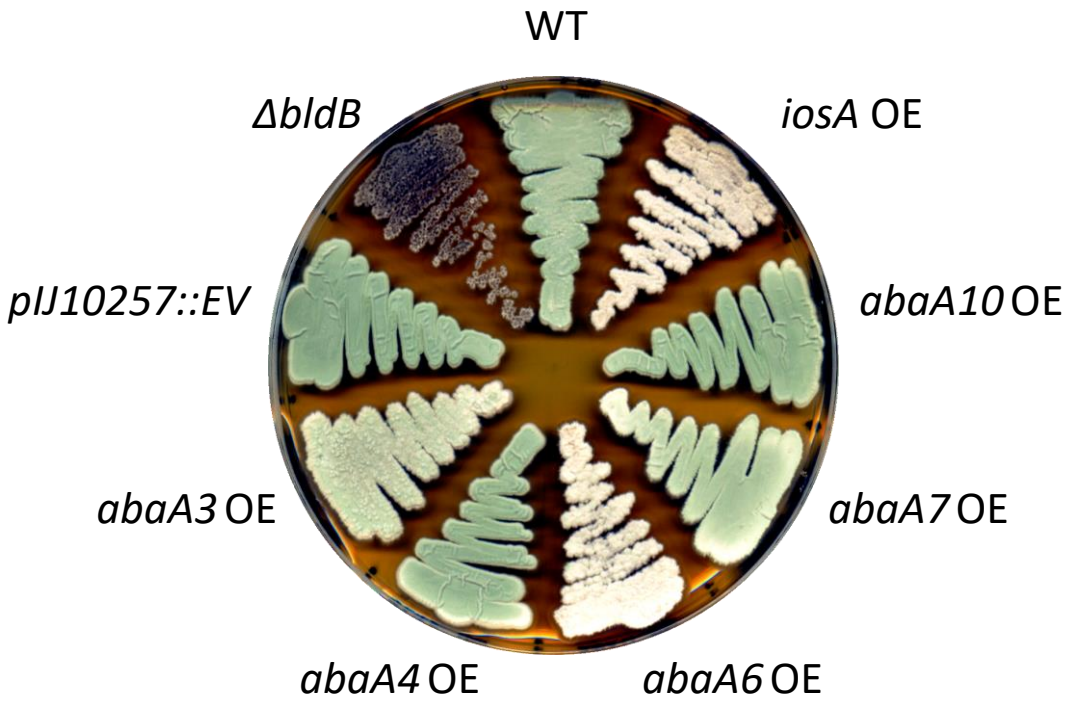

Figure 4.8. Overexpression Phenotypes for the *abaA* Homologues and *iosA*.

Plate depicting the growth of the overexpression strains for the 5 *abaA* homologues and *iosA* on MYM agar. EV stands for empty pIJ10257 vector control. Plate image was taken after a 4-day incubation at 28˚C.

In order to better visualise the phenotypes of these two overexpression lines, SEM imaging on single colonies was performed by Kim Findlay. In comparison to wild-type *S. venezuelae* (**Fig. 4.9A**) and the overexpression negative control (**Fig. 4.9D**), both the *abaA6* and the *iosA* overexpression lines exhibited impaired development with similar patterns of growth (**Fig. 4.9B, 4.9C, 4.9E, 4.9F**). The centres of the imaged colonies for both overexpression lines largely consisted of vegetative mycelial growth, with some bigger cone-like structures being raised, which possibly consisted of future aerial hyphae (**Fig. 4.9B**, **4.9E**). Moving on to the periphery of the colonies, a lot of undifferentiated hyphae, some lysed hyphae and a few chains with spores of varying sizes could be observed for both strains (**Fig. 4.9C**, **4.9F**). This suggests that the single overexpressions of *abaA6* and *iosA* might contribute to the Δ*bldB* phenotype.

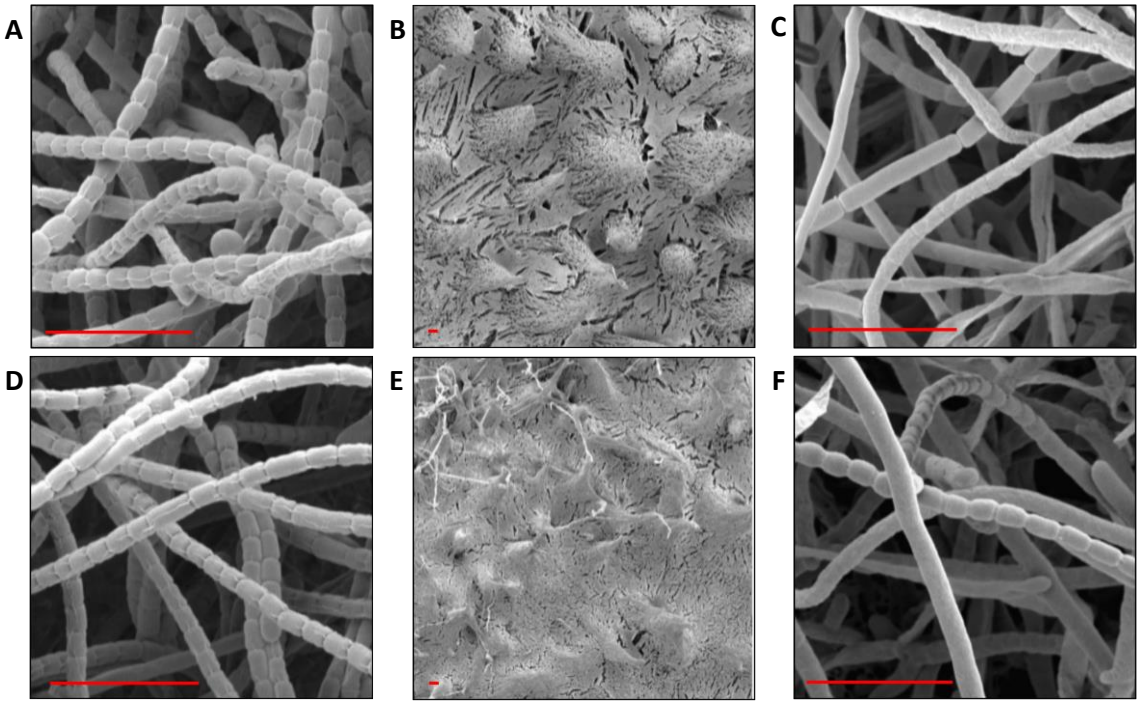

Figure 4.9. Phenotype Characterisation of the *abaA6* and *iosA* Single Overexpression Strains.

Scanning electron micrographs comparing the phenotypes of wild-type *S. venezuelae* **(A)**, the colony centre of the *abaA6* overexpression strain **(B)**, the colony periphery of the *abaA6* overexpression strain **(C),** the pIJ10257 empty vector control **(D)**, the colony centre of the *iosA* overexpression strain **(E)**, and the colony periphery of the *iosA* overexpression strain **(F).** Scale bars in red indicate 5 µm.

The Double Overexpression of *abaA6* and *iosA* Recapitulates the *ΔbldB* Mutant Phenotype

Since RNA-seq showed that *abaA6* and *iosA* were the two most dramatically upregulated genes in the Δ*bldB* mutant (**Fig. 4.6**, **Table 4.1**), and the single overexpressions of these genes led to white phenotypes (**Fig. 4.8**, **4.9**), I wondered if overexpressing *abaA6* and *iosA* at the same time in wild-type *S. venezuelae* would result in a phenotype that more closely resembles that of the Δ*bldB* mutant (**Fig. 3.7**, **3.8**). Thus, I constructed a strain in which both genes were overexpressed under the same *ermE** promoter, with a ribosome binding site inserted between the two genes, as described by Gallagher *et al.* (2020). On agar, the resulting double overexpression strain appeared bald and resembled the Δ*bldB* mutant much more closely than the single overexpression strains, which appeared white (**Fig. 4.10**).

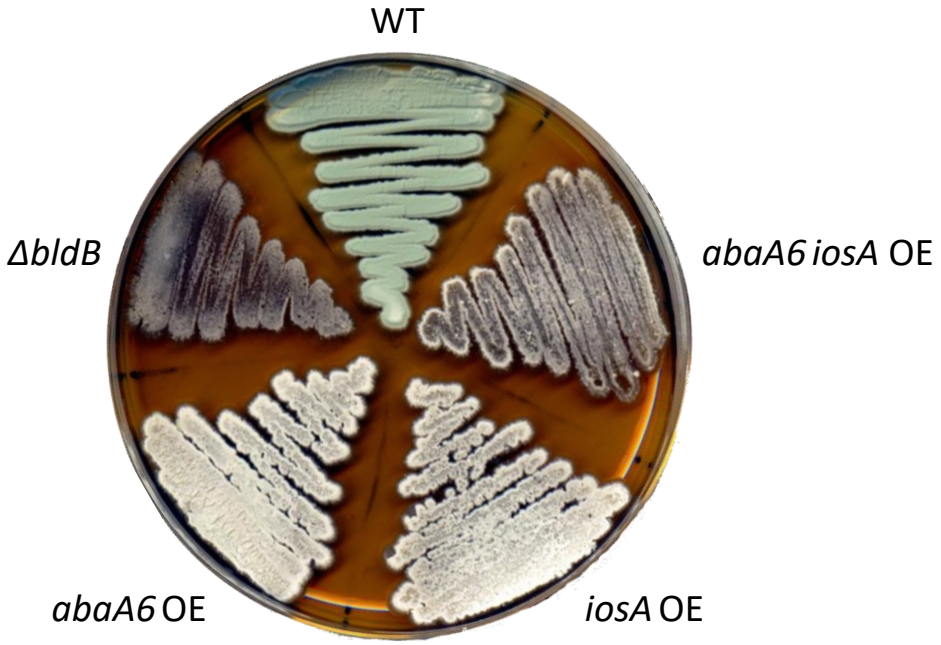

Figure 4.10. The Phenotype of the *abaA6 iosA* Double Overexpression Strain.
Plate depicting the growth of the single and double overexpression strains for *abaA6* and *iosA* on MYM agar. Plate image was taken after a 4-day incubation at 28˚C.

Under the electron microscope, the Δ*bldB* mutant and the *abaA6 iosA* double overexpression strains looked very similar, with vegetative mycelium growth only in the centre of the colonies, and sparse formation of undifferentiated hyphae in the periphery of the colonies (**Fig. 4.11**). Thus the double overexpression of just two genes, *abaA6* and *iosA*, was sufficient to cause a Δ*bldB*-like phenotype.

To extend this analysis, I used both phage transduction and the CRISPR/Cas9 system (Cobb, Wang and Zhao, 2015) to construct an Δ*abaA6* Δ*iosA* Δ*bldB* triple mutant, to see if the loss of *abaA6* and *iosA* would restore wild-type development to the Δ*bldB* mutant.

To make the triple mutant, I decided to make two of the mutations via CRISPR to get a markerless double mutant, and to introduce the final mutation via SV1-mediated phage transduction. Being wary of possible suppressor mutations that could arise when deleting *bldB*, something that I already experienced while constructing the Δ*bldB* mutant (as discussed in Chapter 3), I decided to introduce the *bldB* mutation last by SV1-mediated transduction. Thus, I generated the Δ*iosA* CRISPR mutant first and then deleted *abaA6* in that mutant via CRISPR again to generate the Δ*abaA6* Δ*iosA* double mutant (**Fig. 4.12**). As I showed previously, the Δ*abaA6* and Δ*iosA* single mutants were able to sporulate at levels comparable to wild-type (**Fig. 4.7**). Similarly to the single mutants, the Δ*abaA6* Δ*iosA* double mutant also had no developmental phenotype, as observed both on a plate and under the microscope (**Fig. 4.12**, **4.13**).

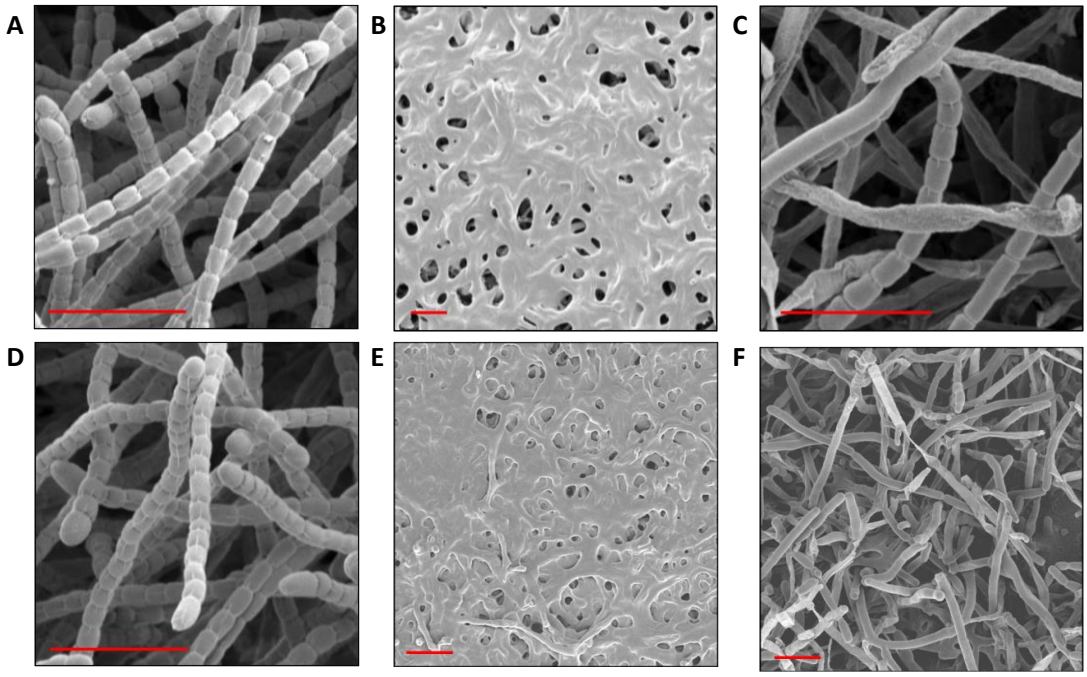

Figure 4.11. Phenotypic Characterisation of the *abaA6 iosA* Double Overexpression Strain.

Scanning electron micrographs comparing the phenotypes of wild-type *S. venezuelae* **(A)**, the colony centre of the *abaA6 iosA* double overexpression strain **(B)**, the colony periphery of the *abaA6 iosA* double overexpression strain **(C),** the pIJ10257 empty vector control **(D)**, the colony centre of the Δ*bldB* mutant strain **(E)**, and the colony periphery of the Δ*bldB* mutant strain **(F).** Scale bars in red indicate 5 µm.

Next, I used the wild-type SV1 phage to infect the Δ*bldB::apr* Redirect mutant, and then used the resulting mutant lysate to infect the Δ*abaA6* Δ*iosA* double mutant. The generated Δ*abaA6* Δ*iosA* Δ*bldB* triple mutant looked white on a plate, a phenotype that could be complemented by providing *bldB in trans* (**Fig. 4.12**). The triple mutant did exhibit some patches of green growth upon prolonged incubation, but did not go on to fully develop the spore pigment on a plate. As could be observed in the SEM images, the Δ*abaA6* Δ*iosA* Δ*bldB* triple mutant largely consisted of spore chains with spores of varying sizes, and a few undifferentiated hyphae (**Fig. 4.13**). In terms of progression through the life cycle, the triple mutant exhibited levels of differentiation much closer to those of wild type than to those of the Δ*bldB* mutant (**Fig. 4.13**).

Unfortunately, whole genome resequencing of the Δ*abaA6* Δ*iosA* Δ*bldB* triple mutant strain showed that a 28.25 kb segment of the *S. venezuelae* genome was unintentionally deleted. This deleted segment covered 32 genes: *vnz19660* to *vnz19800*. Analysis of the parental strains showed that the deletion occurred during the first CRISPR-mediated deletion - that of *iosA*.

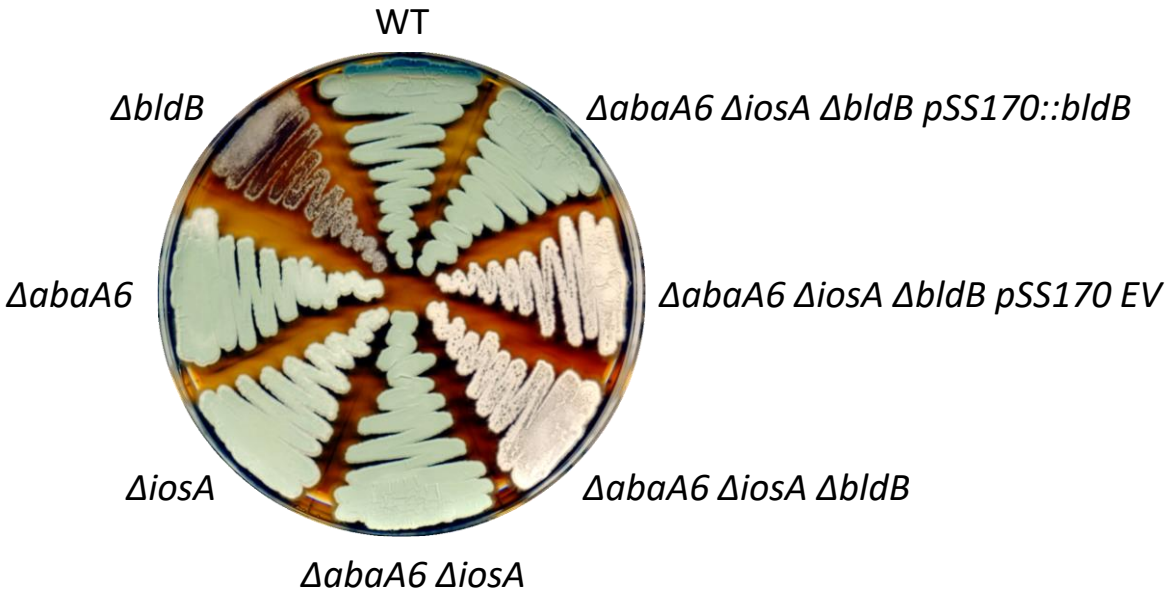

Figure 4.12. The Phenotype of the *ΔabaA6 ΔiosA ΔbldB* Triple Mutant Strain.

Plate depicting the growth of the Δ*abaA6* Δ*iosA* double mutant and Δ*abaA6* Δ*iosA* Δ*bldB* triple mutant on MYM agar. EV stands for empty pSS170 vector control. Plate image was taken after a 4-day incubation at 28˚C.

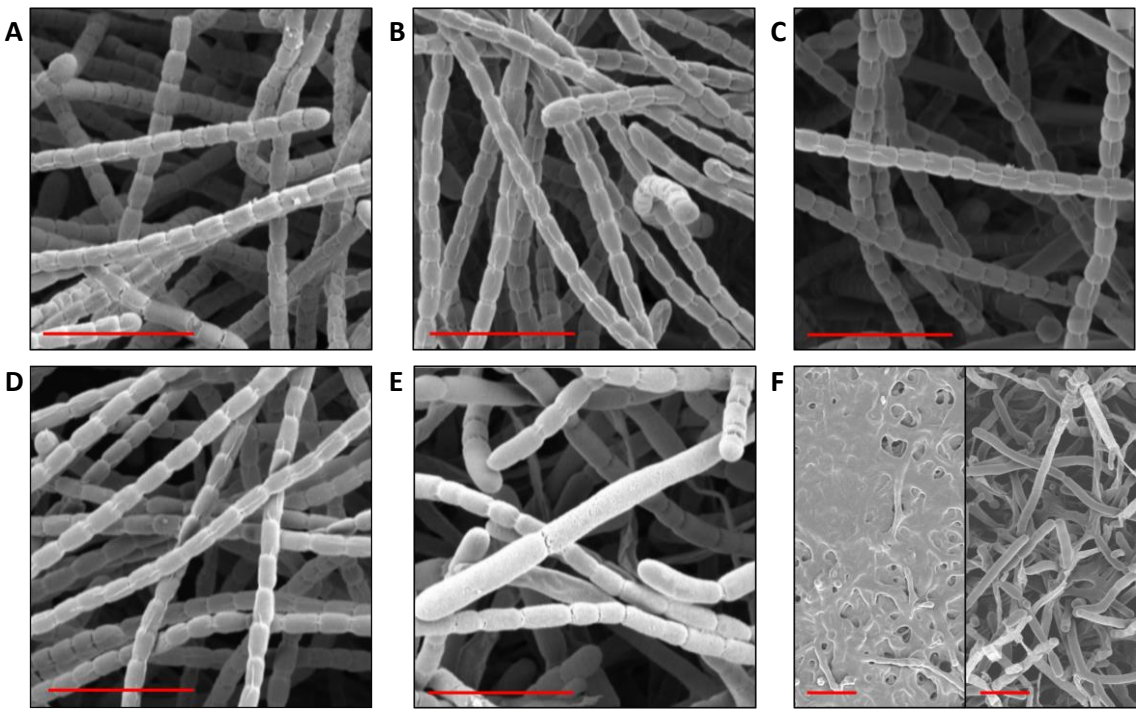

Figure 4.13. Phenotypic Characterisation of the *ΔabaA6 ΔiosA ΔbldB* Triple Mutant.

Scanning electron micrographs comparing the phenotypes of wild-type *S. venezuelae* **(A)**, the Δ*abaA6* mutant **(B)**, the Δ*iosA* mutant **(C),** the Δ*abaA6* Δ*iosA* double mutant **(D)**, the Δ*abaA6* Δ*iosA* Δ*bldB* triple mutant **(E)**, and the colony centre (left panel) and colony periphery (right panel) of the Δ*bldB* mutant strain **(F).** Scale bars in red indicate 5 µm.

Discussion

In this chapter, I described my efforts towards finding out if BldB is a transcription factor, characterising its 'regulon', and identifying candidate regulators that might mediate the Δ*bldB* mutant phenotype.

From an existing microarray study (Bibb *et al.*, 2012), I established that in wild-type *S. venezuelae* the expression of *bldB* peaked at early to mid-development (12 hours) and then tailed off to base levels (**Fig. 4.2**). In comparison, my automated Western blots revealed that the protein abundance of BldB is lower during early development, but then rises and maintains a steady high level in mid- to late development with a moderate decrease during late sporulation (36 hours) (**Fig. 4.1A**, **4.1C**). A similar pattern could be observed in the Western blot, where I measured the levels of 3xFLAG-BldB from the Δ*bldB::*3xFLAG-BldB strain (**Fig. 4.1B**, **4.1D**).

The time points used for the microarray dataset and my Western blots cannot be directly compared, as the experiments were performed years apart and under slightly different conditions. Nevertheless, the broader patterns might be comparable - an early peak of *bldB* expression followed by a peak and sustained levels of BldB protein during mid- and late development might indicate a repression of *bldB* expression or degradation of *bldB* mRNA after the early developmental stages, with BldB protein levels remaining high because the protein is very stable, with little turnover, or possibly because the protein is locked in an interaction (*e.g.* with the BldB homologues). In *S. coelicolor* a slightly different pattern was reported - both the levels of *bldB* expression and the protein levels of BldB were found to be higher during the later stages of development (Yagüe *et al.*, 2014; Rioseras *et al.*, 2018). The difference in expression patterns could be attributed to the use of different species and methods of sampling - Yagüe *et al.* (2014) and Rioseras *et al.* (2018) sampled from solid and liquid cultures of *S. coelicolor*, which cannot be directly compared with the growth and expression patterns of *S. venezuelae*.

My Western blots informed my choice of time points for sampling for my ChIP-seq and RNA-seq experiments. I chose the vegetative growth time point to be at 10 hours, so that I would be confident that I would get enough biomass, from which I could extract nucleic acids. The middle time point was 14 hours, which marked the beginning stages of fragmentation growth in liquid. The final time point was at 22 hours, when the cultures were in the middle of sporulation.

I decided that these 3 time points would appropriately represent the different developmental stages of *S. venezuelae* and give me a comprehensive view into the function of BldB throughout the life cycle.

The anti-BldB antibody ChIP-seq experiment showed a lot of peaks of enrichment, however, most of these were also found in the Δ*bldB* mutant negative control. This suggests that the anti-BldB polyclonal antibody crossreacts non-specifically with one or more DNA-binding proteins. This was unexpected given that the anti-BldB antibody produced clean Western blots, with very little non-specific binding (**Fig. 4.1A**). Upon subtracting the control enrichment from each of the 3 experimental samples genome-wide, there were still a few significant peaks, which possibly represented BldB binding (**Fig. 4.3**). However, all of these peaks corresponded to stable RNA genes, which is a known artefact in ChIP-seq experiments, possibly caused by the high levels of transcription of these genes and the protection of their promoters by RNA polymerase (Vora, Hottes and Tavazoie, 2009).

It is possible that the DNA-binding protein(s) that the anti-BldB antibody bound could actually be one or more of the BldB homologues. The predicted molecular weights for the BldB homologues are quite low, ranging from 6.6 to 9.6 kDa, which could be why they were not detected in any automated Western blots conducted with the polyclonal antibody (the separation range used was 12 to 230 kDa). Further work could be undertaken to determine if any of the BldB homologues are responsible for the enrichment peaks seen in the polyclonal ChIP-seq experiment. Data in Chapter 7 raise the possibility that BldB homologues might interact with DNA indirectly via their partner WhiJ DNA-binding proteins.

Fortunately, I also did the alternative ChIP-seq experiment, where I precipitated 3xFLAG-BldB using an anti-FLAG antibody (**Fig. 4.4**). For the 14- and 22-hour time points, the observed significant peaks corresponded to stable RNA genes, mirroring what I observed in the polyclonal anti-BldB experiment. For the 10-hour sample, there was a lot more differential enrichment, most of which again corresponded to stable RNA genes. One peak seen across all time points corresponded to the *bldB* promoter region. Looking at the raw data, some of the other peaks were often present in the wild-type negative control as well, albeit smaller in size. To investigate this, I used the SPR-derived ReDCaT method (Stevenson *et al.*, 2013) to see if purified 6xHis-BldB would be able to bind its own promoter in an *in vitro* SPR experiment.

My ReDCaT experiment showed no binding of 6xHis-BldB to its promoter, so I concluded that BldB is unlikely to be a DNA-binding protein (**Fig. 4.5**). The peaks observed in the *bldB* promoter in the anti-FLAG ChIP-seq experiment are likely to be an artefact of the construction of the Δ*bldB::*3xFLAG-BldB strain, where the promoter region is present twice - once in its native locus, and once in the pSS170 integrative vector, where I placed 3xFLAG-BldB under the control of its own promoter. In order to definitively state that BldB is not a DNA-binding protein, I plan to use SPR to test binding of 6xHis-BldB to a few more promoters, including the intergenic regions between *lexA* and *nrdR,* and between *vnz35960* and *vnz35965*, as there was modest, but significant enrichment at those positions (peaks indicated in **Fig. 4.4**).

The evidence in previous literature that BldB is a DNA-binding protein is weak. It was proposed that BldB is involved in its own regulation based on the temporal pattern of its promoter activity, when the strain expressing the reporter fusion was grown on media with different carbon sources (Pope, Green and Westpheling, 1998). In opposition to this report, Eccleston *et al*. (2002) did not observe any binding of BldB to DNA in *S. coelicolor*. The only experimental evidence supporting DNA binding was an EMSA performed with purified *S. lividans* BldB and its promoter region, in which a specific and concentration-dependent binding of BldB to the labelled probe was observed (Mishig-Ochiriin *et al.*, 2003). However, EMSA experiments are well known to produce artefacts, which is why *in vivo* ChIP-seq is the favoured technique to demonstrate physiologically relevant DNA binding.

My RNA-seq produced much more interesting results, on which the rest of my research was based. Across all 3 time points in the Δ*bldB* mutant, there was a striking level of upregulation of the *abaA* homologues (**Fig. 4.6**, **Table 4.1**), which are encoded in the vicinity of the *bldB* homologues (**Fig. 3.6**). As well as the *abaA* homologues, one of the genes with the highest level of upregulation was *iosA* (*vnz16670*). Interestingly, *iosA* is encoded divergently and upstream of *whiJ9* and *bldB9* - this is the same genomic context, in which the *abaA* homologues are found. However, IosA is not an AbaA homologue, and it has no bioinformatically predicted conserved domains. IosA is not very well-conserved in *Streptomyces*, and there is a dearth of literature on it. Only one study has reported a homologue of *iosA* to be encoded next to homologues of *bldB* and *whiJ*, and that is in the skyllamycin gene cluster in *Streptomyces* sp. Acta 2897, where the WhiJ homologue was suggested to be a transcriptional regulator for the cluster (Pohle *et al.*, 2011).

In contrast to the *abaA* homologues, expression of the *bldB* and *whiJ* homologues was not dramatically changed in the *ΔbldB* mutant relative to the wild type (**Table 4.1**). There was no significant change in expression for any of them at the 10-hour time point, and at the 14-hour point only *bldB7* and *whiJ10* were upregulated. At 22 hours, the expression of *bldB2*, *bldB6*, *whiJ2*, *whiJ5* and *whiJ6* was significantly lower in the *ΔbldB* mutant, and the expression of *bldB7* was higher. Overall, there was no strong unifying pattern of expression of the *bldB* and *whiJ* homologues in the *ΔbldB* mutant, in contrast to the *abaA* homologues.

Looking at the expression of other key developmental players in the *ΔbldB* mutant, there were generally no changes in expression at the 10-hour time point, with the exception of one of the chaplins, *chpG*, which was slightly upregulated (**Table 4.1**). During the later developmental time points, the expression of the chaplins, the rodlins, and the *ram* genes (responsible for producing the secreted surfactant SapB) was significantly decreased, which is to be expected for a bald phenotype mutant grown in liquid culture. Curiously, there was no change in the expression of any of the *whiE* genes, which are responsible for producing the spore pigment. Out of the other *bld* and *whi* regulators, the expression of *bldM*, *bldN*, *whiB*, *whiG*, *whiH* and *whiI* was significantly decreased. All of these genes are under the repression of the master regulator BldD (den Hengst *et al.*, 2010). Expression of *bldD* itself was unchanged in the *ΔbldB* mutant, but BldD activity is controlled post-translationally by c-di-GMP (Tschowri *et al*., 2014), perhaps suggesting altered c-di-GMP levels in the *bldB* mutant.

Looking at the expression of type VII secretion-related genes, only the expression of *eccC* and *eccE* was elevated in the *ΔbldB* mutant at 22 hours. In contrast to the *S. coelicolor ΔbldB* mutant, in which *esxA* and *esxB* were upregulated (Akpe San Roman *et al.*, 2010), there was no change of expression for these two T7SS-related genes in the *S. venezuelae ΔbldB* mutant.

Overall, these RNA-seq results suggest that in wild-type *S. venezuelae*, BldB must be repressing the expression of the 5 *abaA* homologues and *iosA*. This repression must be indirect, as the ChIP-seq and SPR results suggested that BldB is not a DNA-binding protein, and no peaks were found in the promoters of the 6 genes at any time point. The similar genomic arrangement of *iosA* and the *abaA* homologues in relation to the *bldB* and *whiJ* homologues and their upregulation in the *ΔbldB* mutant might indicate a collaborative function, despite the fact that IosA is not an AbaA homologue (*i.e.* lacks a HATPase_c domain).

To see whether the AbaA homologues and IosA indeed have a role in *Streptomyces* development, I generated mutant and overexpression strains for all 6 genes. None of the mutants exhibited any developmental phenotypes (**Fig. 4.7**). This was not unexpected; given the *abaA* homologues and *iosA* are dramatically upregulated in the *ΔbldB* mutant, it seemed more likely that their overexpression might result in developmental aberrations, rather than their loss. Indeed, two of the single overexpression strains exhibited white phenotypes on a plate - the *abaA6* and *iosA* overexpression strains (**Fig. 4.8**). It was because of this finding that I named *vnz16670 iosA* - for **i**nhibitor **o**f **s**porulation **A**. Since the single overexpression of these two genes had an impact on development, but did not abolish the formation of aerial hyphae, I wondered if their tandem overexpression would result in a strain with a phenotype closer to that of the *ΔbldB* mutant.

To address this question, I put *iosA* and *abaA6* under the control of the same *ermE** promoter in wild-type *S. venezuelae*. The resulting double overexpression strain resembled the *ΔbldB* mutant more closely than the single overexpression strains, with a noticeable reduction in white fuzzy growth on MYM agar (**Fig. 4.10**). Looking at the phenotypes under the electron microscope, both the single and double overexpression strains featured a vegetative mycelium-rich centre of the colony, with formation of aerial hyphae around the edges (**Fig. 4.9**, **4.11**). In the single overexpression strains, some beginnings of aerial growth breaking the surface at the centre of the colonies could be observed (**Fig. 4.9**). This was not typical aerial growth, however, as the structures were bigger and cone-shaped, perhaps representing clusters of aerial hyphae trying to escape the extracellular matrix. This pattern of growth was absent in the *abaA6 iosA* double overexpression strain, which looked comparable to the *ΔbldB* mutant (**Fig. 4.11**). Thus, upregulation of *abaA6* and *iosA* alone was sufficient to cause a *ΔbldB* mutant-like phenotype.

To extend this analysis, I generated a *ΔabaA6 ΔiosA ΔbldB* triple mutant, reasoning that if the upregulation of *abaA6* and *iosA* caused the *ΔbldB* mutant phenotype, their deletion might restore normal development to the *ΔbldB* mutant. I first deleted *iosA* via CRISPR, then *abaA6* via CRISPR as well, with the resulting single and double mutants having no developmental phenotypes (**Fig. 4.12**, **4.13**). Finally, I used phage transduction in the *ΔabaA6 ΔiosA* double mutant to replace *bldB* with the apramycin resistance cassette from the original *ΔbldB* mutant.

Unfortunately, whole-genome resequencing of the triple mutant revealed an off-target 28.25 kb deletion. The deletion covered 32 genes: *vnz19660* to *vnz19800*. PCR analysis showed that the unintended deletion had occurred at the first stage of triple mutant construction, *i.e* the deletion of *iosA* via CRISPR. The deletion seems to cover a phage-like mobile genetic element carrying a predicted excisionase gene, *vnz19745*. Most of the deleted genes encode hypothetical proteins, but several of them encode predicted DNA-binding proteins, including Vnz19650 and Vnz19735, which have a WhiJ-like helix-turn-helix Xre motif. The only deleted gene that has been reported to have an impact on *Streptomyces* development was *vnz19760*, which encodes the diguanylate cyclase CdgD. It was only when *cdgD* was overexpressed that it produced a developmental phenotype in *S. coelicolor* - when it was deleted, the strain was reported to exhibit regular development (Liu *et al.*, 2019). Additionally, the deletion of *cdgD* in *S. venezuelae* resulted in a wild-type phenotype (Al-Bassam *et al.*, 2018). This means that the unintentional deletion of *vnz19760* in the triple mutant should pose no ambiguity in terms of developmental phenotypes.

Remaking the triple mutant without the off-target ~28 kb deletion would clearly be desirable. However, the deletion did not cause any developmental aberrations in the *ΔiosA* single mutant and the *ΔabaA6 ΔiosA* double mutant (**Fig. 4.12**, **4.13**). Furthermore, the mild developmental phenotype of the *ΔabaA6 ΔiosA ΔbldB* triple mutant could only be attributed to the loss of *bldB*, given that providing *bldB in trans* restored sporulation completely (**Fig. 4.12**).

On MYM agar, the triple mutant exhibited white growth with some green pigment formation upon prolonged incubation (**Fig. 4.12**). Scanning electron microscopy conducted on the triple mutant showed an abundance of mostly sporulating hyphae with some variation in spore sizes, and also some undifferentiated hyphae (**Fig. 4.13**). Taken together, this means that the *ΔabaA6 ΔiosA ΔbldB* triple mutant is able to sporulate, but has defects in the regular placement of sporulation septa and a lack of spore pigment formation. When I complemented the triple mutant with *bldB in trans*, it completely restored sporulation and spore pigment deposition (**Fig. 4.12**). Taken together, this means that the deletion of *abaA6* and *iosA* significantly, but not completely, restored sporulation to the *ΔbldB* mutant. In summary, I can conclude that the joint upregulation of *abaA6* and *iosA* is significantly responsible for the bald phenotype of the *ΔbldB* mutant. This does not rule out the possibility that the other AbaA homologues may contribute significantly as well.

The presence of an HATPase_c domain in all AbaA homologues might suggest they act as anti-sigma factors. Given that there are some less well characterised SigB-like sigma factors without cognate anti-sigma factors, it was entirely possible that AbaA6 in particular might bind one of these sigma factors in *S. venezuelae*, thus indirectly providing a transcriptional output for the *ΔbldB* mutant phenotype. In the next chapter, I investigate whether AbaA6 is a part of any regulatory partner-switching mechanisms involving a SigB-like sigma factor, an RsbV/SpoIIAA-like anti-sigma antagonist, and a RsbU/SpoIIE-like phosphatase.

Page intentionally left blank

5. Protein-protein Interaction Network Involving the Putative Anti-Sigma Factor AbaA6

Introduction

The Role of Osmoregulation in Bacterial Growth

Homeostasis is an umbrella term for the different processes all living organisms undergo in order to maintain a stable physiological state. All bacteria face unique challenges in maintaining homeostasis based on the environment they are found in. Different stresses include changes in osmolarity, pH, temperature, oxidation and nutrient availability.

Water flows in and out of the bacterial cell by osmosis through the cell envelope. The difference in solute concentration between the intracellular and extracellular environment of the bacterial cell creates osmotic potential. When the osmolarity of the extracellular environment is lower than that of the cell, this leads to hypoosmotic shock, in which the influx of water into the cell ultimately leads to cell swelling and high turgor pressure. When the osmolarity of the external environment is higher than that of the cell, this leads to hyperosmotic shock, in which water flows out of the cell, leading to the shrinking of the cell cytoplasm and plasmolysis - a partial separation of the inner membrane from the cell wall (Rojas and Huang, 2018). It has been shown that shrunken plasmolysed bacteria exhibit poor diffusion of macromolecules through the dehydrated and crowded cytoplasm, in which DNA and proteins become compartmentalised and practically immobile (van den Bogaart *et al.*, 2007; Konopka *et al.*, 2009; Mika *et al.*, 2010; Wu *et al.*, 2019). This has huge implications for the overall biochemistry of the bacterial cell; therefore it is essential that bacteria develop ways to manage osmotic stress.

Osmotic stress has been shown to have an effect on bacterial growth and cell division. The cell growth of *B. subtilis* and other gram-positive bacteria was shown to depend on turgor pressure induced by osmotic shock (Rojas, Huang and Theriot, 2017). Briefly, these authors' model suggests that a rise in turgor pressure leads to cell wall expansion, while a rise in membrane tension negatively impacts it, by prohibiting peptidoglycan precursors from crossing the membrane.

An increase in membrane synthesis relieves the membrane tension and the repression on cell wall expansion, thus making sure that the cell wall and membrane expand at similar rates. In contrast, osmolarity-induced turgor pressure was not found to be the major driver of cell growth in the gram-negative *E. coli* (Rojas, Theriot and Huang, 2014).

It has been suggested that in *E. coli*, the cell division protein FtsZ is able to bind McsS - a component of a mechanosensitive channel (Koprowski *et al.*, 2015). Since mechanosensitive channels have been shown to open to release cytoplasmic solutes to relieve turgor pressure when bacteria enter hypoosmotic environments (Haswell, Phillips and Rees, 2011), this could directly link FtsZ function to the osmotic stress response.

Osmotic Stress and Development in *Streptomyces*

When colonies of *S. coelicolor* were transferred from standard YEME medium without osmolytes to YEME with either sucrose or NaCl, there was an observed cessation in growth for 2 -3 hours (Fuchino *et al.*, 2017). Growth eventually resumed, but strikingly, multiple new hyphae began to emerge from the lateral walls of the existing hyphae, instead of continued growth from the existing hyphal tips. When the authors tested growth in hypoosmotic stress conditions, they still observed a lag in growth (albeit a shorter one), but this time growth resumed from the existing hyphal tips. Acid stress also induced a long lag in growth, but further growth began again from the existing hyphal tips. This means that it was the hyperosmotic stress conditions that induced the shift in cell polarity - a phenomenon that was also observed in *S. venezuelae*. Interestingly, the *Streptomyces* chromosome was found to condense during the hyperosmotic stress-induced growth lag (Fuchino *et al.*, 2017). This is consistent with the observations that under high osmolarity, the cytoplasm shrinks and its components become more static (van den Bogaart *et al.*, 2007; Konopka *et al.*, 2009; Mika *et al.*, 2010; Wu *et al.*, 2019).

A direct reason why the *Streptomyces* chromosome becomes more compact could be found in the histone-like protein DdbA (Aldridge *et al.*, 2013). DdbA was found to bind to supercoiled DNA during the beginning of sporulation and condense it - a function that was impaired under osmotic stress conditions. The *ΔddbA* mutant exhibited a delay in sporulation when grown on NMMP agar containing a high concentration of KCl. The *S. coelicolor* Dps proteins have been proposed to have a similar role in nucleoid compaction under osmotic stress conditions (Facey *et al.*, 2009).

The nucleotide second messenger c-di-AMP has been implicated in osmoregulation in bacteria (Commichau *et al.*, 2018). The *S. venezuelae* DNA integrity scanning protein DisA was found to have diadenylate cyclase activity and to be able to synthesise c-di-AMP out of ATP (Latoscha *et al.*, 2020). After a conserved domain search, a candidate phosphodiesterase (designated AtaC) was identified and found to be able to break down c-di-AMP into AMP and 5′-pApA. Whereas the *ΔdisA* mutant had no developmental phenotype, the *ΔataC* mutant had a white phenotype, with a presence of undifferentiated and lysed aerial hyphae. When grown on DN medium supplemented with 0.5 M NaCl, however, it was the *ΔdisA* mutant that exhibited reduced growth when serially diluted, whereas the *ΔataC* mutant grew in a pattern comparable to wild-type *S. venezuelae*. Taken together, these results point to developmental defects caused by a high concentration of c-di-AMP, and susceptibility to osmotic stress caused by a low concentration of c-di-AMP (Latoscha *et al.*, 2020).

The OsaABC System in *Streptomyces*

The hybrid histidine kinase OsaA and the response regulator OsaB were first characterised in a transposon mutagenesis study in *S. coelicolor* (Bishop *et al.*, 2004). The *ΔosaB* mutant in *S. coelicolor* was found to have a bald phenotype when grown on osmolyte-supplemented media, whereas the *ΔosaA* mutant was observed to only have a slight developmental delay. OsaA was shown to be pupylated - pupylation is a post-translational modification that targets proteins for degradation by the proteasome (Boubakri *et al.*, 2015). Turnover of OsaA must have implications for the ability of *S. coelicolor* to sense and relay signals concerning the osmolarity of the extracellular environment.

The study of the effects of SigB on one of the *osaB* promoters led to the discovery of OsaC, a multidomain protein necessary for the osmoadaptation response in *S. coelicolor* (Fernández Martínez *et al.*, 2009). The *osaBp2* promoter was induced in a SigB-dependent manner after addition of an osmolyte (NaCl or sucrose) to the medium. OsaC, which is encoded by a gene divergently transcribed to *osaA*, was hypothesised to contribute to this process. OsaC contains 5 domains - an N-terminal HATPase_c domain (like the ATPase domain found in SpoIIAB/RsbW and the AbaA homologues), a PAS domain and 2 GAF domains proposed to be sensory domains, and finally, a C-terminal phosphatase domain (like the PP2C domain found in SpoIIE/RsbU).

PAS and GAF domains are sensory domains often found in tandem - PAS domains are able to sense redox potential and light among other stimuli, whereas GAF domains are able to bind cyclic nucleotides, and are found in phosphodiesterases, adenylyl cyclases and FhlA (Taylor and Zhulin, 1999; Ho, Burden and Hurley, 2001).

Fernández Martínez *et al.* (2009) observed sporulation-deficient phenotypes when they knocked out or overexpressed OsaC and grew the resulting strains on NMMP agar supplemented with an osmolyte. The *ΔosaC* mutant phenotype could not be complemented when OsaC lacking the phosphatase domain was provided *in trans*, meaning that the phosphatase domain is important for the function of OsaC in osmotic stress conditions (Fernández Martínez *et al.*, 2009).

OsaC was proposed to be an alternative anti-sigma factor for SigB, a previously discussed sigma factor involved in the osmotic and oxidative response in *S. coelicolor* (Cho *et al.*, 2001; Lee *et al.*, 2005). OsaC was co-purified with SigB, and the N-terminal ATPase domain was proposed to be the one necessary for SigB binding (Fernández Martínez *et al.*, 2009). The overexpression of OsaC was found to affect SigB function, resulting in altered activity of the *osaB* promoter and of the *sigB* promoter itself. SigB has an anti-sigma factor, RsbA, and an anti-sigma factor antagonist, RsbV (Lee *et al.*, 2004), which are proposed to be the anti-sigma and anti-sigma antagonist under “normal conditions”, in contrast to the “osmotic stress” anti-sigma OsaC and a yet unknown OsaC antagonist (Fernández Martínez *et al.*, 2009).

Deleting either *osaB* or *osaC* from *S. avermitilis* resulted in bald phenotypes and higher production of ivermectin and oligomycin - for this reason the authors proposed that the two mutant strains could be used for the industrial production of these secondary metabolites (Godinez *et al.*, 2015).

OsaC-Like Proteins in Bacteria

In addition to characterising OsaC, Fernández Martínez *et al.* (2009) identified 4 more OsaC-like proteins in *S. coelicolor*. None of the mutants lacking these OsaC-like proteins exhibited any developmental defects when grown on osmolyte-containing media, meaning that the role of OsaC in osmoregulation is non-redundant.

It is not uncommon to find other examples of such multidomain proteins, especially ones related to modulating the function of a SigB-like sigma factor (Bouillet *et al.*, 2018). There are 2 well-characterised fusion proteins that have the HATPase_c anti-sigma domain and the PP2C phosphatase domain, along with a REC domain. The first one is SypE, which binds to and regulates the function of the STAS-domain protein SypA - a major contributing factor for biofilm formation in *Vibrio fischeri* acting via an unidentified sigma factor (Morris and Visick, 2013). The second one is CrsR, which is able to bind anti-sigma antagonist CrsA to control SigS function in chemosensing and stress response in *Shewanella oneidensis* (Bouillet *et al.*, 2016, 2017).

PdtaS is a cytosolic sensor kinase, part of the PdtaS-PdtaR two-component system in *Mycobacterium tuberculosis*. PdtaS has PAS and GAF domains in its N-terminus, and HisKA and HATPase_c domains in its C-terminus (Preu *et al.*, 2012). Its response regulator PdtaR is unusual in its control of transcription - it has been proposed to serve as a transcriptional anti-terminator, rather than an activator (Morth *et al.*, 2004).

One even more striking example from *Mycobacterium tuberculosis* is Rv1364c, which contains a PAS domain, a PP2C phosphatase domain, a HATPase_c anti-sigma domain, and a STAS anti-sigma antagonist domain (King-Scott *et al.*, 2011). It was shown to interact with SigF via its anti-sigma and phosphatase domains (Parida *et al.*, 2005), and can presumably perform all the functions of the *Bacillus* SpoIIE-SpoIIAA-SpoIIAB cascade by itself. Interestingly, homologues of *M. tuberculosis* SigF have only been reported in other pathogenic, slow-growing species, and not in non-pathogenic fast-growing species like *Mycobacterium smegmatis* (DeMaio *et al.*, 1996). Expression of *sigF* and Rv1364c was found to be induced under stress conditions, particularly during survival after phagocytosis (DeMaio *et al.*, 1996; Li *et al.*, 2004).

In this chapter I describe a protein-protein interaction network I discovered via bacterial two-hybrid screens, which involves the putative anti-sigma factor AbaA6, two anti-sigma factor antagonists, and the multidomain proteins OsaC and OsaC2.

Results

A Bacterial-Two-Hybrid Library Screen Found Potential Anti-Sigma Antagonist Partners for AbaA6

Seeing as *abaA6* and *iosA* were among the most highly upregulated genes in the *ΔbldB* mutant (**Fig. 4.6, Table 4.1**), and since their joint overexpression recapitulates the *ΔbldB* mutant phenotype (**Fig. 4.10, 4.11, 4.12, 4.13**), I undertook a bacterial-two-hybrid library screen to establish whether I could find any binding partners for AbaA6 and IosA. I fused each of the two full-length proteins to the N-terminus of the T18 peptide and to the C-terminus of the T25 peptide and used these fusions as baits to screen the T25 and T18C genomic libraries respectively.

In the case of AbaA6, I identified 31 in-frame library inserts as 'strong' or 'medium' interaction hits simply via visual inspection of colony colour when grown on MacConkey agar. Out of those, 13 hits originated from Vnz10850, 4 hits from Vnz03680, and 6 hits from Vnz10530 (**Table 5.1**). For IosA, 14 out of 16 in-frame strong-interacting hits originated from Vnz10530 (**Table 5.1**).

Vnz10850 and Vnz03680 are both hypothetical proteins with predicted STAS (Sulphate Transporter and Anti-Sigma factor antagonist) domains, characteristic of anti-sigma factor antagonists such as SpoIIAA and RsbV in *B. subtilis* (Dufour and Haldenwang, 1994; Magnin *et al.*, 1996; Aravind and Koonin, 2000). From here onwards, I will refer to Vnz03680 and Vnz10850 as AsfA1 and AsfA2, respectively (AsfA standing for **A**nti-**S**igma **F**actor **A**ntagonist). The hypothetical protein Vnz10530 was a joint hit for both AbaA6 and IosA (**Table 5.1**).

These findings were interesting, as they hinted at a possible role of AbaA6 (and perhaps that of its homologues by means of extrapolation) as an anti-sigma factor. The findings could also provide a clue as to what the biochemical function of IosA is. It is important to note however, that no interacting sigma factor was identified in this library screen, so AbaA6 might have an alternative function.

Table 5.1. AbaA6 and IosA Bacterial-Two-Hybrid Library Screen Results.

Bait	Protein	Number of Hits	Predicted Function and Domains of Interest
AbaA6	Vnz33785	1	Gas vesicle protein
AbaA6	Vnz28805	1	3-hydroxyacyl-CoA dehydrogenase
AbaA6	Vnz20510	1	2'-5' RNA ligase
AbaA6	Vnz18680	1	Prolyl aminopeptidase
AbaA6	Vnz16070	1	Inorganic pyrophosphatase
AbaA6	Vnz15575	1	Heat-shock protein Hsp20
AbaA6	Vnz13795	1	Putative anti-sigma antagonist ArsI, STAS domain
AbaA6	**Vnz10850**	**13**	**Anti-sigma factor antagonist, STAS domain**
AbaA6	**Vnz10530**	**6**	**Hypothetical protein**
AbaA6	Vnz03925	1	Glyoxalase
AbaA6	**Vnz03680**	**4**	**Hypothetical protein, STAS domain**
IosA	Vnz19610	1	Cysteinyl-tRNA synthetase
IosA	**Vnz10530**	**14**	**Hypothetical protein**
IosA	Vnz11595	1	Glutamate 5-kinase ProB

AbaA6 Interacts with Two Predicted Anti-Sigma Factor Antagonists - AsfA1 and AsfA2

In order to quantify the interactions between AbaA6, IosA and their respective and shared library screen hits AsfA1, AsfA2 and Vnz10530, I performed β-galactosidase assays with the full-length proteins. Indeed, AbaA6 interacted strongly with both predicted anti-sigma antagonists AsfA1 and AsfA2 (**Fig. 5.1**). As for the hypothetical protein Vnz10530, it interacted strongly with the T18 peptide in the empty vector negative control, so its supposed interactions with AbaA6 and IosA were false positives, and not represented here. Additionally, there was no interaction between AbaA6 and IosA themselves, as well as low-strength or background level self-interactions for AbaA6, AsfA1 and AsfA2 (**Fig. 5.1**).

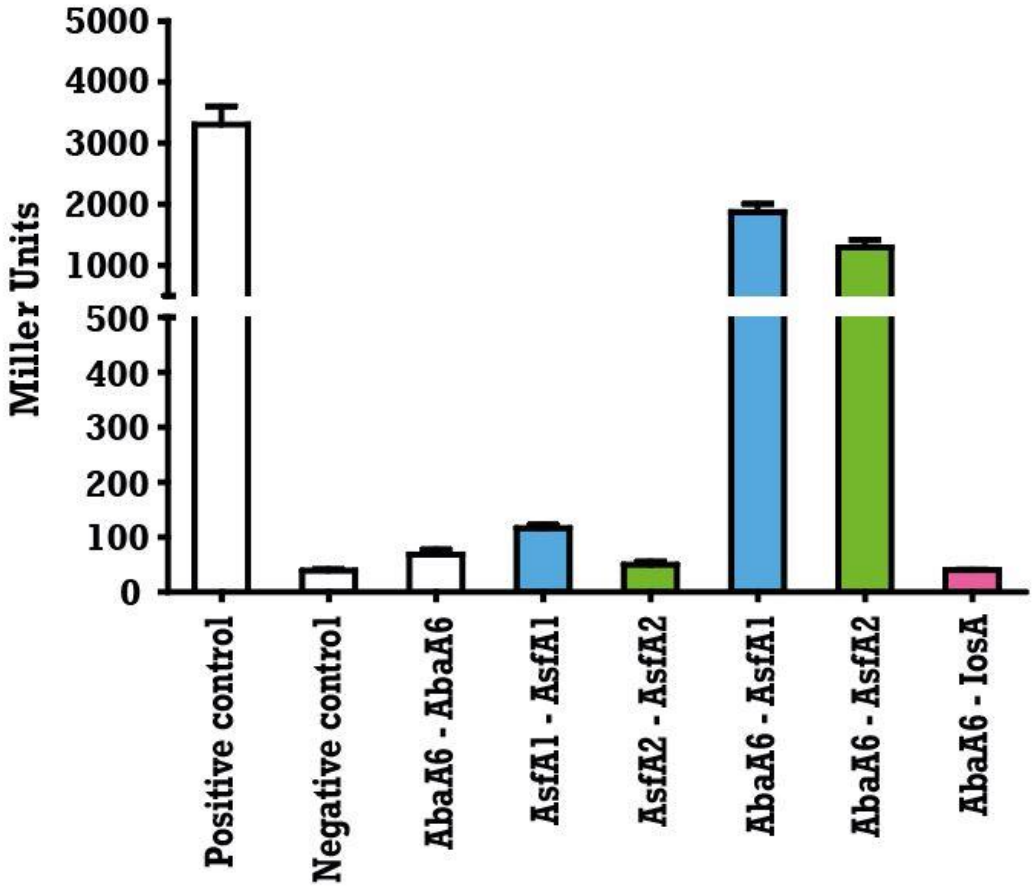

Figure 5.1. Interactions Between AbaA6, IosA and the AsfA Homologues.

β-galactosidase assays were performed to measure strength of protein-protein interactions (in Miller units). The strong interaction between the leucine zipper domains of leucine zipper of GCN4 (T18C-zip and T25-zip) was used as a positive control. Empty vector negative controls were performed for every interaction displayed here, but for the sake of clarity, only one representative negative control is displayed. Results are the average of three independent experiments, with two technical replicates per experiment. Error bars indicate the SEM.

AbaA6 Does Not Interact with 7 SigB Homologues

The strong interaction between AbaA6 (a protein with a predicted anti-sigma domain) and both AsfA1 and AsfA2 (proteins with predicted anti-sigma antagonist domains) suggested that those interactions might be a part of a bigger sigma - anti-sigma factor network similar to those described in *B. subtilis* (Diederich *et al.*, 1994; Magnin *et al.*, 1996). However, the bacterial-two-hybrid library screen that used AbaA6 as bait did not return any sigma factors as hits (**Table 5.1**). In case the library was not representative enough, I performed targeted one-on-one β-galactosidase assays between AbaA6 and 7 full-length *S. venezuelae* homologues of *B. subtilis* SigB and SigF.

To find these 7 SigB homologues, a comprehensive BLAST search was performed by Dr Govind Chandra, using *B. subtilis* SigB and SigF as queries (BSU04730 and BSU23450, respectively). This resulted in a list of 11 potential SigB homologues in *S. venezuelae.* Deciding what is a genuine homologue can be challenging when dealing with protein families, especially with sigma factors. For this reason, a further reciprocal BLAST search using the 11 SigB homologue candidates was performed, as summarised in **Table 5.2**.

Out of the 11 candidates, 7 mapped back to the *B. subtilis* SigB (highlighted in bold in **Table 5.2**), so I concluded that they are genuine SigB homologues, and used them in the next two-hybrid experiments described in this chapter. The remaining 4 sigma factors from the initial search were actually the well-studied sigma factors HrdA, HrdB, HrdD and WhiG, so I did not use them in these SigB-centric two-hybrid assays. Among the 7 candidates I found the homologues for *S. coelicolor* SigB, SigI, SigN, SigF and SigH (**Table 5.2**). Notably, the *S. coelicolor* SigB homologues SigG, SigK, SigL and SigM are not present in *S. venezuelae*. *S. venezuelae* instead has two extra SigB-like sigma factors that I designated SigB2 and SigB3 (**Table 5.2**).

Table 5.2. List of Reciprocal Best Hits for Potential *S. venezuelae* SigB Homologues.

Query (vnz)	Hit (BSU)	Reverse Hit (vnz)	Query Cover	Hit Cover	Fraction Identity	P value	SCO Homologue	Designation	Referenced in:
Vnz01715	**BSU04730**	**Vnz18615**	**0.82**	**0.885**	**0.371**	**3E-51**	**SCO0600**	**SigB**	**Cho *et al.* (2001)**
Vnz01090	**BSU04730**	**Vnz18615**	**0.803**	**0.885**	**0.356**	**3E-49**	**No SCO**	**SigB2**	**This study**
Vnz02255	**BSU04730**	**Vnz18615**	**0.698**	**0.866**	**0.388**	**1E-48**	**No SCO**	**SigB3**	**This study**
Vnz13800	**BSU04730**	**Vnz18615**	**0.851**	**0.954**	**0.389**	**3E-50**	**SCO3068**	**SigI**	**Homerova *et al.* (2012)**
Vnz18615	**BSU04730**	**Vnz18615**	**0.743**	**0.863**	**0.422**	**2E-53**	**SCO4034**	**SigN**	**Dalton *et al.* (2007)**
Vnz18620	**BSU04730**	**Vnz18615**	**0.804**	**0.874**	**0.394**	**1E-48**	**SCO4035**	**SigF**	**Potúcková *et al.* (1995)**
Vnz24270	**BSU04730**	**Vnz18615**	**0.634**	**0.844**	**0.413**	**7E-51**	**SCO5243**	**SigH**	**Viollier *et al.* (2003)**
Vnz11045	BSU25200	Vnz27210	0.949	0.736	0.583	2E-120	SCO2465	HrdA	Buttner and Lewis (1992)
Vnz15035	BSU25200	Vnz27210	0.865	0.698	0.483	3E-87	SCO3202	HrdD	Buttner, Chater and Bibb (1990)
Vnz26215	BSU16470	Vnz26215	0.881	0.953	0.42	6E-59	SCO5621	WhiG	Chater *et al.* (1989)
Vnz27210	BSU25200	Vnz27210	0.703	0.906	0.558	2E-133	SCO5820	HrdB	Buttner, Chater and Bibb (1990)

The β-galactosidase assays revealed that there are no interactions between AbaA6 and the 7 SigB homologues, and (as expected) no self-interactions between the 7 SigB homologues (**Fig. 5.2**). Furthermore, when IosA and each of those 7 SigB homologues were co-transformed into the *E. coli* BTH101 cells and plated on media supplemented with IPTG and X-Gal, the resulting colonies were white. For this reason, I concluded that IosA also does not interact with the 7 SigB homologues, and so I did not follow this up with β-galactosidase assays.

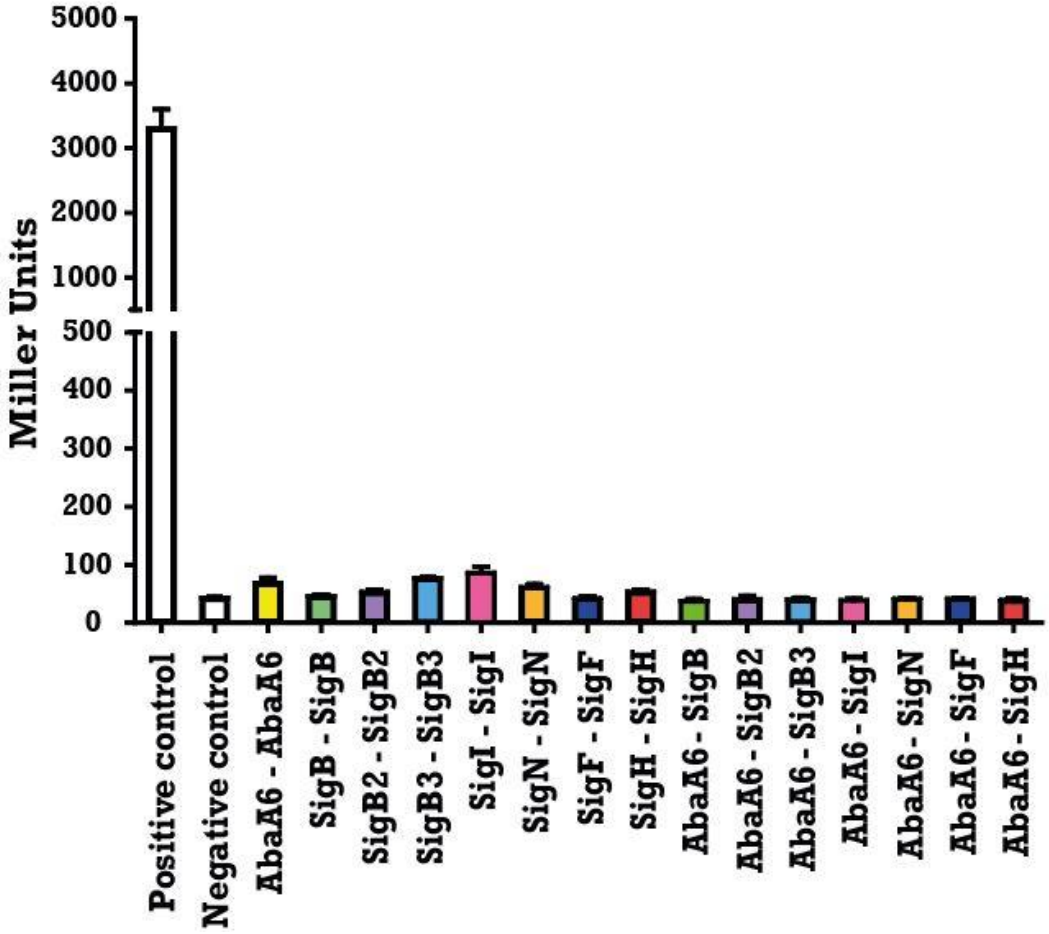

Figure 5.2. Interactions Between AbaA6 and 7 SigB Homologues.

β-galactosidase assays were performed to measure strength of protein-protein interactions (in Miller units). The strong interaction between the leucine zipper domains of leucine zipper of GCN4 (T18C-zip and T25-zip) was used as a positive control. Empty vector negative controls were performed for every interaction displayed here, but for the sake of clarity, only one representative negative control is displayed. Results are the average of three independent experiments, with two technical replicates per experiment. Error bars indicate the SEM.

AsfA1 and AsfA2 Interact with OsaC and OsaC2

In order to see if AsfA1 and AsfA2 might be dephosphorylated in a way similar to the dephosphorylation of the anti-sigma antagonist SpoIIAA by the phosphatase SpoIIE (Arigoni *et al.*, 1996), I performed another set of bacterial-two-hybrid library screens with AsfA1 and AsfA2 as baits. For both baits, the hits predominantly came from the same two multidomain proteins: Vnz26705 and Vnz17535 (**Table 5.3**). The *S. coelicolor* homologue of Vnz26705 has already been studied and was designated OsaC, as it was found to have a role in osmoregulation, and was suggested to act as an anti-sigma factor for *S. coelicolor* SigB (Fernández Martínez *et al.*, 2009). OsaC and Vnz17535 contain the same set of domains (PAS, GAF, PP2C phosphatase and HATPase_c), although in different configurations (**Fig. 5.3**); for this reason, I will refer to Vnz17535 as OsaC2 from here onwards. Other similar hits came up in both screens, where the proteins contained various combinations of the same PAS, GAF, phosphatase and ATPase domains, but not as many times as OsaC and OsaC2 did.

Other hits of interest included AbaA10 for both AsfA1 and AsfA2, and AbaA6 for AsfA1 (**Table 5.3**). AbaA6 being among the hits is unsurprising, as a reciprocal hit is to be expected, given the strong interaction between AbaA6 and AsfA1 (**Fig. 5.1**). The fact that AbaA10 came up suggests that some AbaA homologues might have similar or perhaps even redundant functions, creating crosstalk between them and their interacting partners. Other HATPase_c domain-only containing proteins came up in the screens - those could be considered AbaA homologues as well, though in this study I reserved the AbaA designation for HATPase_c domain-containing proteins encoded next to one of the *bldB* homologues.

There is one predicted methyltransferase hit (Vnz10030) for AsfA1 - this is potentially interesting, given that methyltransferases are sometimes found encoded near *bldB* and *whiJ* homologues, and that there are “long” BldB homologues that contain a methyltransferase domain in addition to a DUF397 domain (**Table 3.1**). PstA (hit for AsfA1) is also potentially interesting, as it was one of the most differentially expressed genes in the Δ*bldB* mutant, although its massive downregulation at 10 hours was not statistically significant. Vnz10530, which was a library screen hit for both AbaA6 and IosA (**Table 5.1**) but turned out to be a false positive, also features as a multiple hit in the AsfA1 library screen (**Table 5.3**). Naturally, I did not follow up this established false positive hit with any further experiments.

Table 5.3. AsfA1 and AsfA2 Bacterial-Two-Hybrid Library Screen Results.

Bait	Protein	Number of Hits	Predicted Function	Domains of Interest
AsfA1	Vnz33580	1	Probable regulatory protein	PAS, GAF, SpoIIE, HATPase
AsfA1	Vnz31495	1	**AbaA10**	HATPase only
AsfA1	Vnz29960	1	ATP-binding protein	HATPase only
AsfA1	Vnz26705	6	PAS domain S-box protein - **OsaC**	HATPase, PAS, 2x GAF, SpoIIE
AsfA1	Vnz23470	2	PAS sensor protein	2x PAS, GAF, SpoIIE, HATPase
AsfA1	Vnz23260	1	Serine/threonine protein phosphatase	GAF, SpoIIE, HATPase
AsfA1	Vnz19255	1	Phosphate transport system permease PstA	
AsfA1	Vnz17535	16	Phosphatase – **OsaC2**	PAS, GAF, SpoIIE, HATPase
AsfA1	Vnz10530	5	Hypothetical protein	
AsfA1	Vnz10030	1	Methyltransferase	
AsfA1	Vnz09905	1	**AbaA6**	HATPase only
AsfA1	Vnz04050	1	Hypothetical protein	HATPase only
AsfA2	Vnz33580	1	Protein phosphatase	PAS, GAF, SpoIIE, HATPase
AsfA2	Vnz31495	1	**AbaA10**	HATPase only
AsfA2	Vnz26705	1	PAS domain S-box protein - **OsaC**	HATPase, PAS, 2x GAF, SpoIIE
AsfA2	Vnz25480	1	TesB-like acyl-CoA thioesterase 3	
AsfA2	Vnz19970	1	Hypothetical protein	
AsfA2	Vnz17535	16	Phosphatase – **OsaC2**	PAS, GAF, SpoIIE, HATPase
AsfA2	Vnz04050	1	Hypothetical protein	HATPase only

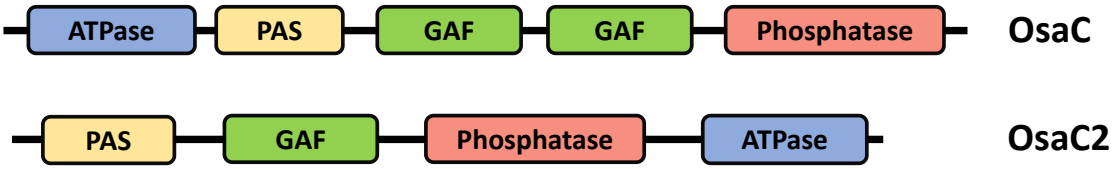

Figure 5.3. OsaC and OsaC2 Are Multidomain Proteins.

Both OsaC and OsaC2 have the same 4 domains in different configurations - an HATPase_c domain, PAS domain, GAF domain(s) and a PP2C-SIG phosphatase domain.

I performed another set of β-galactosidase assays to quantify the interactions between AsfA1 and AsfA2 and two of their shared and most frequently found library screen hits - OsaC and OsaC2. Indeed, both AsfA1 and AsfA2 interact strongly with OsaC and OsaC2, confirming the library screen findings (**Fig. 5.4**). When compared to the negative control, there is a low level of self-interaction for OsaC and OsaC2 and no self-interaction for AsfA2. AsfA1 is a more confusing case - in this latest assay (**Fig. 5.4**), the strength of self-interaction is higher than I previously observed (**Fig. 5.2**). This discrepancy is not particularly concerning, as neither observed self-interaction for AsfA1 is particularly high. If the self-interaction of AsfA1 does prove to be important in the future, it could be better studied via various biochemical methods, such as analytical gel filtration and ITC.

OsaC Does Not Interact with SigB or BldB in a Bacterial-Two-Hybrid Experiment

Interestingly, OsaC came up as a single hit in my initial bacterial-two-hybrid library screen, which used BldB as bait (**Table 3.2**). At the time, I placed higher priority on confirming the potential interactions between BldB and its homologues, which came up in the screen multiple times. With these new findings however, validating an interaction between BldB and OsaC became more relevant, as it could help elucidate the roles of BldB and OsaC in this complex developmentally regulated network.

Additionally, the original study of OsaC in *S. coelicolor* suggested that it interacts with SigB and serves as its anti-sigma factor through the HATPase_c domain that is characteristic of the AbaA homologues in this thesis (Fernández Martínez *et al.*, 2009). The reciprocal best hit for the *S. coelicolor* SigB (SCO0600) in *S. venezuelae* is Vnz01715, which I also designated as SigB (**Table 5.2**), so I also tested the interaction between *S. venezuelae* OsaC and SigB.

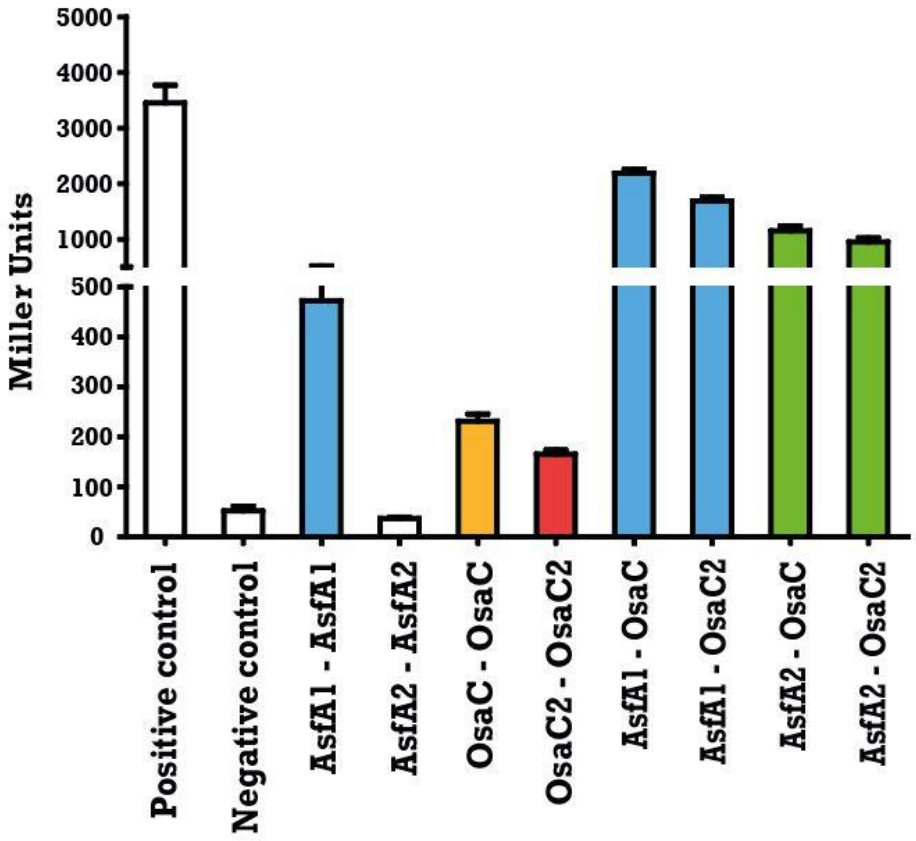

Figure 5.4. Interactions Between the AsfA Homologues and the OsaC Homologues.

β-galactosidase assays were performed to measure strength of protein-protein interactions (in Miller units). The strong interaction between the leucine zipper domains of leucine zipper of GCN4 (T18C-zip and T25-zip) was used as a positive control. Empty vector negative controls were performed for every interaction displayed here, but for the sake of clarity, only one representative negative control is displayed. Results are the average of three independent experiments, with two technical replicates per experiment. Error bars indicate the SEM.

The β-galactosidase assays showed very low levels of self-interaction for BldB, OsaC and OsaC2, and no self-interaction for SigB (**Fig. 5.5**). In the case of BldB, this is not surprising, as it agrees with my previous two-hybrid experiments (**Fig. 3.8**). No interaction was found between BldB and OsaC or OsaC2, nor between SigB and OsaC or OsaC2 (**Fig. 5.5**).

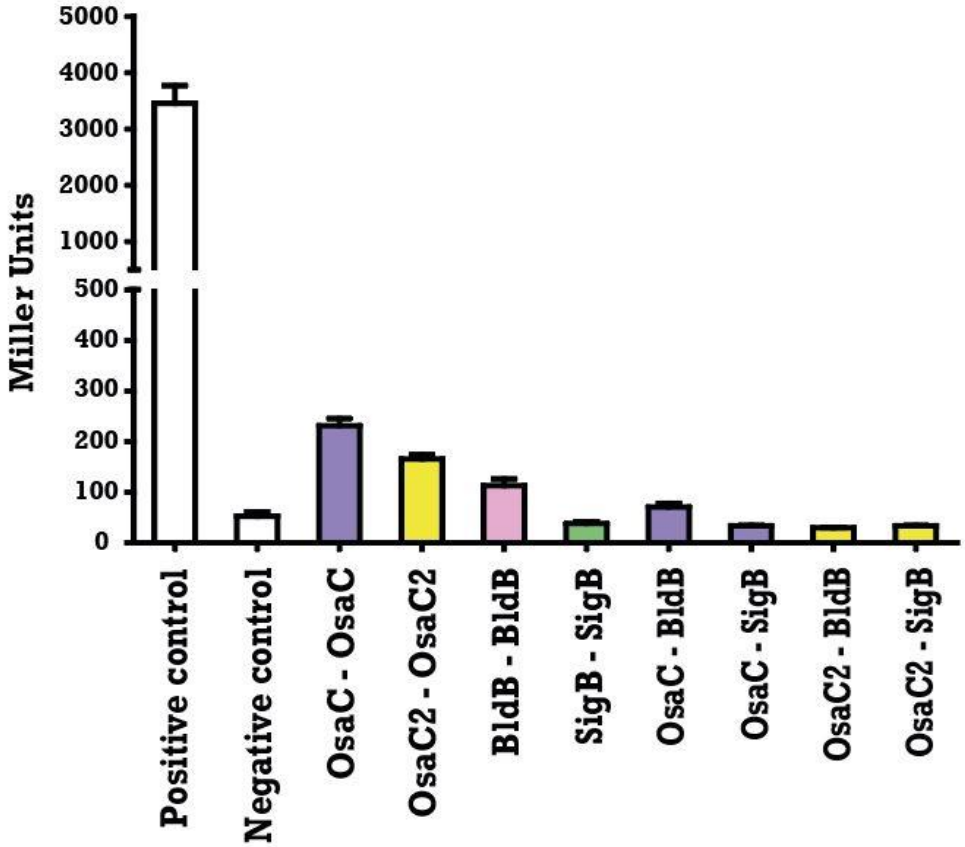

Figure 5.5. Interactions Involving the Multidomain Proteins OsaC and OsaC2.

β-galactosidase assays were performed to measure strength of protein-protein interactions (in Miller units). The strong interaction between the leucine zipper domains of leucine zipper of GCN4 (T18C-zip and T25-zip) was used as a positive control. Empty vector negative controls were performed for every interaction displayed here, but for the sake of clarity, only one representative negative control is displayed. Results are the average of three independent experiments, with two technical replicates per experiment. Error bars indicate the SEM.

The Involvement of the AsfA and OsaC Homologues in *Streptomyces* Development

Through all the bacterial-two-hybrid experiments described in this chapter, I revealed a potential partner-switching network of interacting proteins, arising from the predicted anti-sigma factor AbaA6. I constructed mutant and overexpression lines for all relevant genes mentioned so far in this chapter - *asfA1, asfA2, osaC, osaC2* and *sigB*, in order to see whether this results in any developmental phenotypes. Due to the initial use of a wild-type strain with secondary mutation(s), I remade all strains featured in **Fig. 5.6** using a clean wild-type background - the overexpression constructs were simply re-conjugated, and the initial mutants were transduced using SV1 phage.

On MYM agar, the *ΔasfA1*, *ΔasfA2*, *ΔosaC2* and *ΔsigB* mutants all sporulated at a rate comparable to that of the wild type (**Fig. 5.6**). The *ΔosaC* mutant, however, appeared white, suggesting it is developmentally impaired. Similarly, the overexpression strains for *asfA1*, *asfA2*, *osaC2* and *sigB* appeared wild type-like on MYM agar, but the overexpression strain for *osaC* appeared white (**Fig. 5.6**).

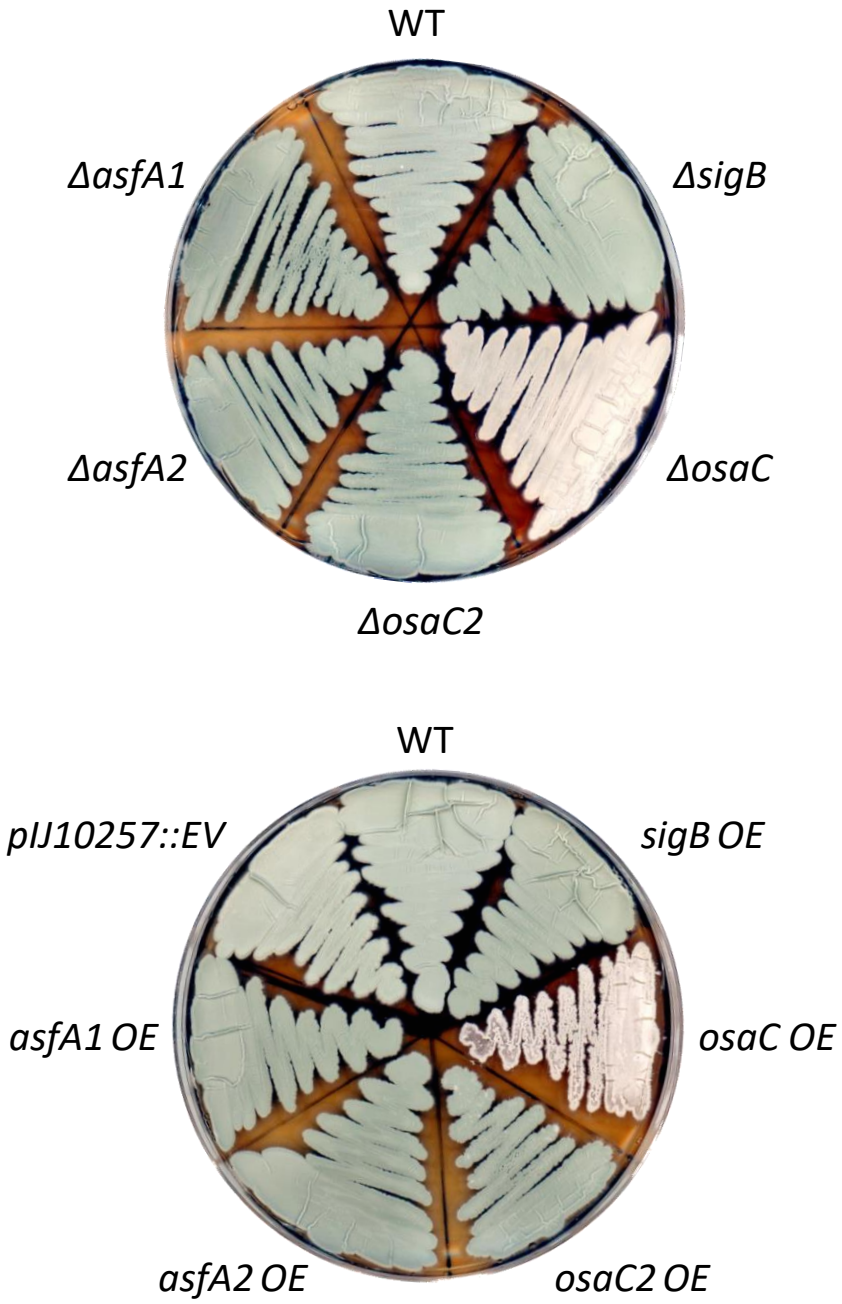

Figure 5.6. Mutant and Overexpression Phenotypes for the *asfA* and *osaC* Homologues.

Plates depicting the growth of the mutant and overexpression strains for the *asfA* homologues, the *osaC* homologues and *sigB* on MYM agar. Plate images were taken after a 4-day incubation at 28˚C.

Discussion

Through multiple bacterial-two-hybrid library screens and subsequent β-galactosidase quantitation, I uncovered an extensive protein-protein interaction network involving AbaA6. Unfortunately, I did not discover any proteins that could interact with IosA (apart from one false positive hit), so the molecular function of IosA remains a mystery.

I confirmed the strong interactions between AbaA6 and the predicted anti-sigma antagonists AsfA1 and AsfA2 (**Fig. 5.1**) but did not find any sigma factors that bind AbaA6 (**Fig. 5.2**). In *S. venezuelae*, there are 55 predicted sigma factors (McLean *et al.*, 2019) so it is possible that AbaA6 binds a non-SigB sigma factor. However, no sigma factors appeared as hits in the initial AbaA6 bacterial-two-hybrid library screen (**Table 5.1**). This might indicate that AbaA6 does not bind a sigma factor, or that bacterial-two-hybrid assays are not an appropriate method to identify these particular sigma - anti-sigma interactions. If AbaA6 binds a given sigma factor as a dimer – reminiscent of the way SpoIIAB binds SigF as a dimer (Campbell *et al.*, 2002), then bacterial-two-hybrid assays would not be able to capture the multimeric AbaA6-sigma factor interaction.

AbaA6 did bind the two predicted anti-sigma factor antagonists with STAS domains (AsfA1 and AsfA2), so there might still be similarities with the secondary partner-switching module (RsbT-RsbRS-RsbX) that acts on the stress response sigma factor SigB from *Bacillus.* In *Bacillus*, the activation state of the phosphatase RsbU (part of the primary partner-switching mechanism involving SigB-RsbW-RsbV-RsbU) is controlled by the secondary partner-switching mechanism involving RsbT-RsbRS-RsbX (Hecker, Pané-Farré and Uwe, 2007). Both the primary and the secondary partner switching mechanisms involve AbaA-like anti-sigma factors (RsbW and RsbT) and AsfA-like antagonists (RsbV, RsbR, RsbS). Thus, AbaA6 and its proposed antagonists AsfA1 and AsfA2 might function in a similar way to the secondary partner-switching module, and only indirectly modulate the activation state of a SigB-like sigma factor – something that remains to be discovered.

I did further bacterial-two-hybrid experiments, focusing on AsfA1 and AsfA2 as baits, anticipating to find RsbU-like phosphatases that might dephosphorylate the predicted anti-sigma factor antagonists. What I found was that AsfA1 and AsfA2 both bind OsaC and OsaC2 - multidomain proteins that indeed contain RsbU-like phosphatase domains, in addition to PAS, GAF, and histidine kinase-like HATPase_c domains.

Through its PAS and GAF domains, OsaC could ostensibly sense the osmotic state of the cell and act on its transcriptional regulator - proposed to be SigB in *S. coelicolor* (Fernández Martínez *et al.*, 2009).

I had hoped that OsaC, via the proposed interaction with SigB, would lead me to discover the molecular basis of the massive upregulation of *iosA* and the *abaA* homologues in the *ΔbldB* mutant (**Fig. 4.6, Table 4.1**). In addition, if there was also an interaction between BldB and OsaC, as the initial BldB two-hybrid-library screen suggested (**Table 3.1**), it would have closed the loop involving 4 levels of interaction, namely: AbaA6, AsfA1/ AsfA2, OsaC and BldB. This would have directly connected osmoregulation to the developmental life cycle of *Streptomyces*. However, my one-on-one β-galactosidase assays did not demonstrate interactions between OsaC and SigB or BldB (**Fig. 5.5**). Thus, I could not reproduce the results of Fernández Martínez *et al.* (2009) in the two-hybrid system with the *S. venezuelae* homologues. Vnz01715 (which I designated SigB) was the obvious homologue to use in my experiments, based on both synteny and homology with *S. coelicolor* SigB (SCO0600). However, it is still possible that *S. venezuelae* OsaC interacts with an alternative SigB homologue, such as the ones I tested for interaction with AbaA6. Alternatively, the two-hybrid system may not be an appropriate method to test for these interactions due to steric occlusion of the adenylate cyclase peptides, given the size and multidomain structure of OsaC. This might also be the reason why I did not observe an interaction between OsaC and BldB.

Future two-hybrid based work could focus on testing the interaction between BldB and the ATPase and PAS domains of OsaC in isolation, as the OsaC peptide from the initial BldB library screen (**Table 3.1**) covered these 2 OsaC domains. What is more encouraging is that in a preliminary Co-IP coupled to mass spectrometry experiment, where I used the polyclonal anti-BldB antibody to isolate BldB and any interacting partners, I found OsaC among the top hits (data not shown). More replicates and further biochemical experiments would be needed to confirm an interaction between OsaC and BldB, but the negative results from the one-on-one two-hybrid experiments alone do not rule out that interaction (or a potential interaction between OsaC and SigB).

The *S. coelicolor asfA2* homologue (*sco7754*), and *sigB* were upregulated after the application of acidic pH shock (Kim *et al.*, 2008), which is consistent with the involvement of SigB in the general stress response, and potentially links AsfA2 to SigB function. In both the *Bacillus* and the *Mycobacterium* stressosomes, the STAS domain-containing RsbR and RsbS were found to interact specifically via their STAS domains (Chen *et al.*, 2003; Marles-Wright *et al.*, 2008; Ramesh *et al.*, 2021).

It would be interesting to test whether AsfA1 and AsfA2 form a heterooligomer, which might make sense, considering they both interact strongly with AbaA6, OsaC and OsaC2.

Finally, I wanted to assess whether the AsfA homologues, the OsaC homologues, or SigB have any involvement in *S. venezuelae* development, so I generated mutant and overexpression strains for all 5 genes. One might expect that if the AsfA homologues act as anti-sigma antagonists for AbaA6 (the overexpression of which causes a white phenotype), they might also have developmental phenotypes when deleted. However, that was not the case - both the mutant and overexpression strains for *asfA1* and *asfA2* appear to sporulate normally (**Fig. 5.6**). This could be caused by AsfA1 and AsfA2 having redundant functions and thus compensating for each other, in which case the phenotype of a Δ*asfA1* Δ*asfA2* double mutant could be informative.

When grown on MYM agar, the *S. venezuelae ΔsigB* mutant did not exhibit a developmental phenotype, and neither did the *sigB* overexpression strain (**Fig. 5.6**). This was consistent with what was observed for the *S. avermitilis ΔsigB* mutant, which had a wild-type phenotype (Sun *et al.*, 2017). In comparison, the *S. coelicolor ΔsigB* mutant exhibited a bald phenotype on osmolyte-supplemented media (Cho *et al.*, 2001). In future work, I could grow my strains on different types of solid media with or without osmolyte supplementation, in order to observe any differences in phenotype.

OsaC2 did not produce any developmental phenotypes when deleted or overexpressed, unlike OsaC, where both the Δ*osaC* mutant and the *osaC* overexpression strain had white phenotypes (**Fig. 5.6**). The fact that both the deletion and overexpression of *osaC* resulted in developmental phenotypes is consistent with the findings of Fernández Martínez *et al.* (2009). In the *S. coelicolor* study, both the deletion and the overexpression strains for *osaC* lacked aerial hyphae. However, these phenotypes were only observed when the strains were plated on agar supplemented with 250 mM KCl - on NMMP agar both strains sporulated. Throughout my work, I used standard MYM agar with trace elements added to look at the *S. venezuelae* phenotypes. MYM contains maltose, which is a non-ionic osmolyte, so this could explain why I see the same developmental phenotypes as the authors of the initial OsaC study. Overall, my findings and those of Fernández Martínez *et al.* (2009) show would suggest that an optimal physiological concentration of OsaC is needed for sporulation in *Streptomyces*.

In summary, while studying the protein-protein interactions of AbaA6 did reveal a potential partner-switching network involving the AsfA and OsaC homologues, it did not find the expected transcriptional regulator(s) that might be responsible for the dramatic upregulation of *iosA* and the *abaA* homologues in the Δ*bldB* mutant in *S. venezuelae*.
For this reason, I decided to switch gears and see if I could find these transcriptional regulator(s) among the DNA-binding WhiJ homologues encoded in the vicinity of the *bldB* and *abaA* homologues.

Page intentionally left blank

6. WhiJ9 is a Transcription Factor, which is Linked to BldB Function

Introduction

The HTH-Xre Family of Transcriptional Regulators in Bacteria

DNA-binding proteins with helix-turn-helix Xre domains comprise one of the biggest families of transcriptional regulators in bacteria (Santos *et al.*, 2009). The classical example of a regulator with a HTH-Xre-like domain is the bacteriophage lambda repressor (Beamer and Pabo, 1992; Brady *et al.*, 2021). Indeed, many of the well-characterised HTH-Xre proteins are transcriptional repressors (which is why the whole HTH-Xre family of regulators gets described as repressors), though there are numerous examples where Xre regulators serve as activators of expression. Typically, the HTH-Xre domain is found in the N-terminus of proteins, whereas the C-terminus is more variable and often serves as an oligomerisation domain (Romero-Rodríguez, Robledo-Casados and Sánchez, 2015).

While most literature uses the "Xre" designation as an acronym for "xenobiotic response element", the name also found its roots from a study on the *B. subtilis* PBSX prophage. A gene divergently transcribed to the PBSX prophage genes, which was required for the sustained repression of the prophage was discovered and designated *xre*, standing for "PBS**X** **re**pressor" (Wood, Devine and McConnell, 1990). The Xre protein has been shown to bind 4 palindromic sites in its own intergenic region, thus blocking the transcription of the divergent prophage genes (McDonnell and McConnell, 1994). The *xre* gene was found to be essential in *Bacillus*, as expression of the prophage is fatal and leads to bacterial lysis (McDonnell *et al.*, 1994; Koo *et al.*, 2017).

Another well-characterised example of a transcriptional regulator with a HTH-Xre motif is SinR - a master regulator of biofilm formation in *Bacillus* (Gaur, Oppenheim and Smith, 1991). SinR directly represses the expression of genes in the *epsA-E* and *yqxM-sipW-tasA* operons, which are responsible for the biosynthesis of different extracellular matrix components (Kearns *et al.*, 2004; Chu *et al.*, 2006).

Before its role in biofilm formation was discovered however, SinR was already well-known for being a repressor of *Bacillus* sporulation. SinR was first identified when it was overexpressed on a high-copy plasmid, resulting in a sporulation-deficient phenotype, which is how it got its name, which stands for **s**porulation **in**hibition **r**egulator (Gaur, Dubnau and Smith, 1986). SinR was shown to repress the expression of important sporulation regulators such as Spo0A, ultimately leading to control over the SigF partner-switching pathway (Mandic-Mulec, Doukhan and Smith, 1995).

Given its important role in sporulation and biofilm formation in *Bacillus*, it is unsurprising that SinR itself is under strict regulation. The gene upstream of *sinR* encodes its antagonist SinI, which binds SinR to take it off DNA in stationary phase (Bai, Mandic-Mulec and Smith, 1993). Looking at the molecular details of the interaction, it was revealed that SinR binds DNA as a homotetramer, until SinI binding forces it to dissociate and to form the SinR-SinI heterodimer instead (Lewis *et al.*, 1998; Colledge *et al.*, 2011). Interestingly, another DNA-binding protein of the Xre family - SlrR was found to also be involved in the regulation of SinR function. In a double negative feedback loop, SinR represses the expression of *slrR*, but SlrR binds to SinR and antagonises this repression (Chai *et al.*, 2010). The SinR-SlrR complex was reported to jointly repress genes involved in cell separation and motility in *Bacillus* (Chai *et al.*, 2010).

Proteins with HTH-Xre domains have also been described as key players in bacterial type II toxin-antitoxin systems. Type II toxin-antitoxin systems encode a stable toxin and an unstable antitoxin and have been shown to play a role in bacterial cell growth, stress responses and plasmid maintenance (Gerdes, Christensen and Løbner-Olesen, 2005). Under normal conditions, the antitoxin binds and neutralises the toxin, then the toxin-antitoxin complex binds DNA and represses the expression of its own operon (Fraikin, Goormaghtigh and Van Melderen, 2020). Under stress conditions, the antitoxin is degraded, leading to the release and activity of the toxin. Multiple described toxin-antitoxin systems involve antitoxins with N-terminal HTH-Xre domains, such as the RES-Xre, HipA-HipB and HigA-HigB systems (Schumacher *et al.*, 2009; Skjerning *et al.*, 2019; Liu *et al.*, 2020).

It is because of this common occurrence of antitoxins having HTH-Xre domains that the loci encoding paired homologues of *bldB* and *whiJ* have been suggested to be novel toxin-antitoxin systems (Makarova, Wolf and Koonin, 2009). This description is only based on their genomic context and co-evolution, as currently there is no published experimental evidence of BldB homologues acting as toxins or binding to WhiJ homologues, though some studies have suggested that adjacently-encoded BldB and WhiJ homologues might be able to interact with one another (Aínsa *et al.*, 2010; Santamaría *et al.*, 2018).

Regulators with HTH-Xre Motifs in *Streptomyces*

All homologues of WhiJ share an N-terminal helix-turn-helix Xre motif, suggesting that these proteins potentially function as DNA-binding transcription factors. Indeed, there are multiple examples of HTH-Xre domain proteins (not encoded next to *bldB* homologues) that directly regulate the expression of target genes, and impact all kinds of cell functions, including secondary metabolite production and development in *Streptomyces*.

There are many examples in literature where proteins with HTH-Xre domains are found encoded in biosynthetic gene clusters, but the majority of the studies simply note their presence and do not go on to characterise their functions. The studies that did look into the regulatory functions of these HTH-Xre domain-containing proteins found that they can act as either repressors or activators of secondary metabolite production.

One such example is found in the methylenomycin A biosynthetic gene cluster, which is located on the SCP1 plasmid in *S. coelicolor* (Wright and Hopwood, 1976; Kirby and Hopwood, 1977). MmyB, a protein with an N-terminal HTH-Xre motif was found to be an activator of methylenomycin A synthesis, as its deletion abolished the production of the antibiotic (O'Rourke *et al.*, 2009). Another example can be found in the production of reedsmycin (RDM), which is an antifungal antibiotic isolated from *Streptomyces youssoufiensis* OUC6819 (Yao *et al.*, 2018). The HTH-Xre domain-containing RdmA was shown to be a repressor for RDM production, as synthesis of the antibiotic was enhanced by the deletion of RdmA and attenuated by its overexpression. The neighbouring genes of *rdmA* - *rdmD* and *rdmE* encode regulatory sensor kinases with HisKA and HATPase_c domains, with RdmE reported to influence RDM biosynthesis (Yao *et al.*, 2018).

Among the best characterised examples of developmental regulators with HTH-Xre motifs is BldD - the master regulator of *Streptomyces* development. BldD has been shown to form homodimers through association with tetrameric cyclic-di-GMP via its C-terminal domain (Tschowri *et al.*, 2014; Schumacher *et al.*, 2017). The $BldD_2$-$(c\text{-}di\text{-}GMP)_4$ complex then goes on to bind DNA via the N-terminal HTH-Xre domains, and regulate the expression of ~170 genes, including ones encoding other important developmental regulators (Den Hengst *et al.*, 2010).

The *S. venezuelae* orthologue of canonical *S. coelicolor* WhiJ is not straight-forward to determine - in a BLAST search, the closest *S. venezuelae* match for canonical WhiJ is Vnz31570 (encoded next to an *abaA* homologue, but not a *bldB* homologue). However, in a reverse BLAST search Vnz31570 did not map back to *S. coelicolor* WhiJ. Looking at the synteny, the wider genomic region containing *S. coelicolor whiJ* appears to be missing from *S. venezuelae.* Therefore, there is no reciprocal best hit for WhiJ in *S. venezuelae*.

A recent study on the *S. coelicolor* homologue of WhiJ10 (SCO1979) showed that SCO1979 bound its own intergenic region in an *in vitro* EMSA experiment (Zhu *et al.*, 2020). The authors constructed a *Δsco1979* mutant strain by replacing the middle part of the gene with an apramycin resistance cassette, leaving an intact left and right *sco1979* flank. This reportedly resulted in the removal of part of the HTH-XRE motif. In a qRT-PCR experiment, it was shown that while no expression of the deleted part of the gene could be detected, the expression of the intact flanks was upregulated, meaning that SCO1979 directly repressed its own expression. The Δ*sco1979* mutant exhibited a higher production of actinorhodin, prodiginine and CDA, along with reduced sporulation rates (Zhu *et al.*, 2020). The authors did not report any involvement of the adjacently encoded *abaA* and *bldB* homologues in the activity of the *S. coelicolor* WhiJ10 homologue.

Nothing else has been reported in literature about the other *whiJ* homologues, which are genetically linked to homologues of *bldB* (except what is already covered in Chapter 3). In the current chapter, I describe my work towards the characterisation of two such WhiJ homologues - WhiJ6 and WhiJ9.

Results

The Deletion of Two *whiJ* Homologues Has No Impact on *Streptomyces* Development

In my search for proteins that interact with BldB, I discovered that 7 of its 10 homologues interacted strongly with BldB in a bacterial-two hybrid experiment (**Fig. 3.12**). When I deleted 2 out of those 7 strongly interacting homologues (BldB6 and BldB9) from *S. venezuelae*, the resulting mutant strains exhibited white phenotypes (**Fig. 3.13, 3.14, 3.15, 3.16**). The loci encoding *bldB6* and *bldB9* also encode *abaA6* and *iosA* respectively - the two genes with the highest degree of upregulation in the *ΔbldB* mutant, as demonstrated by my RNA-seq results (**Fig. 4.6, Table 4.1**). The single overexpression strains I generated for *abaA6* and *iosA* also exhibited white phenotypes (**Fig. 4.8, 4.9**). Building up on this, I confirmed that the joint overexpression of *abaA6* and *iosA* recapitulated the *ΔbldB* mutant phenotype (**Fig. 4.10, 4.11, 4.12, 4.13**). All of this shows that the two loci encoding *bldB6-abaA6* and *bldB9-iosA* are especially important for BldB function. For this reason, in my search for transcriptional regulators that might contribute to the impressive upregulation of *abaA6* and *iosA* in the *ΔbldB* mutant, I turned to the predicted DNA-binding proteins WhiJ6 and WhiJ9, which are also encoded in the two loci (**Fig. 3.6**).

I decided to do ChIP-seq to test whether WhiJ6 and WhiJ9 could indeed bind DNA, and in particular, if they bound their own intergenic regions, resulting in control over the expression of the divergently transcribed *abaA6* and *iosA*. To do so, I decided to construct *ΔwhiJ6* and *ΔwhiJ9* mutant strains and complement them with plasmids producing 3xFLAG-WhiJ6 or 3xFLAG-WhiJ9 (expressed from their native promoters). I would then go on to use these complemented strains to isolate the tagged WhiJ homologues bound to DNA with an anti-FLAG antibody in the ChIP-seq experiments.

Being wary of any polar effects that might arise upon the deletion of *whiJ6* and *whiJ9*, I decided to first look at the transcriptional start sites of the downstream *bldB6* and *bldB9* from an existing 5' triphosphate end-capture dataset in the Buttner lab. The data showed that the transcription start sites for *bldB6* and *bldB9* lie within the upstream *whiJ6* and *whiJ9* genes. In order not to disturb the regulatory elements necessary for control of *bldB6* and *bldB9* expression, I decided to only truncate the *whiJ6* and *whiJ9* genes instead of deleting them fully. Thus, for both *whiJ6* and *whiJ9* I deleted the first 159 codons using Redirect, leaving the downstream sequences intact.

The resulting *ΔwhiJ6* and *ΔwhiJ9* mutants appeared to develop normally on MYM agar (**Fig. 6.1**). Under the electron microscope, both mutant strains exhibited the formation of regularly sized spores (**Fig. 6.2**). This normal growth confirmed that the partial deletions of *whiJ6* and *whiJ9* did not disturb the expression of the downstream *bldB6* and *bldB9* (whose deletion results in white phenotypes). When I complemented each mutant with an N- or C-terminally 3xFLAG-tagged allele of the complete wild-type gene, the resulting strains developed normally as well (**Fig. 6.1**). Unfortunately, as the *ΔwhiJ6* and *ΔwhiJ9* mutants did not have developmental phenotypes to rescue, I had no way of knowing whether the 3xFLAG-WhiJ6 and 3xFLAG-WhiJ9 fusions were functional, *i.e.,* whether the 3xFLAG tag placed on either terminus interfered with any DNA binding activity.

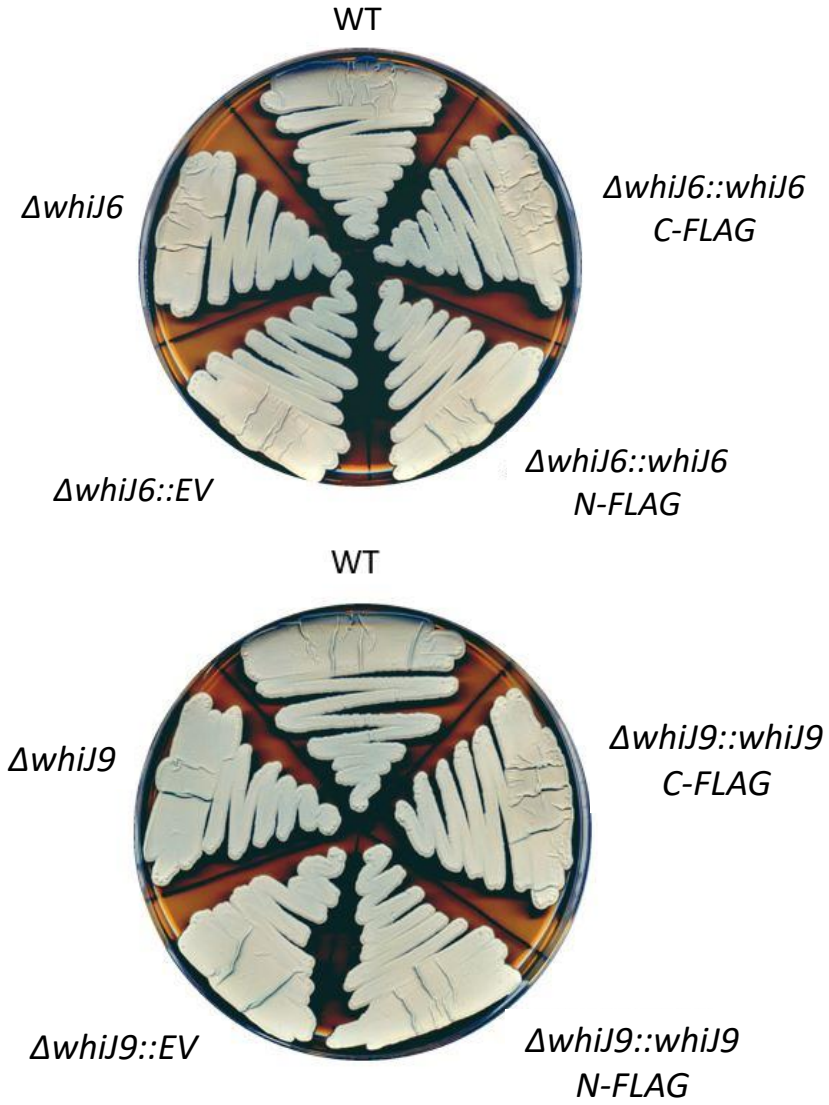

Figure 6.1. Mutant Phenotypes of the *ΔwhiJ6* and *ΔwhiJ9* Strains.

Plates depicting the growth of the mutant and complementation strains for *whiJ6* and *whiJ9* on MYM agar. EV stands for empty pSS170 vector control. N-FLAG and C-FLAG stand for N-terminal 3xFLAG tag and C-terminal 3xFLAG tag, respectively. Plate images were taken after a 4-day incubation at 28˚C.

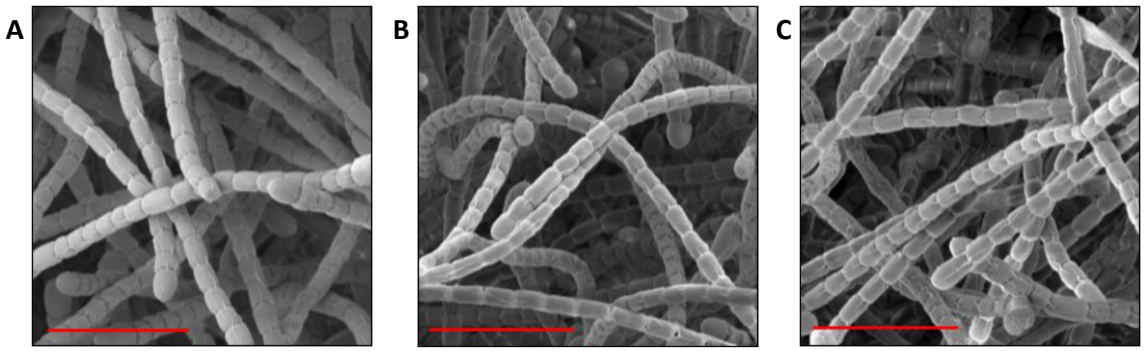

Figure 6.2. Phenotypic Characterisation of the *ΔwhiJ6* and *ΔwhiJ9* Mutant Strains.

Scanning electron micrographs comparing the phenotypes of wild-type *S. venezuelae* **(A)**, the *ΔwhiJ6* mutant strain **(B)**, and the *ΔwhiJ9* mutant strain **(C).** Scale bars in red indicate 5 µm.

The Overexpression of *whiJ9* Results in Impaired Sporulation

Since the partial deletions of *whiJ6* and *whiJ9* resulted in mutants without developmental phenotypes, I decided to see if the overexpression of each gene would result in any developmental aberrations instead. As standard, I placed each gene under the control of the constitutive *ermE** promoter on the integrative plasmid pIJ10257. The resulting *whiJ9* overexpression strain looked white on MYM agar, whereas the *whiJ6* overexpression strain appeared to develop normally (**Fig. 6.3**). When I looked at the effects of *whiJ9* overexpression in microscopic detail, I could see 3 developmentally distinct regions of the colony - a “white” centre showing growth of mostly undifferentiated aerial hyphae (**Fig. 6.4D**), a bald inner ring around this centre, which only exhibited vegetative growth (**Fig. 6.4E**), and a “white” outer ring, which again contained undifferentiated aerial hyphae, but also some spore chains (**Fig. 6.4F**). In comparison, the *whiJ6* overexpression strain (**Fig. 6.4C**), as well as wild-type *S. venezuelae* and the empty vector control strain (**Fig. 6.4A, 6.4B**), were able to form mature spores.

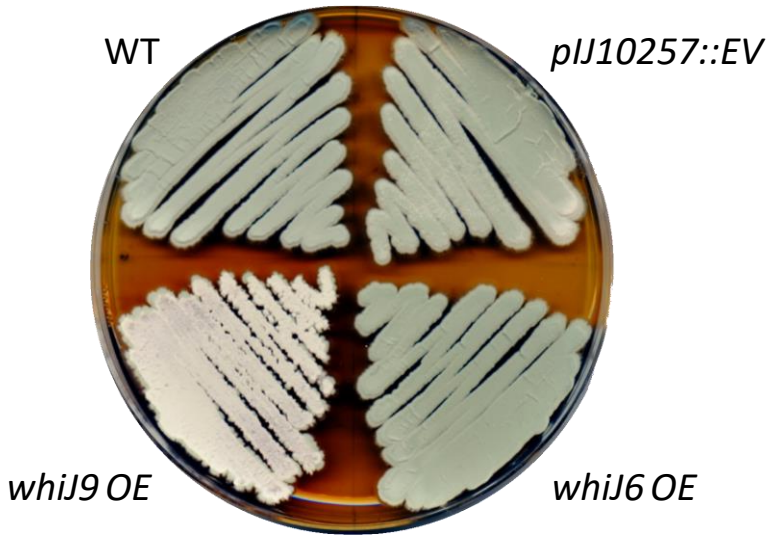

Figure 6.3. Overexpression Phenotypes for *whiJ6* and *whiJ9*.

Plate depicting the growth of the overexpression strains for *whiJ6* and *whiJ9* on MYM agar. EV stands for empty pIJ10257 vector control. Plate image was taken after a 4-day incubation at 28˚C.

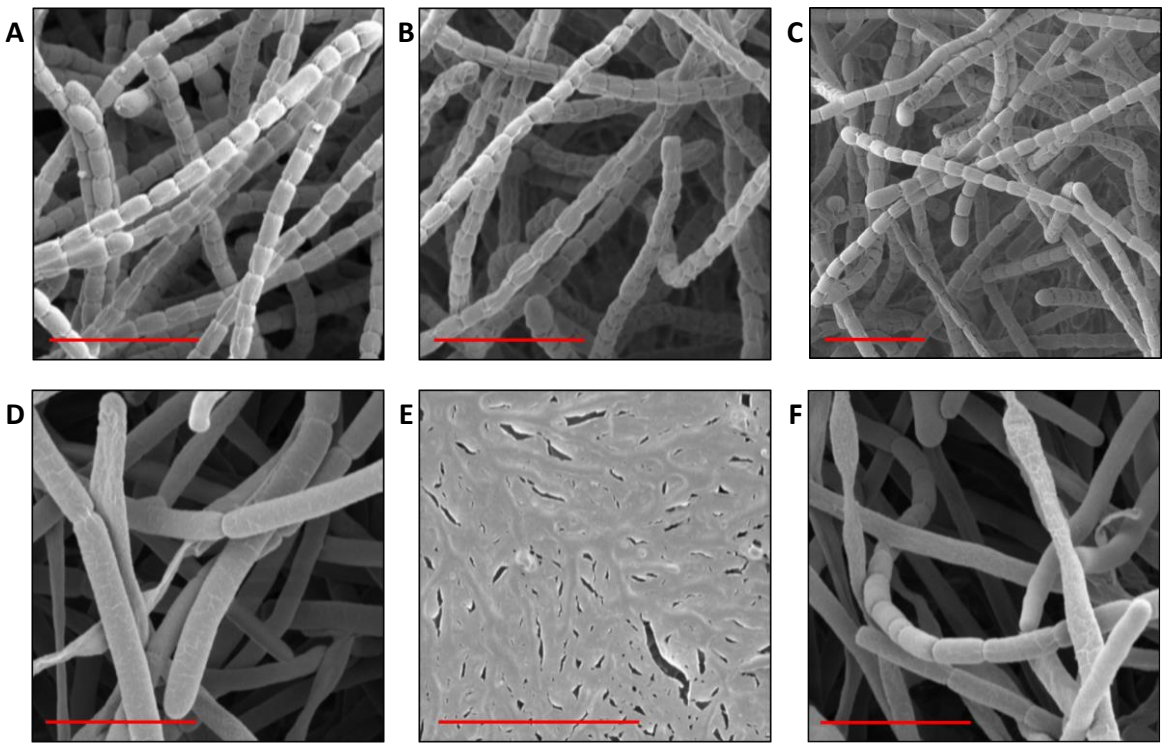

Figure 6.4. Phenotypic Characterisation of the *whiJ6* and *whiJ9* Overexpression Strains.

Scanning electron micrographs comparing the phenotypes of wild-type *S. venezuelae* **(A)**, the pIJ10257 empty vector control **(B)**, the *ΔwhiJ6* overexpression strain **(C)**, the colony centre of the *ΔwhiJ9* overexpression strain **(D)**, the inner ring of the *ΔwhiJ9* overexpression strain **(E)**, the outer ring of the *ΔwhiJ9* overexpression strain **(F).** Scale bars in red indicate 5 µm.

Because the *whiJ9* overexpression strain was developmentally impaired, I decided to overexpress N- or C-terminally 3xFLAG-tagged WhiJ9 in wild-type *S. venezuelae* to see if it would result in the same overexpression phenotype. On a plate, both of the resulting strains looked exactly like the strain in which I overexpressed untagged *whiJ9* (**Fig. 6.5**). This proved that both 3xFLAG versions of WhiJ9 were fully functional, with no steric occlusion caused by the tag placed on either end. Unfortunately, I still had no way of telling whether the 3xFLAG-tagged alleles of WhiJ6 were functional, as there was no phenotypic output from the deletion or overexpression of the gene.

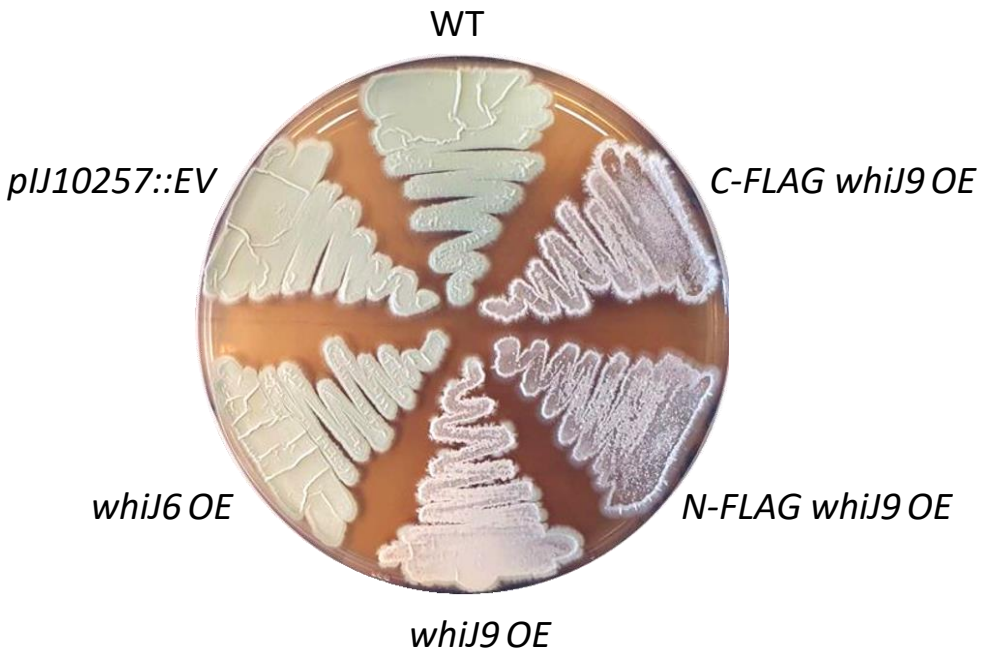

Figure 6.5. Overexpression Phenotypes for the 3xFLAG-tagged Alleles of *whiJ9*.

Plate depicting the growth of the overexpression strains for *whiJ6* and *whiJ9* on MYM agar. EV stands for empty pIJ10257 vector control. N-FLAG and C-FLAG stand for N-terminal 3xFLAG tag and C-terminal 3xFLAG tag, respectively. Plate image was taken after a 4-day incubation at 28˚C.

Protein Abundance Levels of the WhiJ6 and WhiJ9 Homologues

To choose which of the aforementioned *ΔwhiJ6* and *ΔwhiJ9* mutant strains complemented with 3xFLAG-tagged alleles of the respective genes to use for ChIP-seq, I performed an automated Western blot using an anti-FLAG antibody. For the ChIP-seq experiments on the 2 WhiJ homologues, I decided to mirror what I did for my BldB-focused RNA-seq and ChIP-seq experiments and use 3 time points for sampling - representing early, mid- and late development. Therefore, I took samples for Western blotting at 10-, 16- and 22-hours post-inoculation.

The levels of WhiJ6 increased as the strains progressed through development, although I could not detect any C-terminally 3xFLAG-tagged WhiJ6 at 10 hours (**Fig. 6.6**). Because I could not tell which allele was functional, and the N-terminally tagged allele performed better in the Western blot, I chose to use the *ΔwhiJ6* mutant complemented with an N-terminally 3xFLAG-tagged WhiJ6 in my ChIP-seq experiment.

Unfortunately, I did not get the same robust protein levels for 3xFLAG-WhiJ9. The N-terminally tagged WhiJ9 allele could not be detected at all, whereas the C-terminally tagged allele could be detected at very low levels, and only at 16- and 22-hours post-inoculation (**Fig. 6.6**). For this reason, I chose to do ChIP-seq with the *ΔwhiJ9* mutant complemented with a C-terminally 3xFLAG-tagged WhiJ9. However, I was worried about potential low enrichment levels caused by the low protein abundance of 3xFLAG-WhiJ9. For this reason, I decided to test whether one of the 3xFLAG-WhiJ9 overexpression strains I previously generated (**Fig. 6.5**) could also be used in a ChIP-seq experiment.

I performed another Western blot using the 3xFLAG-WhiJ9 overexpression strains (**Fig. 6.5**). As expected, I could detect 3xFLAG-WhiJ9 at high levels at all time points, irrespective of where the tag was placed (**Fig. 6.7**). In comparison, this time I could not detect any 3xFLAG-WhiJ9 from the *ΔwhiJ9* mutant complemented with a C-terminally 3xFLAG-tagged WhiJ9. For this reason, I decided to perform ChIP-seq on one of the overexpression strains, in addition to the *ΔwhiJ9* mutant complemented with a C-terminally 3xFLAG-tagged WhiJ9. To be consistent, I decided to use the C-terminally tagged WhiJ9 overexpression strain for ChIP-seq.

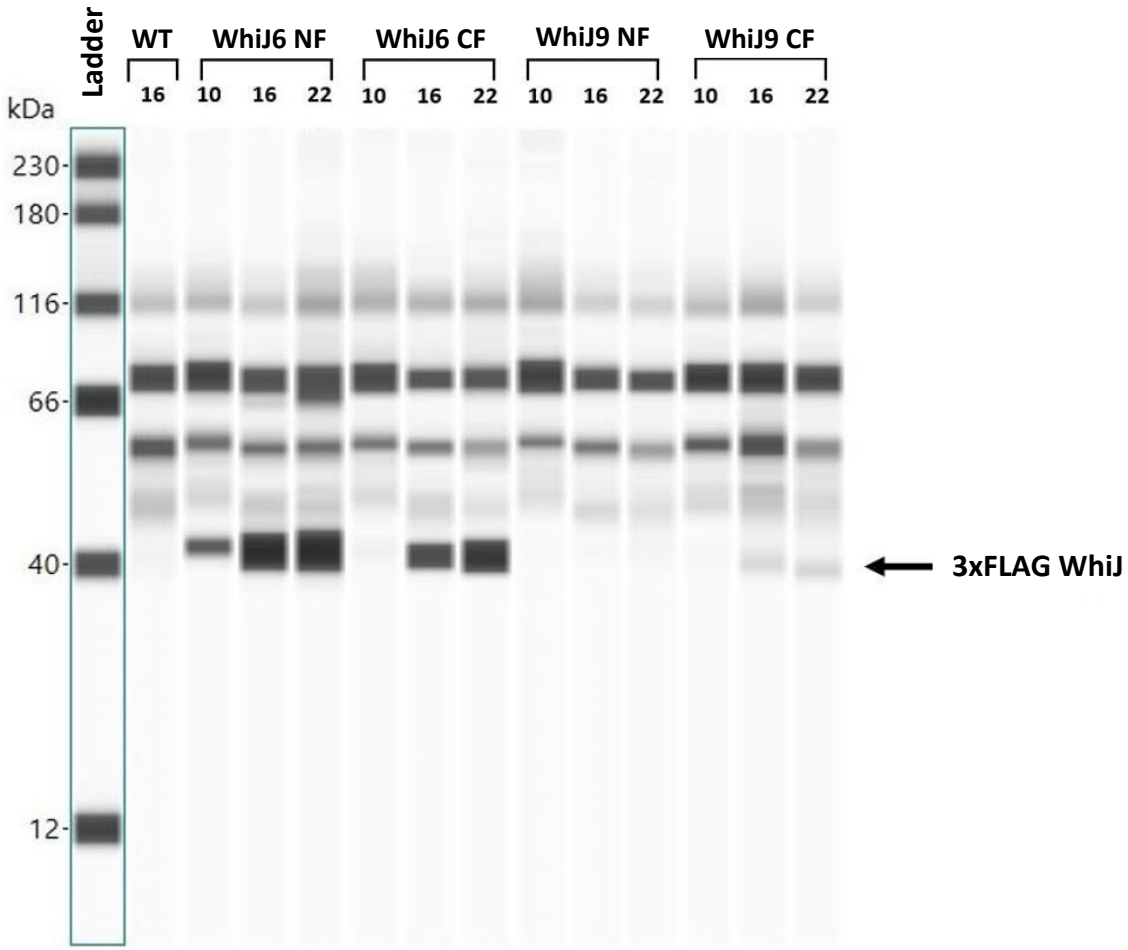

Figure 6.6. WhiJ6 and WhiJ9 Abundance Throughout Development.

The levels of 3xFLAG-WhiJ6 and 3xFLAG-WhiJ9 were measured using an automated Western blot. Samples were taken at 10-, 16- and 22-hours post-inoculation from the Δ*whiJ6::*3xFLAG-WhiJ6 and the Δ*whiJ9::*3xFLAG-WhiJ9 strains, with the 3xFLAG tag placed at the N-terminus (NF), or the C-terminus (CF) of the protein. Sample from wild-type *S. venezuelae* taken at 16 hours post-inoculation was used as a negative control. All samples were diluted to the same total protein concentration, as determined by Bradford assays. A single replicate is shown for each timepoint. Arrow indicates the 3xFLAG-WhiJ6 and 3xFLAG-WhiJ9 bands.

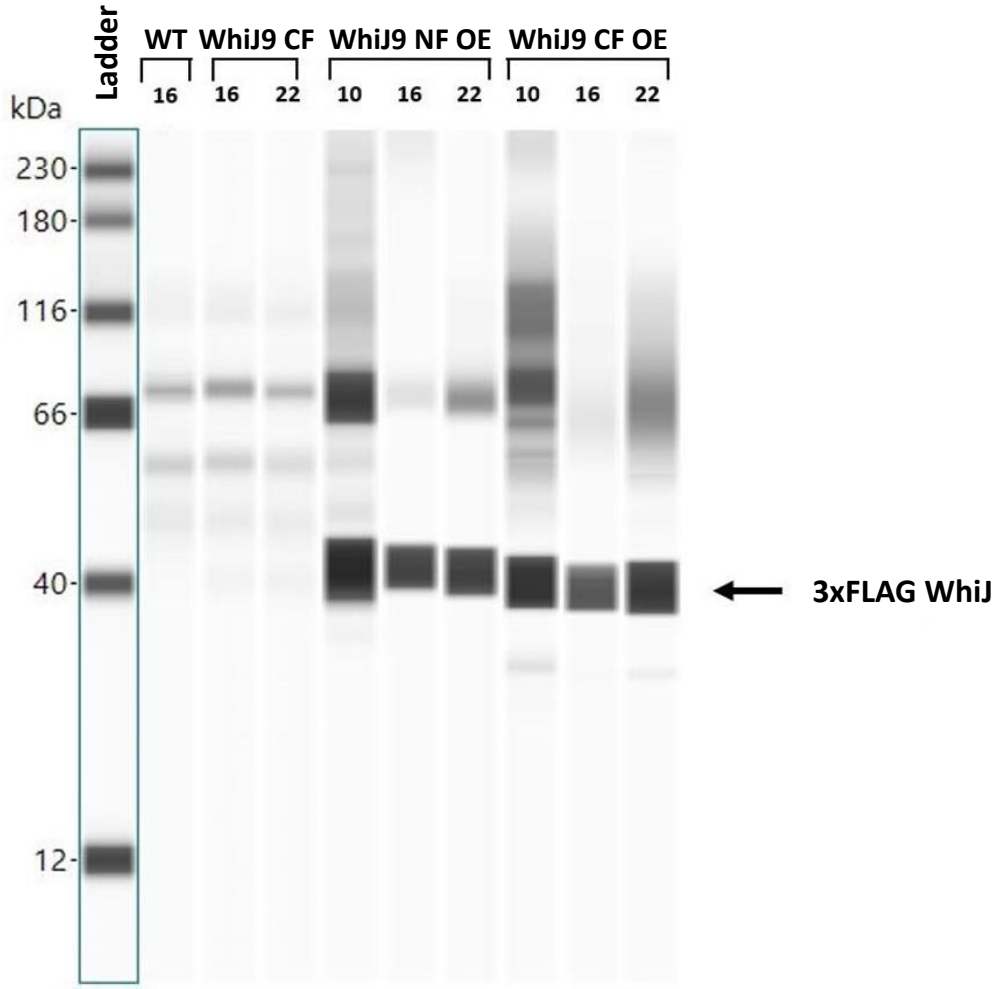

Figure 6.7. WhiJ9 Abundance in WhiJ9 Overexpression Strains.

The levels of 3xFLAG-WhiJ9 were measured using an automated Western blot. Samples were taken at 10-, 16- and 22-hours post-inoculation from the 3xFLAG-WhiJ9 strains, with the 3xFLAG tag placed at the N-terminus (NF), or the C-terminus (CF) of the protein. In these strains 3xFLAG-WhiJ9 was either expressed from its own promoter, or from the constitutive *ermE** promoter (OE samples). Sample from wild-type *S. venezuelae* taken at 16 hours post-inoculation was used as a negative control. All samples were diluted to the same total protein concentration, as determined by Bradford assays. A single replicate is shown for each timepoint. Arrow indicates the 3xFLAG-WhiJ9 bands.

WhiJ9 is a DNA-binding Protein

In my ChIP-seq experiment looking at 3xFLAG-WhiJ6 binding to DNA, there were peaks representing differential enrichment compared to the wild-type control, especially in the 10-hour sample (**Fig. 6.8**). As in the BldB ChIP-seq experiment however, these peaks were next to genes encoding stable RNAs (a known false positive); there were no significant peaks next to protein-encoding genes. This meant that under the conditions I used, 3xFLAG-WhiJ6 did not bind DNA. However, this does not necessarily mean that WhiJ6 is not a transcription factor. It is possible that the 3xFLAG tag at the N-terminus might have impeded binding of the N-terminal helix-turn-helix Xre domain to DNA in this experiment.

To identify enrichment caused by 3xFLAG-WhiJ9 binding to DNA, I used a strain where production of 3xFLAG-WhiJ9 was driven from its own promoter, and a strain where its production was driven from the strong *ermE** promoter, resulting in a confirmed overproduction of the protein (**Fig. 6.6, 6.7**). When produced from its own promoter, there was no observed binding of 3xFLAG-WhiJ9 to DNA in the 16- and 22-hour samples. In the 10-hour sample, there were statistically significant albeit low levels of enrichment at intergenic regions flanking protein-coding genes. This was likely caused by the low protein levels of 3xFLAG-WhiJ9 in the complementation strain. In comparison, the overexpression strain exhibited significantly higher enrichment across all time points (**Fig. 6.9**).

I compiled a list of the promoter regions with significant enrichment peaks from both 3xFLAG-WhiJ9 datasets and visually inspected them to omit any “ambiguous” peaks, *e.g* ones with corresponding smaller peaks in the wild-type control. The remaining 46 “good quality” peaks are shown in **Table 6.1**. The genes flanking enrichment peaks that are highlighted in bold are the genes that were differentially expressed in the later-described RNA-seq experiment performed on the *ΔwhiJ9* mutant (**Table 6.2**).

In both 3xFLAG-WhiJ9 datasets, the most statistically significant peak, and also the most interesting peak from the perspective of this project, was found in the intergenic region between *iosA* and *whiJ9* itself - suggesting that WhiJ9 potentially controls its own expression and/or that of *iosA* (**Fig. 6.10, Table 6.1**). This finding will be explored in greater detail later in this chapter.

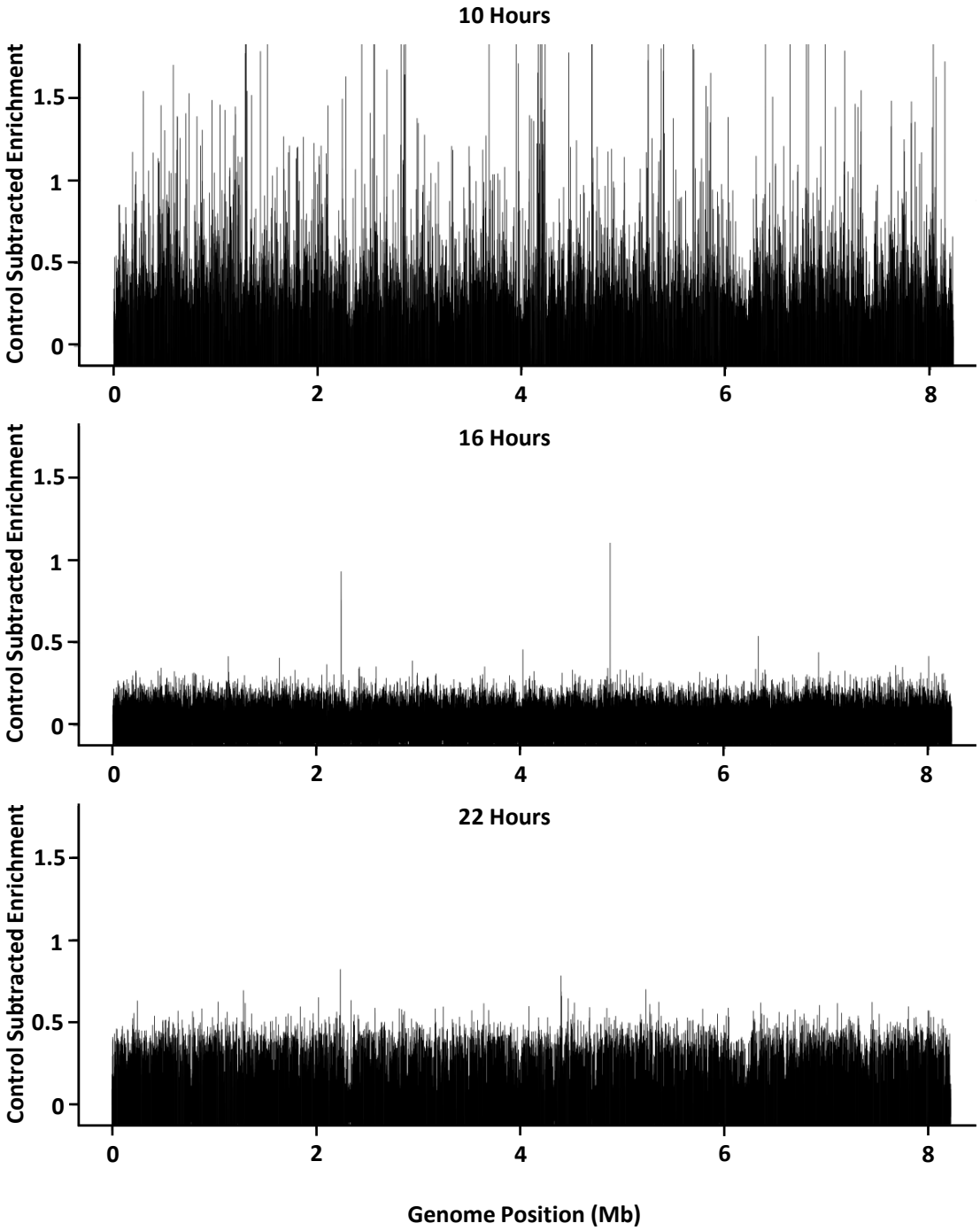

Figure 6.8. Anti-FLAG WhiJ6 ChIP-Seq Whole Genome Enrichment.

ChIP-seq results representing levels of 3xFLAG-WhiJ6 binding to DNA across the whole genome, with protein-DNA complexes captured from the Δ*whiJ6::*3xFLAG-WhiJ6 strain using an anti-FLAG antibody. Wild-type *S. venezuelae* was used as a negative control. The x-axes indicate the genome position in megabases, and the y-axes represent the control subtracted enrichment for each time point.

Page intentionally left blank

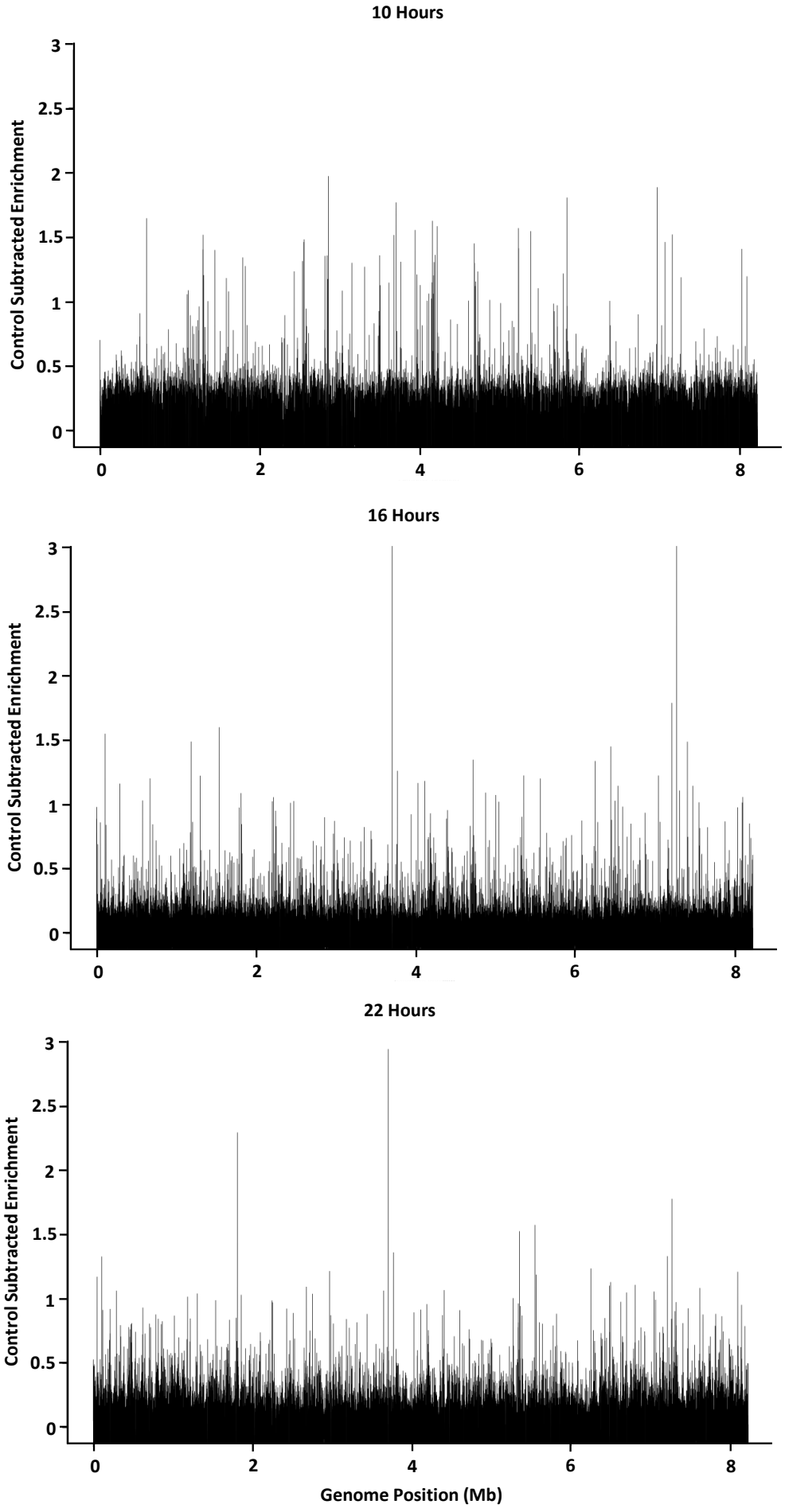
10 Hours
Control Subtracted Enrichment
3
2.5
2
1.5
1
0.5
0
0
2
4
6
8
16 Hours
Control Subtracted Enrichment
3
2.5
2
1.5
1
0.5
0
0
2
4
6
8
22 Hours
Control Subtracted Enrichment
3
2.5
2
1.5
1
0.5
0
0
2
4
6
8
Genome Position (Mb)

Figure 6.9. Anti-FLAG WhiJ9 ChIP-Seq Whole Genome Enrichment.

ChIP-seq results representing levels of 3xFLAG-WhiJ9 binding to DNA across the whole genome, with protein-DNA complexes captured from the 3xFLAG-WhiJ9 overexpression strain using an anti-FLAG antibody. Wild-type *S. venezuelae* was used as a negative control. The x-axes indicate the genome position in megabases, and the y-axes represent the control subtracted enrichment for each time point.

Looking at the other 45 enrichment peaks from **Table 6.1**, while they are good candidates for direct WhiJ9 targets, it is possible that not all of them represent actual WhiJ9 binding, as for some of them the enrichment values were low (though still statistically significant). Further experiments would need to be performed to confirm and test the strength of WhiJ9 binding to the promoters of interest. While most of these potential WhiJ9 targets are not well-characterised (**Table 6.1**), for a select few there is a considerable amount of information in existing literature, as detailed below.

The expression of the *vnz16980* homologue in *S. coelicolor* (*sco7630*, encoding a predicted phosphoglycerate mutase) has been shown to be controlled by the response regulator PhoP under phosphate stress conditions (Rodríguez-García *et al.*, 2007). Interestingly, when I looked more closely into the direct targets of PhoP in *S. coelicolor* (Sola-Landa *et al.*, 2008; Allenby *et al.*, 2012), I saw that for 13 of their *S. venezuelae* homologues there was significant enrichment in my 3xFLAG-WhiJ9 ChIP-seq dataset, as detailed in **Table 6.1**. More work would need to be performed to establish a link between WhiJ9 and PhoP in *S. venezuelae* specifically, but an overlap in binding sites could for example indicate competition between WhiJ9 and PhoP for binding of the same promoter regions.

One interesting potential target of WhiJ9 was the predicted histidine kinase *vnz00475* (**Table 6.1**). The *S. coelicolor* homologue of *vnz00475* is *cvnA6* - the first gene in the *cvn6* conservon, also found among the PhoP direct targets (Allenby *et al.*, 2012). Conservons (*cvn*) in *Streptomyces* are conserved operons that were first characterised when the *S. coelicolor* genome was sequenced (Bentley *et al.*, 2002). These conservons (13 in *S. coelicolor*) contain 4-5 genes, 2 of which typically encode a histidine kinase-like protein and an ATP/GTP-binding protein (Bentley *et al.*, 2002). As WhiJ9 bound upstream of the *S. venezuelae cvnA6* homologue (**Table 6.1**), it presumably regulates the expression of the whole *cvn6* conservon. Notably, CvnA6 and all other CvnA(1-13) histidine kinase homologues contain a HATPase_c domain, also found in the AbaA homologues and anti-sigma factors for SigB-like systems.

One of the best-characterised conservons is *cvn9* - it has been shown to encode proteins that form a membrane-associated signal transduction complex in *S. coelicolor* (Komatsu *et al.*, 2006). An earlier study by the same authors found that the *cvn9* conservon in *S. griseus* restored sporulation to the bald *ΔamfR* mutant, when it was introduced on a high-copy plasmid (Komatsu *et al.*, 2003). For this reason, they labelled the genes in the conservon *rarA-E* (for "**r**estoration of **a**erial mycelium formation in an amf**R** mutant"). This restoration of sporulation could be recapitulated by the introduction of N-terminally truncated RarA (CvnA9) alone, containing only the HATPase_c domain in its C-terminus. The *S. griseus ΔrarA* mutant exhibited precocious aerial mycelium formation and production of streptomycin, however, this phenotype was only partially restored upon complementation, suggesting that the mutant phenotype was partially caused by polar effects on the downstream genes in the conservon (Komatsu *et al.*, 2003).

In *S. coelicolor*, the deletions of *cvnA9* and *cvnD9* (*rarA* and *rarD* in *S. griseus*), and the deletion of *cvnA10* (homologue of *cvnA9*), resulted in the same developmental and antibiotic production phenotypes seen in the *S. griseus ΔrarA* mutant; this time the phenotypes were successfully complemented by re-introduction of the respective wild-type genes (Komatsu *et al.*, 2003, 2006). Furthermore, the HATPase_c domain of CvnA9 was shown to hydrolyse ATP *in vitro* (Komatsu *et al.*, 2006).

Another operon that might be under the dual control of WhiJ9 and PhoP is *vnz25450 - vnz25465* (**Table 6.1**). Interestingly, the genes in this operon were among the most upregulated genes in *S. venezuelae* 'explorer cells' and their products were proposed to play a role in the uptake of iron-complexed siderophores (Jones *et al.*, 2017, 2019).

Another likely WhiJ9 target is *vnz07825*, a gene encoding a tellurium resistance TerC-like protein. This gene was found to be greatly induced following nitrogen starvation, but then repressed after addition of ammonium, in a way that was dependent on the response regulator GlnR in *S. venezuelae* (Pullan *et al.*, 2011). Another potential target of WhiJ9 from my ChIP-seq dataset, which was also found to be a direct target of GlnR was *vnz13910*, which encodes a hypothetical protein, with potential function in beta-glucan synthesis (Pullan *et al.*, 2011).

SppA (encoded by *vnz18225*, and a potential PhoP target) has been described as a dual-specificity phosphatase, as it was shown to dephosphorylate peptides containing pSer, pThr, and pTyr *in vitro* (Umeyama, Naruoka and Horinouchi, 2000). Growth of the *S. coelicolor ΔsppA* mutant was found to be severely delayed and impaired, though after prolonged incubation the strain was able to sporulate (Umeyama, Naruoka and Horinouchi, 2000). SppA has been shown to dephosphorylate DivIVA *in vivo* and *in vitro*, although the *ΔsppA* mutant phenotype was not caused by hyperphosphorylation of DivIVA (Passot, Cantlay and Flärdh, 2021).

Other peaks of interest included the promoter region of *sigF* (**Fig. 6.10**), and the intergenic region between *sigB3* and a gene encoding its potential anti-sigma factor, which has a HATPase_c domain (**Table 6.1**). The sporulation sigma factor SigF and the uncharacterised SigB3 were among the SigB-like sigma factors I previously tested for interaction with AbaA6, though no interactions were found in the bacterial two-hybrid experiment (**Fig. 5.2**).

Finally, a peak corresponding to potential WhiJ9 binding was found in the intergenic region between *lexA* and *nrdR* (**Fig. 6.10, Table 6.1**). LexA is a well-characterised repressor of the SOS response in bacteria (Butala, Žgur-Bertok and Busby, 2009; Smollett *et al.*, 2012). NrdR is a repressor of the ribonucleotide reductase encoding genes *nrdAB* and *nrdJ* in *S. coelicolor* (Grinberg et al., 2006). Ribonucleotide reductases catalyse a step in the *de novo* synthesis of dNTPs, thereby influencing the rate of DNA replication (Herrick and Sclavi, 2007).

Table 6.1. WhiJ9 ChIP-seq Results.

Flanking Gene(s)	SCO Homologue(s)	Product(s)	Adjusted P Value			Bound by PhoP?
			10 hours	16 hours	22 hours	
vnz16670, ***vnz16675***	-	**IosA, WhiJ9**	4.87E-08	6.78E-58	6.15E-21	-
vnz36245	*sco7013*	Sugar-binding protein	0.000522	6.84E-10	0.000362	Y
vnz07825	*sco1963*	**Tellurium resistance protein TerC**	0.000557	2.97E-07		-
vnz00475	*sco6069*	**Histidine kinase CvnA6**		3.23E-21	1.97E-05	Y
vnz28425	-	**Hypothetical protein**		8.33E-16	0.000141	-
vnz16975, ***vnz16980***	*sco2840, sco7630*	LysR family transcriptional regulator, **Phosphoglycerate mutase**		1.63E-14	1.58E-05	-
vnz25450	*sco5476*	**Peptide ABC transporter permease**		1.88E-13	0.000239	Y
vnz07930	-	**Hypothetical protein**		2.84E-07	4.43E-09	-
vnz28940, vnz28945	*sco4261, sco4257*	**Helix-turn-helix transcriptional regulator, Hydrolytic protein**	2.99E-11			Y
vnz18930	*sco4088*	Hypothetical protein	1.95E-08			-
vnz28740, vnz28745	*- , sco5999*	Extradiol dioxygenase, Aconitate hydratase	3.72E-08			Y
vnz13910	-	Hypothetical protein	5.51E-08			-

Flanking Gene(s)	SCO Homologue(s)	Product(s)	Adjusted P Value			Bound by PhoP?
			10 hours	16 hours	22 hours	
vnz04645, vnz04650	*sco1378, sco1379*	Glycine dehydrogenase, Photosystem reaction center subunit H	4.68E-07			-
***vnz35960**, vnz35965*	*sco2347, -*	**Hypothetical protein**, TetR family transcriptional regulator	7.40E-07			Y
vnz24420, vnz24425	*-*	DNA-binding protein, Transcriptional regulator	9.78E-07			-
***vnz02250**, vnz02255*	*-*	**HATPase_c domain protein**, SigB3	2.37E-06			-
vnz25170	*sco5439*	Helicase	2.94E-06			-
vnz27470	*sco5901*	RNA methyltransferase	5.28E-06			Y
vnz07295, vnz07300	*sco1840, -*	ABC transporter, Hypothetical protein	1.56E-05			Y
vnz21010, vnz21015	*sco4505, sco4506*	Cold-shock protein, menaquinone biosynthesis protein	9.62E-05			Y
vnz20385, vnz20390	*sco4318, -*	Helicase, Hypothetical protein	0.000165			-
vnz06905, vnz06910	*sco1776, sco1777*	CTP synthase, Glucoamylase	0.000324			Y
vnz15670	*sco3326*	NAD-dependent dehydratase	0.000328			-
*vnz02185, **vnz02190***	*sco3748, -*	Cold shock domain protein CspD, **RNA helicase**	0.000357			-

Flanking Gene(s)	SCO Homologue(s)	Product(s)	Adjusted P Value			Bound by PhoP?
			10 hours	16 hours	22 hours	
vnz15370	*sco4493*	**AsnC family transcriptional regulator**	0.000777			-
vnz29240	*sco6095*	Sulfate ABC transporter ATP-binding protein		1.99E-19		Y
vnz06685	-	Ectoine/hydroxyectoine ABC transporter ATP-binding protein EhuA		2.37E-18		-
vnz33340	*sco7545*	ABC transporter ATP-binding protein		3.78E-18		-
vnz05040	*sco1442*	**Hypothetical protein**		1.06E-16		-
vnz18620	*sco4035*	**SigF**		2.03E-16		-
vnz18225	*sco3941*	Protein phosphatase SppA		7.42E-14		Y
vnz33625, vnz33630	*sco0942, sco0941*	**RNA polymerase subunit sigma, Hypothetical protein**		1.03E-13		Y
vnz32940	-	**Hypothetical protein**		1.62E-12		-
vnz23160	*sco5015*	Hypothetical protein		1.12E-10		-
vnz19010	-	Hypothetical protein		1.50E-10		-
vnz00025	-	AAA family ATPase		9.50E-10		-

Flanking Gene(s)	SCO Homologue(s)	Product(s)	Adjusted P Value			Bound by PhoP?
			10 hours	16 hours	22 hours	
vnz36265, *vnz36270*	-	**SAM-dependent methyltransferase**, Hypothetical protein		2.74E-09		-
vnz21540	-	Hypothetical protein		8.51E-09		-
vnz19990	*sco4295*	**Cold-shock protein**		1.22E-08		-
vnz00215	-	NADPH:quinone reductase		1.60E-06		-
vnz05125	*sco1461*	Inosine 5-monophosphate dehydrogenase		4.60E-06		-
vnz32310, vnz32315	*sco0281, sco0282*	DUF4406 domain-containing protein, DeoR family transcriptional regulator		6.16E-06		-
vnz15450	*sco4473*	**Cytochrome C biogenesis protein ResC**		3.69E-05		-
vnz27115, *vnz27120*	*sco5803, sco5804*	**Repressor LexA**, Transcriptional regulator NrdR		3.88E-05		-
vnz00075, ***vnz00080***	*- , sco7647*	Serine/threonine protein kinase, **Calcium-binding protein**		9.55E-05		-
vnz15035, ***vnz15040***	*sco3202, sco0224*	Sigma factor HrdD, **Hypothetical protein**		0.000276		-

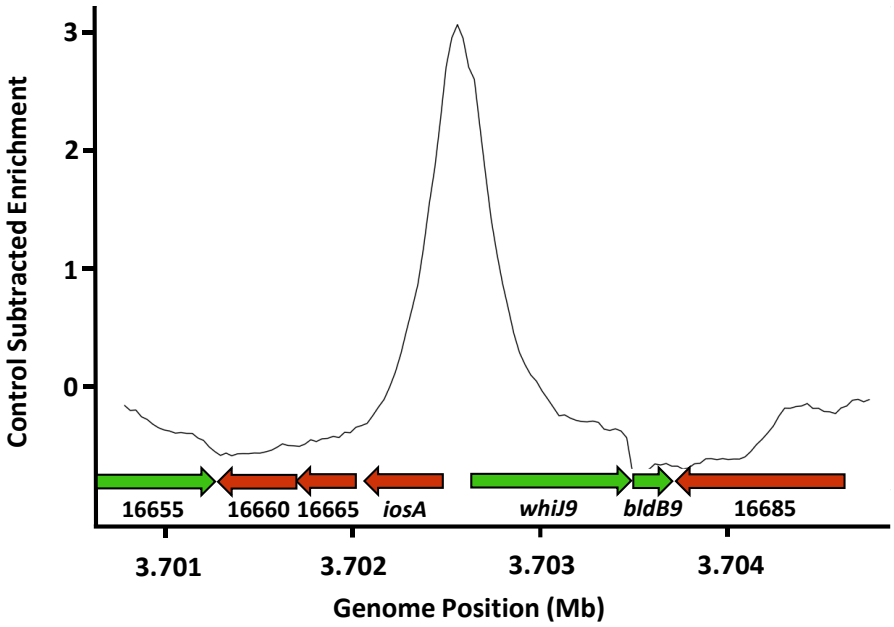

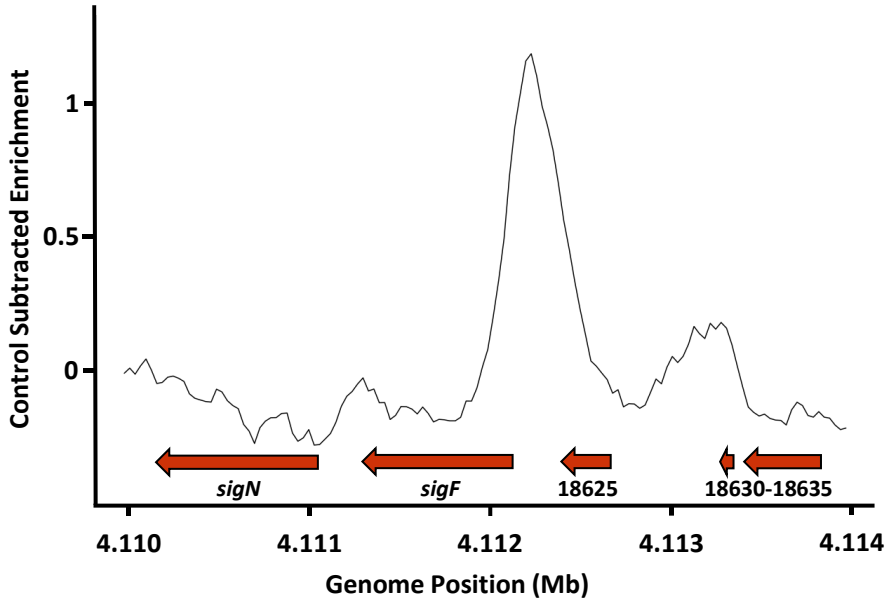

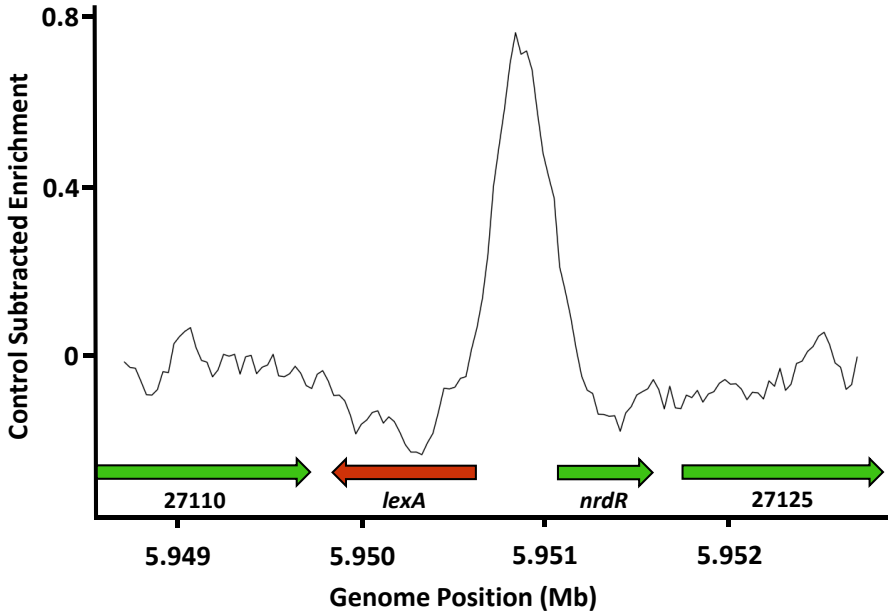

(Continued on next page)

Figure 6.10. Anti-FLAG WhiJ9 ChIP-Seq Selected Peaks.

ChIP-seq results representing levels of 3xFLAG-WhiJ9 binding to 3 promoter regions, with protein-DNA complexes captured from the 3xFLAG-WhiJ9 overexpression strain using an anti-FLAG antibody. Wild-type *S. venezuelae* was used as a negative control. The x-axes indicate the genome position in megabases, and the y-axes represent the control subtracted enrichment.

WhiJ9 Acts as an Activator for the Expression of *iosA*, and a Repressor for Its Own Expression

The most statistically significant peak of enrichment in my 3xFLAG-WhiJ9 ChIP-seq experiment was the intergenic region between *iosA* and *whiJ9* itself, raising the possibility that WhiJ9 controls the expression of one or both genes (**Fig. 6.10, Table 6.1**). Although this particular ChIP-seq result was robust on its own, I wanted to follow it up with another experiment in order to validate it. Thus, I used the SPR-derived ReDCaT method again (Stevenson *et al.*, 2013; Stevenson and Lawson, 2021), in order to see if purified 6xHis-WhiJ6 and 6xHis-WhiJ9 would bind their own promoters *in vitro*.

Under the conditions used in my ChIP-seq experiment, N-terminally 3xFLAG-tagged WhiJ6 did not bind DNA (**Fig. 6.8**). However, I decided to test if 6xHis-WhiJ6 would bind the *abaA6-whiJ6* intergenic region *in vitro*, as its homologue WhiJ9 bound its own promoter in the ChIP-seq experiments (**Fig. 6.10, Table 6.1**). I split the *abaA6-whiJ6* intergenic region into 4 overlapping oligos and captured them on an SPR chip to test binding of 6xHis-WhiJ6 at 3 different concentrations. Consistent with what I observed in the ChIP-seq results, there was no binding of 6xHis-WhiJ6 to any of the 4 oligos *in vitro*.

To do the same experiment with WhiJ9, I split the *iosA-whiJ9* intergenic region into 6 overlapping oligos, as indicated in **Fig. 6.11**. I had to do some troubleshooting to find the optimal conditions for this ReDCaT experiment, as WhiJ9 was a sticky protein and would bind non-specifically to the SPR chip. Increasing the NaCl concentration of the running buffer reduced this non-specific binding significantly. I found that WhiJ9 specifically bound to oligos O1 and O2 in the promoter region (**Fig. 6.11, 6.12**), with more protein binding to O2 (**Fig. 6.12**). The apex of the ChIP-seq enrichment peak mapped exactly to O1 and O2 (**Fig. 6.11**).

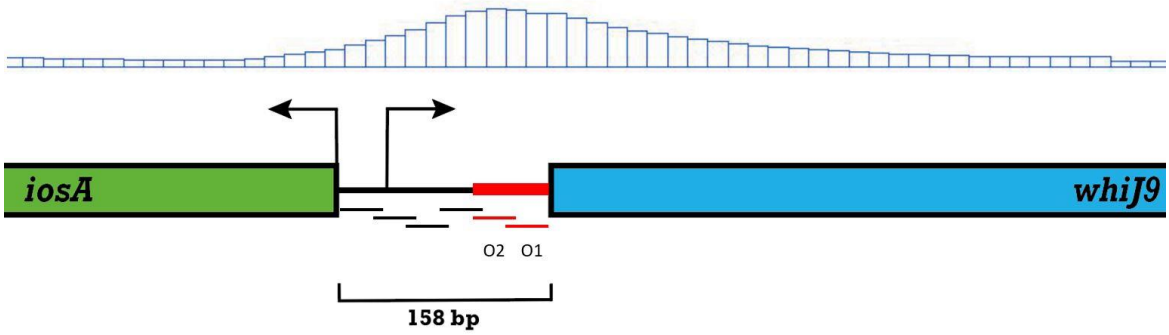

Figure 6.11. The WhiJ9 Binding Site on the *iosA-whiJ9* Intergenic Region.

Representation of the *iosA-whiJ9* intergenic region drawn to scale. ChIP-seq enrichment peak is represented in blue on top. The arrows represent the transcriptional start sites for *iosA* and *whiJ9*. The 6 overlapping oligos used in the ReDCaT experiment are represented as lines under the intergenic region in black for O3-O6 (indicating no WhiJ9 binding) and red for O1 and O2 (indicating specific WhiJ9 binding, as assayed by SPR).

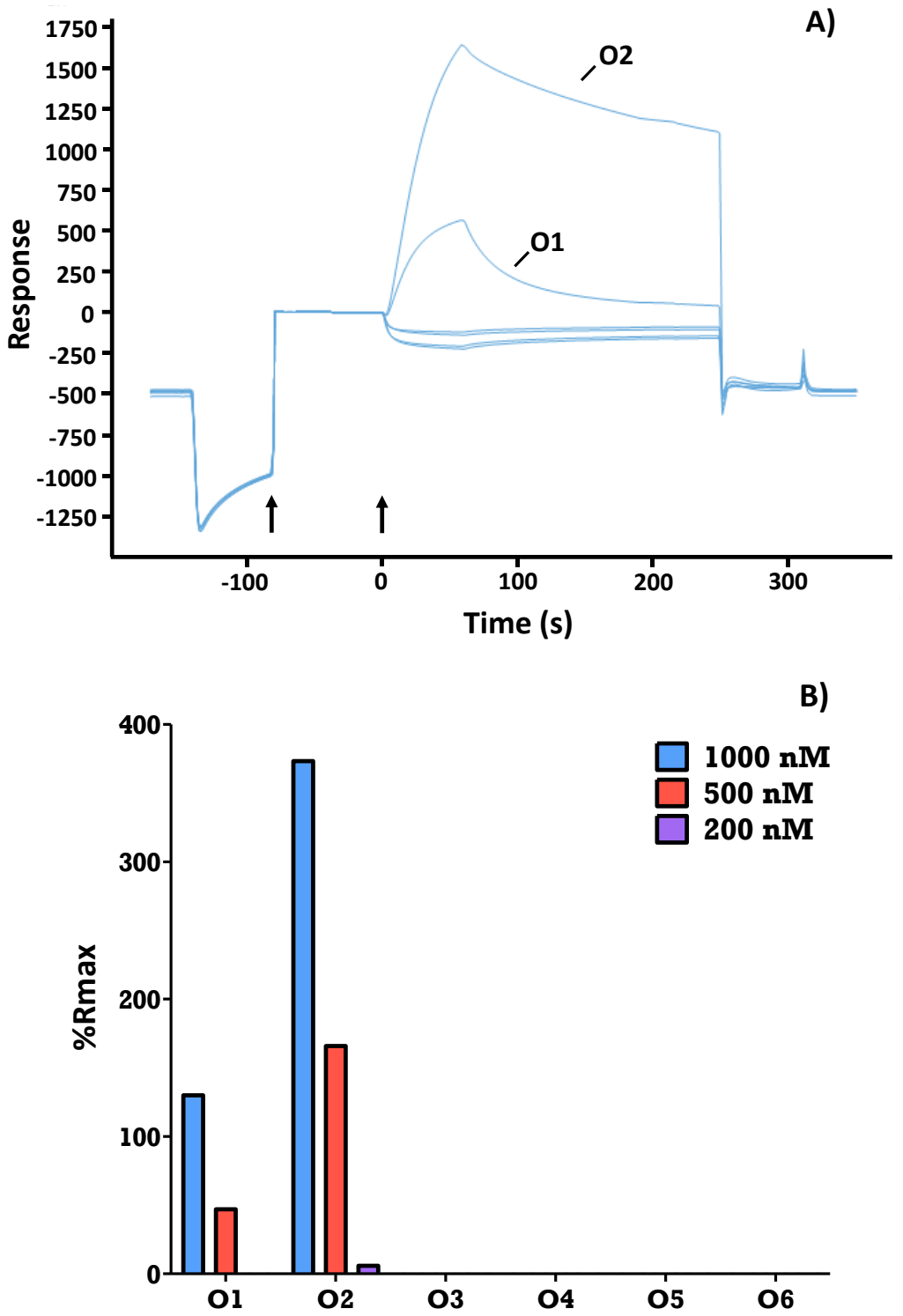

Figure 6.12. Binding of 6xHis-WhiJ9 to 6 Overlapping Oligos from Its Promoter.

Surface Plasmon Resonance (SPR) was used to measure the level of binding of 6xHis-WhiJ9 to 40 bp overlapping dsDNA oligos (O1-O6) from its promoter region. (**A**) SPR sensorgram measuring binding response (y-axis) over time (x-axis). Arrows indicate the subsequent injections of DNA and 6xHis-WhiJ9. (**B**) Bar chart showing the level of 6xHis-WhiJ9 binding to DNA, expressed as a percentage of the theoretical maximum response Rmax, assuming that one monomer of WhiJ9 bound to one dsDNA molecule. Bars represent a single replicate.

The fact that the WhiJ9 binding site lies downstream of the *whiJ9* transcription start site suggests that WhiJ9 binding would block RNA polymerase from transcribing *whiJ9*, such that WhiJ9 would repress its own expression. Additionally, WhiJ9 might activate expression of *iosA*. To test this, I decided to perform an RNA-seq experiment on a *ΔwhiJ9 ΔbldB* double mutant strain. If the striking upregulation of *iosA* in the *ΔbldB* mutant was attenuated by the additional deletion of *whiJ9*, it would strongly suggest that WhiJ9 directly activates *iosA* expression.

I decided to first delete *whiJ9* via CRISPR to obtain a markerless mutant, and then do SV1-mediated phage transduction to delete *bldB*, making use of the original *ΔbldB* mutant. I recreated exactly what I did when I first deleted *whiJ9* via Redirect, removing only the N-terminal 159 amino acids (thus removing the DNA-binding domain), in order not to disturb the promoter of the downstream *bldB9* gene, which is internal to the *whiJ9* coding sequence. Once I obtained the *ΔwhiJ9* CRISPR mutant, I replaced *bldB* in its native locus with the apramycin resistance cassette from the original *ΔbldB* mutant via SV1-mediated phage transduction. I confirmed that no unintended mutations had occurred during the construction of the *ΔwhiJ9 ΔbldB* double mutant via whole genome resequencing.

While the *ΔwhiJ9* single mutant had no developmental phenotype, the *ΔwhiJ9 ΔbldB* double mutant exhibited a bald phenotype on MYM agar and looked exactly like the *ΔbldB* single mutant (**Fig. 6.13**). Scanning electron microscopy showed that the *ΔwhiJ9 ΔbldB* double mutant looked indistinguishable from the *ΔbldB* single mutant, with both strains exhibiting vegetative mycelial growth in the centre of the colonies, and some formation of undifferentiated aerial hyphae in the outer edges of the colonies (**Fig. 6.14**). The phenotype of the double mutant was successfully complemented by introducing *bldB in trans* (**Fig. 6.13**, **6.14**).

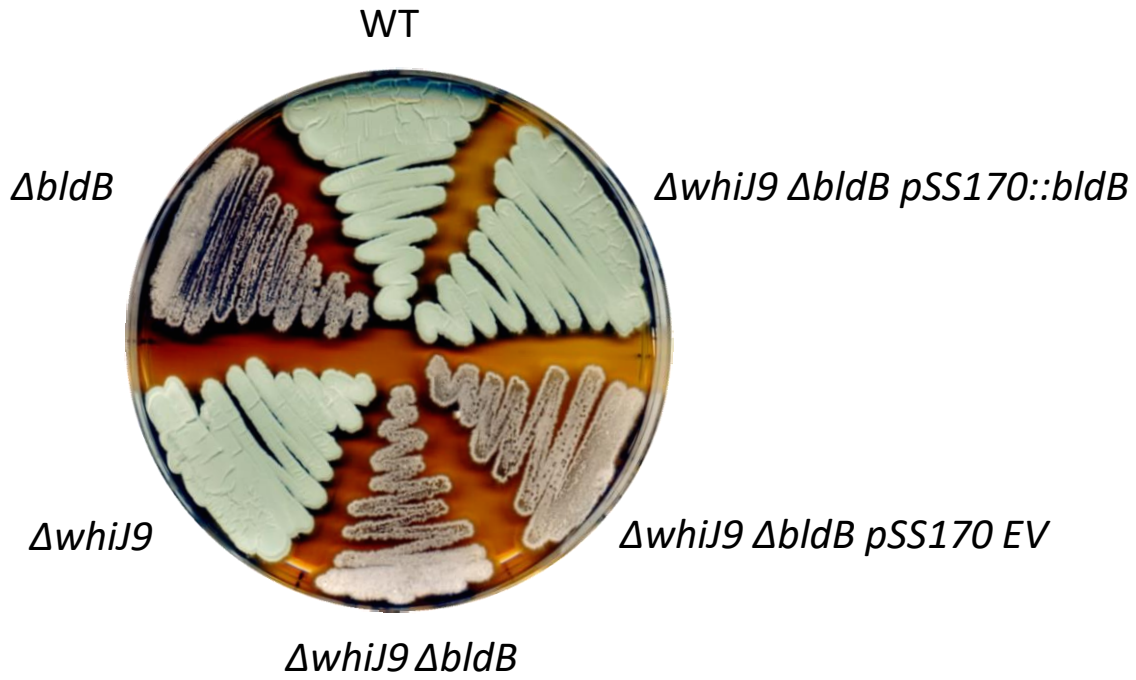

Figure 6.13. Mutant Phenotype of the *ΔwhiJ9 ΔbldB* Double Mutant Strain.

Plate depicting the growth of the *ΔwhiJ9 ΔbldB* double mutant on MYM agar. EV stands for empty pSS170 vector control. Plate image was taken after a 4-day incubation at 28˚C.

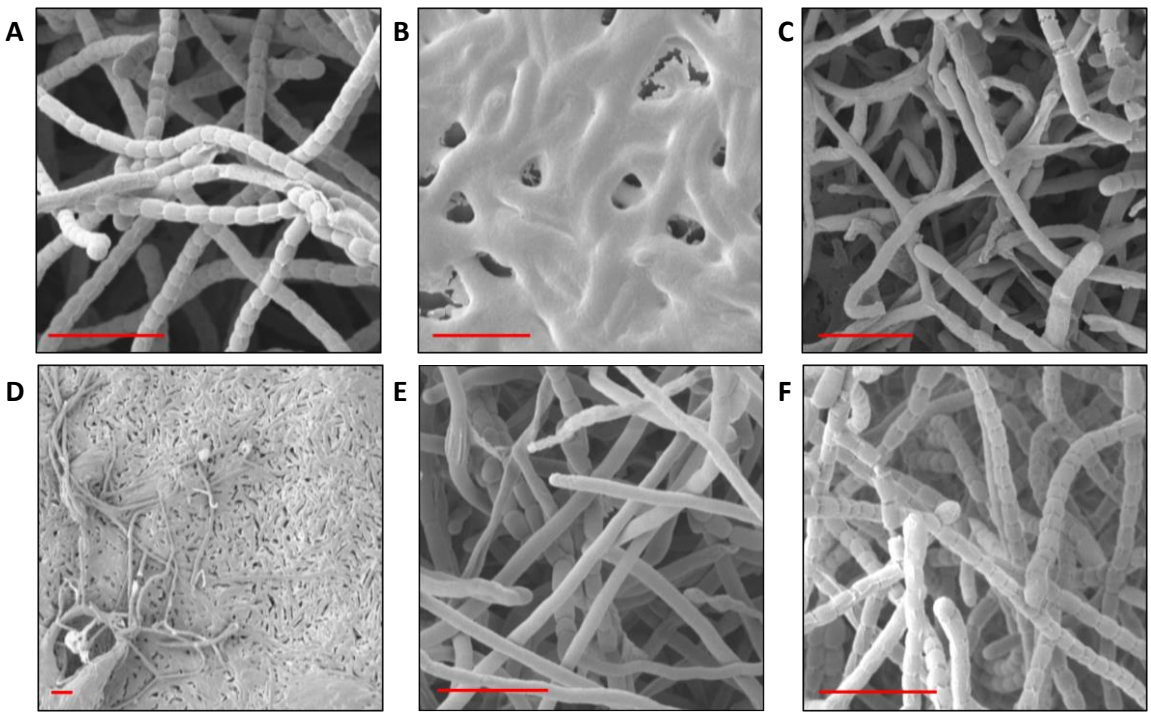

Figure 6.14. Phenotypic Characterisation of the *ΔwhiJ9 ΔbldB* Double Mutant.

Scanning electron micrographs comparing the phenotypes of wild-type *S. venezuelae* **(A)**, the colony centre of the Δ*bldB* mutant **(B)**, the colony periphery of the Δ*bldB* mutant **(C),** the colony centre of the Δ*whiJ9* Δ*bldB* mutant **(D)**, the colony periphery of the Δ*whiJ9* Δ*bldB* mutant **(E)**, and the Δ*whiJ9* Δ*bldB* pSS170::*bldB* complementation strain **(F).** Scale bars in red indicate 5 µm.

Page intentionally left blank

For my RNA-seq experiment, I used 4 strains - wild-type *S. venezuelae*, the *ΔbldB* single mutant, the *ΔwhiJ9* single mutant and the *ΔwhiJ9 ΔbldB* double mutant. Even though I had already done RNA-seq on the *ΔbldB* mutant (**Fig. 4.6, Table 4.1**), I decided to repeat it, so that I could directly compare the new *ΔbldB* dataset to the one from the *ΔwhiJ9 ΔbldB* double mutant. I also wished to fully characterise the regulon of WhiJ9, so I did RNA-seq on the *ΔwhiJ9* single mutant generated via CRISPR. For this RNA-seq experiment I used 2 time points only, 10- and 14-hours post-inoculation, as these were the early and mid- time points, I used for the initial *ΔbldB* mutant RNA-seq experiment.

In this extended experiment, I once again observed the impressive upregulation of the *abaA* homologues and *iosA* in the *ΔbldB* mutant (**Fig. 6.15**). In the *ΔwhiJ9 ΔbldB* double mutant, the expression of all *abaA* homologues was as strikingly elevated as it was in the *ΔbldB* single mutant at 14 hours. However, the expression of *iosA* had significantly decreased in the *ΔwhiJ9 ΔbldB* double mutant - down to a fold change of 1.65 at 14 hours (compared to a fold change of >790 in the *ΔbldB* mutant) (**Fig. 6.15**), proving that WhiJ9 serves as an activator for *iosA* expression in the *ΔbldB* single mutant, thus providing a link between the functions of WhiJ9 and BldB.

Focusing on the dataset from the *ΔwhiJ9* single mutant in comparison to wild type, I represented the differential expression patterns of selected genes of interest in **Table 6.2**.

In the simplest case scenario, one would expect a downregulation or no change of *iosA* expression if its proposed transcriptional activator is missing. Curiously, *iosA* was slightly upregulated in the *ΔwhiJ9* mutant at 10 hours (fold change of 4.79), though not as highly as in the *ΔbldB* mutant (fold change of ~750). At 14 hours, the expression of *iosA* in the *ΔwhiJ9* mutant was not significantly different from wild-type levels. The implications of these results will be discussed at length later in this chapter and in Chapter 7.

Looking at the expression of the *abaA* homologues in the *ΔwhiJ9* mutant, only *abaA4* was slightly upregulated at 10 hours (**Table 6.2**). Out of the *bldB* homologues, only *bldB2* and *bldB5* exhibited a change in expression levels - they were upregulated at 10 hours.

Focusing next on the *whiJ* homologues, the expression of *whiJ5*, *whiJ6* and *whiJ9* itself was elevated at 10 hours. The slight upregulation of *whiJ9* in the *ΔwhiJ9* CRISPR mutant must have occurred because only the first half of the gene was deleted in making the mutant, thus the truncated WhiJ9 protein lacking its N-terminal DNA binding domain could not inhibit its own expression. I confirmed this by looking at where the RNA reads mapped on the *whiJ9* gene. No reads mapped to the first half of the gene, once more validating the deletion; all the reads mapped to the second half of the gene, which was left intact. This validated the hypothesis that WhiJ9 represses its own expression.

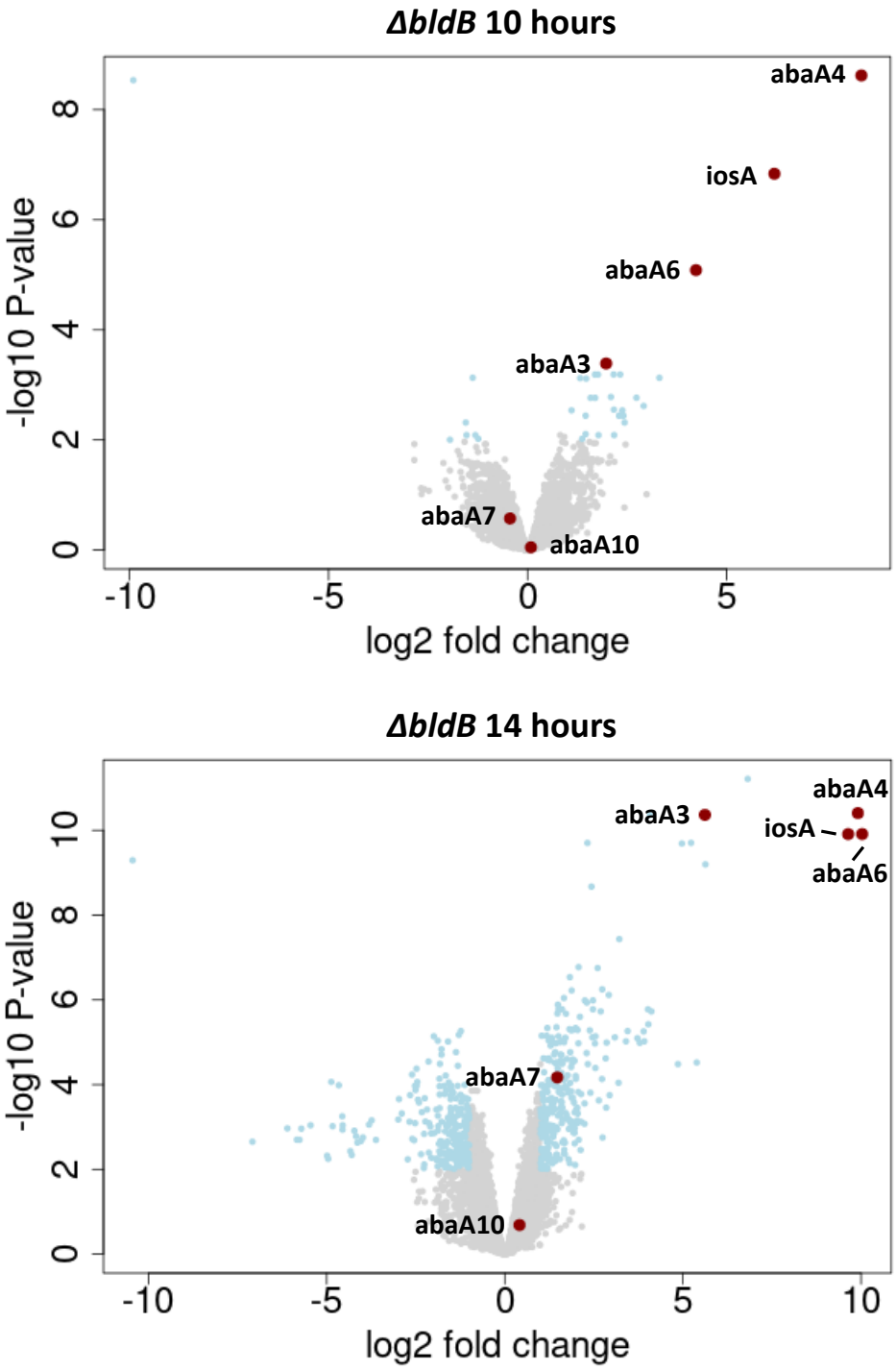

(Figure continued on next page)

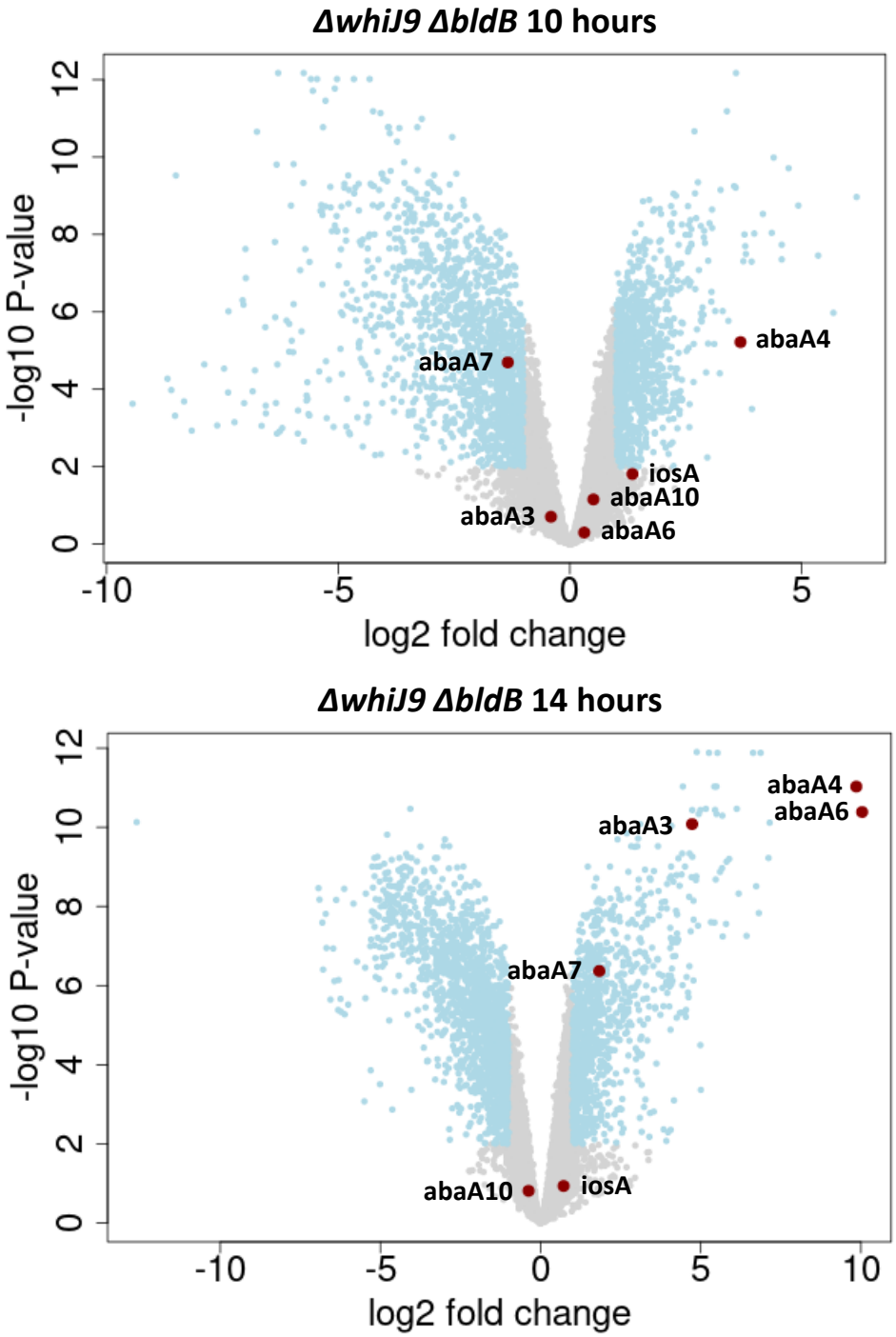

Figure 6.15. Differential Gene Expression in the *ΔbldB* Mutant and the *ΔwhiJ9 ΔbldB* Double Mutant from an RNA-seq Experiment.

Volcano plots were generated to illustrate the differential expression in the *ΔbldB* mutant and the *ΔwhiJ9 ΔbldB* double mutant compared to wild type *S. venezuelae* as assayed by RNA-seq using three biological replicates per time point. The x-axes represent the $\log_2$ fold change of gene expression in the mutants, compared to wild type. The y-axes represent the $-\log_{10}$ P-value. Represented by blue dots are all significantly down- or up-regulated genes with a $\log_2$ fold change less than -1 or above 1 respectively, and P-value ≤ 0.01. The *abaA* homologues and *iosA* are highlighted in red.

It is interesting that while the expression of *whiJ9* in the *ΔwhiJ9* mutant was elevated, the expression of the downstream *bldB9* was unchanged (**Table 6.2**). This confirmed that even though *bldB9* is encoded downstream of *whiJ9*, the two genes are not co-transcribed as an operon, which is consistent with *bldB9* having its own transcriptional start site within the *whiJ9* gene (**Fig. 6.11**).

There was no change in expression levels in the *ΔwhiJ9* mutant for the genes encoding the SigB-like network involving AbaA6, namely *asfA1*, *asfA2*, *osaC* and *osaC2* (**Table 6.2**). Out of the *sigB* homologues in *S. venezuelae*, only the expression of *sigF* was downregulated at 14 hours. SigF was found among the targets of WhiJ9 as shown by ChIP-seq (**Fig. 6.10, Table 6.1**), so this downregulation of *sigF* expression was likely directly caused by WhiJ9. Looking at the Type VII secretion components, only the expression of *eccD* was upregulated at 14 hours (**Table 6.2**).

Out of the other *bld* regulators, there was an upregulation of *bldC*, *bldM* and *bldN* at 10 hours, and *bldH* at 14 hours. Out of the other *whi* regulators, *whiH* and *whiI* were upregulated at 10 hours, though *whiI* expression was significantly reduced at 14 hours. The expression of *whiD* and *whiE orfVIII* was modestly downregulated at 14 hours. All of the chaplins and rodlins, as well as *geoA*, were highly upregulated at 10 hours, but their expression was reduced at 14 hours. Out of the *ram* genes, only *ramC* was slightly upregulated at 10 hours.

Interestingly, the expression of the whole *rarA-E* operon (*cvn9* conservon) was very highly upregulated in the *ΔwhiJ9* mutant at 10 hours (**Table 6.2**). WhiJ9 did not bind directly to the promoter of this conservon, so this upregulation is indirect. WhiJ9 did bind upstream of the *cvn6* conservon (**Table 6.1**). Indeed, the expression of all *cvn6* conservon genes was downregulated at 10 hours and upregulated at 14 hours (**Table 6.2**).

Out of the rest of the WhiJ9 targets identified via ChIP-seq (**Table 6.1**), only the ones with a significant change in expression at 10 or 14 hours are included in **Table 6.2**; they were also highlighted in bold in **Table 6.1**.

All genes in the operon *vnz25450* - *vnz25465*, which were previously found to be upregulated in explorer cells (Jones *et al.*, 2017, 2019) were downregulated in the *ΔwhiJ9* mutant at 14 hours (**Table 6.2**). WhiJ9 binds in the *vnz02250* - *sigB3* intergenic region, and the expression of *vnz02250* encoding the HATPase_c domain-containing predicted anti-sigma factor was significantly downregulated at 14 hours, whereas *sigB3* expression was unchanged. Another direct WhiJ9 target - *vnz33625*, encoding an uncharacterised non-SigB-like sigma factor was downregulated at 14 hours. Finally, WhiJ9 binds in the *lexA-nrdR* intergenic region (**Fig. 6.10**), and only the expression of *lexA* was significantly changed in the *ΔwhiJ9* mutant - it was upregulated at 10 hours post-inoculation (**Table 6.2**).

Table 6.2. WhiJ9 RNA-seq Results.

S. venezuelae **Gene**	***S. coelicolor*** **Homologue**	**Product**	**LFC 10 Hours**	**FDR 10 Hours**	**LFC 14 Hours**	**FDR 14 Hours**
vnz29085	*sco6237*	AbaA3	n.s	n.s	n.s	n.s
vnz25565	*sco6130*	AbaA4	1.7	0.034	n.s	n.s
vnz09905	*scp1.59, scp1.294*	AbaA6	n.s	n.s	n.s	n.s
vnz16135	*sco3423*	AbaA7	n.s	n.s	n.s	n.s
vnz31495	*sco1980*	AbaA10	n.s	n.s	n.s	n.s
vnz16670	-	IosA	2.26	6.41E-04	n.s	n.s
vnz26620	-	BldB	n.s	n.s	n.s	n.s
vnz15145	*sco4442*	BldB2	1.56	2.56E-04	n.s	n.s
vnz29075	*sco6235*	BldB3	n.s	n.s	n.s	n.s
vnz25555	*sco6128*	BldB4	n.s	n.s	n.s	n.s
vnz20565	-	BldB5	1.15	0.002	n.s	n.s
vnz09895	-	BldB6	n.s	n.s	n.s	n.s
vnz16140	*sco3424*	BldB7	n.s	n.s	n.s	n.s

***S. venezuelae* Gene**	***S. coelicolor* Homologue**	**Product**	**LFC 10 Hours**	**FDR 10 Hours**	**LFC 14 Hours**	**FDR 14 Hours**
vnz28285	-	BldB8	n.s	n.s	n.s	n.s
vnz16680	-	BldB9	n.s	n.s	n.s	n.s
vnz31505	*sco1978*	BldB10	n.s	n.s	n.s	n.s
vnz28375	*sco2382*	BldB11	n.s	n.s	n.s	n.s
vnz15140	*sco4441*	WhiJ2	n.s	n.s	n.s	n.s
vnz29080	*sco6236*	WhiJ3	n.s	n.s	n.s	n.s
vnz25560	*sco6129*	WhiJ4	n.s	n.s	n.s	n.s
vnz20560	*sco3365*	WhiJ5	2.15	1.52E-05	n.s	n.s
vnz09900	-	WhiJ6	1.66	7.60E-04	n.s	n.s
vnz16130	*sco3421*	WhiJ7	n.s	n.s	n.s	n.s
vnz28280	*sco2865*	WhiJ8	n.s	n.s	n.s	n.s
vnz16675	-	WhiJ9	1.05	0.04	n.s	n.s
vnz31500	*sco1979*	WhiJ10	n.s	n.s	n.s	n.s
vnz28370	-	WhiJ11	n.s	n.s	n.s	n.s
vnz03680	-	AsfA1	n.s	n.s	n.s	n.s

***S. venezuelae* Gene**	***S. coelicolor* Homologue**	**Product**	**LFC 10 Hours**	**FDR 10 Hours**	**LFC 14 Hours**	**FDR 14 Hours**
vnz10850	*sco7754*	AsfA2	n.s	n.s	n.s	n.s
vnz17535	*sco3796*	OsaC2	n.s	n.s	n.s	n.s
vnz26710	*sco5748*	OsaA	n.s	n.s	n.s	n.s
vnz26715	*sco5749*	OsaB	n.s	n.s	n.s	n.s
vnz26705	*sco5747*	OsaC	n.s	n.s	n.s	n.s
vnz01755	*sco7327*	OsaD	n.s	n.s	n.s	n.s
vnz01715	*sco0600*	SigB	n.s	n.s	n.s	n.s
vnz01090	-	SigB2	n.s	n.s	n.s	n.s
vnz02255	-	SigB3	n.s	n.s	n.s	n.s
vnz13800	*sco3068*	SigI	n.s	n.s	n.s	n.s
vnz18615	*sco4034*	SigN	n.s	n.s	n.s	n.s
vnz18620	*sco4035*	SigF	n.s	n.s	-1.37	0.001
vnz24270	*sco5243*	SigH	n.s	n.s	n.s	n.s
vnz05860	*sco1607*	T7SS-associated serine protease mycosin	n.s	n.s	n.s	n.s
vnz13260	*sco5731*	T7SS-associated serine protease mycosin	n.s	n.s	n.s	n.s

***S. venezuelae* Gene**	***S. coelicolor* Homologue**	**Product**	**LFC 10 Hours**	**FDR 10 Hours**	**LFC 14 Hours**	**FDR 14 Hours**
vnz26595	*sco5720*	T7SS secretion protein EccE	n.s	n.s	n.s	n.s
vnz26600	*sco5721*	T7SS secretion protein EccB	n.s	n.s	n.s	n.s
vnz26605	*sco5722*	T7SS-associated serine protease mycosin	n.s	n.s	n.s	n.s
vnz26610	*sco5724*	T7SS-associated protein EsxB	n.s	n.s	n.s	n.s
vnz26615	*sco5725*	T7SS-associated protein EsxA	n.s	n.s	n.s	n.s
vnz26625	*sco5734*	T7SS secretion protein EccC	n.s	n.s	n.s	n.s
vnz26630	*sco5735*	T7SS integral membrane protein EccD	n.s	n.s	1.08	1.58E-04
vnz18945	*sco4091*	BldC	1.32	3.42E-05	n.s	n.s
vnz05285	*sco1489*	BldD	n.s	n.s	n.s	n.s
vnz16350	*sco3549*	BldG	n.s	n.s	n.s	n.s
vnz12630	*sco2792*	BldH	n.s	n.s	1.06	1.01E-04
vnz22005	*sco4768*	BldM	2.1	6.45E-06	n.s	n.s
vnz15655	*sco3323*	BldN	2.78	2.22E-04	n.s	n.s
vnz04660	*sco1381*	BldO	n.s	n.s	n.s	n.s
vnz07750	*sco1950*	WhiA	n.s	n.s	n.s	n.s

***S. venezuelae* Gene**	***S. coelicolor* Homologue**	**Product**	**LFC 10 Hours**	**FDR 10 Hours**	**LFC 14 Hours**	**FDR 14 Hours**
vnz13645	*sco3034*	WhiB	n.s	n.s	n.s	n.s
vnz22000	*sco4767*	WhiD	n.s	n.s	-1.08	0.009
vnz33520	*sco5320*	WhiE ORFI	n.s	n.s	n.s	n.s
vnz33515	*sco5319*	WhiE ORFII	n.s	n.s	n.s	n.s
vnz33510	*sco5318*	WhiE ORFIII	n.s	n.s	n.s	n.s
vnz33505	*sco5317*	WhiE ORFIV	n.s	n.s	n.s	n.s
vnz33500	*sco5316*	WhiE ORFV	n.s	n.s	n.s	n.s
vnz33495	*sco5315*	WhiE ORFVI	n.s	n.s	n.s	n.s
vnz33490	*sco5314*	WhiE ORFVII	n.s	n.s	n.s	n.s
vnz33525	*sco5321*	WhiE ORFVIII	n.s	n.s	-1.29	0.005
vnz26215	*sco5621*	WhiG	n.s	n.s	n.s	n.s
vnz27205	*sco5819*	WhiH	2.1	4.15E-05	n.s	n.s
vnz28820	*sco6029*	WhiI	1.84	1.14E-04	-1.98	1.03E-04
vnz15660	*sco3324*	RsbN	2.67	1.45E-05	n.s	n.s
vnz19430	*sco4184*	RsiG	n.s	n.s	n.s	n.s

***S. venezuelae* Gene**	***S. coelicolor* Homologue**	**Product**	**LFC 10 Hours**	**FDR 10 Hours**	**LFC 14 Hours**	**FDR 14 Hours**
vnz06205	*sco1674*	ChpC	4.05	4.26E-08	n.s	n.s
vnz22895	*sco2717*	ChpD	3.42	5.97E-06	-1.78	0.002
vnz07055	*sco1800*	ChpE	5.37	4.26E-08	1.78	0.001
vnz22960	*sco2705*	ChpF	4.33	3.17E-06	-1.77	0.005
vnz22985	*sco2699*	ChpG	4.23	6.28E-07	n.s	n.s
vnz06210	*sco1675*	ChpH	4.74	5.55E-08	n.s	n.s
vnz22870	*sco2719*	RdlAB-like	3.33	2.45E-06	n.s	n.s
vnz22885	-	RdlAB-like	2.73	1.88E-05	-1.34	0.008
vnz22890	-	RdlAB-like	2.95	9.49E-06	-1.09	0.022
vnz31965	*sco6683*	RamA	n.s	n.s	n.s	n.s
vnz31960	*sco6684*	RamB	n.s	n.s	n.s	n.s
vnz31975	*sco6681*	RamC	1.01	0.003	n.s	n.s
vnz31955	*sco6685*	RamR	n.s	n.s	n.s	n.s
vnz31970	*sco6682*	RamS	n.s	n.s	n.s	n.s
vnz08495	*sco2077*	DivIVA	n.s	n.s	n.s	n.s

***S. venezuelae* Gene**	***S. coelicolor* Homologue**	**Product**	**LFC 10 Hours**	**FDR 10 Hours**	**LFC 14 Hours**	**FDR 14 Hours**
vnz24950	*sco5396*	FilP	n.s	n.s	n.s	n.s
vnz24955	*sco5397*	Scy	n.s	n.s	n.s	n.s
vnz08520	*sco2082*	FtsZ	n.s	n.s	n.s	n.s
vnz01280	*sco6073*	GeoA	4.7	6.83E-08	n.s	n.s
vnz06980	*sco1789*	ParA	n.s	n.s	n.s	n.s
vnz18015	*sco3887*	ParB	n.s	n.s	n.s	n.s
vnz26075	*sco5577*	Smc	n.s	n.s	n.s	n.s
vnz04890	*sco1416*	SffA	n.s	n.s	n.s	n.s
vnz04885	*sco1415*	SmeA	1.13	0.019	n.s	n.s
vnz18205	*sco3926*	SsgA	1.83	1.53E-05	n.s	n.s
vnz05545	*sco1541*	SsgB	n.s	n.s	n.s	n.s
vnz31585	*sco6722*	SsgD	n.s	n.s	n.s	n.s
vnz13140	*sco2924*	SsgG	n.s	n.s	n.s	n.s
vnz00475	*sco6069*	CvnA6	-1.61	1.75E-05	n.s	n.s
vnz00470	*sco6068*	CvnB6	-1.78	2.28E-04	1.03	0.045

***S. venezuelae* Gene**	***S. coelicolor* Homologue**	**Product**	**LFC 10 Hours**	**FDR 10 Hours**	**LFC 14 Hours**	**FDR 14 Hours**
vnz00465	*sco6067*	CvnC6	-1.82	7.94E-05	1.35	0.013
vnz00460	*sco6066*	CvnD6	-1.93	5.50E-05	1.09	0.036
vnz02660	*sco1630*	RarA	4.89	4.29E-05	1.27	n.s
vnz02655	*sco1629*	RarB	4.93	1.05E-05	1.33	n.s
vnz02650	*sco1628*	RarC	5.03	2.53E-05	1.24	n.s
vnz02645	*sco1627*	RarD	5.09	2.91E-05	1.15	n.s
vnz02640	*sco1626*	RarE	4.65	8.86E-06	1.22	n.s
vnz07825	*sco1963*	Tellurium resistance protein TerC	-1.004	0.0247	n.s	n.s
vnz28245	-	Hypothetical protein	2.6	1.44E-04	n.s	n.s
vnz16980	*sco7630*	Phosphoglycerate mutase	3.49	2.21E-07	-1.05	0.008
vnz25450	*sco5476*	Peptide ABC transporter permease	n.s	n.s	-2.26	0.002
vnz07930	-	Hypothetical protein	3.58	1.72E-07	n.s	n.s
vnz28940	*sco4261*	Helix-turn-helix transcriptional regulator	n.s	n.s	1.54	6.29E-04
vnz28945	*sco4257*	Hydrolytic protein	n.s	n.s	1.53	5.05E-04
vnz35960	*sco2347*	Hypothetical protein	n.s	n.s	1.16	1.01E-04

***S. venezuelae* Gene**	***S. coelicolor* Homologue**	**Product**	**LFC 10 Hours**	**FDR 10 Hours**	**LFC 14 Hours**	**FDR 14 Hours**
vnz02250	-	HATPase_c domain protein	n.s	n.s	-1.17	2.24E-04
vnz02190	-	RNA helicase	n.s	n.s	1.38	0.003
vnz15370	*sco4493*	AsnC family transcriptional regulator	-1.62	2.39E-06	n.s	n.s
vnz05040	*sco1442*	Hypothetical protein	-5.60	3.06E-08	n.s	n.s
vnz18620	*sco4035*	SigF	n.s	n.s	-1.37	0.001
vnz33625	*sco0942*	RNA polymerase subunit sigma	n.s	n.s	-1.85	0.003
vnz33630	*sco0941*	Hypothetical protein	n.s	n.s	-1.6	6.20E-06
vnz32940	-	Hypothetical protein	1.86	8.60E-05	n.s	n.s
vnz36265	-	SAM-dependent methyltransferase	1.1	2.34E-04	n.s	n.s
vnz19990	*sco4295*	Cold-shock protein	-1.24	0.007	n.s	n.s
vnz15450	*sco4473*	Cytochrome C biogenesis protein ResC	n.s	n.s	1.1	0.002
vnz27115	*sco5803*	Repressor LexA	1.97	7.09E-06	n.s	n.s
vnz00080	*sco7647*	Calcium-binding protein	3.21	4.30E-06	-1.08	0.028
vnz15040	*sco0224*	Hypothetical protein	n.s	n.s	-1.93	5.83E-04
vnz19575	*sco4228*	PhoU	-4.97	1.53E-06	n.s	n.s

S. venezuelae **Gene**	***S. coelicolor*** **Homologue**	**Product**	**LFC 10 Hours**	**FDR 10 Hours**	**LFC 14 Hours**	**FDR 14 Hours**
vnz19580	*sco4229*	PhoR	-3.9	4.08E-06	n.s	n.s
vnz19585	*sco4230*	PhoP	-4.14	4.31E-06	n.s	n.s
vnz19255	*sco4140*	PstA	-6.45	4.71E-06	n.s	n.s
vnz19250	*sco4139*	PstB	-6.3	5.10E-06	n.s	n.s
vnz19265	*sco4142*	PstS	-6.29	1.20E-05	n.s	n.s
vnz19260	*sco4141*	PstC	-6.26	4.72E-06	n.s	n.s

WhiJ9 Binds 3 Direct Repeats in its Intergenic Region

After establishing the overall regulon of WhiJ9 (**Fig. 6.9, Table 6.1, 6.2**) and revealing its role as an activator of *iosA* expression (**Fig. 6.10, 6.11, 6.12, 6.15**), I wished to understand how WhiJ9 bound the *iosA-whiJ9* intergenic region in finer molecular detail. I knew approximately where WhiJ9 bound, as it bound specifically to the overlapping O1 and O2 oligos in my initial ReDCaT experiment (**Fig. 6.11, 6.12**). Since WhiJ9 was able to bind these two oligos (though more protein bound to O2), I reasoned that the precise binding site must be located at the intersection of the two oligos. Looking at the intersection region, I noticed the presence of 3 direct repeats with a consensus sequence CGxxCTCAAC. From here onwards, I will refer to these direct repeats as DR1, DR2 and DR3 (**Fig. 6.16**).

I decided to use the ReDCaT method in lieu of traditional DNase I footprinting, to find the specific DNA sequence bound by WhiJ9. Taking the relevant sequence from the *iosA-whiJ9* intergenic region, I truncated 2 base pairs at a time from either the left- or right-hand side. I captured the resulting oligos on an SPR chip and measured the levels of WhiJ9 binding to each sequence. A subset of the full dataset is shown in **Fig. 6.16**.

WhiJ9 bound abundantly to the LH1 and RH1 sequences, which contained all 3 direct repeats (**Fig. 6.16**). Truncations from the left-hand side of the DNA sequence (LH2-10) caused WhiJ9 to bind less, resulting in a lower %Rmax (**Fig. 6.16**). However, binding of WhiJ9 was never abolished. WhiJ9 still bound specifically to oligo LH10, the shortest oligo from this dataset, and no further truncations were made from the left-hand side. LH10 contained the full DR3 direct repeat and the last 3 base pairs from the DR2 repeat.

In contrast, when I truncated the first 2 base pairs from the right-hand side of the sequence (resulting in oligo RH2), I observed a drastic drop in binding (**Fig. 6.16**). The deleted 2 base pairs included the final cytosine of the DR3 repeat, meaning that this base pair is very important for WhiJ9 binding. Continuing to delete 2 base pairs at a time from the DR3 repeat resulted in low binding of WhiJ9 (except for RH6, where it was elevated in comparison). WhiJ9 failed to bind oligo RH7, which lacks the final cytosine of the DR2 repeat, and it also failed to bind oligos that were further truncated from the right-hand side (**Fig. 6.16**).

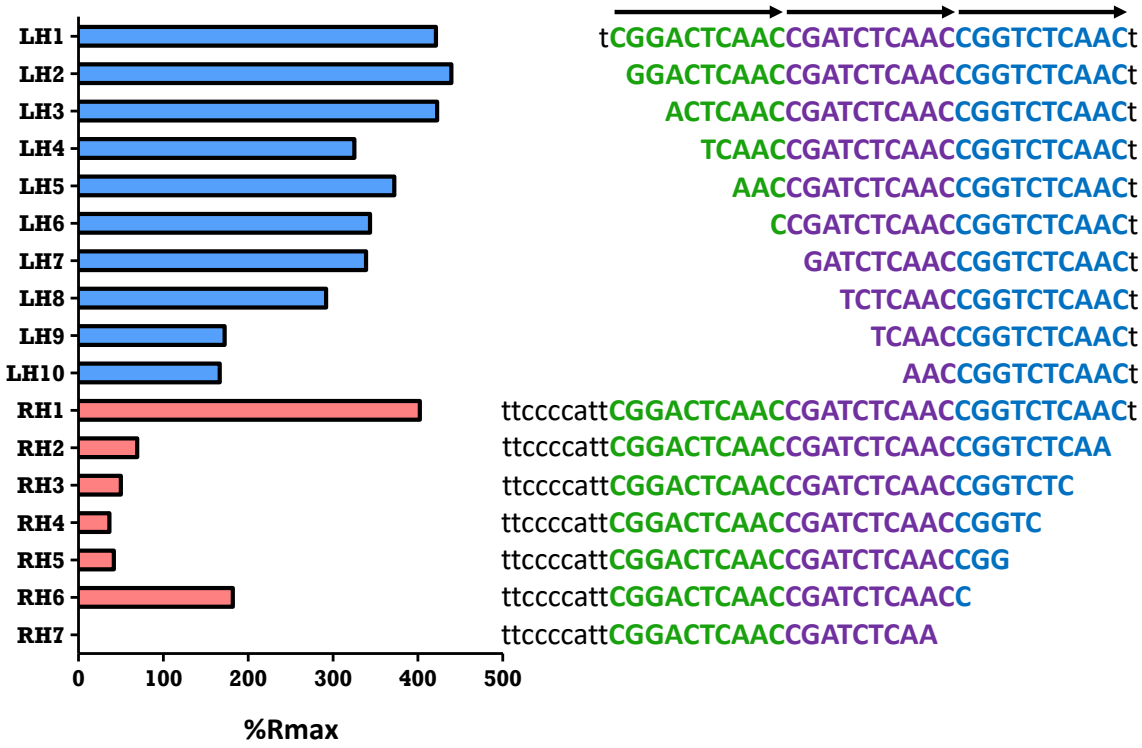

Figure 6.16. 6xHis-WhiJ9 'Footprinting' Using Surface Plasmon Resonance.

Surface Plasmon Resonance (SPR) was used to measure the level of binding of 6xHis-WhiJ9 to dsDNA oligos of varying lengths from its promoter region. Bar chart shows the level of 6xHis-WhiJ9 binding to DNA sequences on the right, expressed as a percentage of the theoretical maximum response Rmax, assuming that one monomer of 6xHis-WhiJ9 bound to one dsDNA molecule. Bars represent the average of two replicates. The 3 direct repeats are indicated with arrows, and highlighted in green (DR1), purple (DR2) and blue (DR3).

Because WhiJ9 bound best to the oligos containing all 3 direct repeats, and the 'footprinting' experiments suggested that DR3 was the most important repeat for binding (**Fig. 6.16**), I wanted to analyse each direct repeat in isolation, and in combination with the others. In this experiment, I took the sequence of the 3 direct repeats, and systematically replaced 1 or 2 repeats at a time with a random DNA sequence to yield 7 DNA sequences of the same length, containing combinations of 1, 2 or all 3 direct repeats, as illustrated in **Fig. 6.17**. As before, I immobilised these oligos onto an SPR chip, and measured WhiJ9 binding.

As expected, the oligo bound best by WhiJ9 was the oligo containing all 3 direct repeats (**Fig. 6.17**). WhiJ9 was able to bind the oligo containing DR2 and DR3 almost as well as it bound the complete sequence, meaning that DR1 did not contribute significantly to overall binding. Interestingly, the oligo containing DR1 and DR3 (with a random DNA sequence between them to replace DR2) was also well bound by WhiJ9, meaning that the direct repeats did not need to be adjacent to achieve a good level of binding.

Out of the oligos containing one direct repeat only, there was no WhiJ9 binding when only DR1 or DR2 was present. There was a modest, but measurable amount of binding when DR3 only was present, confirming that the sequence of DR3 is the most optimal for binding (**Fig. 6.17**).

The %Rmax represented in my ReDCaT experiments (**Fig. 6.17**) is calculated based on the capture and binding level from the SPR experiments, as well as on the molecular weight of the captured dsDNA molecules and the predicted molecular weight of a 6xHis-WhiJ9 monomer (33.684 kDa). In principle, the %Rmax indicates how many protein units are bound per molecule of DNA. For the oligo with all 3 repeats, and the oligo with DR2+DR3 only, the %Rmax was ~400, suggesting that 4 monomers (or 2 dimers) bound to these oligos (**Fig. 6.17**). For the DR1+DR2, and DR1+DR3 oligos, the %Rmax was ~200, suggesting that 2 monomers or 1 dimer bound to these oligos (**Fig. 6.17**).

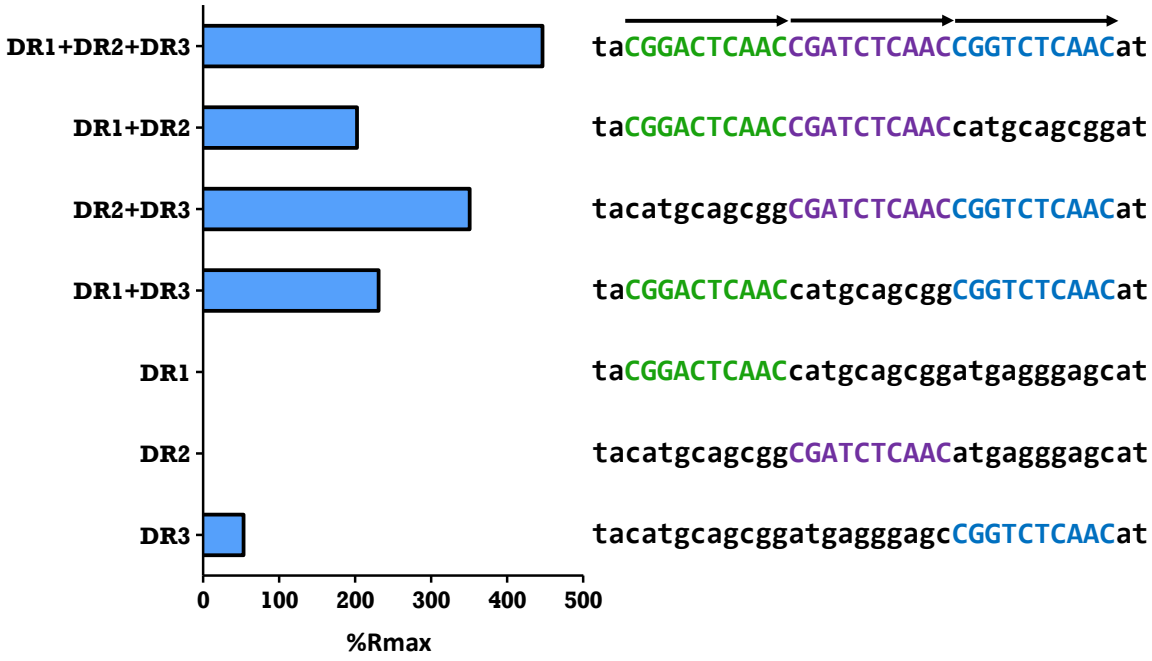

Figure 6.17. Binding of 6xHis-WhiJ9 to Direct Repeats from Its Promoter.

Surface Plasmon Resonance (SPR) was used to measure the level of binding of 6xHis-WhiJ9 to 34bp dsDNA oligos from its promoter region containing 1, 2 or all 3 direct repeats. Bar chart shows the level of 6xHis-WhiJ9 binding to DNA sequences on the right, expressed as a percentage of the theoretical maximum response Rmax, assuming that one monomer of WhiJ9 bound to one dsDNA molecule. Bars represent the average of two replicates. The 3 direct repeats are indicated with arrows, and highlighted in green (DR1), purple (DR2) and blue (DR3).

Attempts to Crystallise a WhiJ9-DNA Complex

As I was interested in finding out precisely how WhiJ9 bound to the direct repeats, I performed X-ray crystallography screens, to see if I could get a structure of WhiJ9 bound to DNA. I performed numerous explorative and focused screens, with DNA of different lengths (as informed by the results of my SPR experiments). While I obtained progressively better crystals (**Fig. 6.18**), they remained quite small and unfortunately did not diffract well.

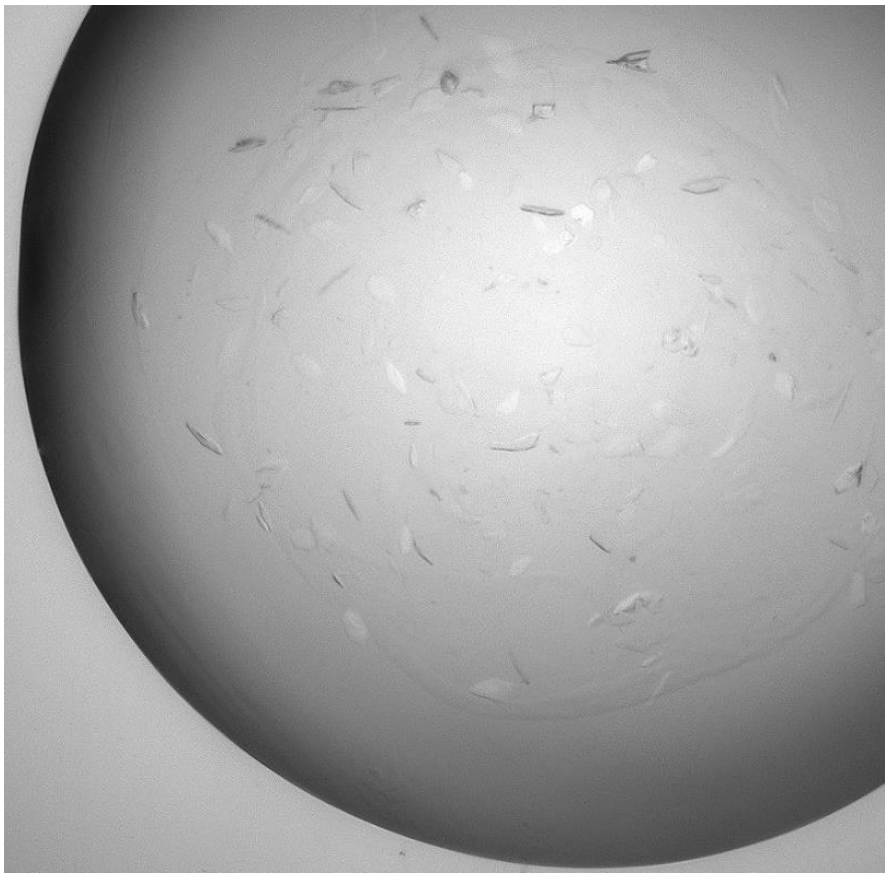

Figure 6.18. Protein-DNA Crystals of 6xHis-WhiJ9 Bound to DNA.

Light microscopy image showing protein-DNA crystals of 6xHis-WhiJ9 bound to dsDNA containing direct repeats DR2+DR3 from its promoter region. Crystals diffracted poorly to ~18Å resolution.

Discussion

In this chapter, I described my work on the genetic and biochemical characterisation of the DNA-binding developmental regulator WhiJ9.

It was clear that out of all 10 loci encoding a non-canonical *bldB* homologue, the two loci encoding *bldB6* and *bldB9* were likely to be the most important ones for this study, as they had multiple connections to the function of canonical BldB. I found that BldB6 and BldB9 directly interacted with BldB in a bacterial-two-hybrid assay (**Fig. 3.12**). When I deleted *bldB6* and *bldB9* in *S. venezuelae*, the resulting mutant strains exhibited white phenotypes (**Fig. 3.13, 3.14, 3.15, 3.16**). Their neighbouring *abaA6* and *iosA* genes showed the highest upregulation in the *ΔbldB* mutant (**Fig. 4.6, Table 4.1**), produced white phenotypes when overexpressed individually (**Fig. 4.8, 4.9**), and recapitulated the *ΔbldB* mutant phenotype when overexpressed in tandem (**Fig. 4.10, 4.11**). It was a logical next step to look into the predicted DNA-binding functions of the adjacently encoded WhiJ6 and WhiJ9 proteins to see if they directly controlled the expression of the divergently transcribed *abaA6* and *iosA* genes. To see if that was the case, I performed ChIP-seq to identify the binding sites of WhiJ6 and WhiJ9 across the *S. venezuelae* genome.

I did not observe any meaningful DNA binding for 3xFLAG-WhiJ6 (**Fig. 6.8**) - the only enrichment peaks were adjacent to genes encoding stable RNAs, which is a known ChIP-seq artefact, as discussed in Chapter 4. While this might suggest that WhiJ6 is not a DNA-binding protein, it is also possible that, for example, placing the 3xFLAG tag on the N-terminus of WhiJ6 might have interfered with the DNA-binding activity of the helix-turn-helix Xre domain on the N-terminus of the protein. I chose N-terminally tagged WhiJ6 for ChIP-seq solely because it gave a better signal in an automated Western blot. I could detect N-terminally tagged WhiJ6 at all 3 time points I tested throughout *S. venezuelae* development, whereas I could not detect C-terminally tagged WhiJ6 at the earliest 10-hour time point (**Fig. 6.6**). Neither the mutant strain nor the overexpression strain for *whiJ6* exhibited any developmental phenotypes (**Fig. 6.1, 6.2, 6.3, 6.4**), which meant that I could not test the functionality of the two 3xFLAG-WhiJ6 alleles. Also, because N-terminally tagged WhiJ9 was functional (**Fig. 6.5**), it seemed reasonable to assume that WhiJ6 would also be functional with an N-terminal 3xFLAG tag. As I later found out, however, there are some clear differences between WhiJ6 and WhiJ9 (despite them being homologues). In future work, I would redo the ChIP-seq experiment with C-terminally tagged WhiJ6 to see if DNA-binding could be detected.

For the 3xFLAG-WhiJ9 ChIP-seq experiment, I used two strains, one where C-terminally tagged WhiJ9 was expressed from its native promoter in a *ΔwhiJ9* mutant background, and in addition, one where it was overexpressed from the constitutive *ermE** promoter in wild-type *S. venezuelae* (**Fig. 6.1, 6.5**). I did this additional ChIP-seq experiment because the production of C-terminally tagged WhiJ9 from its own promoter was barely detectable in a Western blot (**Fig. 6.6, 6.7**). In contrast, the corresponding overexpression strain exhibited high production of C-terminally tagged WhiJ9 at all 3 time points (**Fig. 6.7**). Because overexpressing either N- or C-terminally tagged WhiJ9 resulted in the same white phenotype as overexpressing untagged WhiJ9 (**Fig. 6.3, 6.5**), I was confident that the 3xFLAG-WhiJ9 was fully functional and tag placement did not interfere with DNA binding.

The 3xFLAG-WhiJ9 ChIP-seq experiment revealed 46 “good-quality” enrichment peaks at intergenic regions (**Table 6.1**), which potentially correspond to WhiJ9 binding. While all peaks represent statistically significant enrichment when compared to the wild-type control, some peaks were quite low, so it is possible that not all of them represent meaningful WhiJ9 binding. Out of these 46 peaks, in 22 there was differential expression for one or both of the flanking genes in the *ΔwhiJ9* mutant as compared to the wild type, as shown by RNA-seq (**Table 6.2**). Thus, these 22 peaks must represent true WhiJ9 binding, though I do not discount the remaining ones as false.

Interestingly, I discovered a potential link between the functions of WhiJ9 and the phosphate metabolism response regulator PhoP (Allenby *et al.*, 2012). In *S. coelicolor*, PhoP binds upstream of the homologues of 13 WhiJ9 targets in *S. venezuelae*, as indicated in **Table 6.1**. A PhoP ChIP-seq experiment would need to be performed in *S. venezuelae* to test if overlap and potential competition exists between PhoP and WhiJ9 for the same binding sites in the same species. The *phoPR* operon, and the divergently transcribed *phoU* gene were highly downregulated at 10 hours in the *ΔwhiJ9* mutant (**Table 6.2**). The operon with the highest downregulation in the *ΔwhiJ9* mutant at 10 hours (~73 times lower than wild type) was the *pstABCS* operon (**Table 6.2**), encoding a phosphate uptake system used for scavenging inorganic phosphate under stress conditions. The *pstABCS* and *phoPR* operons have been shown to be under the direct control of PhoPR (Allenby *et al.*, 2004; Sola-Landa *et al.*, 2005). Interestingly, the same downregulation pattern for *phoPRU* and *pstABCS* was found in the *ΔbldB* mutant as well, though not statistically significant due to biological sample variation. However, no enrichment peaks for WhiJ9 (or BldB) were observed near these operons, so this downregulation is indirect.

Among the other interesting direct targets of WhiJ9 is the *cvn6* conservon, the expression of which was downregulated at 10 hours and upregulated at 14 hours (**Table 6.1, 6.2**). The *cvn9* conservon (*rarA-E*) also appears to be influenced by WhiJ9, although indirectly; there was no enrichment peak near the conservon, but it was significantly upregulated in the *ΔwhiJ9* mutant (**Table 6.2**). Interestingly, the *cvn9* conservon was highly downregulated in the *ΔbldB* mutant at 22 hours, though I cannot draw a parallel with the *ΔwhiJ9* mutant RNA-seq data, as I did not include a late time point for analysis. These conservons are of particular interest, as the first genes in the respective operons share the same HATPase_c domain with the AbaA homologues. Another WhiJ9 target with a predicted HATPase_c domain was *vnz02250*, which is transcribed divergently to *sigB3* (**Table 6.1**). The *vnz02250* gene, encoding a possible anti-sigma factor for SigB3, was downregulated at 14 hours in the *ΔwhiJ9* mutant, suggesting that it must be a genuine WhiJ9 target (**Table 6.2**).

Despite 3 genes encoding proteins with HATPase_c domains being targets for WhiJ9 (2 of them direct targets), there were no WhiJ9 enrichment peaks found next to the 5 *abaA* genes (**Table 6.1**), and only the expression of *abaA4* was slightly upregulated at 10 hours in the *ΔwhiJ9* mutant (**Table 6.2**). However, the most significant peak in the 3xFLAG-WhiJ9 ChIP-seq datasets was found in the *iosA-whiJ9* intergenic region (**Table 6.1**), suggesting that WhiJ9 directly controls its own expression and/or that of *iosA*.

I further validated the binding of WhiJ9 to its own promoter region by the SPR-dependent method ReDCaT (Stevenson *et al.*, 2013; Stevenson and Lawson, 2021). WhiJ9 specifically bound to 2 out of the 6 overlapping oligos from its own promoter region - O1 and O2 (**Fig. 6.12**), with the position of binding strongly suggesting that it might repress its own expression by physically obstructing RNA polymerase (**Fig. 6.11**). It was also possible that WhiJ9 might be the activator responsible for the impressive upregulation of *iosA* in the *ΔbldB* mutant. I sought to test this by RNA-seq using the *ΔwhiJ9* mutant, the *ΔbldB* mutant and the *ΔwhiJ9 ΔbldB* double mutant.

In the RNA-seq experiment on the *ΔwhiJ9* mutant there was an upregulation of the truncated *whiJ9* gene (**Table 6.2**), showing that WhiJ9 represses its own expression, consistent with the position of its binding site downstream of the *whiJ9* transcription start site. This auto-repression must in part account for the low production of 3xFLAG-WhiJ9 when expressed from its native promoter (**Fig. 6.6**). By driving the expression from the constitutive *ermE** promoter in the absence of the WhiJ9 binding site, I bypassed the self-repression of WhiJ9 and was able to detect higher levels of 3xFLAG-WhiJ9 (**Fig. 6.7**).

To test if WhiJ9 activated the expression of *iosA* in the *ΔbldB* mutant, I compared expression levels in the *ΔbldB* mutant and the *ΔwhiJ9 ΔbldB* double mutant via RNA-seq. I could once again observe an impressive upregulation of the *abaA* homologues and *iosA* in the *ΔbldB* mutant at 10 and 14 hours (**Fig. 6.15**). In comparison, the expression of *iosA* was significantly reduced in the *ΔwhiJ9 ΔbldB* double mutant (**Fig. 6.15**). This meant that the additional loss of *whiJ9* abolished the upregulation of *iosA*, showing that WhiJ9 directly activates *iosA* expression in the *ΔbldB* mutant. In a qRT-PCR experiment described in the next chapter, I demonstrate that overproduction of WhiJ9 results in even higher levels of transcription of *iosA* than deletion of *bldB* (**Fig. 7.6**), cementing the role of WhiJ9 as the activator of *iosA* expression.

Looking at the expression of the *abaA* homologues in the *ΔwhiJ9 ΔbldB* double mutant compared to the *ΔbldB* mutant from the same RNA-seq dataset, while at 10 hours the expression was a bit more variable, at 14 hours, the patterns of *abaA* homologue expression between the two strains was almost identical (**Fig. 6.15**). This meant that WhiJ9 activated the expression of *iosA* specifically and did not affect the expression of the *abaA* homologues genetically linked to the other *bldB* homologues. The one exception was *abaA4*, which was upregulated at 10 hours in the *ΔwhiJ9* mutant (**Table 6.2**). Further work could investigate whether the other WhiJ homologues control the expression of their adjacent *abaA* homologues (but note that I was unable to demonstrate binding of WhiJ6 to the *abaA6-whiJ6* intergenic region, *in vivo* or *in vitro*). The *S. coelicolor* homologue of WhiJ10 was shown to be able to bind its own promoter region and repress its own transcription much like *S. venezuelae* WhiJ9 does - though the authors of the study did not do any qRT-PCR assays to measure the expression levels of the divergently transcribed *S. coelicolor abaA10* homologue (Zhu *et al.*, 2020).

To define a minimal binding site for WhiJ9, I again used the ReDCaT method to determine how far I could truncate the O1+O2 region before I observed loss of 6xHis-WhiJ9 binding (**Fig. 6.16**). This 'footprinting' experiment revealed that WhiJ9 bound specifically to 3 direct repeats located at the overlap between O1 and O2 (**Fig. 6.16**). The consensus sequence from the 3 direct repeats was CGxxCTCAAC, with the final cytosine of each repeat contributing significantly to WhiJ9 binding.

To further analyse the binding of WhiJ9 to each repeat, separately and in combination, I designed oligos containing 1, 2 or all 3 direct repeats, where instead of deleting the relevant repeats, I replaced them with random DNA sequences, in order to keep all oligos the same length (**Fig. 6.17**).

Because the %Rmax was calculated using the capture and binding values as well as the molecular weights of the protein and DNA used for each sample, in principle it is possible to deduce the number of protein units bound per DNA molecule.

As expected, WhiJ9 bound best to the oligo with all 3 repeats intact - the average %Rmax was at ~400%, suggesting that 4 monomers or 2 dimers bound that sequence (**Fig. 6.17**). For the 3 oligos with different combinations of 2 direct repeats, the %Rmax was at ~200%, suggesting that 2 monomers or 1 dimer bound to those sequences. As the DR2+DR3 oligo bound WhiJ9 best out of the 2-repeat combinations, it meant that the loss of DR1 was not that impactful for WhiJ9 binding (**Fig. 6.17**). Interestingly, the binding of WhiJ9 to the DR1+DR3 oligo, where the 2 repeats were separated by a random DNA sequence, was still at an %Rmax of ~200%, suggesting that the separation of the repeats did not negatively impact overall binding (**Fig. 6.17**). This might suggest that WhiJ9 bound the direct repeats as monomers. Looking at the oligos containing only one direct repeat, there was no binding of WhiJ9 when only DR1 or DR2 were present. When only DR3 was present, there was a low level of binding, corresponding to one monomer binding the oligo (**Fig. 6.17**). In a preliminary SPR experiment aiming to establish the kinetics of WhiJ9 binding to DNA containing DR2+DR3, I found that WhiJ9 bound the DNA with a K_D in the low nM range, which is typical for a transcription factor.

In future work, I would like to use SPR to validate the binding of WhiJ9 (as identified by ChIP-seq) to other promoter regions – including the *sigF* promoter region and the *lexA-nrdR* intergenic region (**Fig. 6.10**). This would allow me to find a consensus binding sequence for WhiJ9 binding that is not solely based on the 3 direct repeats from its own promoter.

Overall, these results demonstrated that out of the 3 direct repeats, WhiJ9 preferentially bound DR3, whereas DR1 was the most expendable one (**Fig. 6.17**). The results also hinted that WhiJ9 possibly bound DNA as non-cooperating monomers. However, a preliminary mass photometry experiment performed by Dr Clare Stevenson suggested that 6xHis-WhiJ9 formed a dimer in solution. No monomeric WhiJ9 was detected, as the predicted molecular weight of 6xHis-WhiJ9 (~33 kDa) is lower than the threshold of detection for this system (40 kDa).

To establish the oligomeric state of WhiJ9, I would need to do more experiments such as native mass spectrometry, or analytical size-exclusion chromatography. For the latter method, I would need to find a way to counteract the concentration-dependent aggregation of the protein.

If the preliminary mass photometry data are correct and WhiJ9 is a dimer in solution, it would seem unlikely that it would dissociate to bind to direct repeats as monomers. To find out precisely how WhiJ9 binds to direct repeats I undertook crystallisation screens, hoping to get diffracting protein-DNA crystals and solve the structure of 6xHis-WhiJ9 bound to DNA. After trying different conditions and varying the length of the DNA used, I did get protein-DNA crystals (**Fig. 6.18**), but they were quite small, flat, and unstable, and unfortunately did not diffract well. Future work could focus on elucidating the structure of WhiJ9 bound to DNA by cryo-EM instead, as that would not require crystallisation of the complex.

Overall, in this chapter I established the role of WhiJ9 as a transcription factor, characterised its regulon, and found that it specifically bound to 3 direct repeats in its promoter. This finding solved a part of the mystery behind the indirect repression of *iosA* by BldB, as I found that WhiJ9 acts as an activator of *iosA* expression. In the next chapter, I present evidence that the direct link between BldB and WhiJ9 is BldB9.

Page intentionally left blank

7. Evidence that BldB9 is the Link Between BldB and WhiJ9 Function

Introduction

The results I presented so far demonstrate that unlike most other Bld regulators, BldB is not a transcription factor or a sigma factor and is not able to directly control the expression of sporulation-related genes (**Fig. 4.3, 4.4**). Nevertheless, the loss of BldB severely impacts *S. venezuelae* development (**Fig. 3.7, 3.8**), which I could attribute to the resulting overexpression of the *abaA* homologues and *iosA* (**Fig. 4.10, 4.11**). As *iosA* was one of the genes with the highest degree of upregulation in the *ΔbldB* mutant (**Fig. 4.6, Table 4.1**), I focused my attention on its locus, which also encodes the *bldB* homologue *bldB9* and the *whiJ9* homologue.

From bacterial-two-hybrid experiments, I knew that BldB9 directly and strongly interacts with BldB (**Fig. 3.12**). I revealed that WhiJ9 represses its own expression and activates the expression of *iosA* (**Fig. 6.15, Table 6.2**). Knowing all of this, I reasoned that the missing link between the indirect repression of *iosA* expression by BldB and its direct activation by WhiJ9 must be either a direct BldB-WhiJ9 interaction, or a partner-switching mechanism with BldB9 in the centre. I set out to test this by a series of protein-protein interaction experiments using BldB, BldB9 and WhiJ9, and by qRT-PCR experiments measuring *iosA* expression.

Results

WhiJ9 Did Not Interact with BldB or BldB9 in a Bacterial-Two-Hybrid Assay

Given that both BldB and WhiJ9 exerted control over the expression of *iosA* (although in antagonistic ways), I considered two possible scenarios. The first one involved the direct binding of BldB to WhiJ9 and subsequent prevention of its function as an activator of *iosA* expression. The second one involved BldB9 being able to swap between binding BldB and binding WhiJ9, in a partner-switching mechanism reminiscent of those involving the anti-sigma factors SpoIIAB and RsbW in the SigF and SigB pathways in *Bacillus* (Benson and Haldenwang, 1993; Diederich *et al.*, 1994; Dufour and Haldenwang, 1994). To investigate these two scenarios experimentally, I tested for interactions between WhiJ9, BldB9 and BldB.

Following my initial bacterial-two-hybrid library screen with BldB as bait, I identified BldB9 as one of the 7 BldB homologues that interacted strongly with canonical BldB (**Fig. 3.12, Table 3.2**). WhiJ9 was not among the hits in this screen, though there were 2 other hits containing a helix-turn-helix Xre domain, characteristic of the WhiJ homologues (**Table 3.2**). To test whether WhiJ9 was able to bind to either BldB or BldB9 (among other interactions), I performed one-on-one bacterial-two-hybrid β-galactosidase assays using full-length proteins.

I once again confirmed the strong interaction between BldB and BldB9, and the low level of self-interaction for BldB (**Fig. 7.1**). In this experiment, no interactions were detected between WhiJ9 and either BldB or BldB9 (**Fig. 7.1**). Additionally, BldB9, WhiJ9 and IosA did not self-interact, and no interactions between IosA and either BldB, BldB9 or WhiJ9 were detected. Finally, I tested whether there were any interactions between the protein counterparts from the two loci of interest encoding *abaA6* and *iosA*. No interactions were detected between BldB6 and BldB9, or between WhiJ6 and WhiJ9, or between AbaA6 and IosA (**Fig. 7.1**).

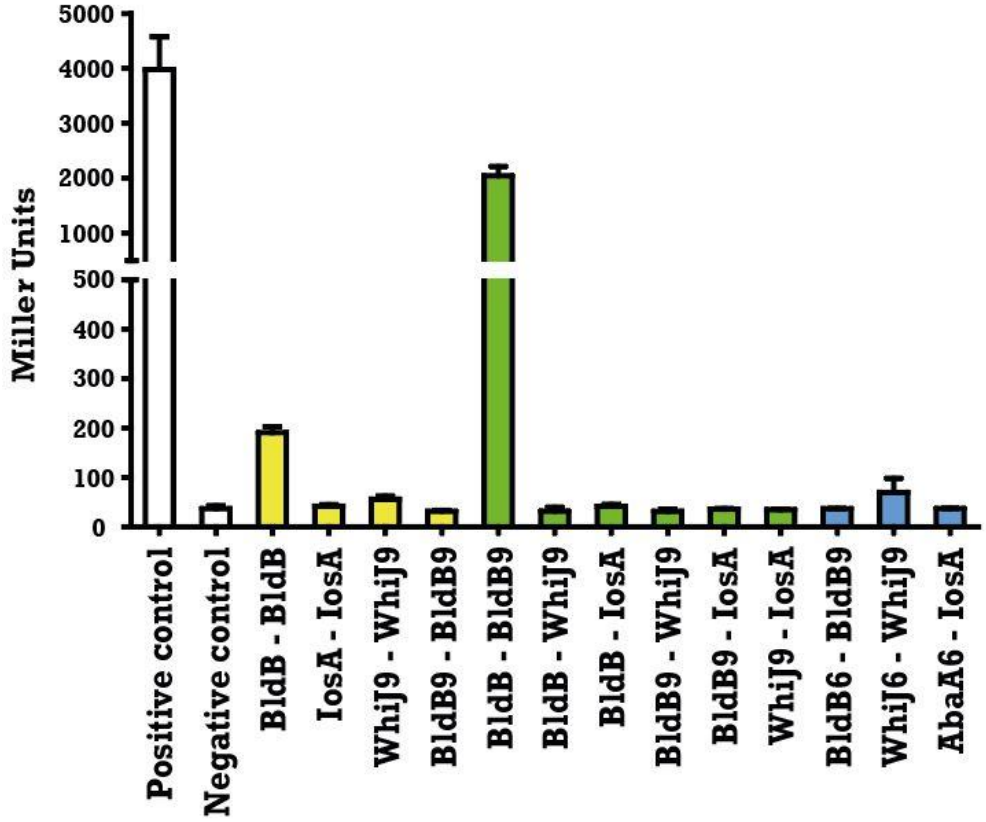

Figure 7.1. Interactions Between BldB and Proteins Encoded by the *iosA-bldB9-whiJ9* Locus.

β-galactosidase assays were performed to measure the strength of protein-protein interactions (in Miller units). The strong interaction between the leucine zipper domains of leucine zipper of GCN4 (T18C-zip and T25-zip) was used as a positive control. Empty vector negative controls were performed for every interaction displayed here, but for the sake of clarity, only one representative negative control is displayed. Results are the average of three independent experiments, with two technical replicates per experiment. Error bars indicate the SEM.

Evidence that WhiJ9 Forms a Complex with BldB9

Although the bacterial-two-hybrid experiment did not detect any interactions between WhiJ9 and either BldB or BldB9, I wished to do another experiment to test this, as two-hybrid assays can produce false-negative results. Thus, I decided to do co-purification experiments to see if I could purify a complex of either WhiJ9-BldB or WhiJ9-BldB9 from *E. coli* using the pCOLADuet-1 system. After several co-purification experiments, I did not find any evidence for a formation of a complex between BldB and WhiJ9.

However, when I used the pCOLA-Duet1 plasmid expressing 6xHis-BldB9 and untagged WhiJ9 (both codon-optimised for expression in *E. coli*; plasmid generated by GenScript), I could see potential double bands corresponding to 6xHis-BldB9 and WhiJ9 in the nickel column eluate, although there were many other proteins also present (**Fig. 7.2**). I excised the candidate WhiJ9 double band and the candidate 6xHis-BldB9 single bands separately and confirmed via mass spectrometry that they mainly consisted of BldB9 and WhiJ9. The presence of double bands for both BldB9 and WhiJ9 on an SDS gel might indicate degradation of the proteins. Unfortunately, 6xHis-BldB9 is a highly insoluble protein, so only a small amount was present in the supernatant and eluted from the nickel column. If BldB9 and WhiJ9 do indeed form a complex, this might explain why the WhiJ9 it co-eluted with was also not abundant (**Fig. 7.2**).

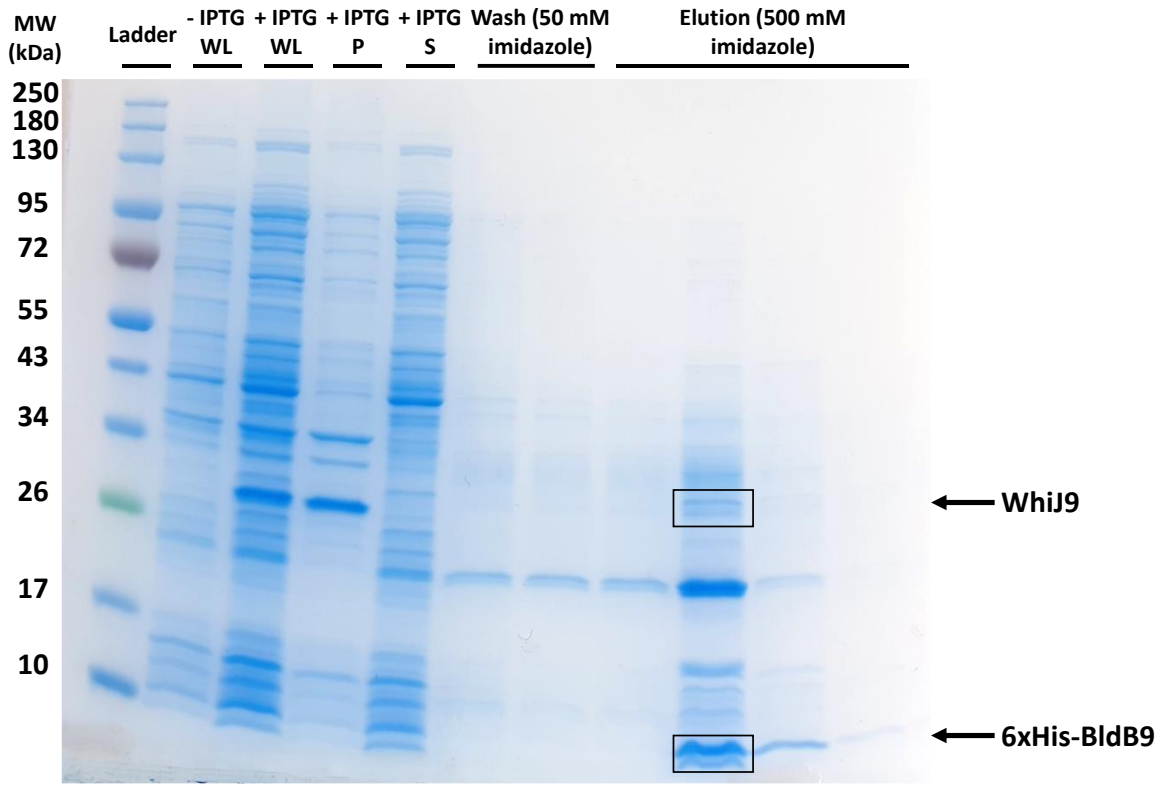

Figure 7.2. Co-purification of a BldB9-WhiJ9 Complex from *E. coli*.

6xHis-BldB9 and WhiJ9 were co-overexpressed in *E. coli* using pCOLADuet-1. The lysed culture supernatant was passed through a nickel column, washes were performed, and bound proteins were eluted and run on a 4-20% SDS-polyacrylamide gel. Color Prestained Protein Standard, Broad Range from New England BioLabs was used as a ladder. WL stands for whole lysate, P stands for pellet fraction, S stands for supernatant.

To see if BldB9-WhiJ9 interaction occurred while WhiJ9 was bound to DNA, I once again employed the SPR method ReDCaT (Stevenson *et al.*, 2013; Stevenson and Lawson, 2021). I immobilized the DR2+DR3 oligo (**Fig. 6.17**) on a SPR chip and then injected 6xHis-WhiJ9 (**Fig. 7.3**). This resulted in the usual increase in response, corresponding to WhiJ9 binding to DNA. After a short injection of running buffer, during which WhiJ9 started dissociating from the DNA, I injected either 6xHis-BldB or 6xHis-BldB9 to see how it would affect the response. Upon addition of BldB, there was no shift in response (**Fig. 7.3**), meaning that BldB did not bind to WhiJ9, consistent with the failure to isolate a BldB-WhiJ9 complex following co-expression in *E. coli*.

When I injected BldB9, however, I saw another increase in response, presumably corresponding to BldB9 binding to WhiJ9 (**Fig. 7.3**), and in agreement with the co-purification experiment (**Fig. 7.2**). Notably, the increase in response due to BldB9 binding to WhiJ9 in this SPR experiment suggested that BldB9 did not take WhiJ9 off DNA, but simply bound to it, with the complex then dissociating at a rate comparable to when WhiJ9 dissociated by itself (**Fig. 7.3**). In a separate control experiment I observed no binding of BldB9 to DNA in the absence of WhiJ9, suggesting that BldB9 bound specifically to WhiJ9 and is not a DNA-binding protein itself.

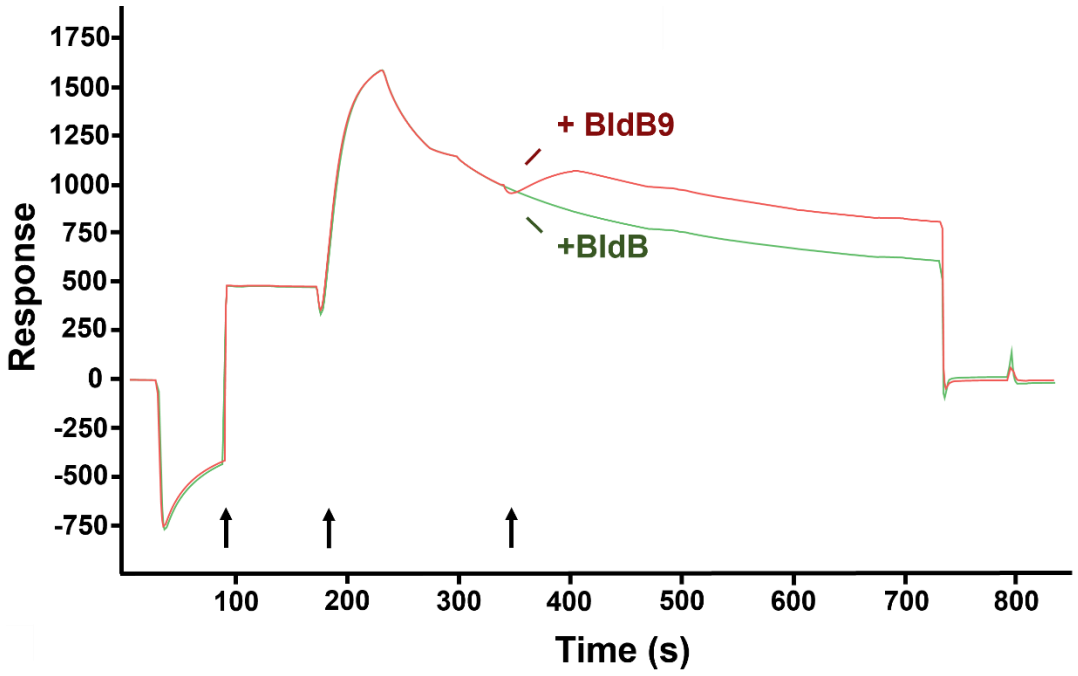

Figure 7.3. Binding of BldB9 to WhiJ9 Captured on DNA.

SPR sensorgram measuring binding response (y-axis) over time (x-axis). Arrows indicate the subsequent injections of DNA, 6xHis-WhiJ9, and either 6xHis-BldB (green line) or 6xHis-BldB9 (red line). One out of four replicates are represented in this sensorgram.

Evidence that BldB9 and WhiJ9 Control the Expression of *iosA* Together

Since my co-purification and SPR results suggested that WhiJ9 and BldB9 interact, I reasoned that the loss or overexpression of BldB9 might affect *iosA* expression. I also wanted to measure the expression of *iosA* in a *ΔbldB9 ΔwhiJ9* double mutant and compare the pattern to that in the *ΔbldB9* and *ΔwhiJ9* single mutants. For this reason, I constructed a *ΔbldB9 ΔwhiJ9* double mutant via Redirect, and performed a series of qRT-PCR experiments using this double mutant and other already characterised strains resulting from the deletion or overexpression of *bldB*, *bldB9* and *whiJ9*.

I previously characterised the phenotypes of the *ΔbldB9* and *ΔwhiJ9* single mutants. The *ΔbldB9* mutant exhibited a white phenotype, with ample production of aerial hyphae, but a lack of mature spore formation (**Fig. 3.13, 3.14, 3.16**). The *ΔwhiJ9* mutant exhibited normal sporulation both on a plate, and under the electron microscope (**Fig. 6.1, 6.2**). Interestingly, the *ΔbldB9 ΔwhiJ9* double mutant developed normally on a plate (**Fig. 7.4**). SEM showed that the double mutant was able to form regular, mature spores (**Fig. 7.5**). This meant that the additional loss of *whiJ9* rescued the white phenotype of the *ΔbldB9* mutant, pointing to linked but antagonistic functions between WhiJ9 and BldB9.

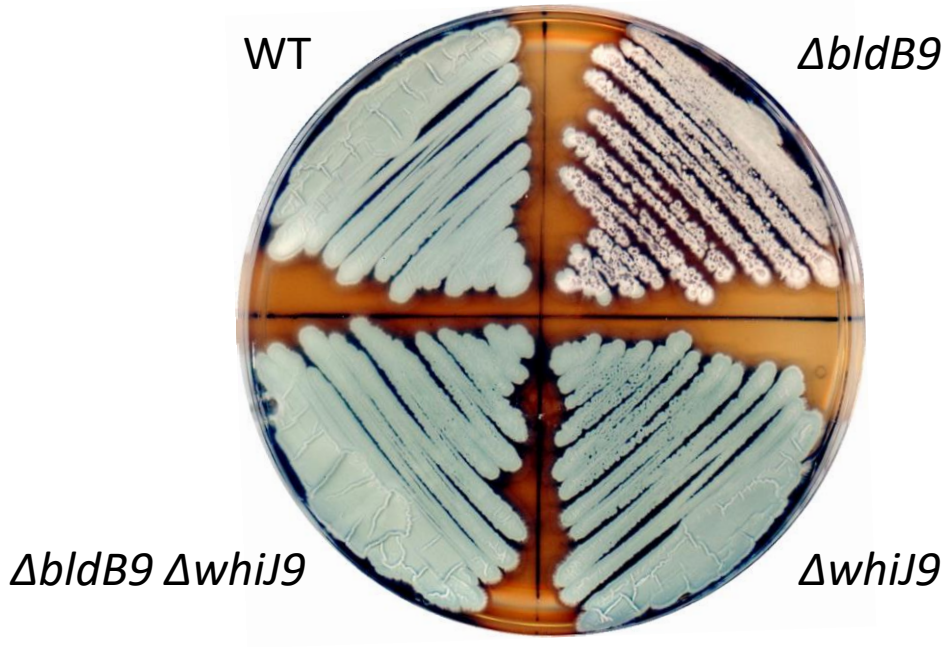

Figure 7.4. Mutant Phenotype of the *ΔbldB9 ΔwhiJ9* Strain.

Plate depicting the growth of the *ΔbldB9 ΔwhiJ9* double mutant on MYM agar. Plate image was taken after a 4-day incubation at 28˚C.

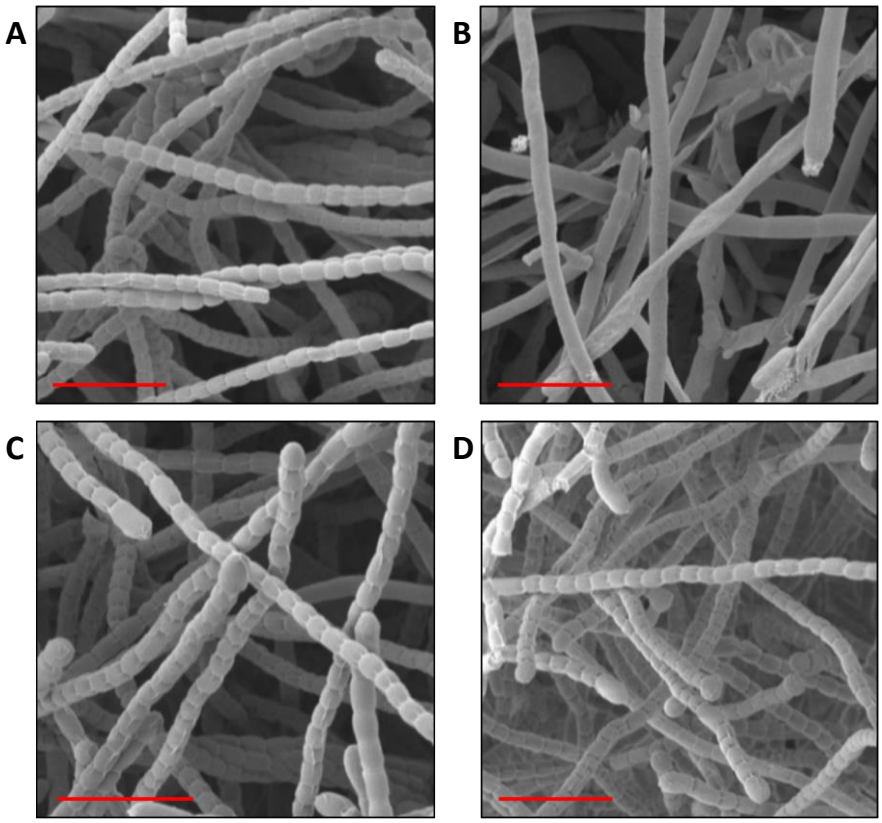

Figure 7.5. Phenotypic Characterisation of the *ΔbldB9 ΔwhiJ9* Double Mutant Strain.

Scanning electron micrographs comparing the phenotypes of wild-type *S. venezuelae* **(A)**, the *ΔbldB9* mutant strain **(B)**, the *ΔwhiJ9* mutant strain **(C)**, and the *ΔbldB9 ΔwhiJ9* double mutant strain **(D).** Scale bars in red indicate 5 µm.

My qRT-PCR results once again confirmed the striking upregulation of *iosA* in the *ΔbldB* mutant (**Fig. 7.6**). In comparison, the levels of *iosA* expression in the *bldB* overexpression strain were identical to wild-type levels. In the *ΔwhiJ9* mutant, the expression levels of *iosA* were only a fraction higher than in wild type, whereas in the *whiJ9* overexpression strain they were even higher than the expression levels in the *ΔbldB* mutant (**Fig. 7.6**). This impressive upregulation of *iosA* in the *whiJ9* overexpression strain confirmed the role of WhiJ9 as a direct activator of *iosA* expression.

Interestingly, the expression of *iosA* was slightly upregulated in the *ΔbldB9* mutant, though not as highly as in the *ΔbldB* mutant or the *whiJ9* overexpression strain (**Fig. 7.6**). The upregulation seen in the *ΔbldB9* mutant was lost with the additional deletion of *whiJ9* in the *ΔbldB9 ΔwhiJ9* double mutant, returning *iosA* expression to wild-type levels.

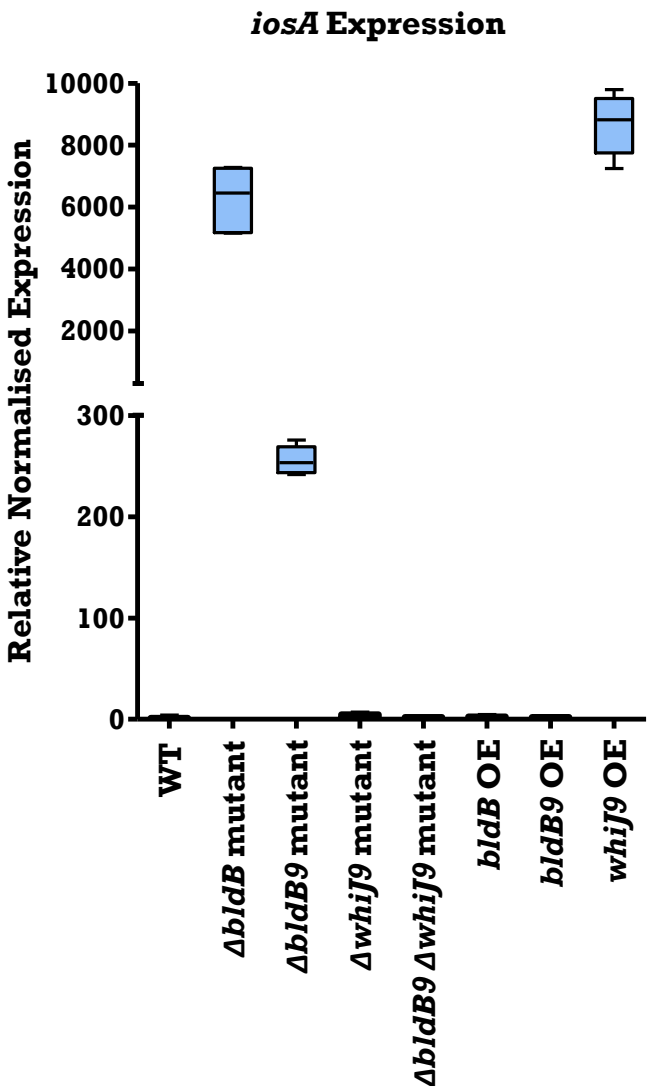

Figure 7.6. Expression of *iosA* in Mutant and Overexpression Strains for *bldB*, *bldB9* and *whiJ9*.

Box-and-whiskers plot representing the absolute quantification of *iosA* expression as assayed by qRT-PCR. Differences in primer efficiency were corrected based on curves from genomic DNA amplification. Expression values for each sample were calculated relative to the *hrdB* reference and normalised to the WT value, which was set to 1. Plots represent the lower quartile (bottom of box), median (horizontal line in box) and upper quartile (top of box) of 2 independent experiments with 3 technical replicates per experiment. The whiskers represent the minimum and maximum expression values.

Discussion

In this chapter I presented evidence that BldB9 can interact with the transcription factor WhiJ9 and proposed that the interactions between BldB9 and both WhiJ9 and BldB might comprise a partner-switching mechanism that regulates the expression of the sporulation inhibitor *iosA*.

I confirmed that WhiJ9 acts as an activator of the expression of *iosA* in two separate experiments. First, I performed RNA-seq on the *ΔbldB ΔwhiJ9* double mutant and observed that the additional loss of *whiJ9* abolished the upregulation of *iosA* in the *ΔbldB* mutant (**Fig. 6.15**). Second, I did qRT-PCR using the *whiJ9* overexpression strain, which showed that it had the highest levels of *iosA* expression out of all assayed strains (**Fig. 7.6**).

I observed a slight elevation of *iosA* expression in the *ΔwhiJ9* mutant in both my RNA-seq (at 10 hours only) and qRT-PCR experiments (**Table 6.2, Fig. 7.6**), which might seem inconsistent with WhiJ9 functioning as an activator of *iosA* expression. However, this observation is not especially meaningful, as the *iosA* expression levels in the *ΔwhiJ9* mutant were far closer to the very low levels of expression found in the wild type that to the dramatically elevated levels of *iosA* expression found in the *ΔbldB* mutant and the *whiJ9* overexpression strain (**Fig. 7.6**).

Given that WhiJ9 is a direct activator of *iosA* expression and BldB is an indirect repressor, I wished to find the missing link between the two regulators. Considering all the results presented thus far, I reasoned that either BldB bound WhiJ9 directly and prevented it from activating *iosA* expression, or BldB9 served as a partner switch between them. To test this, I performed a series of experiments looking at protein-protein interactions between WhiJ9 and either BldB or BldB9.

First, I performed one-on-one bacterial-two-hybrid assays. I once again observed the strong binding between BldB and BldB9 but did not observe any binding between WhiJ9 and either BldB or BldB9 (**Fig. 7.1**). The two-hybrid method is valuable for characterising protein-protein interactions, but some positive interactions can be prevented by steric hindrance arising from the fusion of the proteins to the bulky T18 and T25 peptides, leading to false negative results. For this reason, I decided to perform alternative experiments, using the pCOLA-Duet1 system to co-overexpress 6xHis-BldB9 and WhiJ9 in *E. coli*.

Knowing that BldB9 is very insoluble and difficult to purify, I chose to place the 6xHis-tag on BldB9 instead of WhiJ9, to ensure that I could capture as much of the protein as possible on a nickel column. I also used versions of the *bldB9* and *whiJ9* genes that had been codon-optimised for expression in *E. coli*. Even with those measures taken, I only saw low amounts of BldB9 and WhiJ9 in the eluate (**Fig. 7.2**), and I had to resort to mass spectrometry to verify that the bands indeed corresponded to BldB9 and WhiJ9. Both proteins eluted as double bands on the SDS gel, with the lower bands possibly representing degradation products (**Fig. 7.2**). In future work, I would try fusing alternative tags to BldB9, such as SUMO or MBP, to try to increase its solubility and get a more abundant BldB9-WhiJ9 complex.

Nevertheless, this experiment suggested that BldB9 and WhiJ9 might interact with one another, whereas I did not find evidence that BldB binds WhiJ9. To see if these interactions occurred while WhiJ9 was bound to DNA, I used the ReDCaT method once again (Stevenson *et al.*, 2013; Stevenson and Lawson, 2021). I found that when WhiJ9 was bound to DNA, the further addition of BldB9 caused an increase in response, consistent with BldB9 binding to WhiJ9 (**Fig. 7.3**). In contrast, no shift in response was observed when BldB was injected (**Fig. 7.3**). This strengthened the evidence that the link between BldB and WhiJ9 is their individual interactions with BldB9 (as opposed to a direct interaction between BldB and WhiJ9).

The existence of “long” BldB homologues representing fusions of BldB and WhiJ was an early indication that the separate proteins might be able to interact with one another (**Table 3.1**). After the BldB9-WhiJ9 co-purification experiment (**Fig. 7.2**), I initially thought that the function of BldB9 would be to take WhiJ9 off DNA and prevent the activation of *iosA* expression, reminiscent of the binding of the antagonist SinI to SinR - the master regulator of *Bacillus* sporulation and biofilm formation (Bai, Mandic-Mulec and Smith, 1993; Lewis *et al.*, 1998; Colledge *et al.*, 2011). However, the SPR experiment suggested that BldB9 bound to WhiJ9 but did not dissociate it from DNA (**Fig. 7.3**).

My qRT-PCR experiment further contributed to our understanding of the control of *iosA* expression. The role of WhiJ9 as its activator was confirmed, as the *whiJ9* overexpression strain showed a very high upregulation of *iosA* (**Fig. 7.6**). In the Δ*bldB9* mutant a more moderate level of *iosA* upregulation could be observed (**Fig. 7.6**). In comparison, the *ΔbldB9 ΔwhiJ9* mutant showed levels of *iosA* expression identical to those in the wild-type control, consistent with the proposal that BldB9 antagonises the direct activation of *iosA* expression by WhiJ9.

Out of all strains used in the qRT-PCR dataset (**Fig. 7.6**), none showed a downregulation of *iosA* - the expression of *iosA* was either at wild-type levels (in the *ΔwhiJ9* mutant, the *ΔbldB ΔwhiJ9* double mutant, and the overexpression strains for *bldB* and *bldB9*), or 2-3 orders of magnitude higher (in the *ΔbldB* mutant, the *ΔbldB9* mutant and the *whiJ9* overexpression strain). These results suggest that *iosA* expression is 'switched off' in wild-type *S. venezuelae*. This is confirmed by looking at the raw RNA-seq datasets described in Chapters 4 and 6, where an extremely low number of reads mapping to *iosA* are found in the wild-type samples. Therefore, the sustained repression of *iosA* transcription in *S. venezuelae* seems to be crucial for the normal progression through development.

As there is no annotation of bioinformatically predicted domains for IosA, its biochemical function remains a mystery. It is interesting to note however, that in my qRT-PCR experiment all strains that showed an upregulation of *iosA* exhibited bald (*ΔbldB* mutant) or white (*ΔbldB9* mutant and *whiJ9* overexpression strain) developmental phenotypes, consistent with the designation "**i**nhibitor **o**f **s**porulation". It would be interesting to see what the expression patterns of the other *abaA* homologues are in the *ΔbldB9* mutant and *whiJ9* overexpression strain - either via RNA-seq or more focused qRT-PCR assays. If the expression of the *abaA* homologues is not elevated in these two strains (in contrast to the *ΔbldB* mutant), it might explain why they exhibit white phenotypes, as opposed to the bald phenotype of the *ΔbldB* mutant.

If high *iosA* expression always correlates with a developmental phenotype in *Streptomyces*, then it is logical that the *S. venezuelae ΔwhiJ9* mutant sporulates normally - the truncated WhiJ9 protein lacks the DNA-binding domain and is unable to act as an activator of *iosA* expression. Interestingly, a partial deletion of canonical *whiJ* in *S. coelicolor* exhibited a sporulation-deficient phenotype - the first 93 codons were left intact, so the truncated WhiJ did contain the N-terminal HTH-Xre motif. When the entire *whiJ* gene was deleted, however, the resulting strain was able to sporulate (Aínsa *et al.*, 2010).

In future work I would generate another partial *S. venezuelae ΔwhiJ9* mutant - one which expresses a protein that is missing a portion of the C-terminus (in a way that does not interfere with *bldB9* transcription), but has an intact HTH-Xre motif, to determine if it would lead to a developmental phenotype. If this partial deletion mutant failed to sporulate, that phenotype might be attributable to loss of BldB9 binding. In theory, this might lead to a moderate upregulation of *iosA*, like the one exhibited by the *ΔbldB9* mutant - something that could be examined by qRT-PCR.

This might be what is happening in the *S. coelicolor* locus containing canonical *whiJ*, the *bldB* homologue *sco4542*, and the *abaA* homologue *sco4544* (Aínsa *et al.*, 2010).

A lot more work needs to be done to fully characterise BldB-BldB9-WhiJ9 interactions, but in this chapter I described the first experimental evidence that a non-canonical BldB homologue binds to its genetically paired WhiJ homologue, resulting in control over the expression of the divergently transcribed gene in the locus (in this case *iosA*).

8. General Discussion

Despite the importance of the Bld and Whi regulators for progression through the developmental stages in *Streptomyces*, the precise molecular functions of some of these regulators have eluded researchers for decades. BldB is one such example. The major aims of this study were to determine the biochemical function of BldB, and to gain insights into the global effects of this developmental regulator.

A final model illustrating some of the key findings presented in this thesis is represented in **Figure 8.1**.

Prior to this work, very few studies focused on BldB. The key information that could be gleaned from these studies was that canonical BldB had numerous homologues in various *Streptomyces* species, which were found encoded next to homologues of *whiJ* and *abaA* (Fernández-Moreno *et al.*, 1992; Gehring *et al.*, 2000; Chater and Chandra, 2006; Aínsa *et al.*, 2010; Doroghazi and Buckley, 2014). This is also true for the model organism used in this thesis (**Fig. 3.6**) – *S. venezuelae* has 10 non-canonical *bldB* homologues (designated *bldB2-11*), all of which have a *whiJ* homologue encoded adjacently (designated *whiJ2-11*). In 5 of these loci, there is also an *abaA* homologue encoded divergently to the *whiJ* homologue (**Fig. 3.6**).

This genomic arrangement differs from that of canonical *bldB*, which is instead found encoded next to genes involved in the type VII secretion system (**Fig. 3.1**), something that appears to be characteristic for canonical *bldB* as it occurs in different *Streptomyces* species (Akpe San Roman *et al.*, 2010). None of my results suggest a significant involvement of BldB in the *Streptomyces* type VII secretion system, though I do not discount it - further work focused specifically on the secretion system would need to be done to establish any role for BldB in secretion.

Another key piece of information from previous literature was the claim that BldB binds DNA. Numerous articles that only mention BldB in passing refer to it as a DNA-binding regulator. This recurring statement is largely based on two studies. The first one speculated that BldB auto-regulates its expression solely based on the temporal pattern of the *bldB* promoter activity in *S. coelicolor* (Pope, Green and Westpheling, 1998).

The second study took this suggestion further, presenting some evidence that *S. lividans* BldB was able to bind its own promoter in an EMSA experiment (Mishig-Ochiriin *et al.*, 2003). In contrast to these two studies, Eccleston *et al*. (2002) reported that they did not observe any binding of *S. coelicolor* BldB to DNA.

My *in vivo* ChIP-seq results did not suggest that *S. venezuelae* BldB is able to directly bind to DNA (**Fig. 4.3, 4.4**) and I did not observe binding of 6xHis-BldB to its own promoter using *in vitro* SPR (**Fig. 4.5**). It is formally possible that canonical BldB orthologues in other *Streptomyces* species might bind DNA, as suggested for *S. lividans* BldB (Mishig-Ochiriin *et al.*, 2003), but more robust experiments like ChIP-seq would need to be performed to test this, as EMSA experiments can produce false positive artefacts. It is also possible that BldB indirectly binds DNA through an interaction with other protein(s).

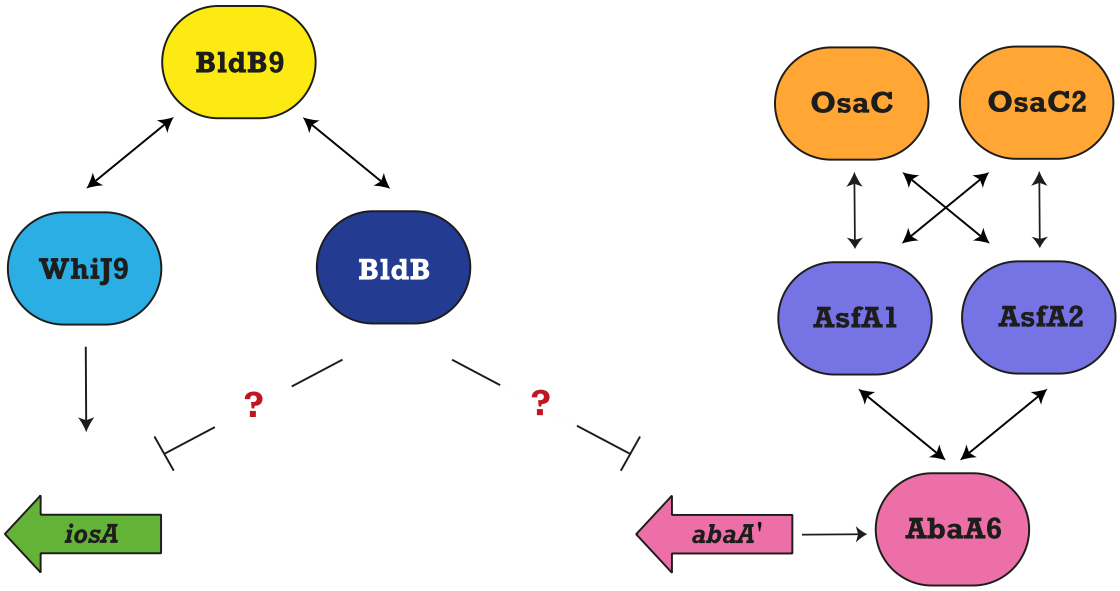

Figure 8.1. A Network of Interactions and Regulation Involving BldB

A final model depicting some of the key findings of this study. Single head arrows indicate activation of expression, double head arrows indicate interaction between proteins, T-shaped lines indicate inhibition of expression. BldB interacts strongly with 7 out of non-canonical 10 BldB homologues (only BldB9 is depicted here). BldB indirectly represses the expression of the 5 *abaA* homologues and *iosA*. Evidence suggests that BldB9 interacts with WhiJ9. WhiJ9 is a DNA-binding transcriptional regulator, which activates the expression of *iosA*. The predicted anti-sigma factor AbaA6 interacts strongly with the predicted anti-sigma antagonists AsfA1 and AsfA2. Both AsfA1 and AsfA2 interact with the multidomain proteins with a role in osmoregulation OsaC and OsaC2.

My bacterial-two-hybrid library screen (**Table 3.2**) and subsequent one-on-one two-hybrid interaction assays (**Fig. 3.12**) revealed that *S. venezuelae* BldB interacts strongly with 7 of its non-canonical BldB homologues *in vivo*. The phylogenetic analysis I conducted suggested that the remaining 3 BldB homologues, with which BldB did not interact, are more similar in sequence to BldB than the 7 strongly interacting ones (**Fig. 3.18, 3.19**). Future work could explore what residues are important for heterodimer formation between BldB and the 7 BldB homologues.

Out of the 7 strongly interacting homologues, 2 are necessary for *S. venezuelae* sporulation - BldB6 and BldB9 (**Fig. 3.13, 3.14, 3.15, 3.16**). The two loci containing *bldB6* and *bldB9* proved to be the most important ones for deciphering the role of BldB in development. My RNA-seq results revealed that in an indirect way, BldB serves to repress the expression of the 5 *abaA* homologues and *iosA* (**Fig. 4.6**). IosA is a hypothetical protein of unknown biochemical function. I gave the *iosA* designation to the gene (standing for "**i**nhibitor **o**f **s**porulation **A**"), as its overexpression led to a sporulation-deficient phenotype in *S. venezuelae* (**Fig. 4.8, 4.9**). The same phenotype could also be observed following the overexpression of *abaA6* (**Fig. 4.8, 4.9**). Furthermore, the joint overexpression of *abaA6* and *iosA* (encoded near *bldB6* and *bldB9*, respectively) recapitulated the classical bald phenotype of the *ΔbldB* mutant (**Fig. 4.10, 4.11**).

IosA, despite having the same genomic context as the *abaA* homologues, does not share significant sequence similarity with them. No *S. venezuelae* proteins were found to interact with it in a bacterial-two-hybrid screen. In comparison, AbaA6 and the other AbaA homologues all share an HATPase_c domain, which is commonly found in anti-sigma factors. Two-hybrid experiments revealed a protein-protein interaction network with AbaA6 at its foundation (**Fig. 8.1**). AbaA6 strongly interacted with two proteins with predicted STAS anti-sigma antagonist domains, which I designated AsfA1 and AsfA2 (**Table 5.1, Fig. 5.1**). These two proteins in turn interact with the multidomain proteins OsaC and OsaC2 (**Table 5.3, Fig. 5.4**), which share a similar domain architecture - they contain HATPase_C, PAS, GAF and PP2C phosphatase domains (**Fig. 5.3**).

The AbaA6 - AsfA1/AsfA2 - OsaC/OsaC2 interaction network has similarities with the partner-switching mechanisms exerting control over the activity of the *Bacillus* sigma factors SigB and SigF (Schmidt *et al*., 1990; Hecker, Pané-Farré and Uwe, 2007). However, I did not identify any interacting sigma factors for AbaA6 or for OsaC (**Fig. 5.2, 5.5**).

More work would need to be done to study the phosphorylation states of the putative anti-sigma antagonists AsfA1 and AsfA2, to identify the transcriptional regulators that presumably function as the target(s) of this pathway and to elucidate the signal received by OsaC/OsaC2 components through their sensor domains. A good candidate for such a signal is osmotic stress, since OsaC has been shown to have a role in osmoregulation in *S. coelicolor* (Fernández Martínez *et al.*, 2009). It would be interesting to know whether any of the other components of the pathway, especially AbaA6, also have a role in osmotic stress.

In an attempt to find the transcriptional regulators responsible for the impressive upregulation of *abaA6* and *iosA* in the *ΔbldB* mutant (**Fig. 4.6, Table 4.1**), I decided to see if the predicted transcription factors WhiJ6 and WhiJ9 are able to bind to the intergenic regions upstream of their own genes and thus control the expression of the divergently transcribed *abaA6* and *iosA* genes (**Fig. 3.6**). While my ChIP-seq and SPR results did not provide any evidence that WhiJ6 binds DNA (**Fig. 6.8**), I did confirm that WhiJ9 is a transcription factor (**Fig. 6.9, 6.10**). Out of 46 candidate binding sites identified in WhiJ9 ChIP-seq, the one with the highest level of enrichment was the *iosA-whiJ9* intergenic region (**Fig. 6.11**). Using SPR, I found the precise sequence that WhiJ9 bound to in this intergenic region - that sequence contains 3 direct repeats, which I designated DR1, DR2 and DR3 (**Fig. 6.12, 6.16, 6.17**). The consensus sequence for these repeats is CGxxCTCAAC.

The precise way in which WhiJ9 binds to these repeats is still unknown as my crystallisation screens did not yield diffracting crystals of 6xHis-WhiJ9 bound to DNA (**Fig. 6.18**). It is still unclear whether WhiJ9 binds these repeats as a monomer or as a dimer - the SPR results better fit the hypothesis that WhiJ9 binds the 3 direct repeats as non-cooperating monomers (**Fig. 6.17**), whereas the preliminary mass photometry data from Dr Clare Stevenson suggest that WhiJ9 is able to form a dimer in solution. More work would be needed to establish the oligomeric state of WhiJ9, and to find out how many WhiJ9 protomers occupy the 3 direct repeats in the *iosA* promoter.

If WhiJ9 bound DNA as a dimer, two obvious questions would be how those dimers bind an odd number of direct repeats, and how the dimers are situated against one another (*e.g.,* in a head-to-tail manner, a dimer of dimers). An example of a protein proposed to bind as head-to-tail homodimer(s) to 3 direct DNA repeats is the *E. coli* response regulator ArcA (Park *et al.*, 2013; Park and Kiley, 2014).

ArcA was suggested to bind the 3 direct repeats cooperatively, and more specifically, it was suggested that the ArcA homodimer bound to the first two direct repeats facilitated binding of ArcA (either as a monomer or a homodimer) to the third repeat, which was otherwise bound with lower affinity (Park and Kiley, 2014). The authors also observed that the position of the third repeat in particular was important for the transcriptional outcome at the *icdA* promoter, which is under ArcA control (Park and Kiley, 2014). It would be interesting to see how the loss of 1 or 2 direct repeats would affect WhiJ9 binding *in vivo* in *Streptomyces*, and how the loss of each repeat would impact the expression of *iosA*.

The position of the direct repeats in the *iosA-whiJ9* intergenic region strongly suggested that WhiJ9 represses its own expression and hinted that it might activate the expression of *iosA* (**Fig. 6.11**). This was confirmed by my second RNA-seq experiment, using the *ΔbldB* mutant, the *ΔwhiJ9* mutant and the *ΔbldB ΔwhiJ9* double mutant (**Fig. 6.15, Table 6.2**). Thus, I established that WhiJ9 directly activates *iosA* expression, whereas BldB indirectly represses it. In an attempt to bridge the functions of BldB and WhiJ9, I performed different experiments to find out if BldB9 might function as the link between them (**Fig. 8.1**).

I presented preliminary evidence that BldB9 and WhiJ9 can form a complex when co-expressed in *E. coli* (**Fig. 7.2**), and that BldB9 can bind to WhiJ9 while the latter is bound to DNA in an *in vitro* SPR experiment (**Fig. 7.3**). No direct interactions between BldB and WhiJ9 were observed (**Fig. 7.3**). More work would be needed to strengthen this evidence, which could include performing CoIP experiments, and further co-purification trials with different solubility tags for BldB9.

If the proposed interaction between BldB9 and WhiJ9 indeed occurs in *Streptomyces*, future work would need to focus on elucidating how BldB9 (with or without the presence of BldB) affects the function of WhiJ9. Looking at my results, the expression of *iosA* was slightly elevated in the *ΔbldB9* mutant but was reduced back to wild-type levels in the *ΔbldB9 ΔwhiJ9* mutant (**Fig. 7.6**), suggesting that BldB9 antagonises the activation of *iosA* expression by WhiJ9. However, the SPR results suggested that BldB9 binds to WhiJ9 without taking it off DNA (**Fig. 7.3**).

One model consistent with both results would be that when WhiJ9 is bound to the direct repeats of the *iosA-whiJ9* intergenic region, BldB9 binds to WhiJ9 and blocks its function as an activator, perhaps by preventing the recruitment of RNA polymerase. If this were true, BldB9 would function as an “anti-activator”.

If BldB9 binds to WhiJ9 while WhiJ9 is bound to DNA, this could be confirmed through BldB9 ChIP-seq experiments in a *whiJ9* overexpression strain (to bypass the repression of *whiJ9* expression). As ChIP-seq works for proteins that are indirectly bound to DNA, this experiment could establish if any BldB9 binding sites coincide with those of WhiJ9 (**Table 6.1**). In addition, *in vitro* transcription could be employed to see if the addition of BldB9 would abolish the transcriptional activation of *iosA* by WhiJ9.

The problem with this model is the placement of BldB within it. Considering that BldB acts antagonistically to WhiJ9, the only explanation that would fit this model would be that the BldB-BldB9 heterodimer jointly binds to WhiJ9. However, the BldB ChIP-seq experiments presented in Chapter 4 failed to show DNA binding by BldB (**Fig. 4.3, 4.4**). In the strains used in those experiments however, the expression of *whiJ9* is presumably low due to its expression auto-inhibition, which could have been the reason behind the low ChIP-seq enrichment. Another 3xFLAG-BldB ChIP-seq experiment using a strain overexpressing untagged *whiJ9* could be performed to definitively establish if BldB indirectly binds to WhiJ9.

Another scenario might be that BldB, BldB9 and WhiJ9 comprise a partner-switching mechanism, with BldB binding to BldB9 to release WhiJ9 to perform its function. However, this model is not well-supported by my expression studies. According to this model, loss of BldB should result in permanent BldB9-WhiJ9 complex formation and no activation of *iosA* expression, whereas loss of BldB actually causes massive upregulation of *iosA* expression (**Fig. 4.6, 7.6, Table 4.1**).

Yet another possibility is that there is a regulatory small RNA encoded in the vicinity of the *iosA-bldB9-whiJ9* locus, as there is in the *sco4677-4679* locus in *S. coelicolor* (Hindra *et al.*, 2014). The sRNA *scr4677* was found to stabilise the polycistronic transcript containing *sco4677* (encoding the AbaA-like anti-sigma factor RsfA) and *sco4676*, presumably aiding the translation of the putative anti-sigma factor.

While I did not determine the precise molecular function of BldB, this work greatly expands our overall understanding of the global effects of this developmental regulator. I found that loss of BldB function causes the dramatic upregulation of *iosA* and the *abaA* homologues, and that co-overexpression of just two of these genes, *iosA* and *abaA6*, was enough to recapitulate the *ΔbldB* mutant phenotype. I showed that the transcription factor WhiJ9 was directly responsible for the activation of *iosA* in the *ΔbldB* mutant, and that BldB9 heterodimerises with BldB.

It is possible that the molecular interactions and dependencies involving the proteins encoded in the *iosA-whiJ9-bldB9* locus might be replicated for the other loci containing *bldB*, *whiJ* and *abaA* homologues, leading to the dramatic upregulation of the *abaA* homologues seen in the *ΔbldB* mutant. Unravelling all these molecular interactions would present an interesting challenge - one that would further enhance our understanding of the function of BldB and its homologues, and perhaps give context to their involvement in managing stress responses.

References

Aínsa, J. A. *et al.* (2000) 'WhiA, a Protein of Unknown Function Conserved among Gram-Positive Bacteria, Is Essential for Sporulation in Streptomyces coelicolor A3(2)', *Journal of Bacteriology*, pp. 5470–5478. doi: 10.1128/jb.182.19.5470-5478.2000.

Aínsa, J. A. *et al.* (2010) 'The complex whiJ locus mediates environmentally sensitive repression of development of Streptomyces coelicolor A3(2)', *Antonie van Leeuwenhoek*, 98(2), pp. 225–236.

Aínsa, J. A., Parry, H. D. and Chater, K. F. (1999) 'A response regulator-like protein that functions at an intermediate stage of sporulation in Streptomyces coelicolor A3(2)', *Molecular microbiology*, 34(3), pp. 607–619.

Akanuma, G. *et al.* (2011) 'Control of aerial mycelium formation by the BldK oligopeptide ABC transporter in Streptomyces griseus', *FEMS microbiology letters*, 315(1), pp. 54–62.

Akpe San Roman, S. *et al.* (2010) 'A heterodimer of EsxA and EsxB is involved in sporulation and is secreted by a type VII secretion system in Streptomyces coelicolor', *Microbiology*, 156(Pt 6), pp. 1719–1729.

Al-Bassam, M. M. *et al.* (2014) 'Response Regulator Heterodimer Formation Controls a Key Stage in Streptomyces Development', *PLoS genetics*, 10(8), p. e1004554.

Al-Bassam, M. M. *et al.* (2018) 'Expression Patterns, Genomic Conservation and Input Into Developmental Regulation of the GGDEF/EAL/HD-GYP Domain Proteins in Streptomyces', *Frontiers in Microbiology*. doi: 10.3389/fmicb.2018.02524.

Aldridge, M. *et al.* (2013) 'A novel bifunctional histone protein in Streptomyces : a candidate for structural coupling between DNA conformation and transcription during development and stress?', *Nucleic Acids Research*, pp. 4813–4824. doi: 10.1093/nar/gkt180.

Allenby, N. E. E. *et al.* (2004) 'Post-transcriptional regulation of the Bacillus subtilis pst operon encoding a phosphate-specific ABC transporter', *Microbiology*, 150(Pt 8), pp. 2619–2628.

Allenby, N. E. E. *et al.* (2012) 'Diverse control of metabolism and other cellular processes in Streptomyces coelicolor by the PhoP transcription factor: genome-wide identification of in vivo targets', *Nucleic acids research*, 40(19), pp. 9543–9556.

Aravind, L. and Koonin, E. V. (2000) 'The STAS domain — a link between anion transporters and antisigma-factor antagonists', *Current Biology*, pp. R53–R55. doi: 10.1016/s0960-9822(00)00335-3.

Arigoni, F. *et al.* (1995) 'Localization of Protein Implicated in Establishment of Cell Type to Sites of Asymmetric Division', *Science*, pp. 637–640. doi: 10.1126/science.270.5236.637.

Arigoni, F. *et al.* (1996) 'SpoIIE governs the phosphorylation state of a protein regulating transcription factor sigma F during sporulation in Bacillus subtilis', *Proceedings of the National Academy of Sciences of the United States of America*, 93(8), pp. 3238–3242.

Bagchi, S. *et al.* (2008) 'Intermediate filament-like proteins in bacteria and a cytoskeletal function inStreptomyces', *Molecular Microbiology*. doi: 10.1111/j.1365-2958.2008.06473.x.

Bai, U., Mandic-Mulec, I. and Smith, I. (1993) 'SinI modulates the activity of SinR, a developmental switch protein of Bacillus subtilis, by protein-protein interaction', *Genes & development*, 7(1), pp. 139–148.

Beamer, L. J. and Pabo, C. O. (1992) 'Refined 1.8 A crystal structure of the lambda repressor-operator complex', *Journal of molecular biology*, 227(1), pp. 177–196.

Becher, P. G. *et al.* (2020) 'Developmentally regulated volatiles geosmin and 2-methylisoborneol attract a soil arthropod to Streptomyces bacteria promoting spore dispersal', *Nature microbiology*, 5(6), pp. 821–829.

Bennett, J. A. *et al.* (2009) 'Medium-Dependent Phenotypes of Streptomyces coelicolor with Mutations in ftsI or ftsW', *Journal of Bacteriology*, pp. 661–664. doi: 10.1128/jb.01048-08.

Benson, A. K. and Haldenwang, W. G. (1993) 'Bacillus subtilis sigma B is regulated by a binding protein (RsbW) that blocks its association with core RNA polymerase', *Proceedings of the National Academy of Sciences of the United States of America*, 90(6), pp. 2330–2334.

Bentley, S. D. *et al.* (2002) 'Complete genome sequence of the model actinomycete Streptomyces coelicolor A3(2)', *Nature*, 417(6885), pp. 141–147.

Bibb, M. J. *et al.* (2012) 'Expression of the chaplin and rodlin hydrophobic sheath proteins in Streptomyces venezuelae is controlled by σBldN and a cognate anti-sigma factor, RsbN', *Molecular microbiology*, 84(6), pp. 1033–1049.

Bibb, M. J. and Buttner, M. J. (2003) 'The Streptomyces coelicolor Developmental Transcription Factor BldN Is Synthesized as a Proprotein', *Journal of bacteriology*, 185(7), pp. 2338–2345.

Bibb, M. J., Janssen, G. R. and Ward, J. M. (1985) 'Cloning and analysis of the promoter region of the erythromycin resistance gene (ermE) of Streptomyces erythraeus', *Gene*, 38(1-3), pp. 215–226.

Bibb, M. J., Molle, V. and Buttner, M. J. (2000) 'sigma(BldN), an extracytoplasmic function RNA polymerase sigma factor required for aerial mycelium formation in Streptomyces coelicolor A3(2)', *Journal of bacteriology*, 182(16), pp. 4606–4616.

Bignell, D. R. *et al.* (2000) 'Study of the bldG locus suggests that an anti-anti-sigma factor and an anti-sigma factor may be involved in Streptomyces coelicolor antibiotic production and sporulation', *Microbiology*, 146 (Pt 9), pp. 2161–2173.

Bignell, D. R. D. *et al.* (2003) 'The putative anti-anti-sigma factor BldG is post-translationally modified by phosphorylation in Streptomyces coelicolor', *FEMS microbiology letters*, 225(1), pp. 93–99.

Bishop, A. *et al.* (2004) 'Systematic Insertional Mutagenesis of a Streptomycete Genome: A Link Between Osmoadaptation and Antibiotic Production', *Genome Research*, pp. 893–900. doi: 10.1101/gr.1710304.

Blin, K. *et al.* (2019) 'antiSMASH 5.0: updates to the secondary metabolite genome mining pipeline', *Nucleic Acids Research*, pp. W81–W87. doi: 10.1093/nar/gkz310.

van den Bogaart, G. *et al.* (2007) 'Protein mobility and diffusive barriers in Escherichia coli: consequences of osmotic stress', *Molecular microbiology*, 64(3), pp. 858–871.

Boubakri, H. *et al.* (2015) 'The Absence of Pupylation (Prokaryotic Ubiquitin-Like Protein Modification) Affects Morphological and Physiological Differentiation in Streptomyces coelicolor', *Journal of bacteriology*, 197(21), pp. 3388–3399.

Bouillet, S. *et al.* (2016) 'The General Stress Response σS Is Regulated by a Partner Switch in the Gram-negative Bacterium Shewanella oneidensis', *The Journal of biological chemistry*, 291(50), pp. 26151–26163.

Bouillet, S. *et al.* (2017) 'Protection of the general stress response σ factor by the CrsR regulator allows a rapid and efficient adaptation of', *The Journal of biological chemistry*, 292(36), pp. 14921–14928.

Bouillet, S. *et al.* (2018) 'Regulation of σ factors by conserved partner switches controlled by divergent signalling systems', *Environmental Microbiology Reports*, pp. 127–139. doi: 10.1111/1758-2229.12620.

Bradford, M. M. (1976) 'A rapid and sensitive method for the quantitation of microgram quantities of protein utilizing the principle of protein-dye binding', *Analytical biochemistry*, 72, pp. 248–254.

Brady, A. *et al.* (2021) 'Molecular Basis of Lysis-Lysogeny Decisions in Gram-Positive Phages', *Annual review of microbiology*, 75, pp. 563–581.

Bucca, G. *et al.* (2009) 'Development and application of versatile high density microarrays for genome-wide analysis of Streptomyces coelicolor: characterization of the HspR regulon', *Genome biology*, 10(1), p. R5.

Bush, M. J. *et al.* (2013) 'Genes required for aerial growth, cell division, and chromosome segregation are targets of WhiA before sporulation in Streptomyces venezuelae', *mBio*, 4(5), pp. e00684–13.

Bush, M. J. *et al.* (2015) 'c-di-GMP signalling and the regulation of developmental transitions in streptomycetes', *Nature reviews. Microbiology*, 13(12), pp. 749–760.

Bush, M. J. *et al.* (2016) 'Genome-Wide Chromatin Immunoprecipitation Sequencing Analysis Shows that WhiB Is a Transcription Factor That Cocontrols Its Regulon with WhiA To Initiate Developmental Cell Division in Streptomyces', *mBio*, 7(2), pp. e00523–16.

Bush, M. J. *et al.* (2017) 'Multi-layered inhibition of Streptomyces development: BldO is a dedicated repressor of whiB', *Molecular microbiology*, 104(5), pp. 700–711.

Bush, M. J. (2018) 'The actinobacterial WhiB-like (Wbl) family of transcription factors', *Molecular microbiology*, 110(5), pp. 663–676.

Bush, M. J. *et al.* (2019) 'BldC Delays Entry into Development To Produce a Sustained Period of Vegetative Growth in Streptomyces venezuelae', *mBio*, 10(1). doi: 10.1128/mBio.02812-18.

Bush, M.J. *et al.* (2022) 'Hyphal compartmentalization and sporulation in Streptomyces require the conserved cell division protein SepX', *Nature communications*, 13(1), p. 71.

Butala, M., Žgur-Bertok, D. and Busby, S. J. W. (2009) 'The bacterial LexA transcriptional repressor', *Cellular and Molecular Life Sciences*, pp. 82–93. doi: 10.1007/s00018-008-8378-6.

Buttner, M. J., Chater, K. F. and Bibb, M. J. (1990) 'Cloning, disruption, and transcriptional analysis of three RNA polymerase sigma factor genes of Streptomyces coelicolor A3(2)', *Journal of bacteriology*, 172(6), pp. 3367–3378.

Buttner, M. J. and Lewis, C. G. (1992) 'Construction and characterization of Streptomyces coelicolor A3(2) mutants that are multiply deficient in the nonessential hrd-encoded RNA polymerase sigma factors', *Journal of bacteriology*, 174(15), pp. 5165–5167.

Campbell, E. A. *et al.* (2002) 'Crystal structure of the Bacillus stearothermophilus anti-sigma factor SpoIIAB with the sporulation sigma factor SigmaF'. Worldwide Protein Data Bank. doi: 10.2210/pdb1l0o/pdb.

Capstick, D. S. *et al.* (2007) 'SapB and the chaplins: connections between morphogenetic proteins in Streptomyces coelicolor', *Molecular microbiology*, 64(3), pp. 602–613.

Capstick, D. S. *et al.* (2011) 'Dual amyloid domains promote differential functioning of the chaplin proteins during Streptomyces aerial morphogenesis', *Proceedings of the National Academy of Sciences of the United States of America*, 108(24), pp. 9821–9826.

Chai, Y. *et al.* (2010) 'An epigenetic switch governing daughter cell separation in Bacillus subtilis', *Genes & development*, 24(8), pp. 754–765.

Chandra, G. and Chater, K. F. (2014) 'Developmental biology of Streptomyces from the perspective of 100 actinobacterial genome sequences', *FEMS microbiology reviews*, 38(3), pp. 345–379.

Chater, K. F. (1972) 'A morphological and genetic mapping study of white colony mutants of Streptomyces coelicolor', *Journal of general microbiology*, 72(1), pp. 9–28.

Chater, K. F. *et al.* (1989) 'The developmental fate of S. coelicolor hyphae depends upon a gene product homologous with the motility sigma factor of B. subtilis', *Cell*, 59(1), pp. 133–143.

Chater, K. F. (2006) 'Streptomyces inside-out: a new perspective on the bacteria that provide us with antibiotics', *Philosophical transactions of the Royal Society of London. Series B, Biological sciences*, 361(1469), pp. 761–768.

Chater, K. F. and Chandra, G. (2006) 'The evolution of development in Streptomyces analysed by genome comparisons', *FEMS microbiology reviews*, 30(5), pp. 651–672.

Chen, C.-C. *et al.* (2003) 'A supramolecular complex in the environmental stress signalling pathway of Bacillus subtilis', *Molecular microbiology*, 49(6), pp. 1657–1669.

Chen, C.-C., Yudkin, M. D. and Delumeau, O. (2004) 'Phosphorylation and RsbX-dependent dephosphorylation of RsbR in the RsbR-RsbS complex of Bacillus subtilis', *Journal of bacteriology*, 186(20), pp. 6830–6836.

Cho, Y. H. *et al.* (2001) 'SigB, an RNA polymerase sigma factor required for osmoprotection and proper differentiation of Streptomyces coelicolor', *Molecular microbiology*, 42(1), pp. 205–214.

Chu, F. *et al.* (2006) 'Targets of the master regulator of biofilm formation in Bacillus subtilis', *Molecular microbiology*, 59(4), pp. 1216–1228.

Cirl, C. *et al.* (2008) ‘Subversion of Toll-like receptor signaling by a unique family of bacterial Toll/interleukin-1 receptor domain–containing proteins’, *Nature Medicine*, pp. 399–406. doi: 10.1038/nm1734.

Claessen, D. *et al.* (2002) ‘Two novel homologous proteins of Streptomyces coelicolor and Streptomyces lividans are involved in the formation of the rodlet layer and mediate attachment to a hydrophobic surface’, *Molecular Microbiology*, pp. 1483–1492. doi: 10.1046/j.1365-2958.2002.02980.x.

Claessen, D. *et al.* (2003) ‘A novel class of secreted hydrophobic proteins is involved in aerial hyphae formation in Streptomyces coelicolor by forming amyloid-like fibrils’, *Genes & development*, 17(14), pp. 1714–1726.

Claessen, D. *et al.* (2004) ‘The formation of the rodlet layer of streptomycetes is the result of the interplay between rodlins and chaplins’, *Molecular microbiology*, 53(2), pp. 433–443.

Cobb, R. E., Wang, Y. and Zhao, H. (2015) ‘High-efficiency multiplex genome editing of Streptomyces species using an engineered CRISPR/Cas system’, *ACS synthetic biology*, 4(6), pp. 723–728.

Colledge, V. L. *et al.* (2011) ‘Structure and organisation of SinR, the master regulator of biofilm formation in Bacillus subtilis’, *Journal of molecular biology*, 411(3), pp. 597–613.

Commichau, F. M. *et al.* (2018) ‘A Delicate Connection: c-di-AMP Affects Cell Integrity by Controlling Osmolyte Transport’, *Trends in microbiology*, 26(3), pp. 175–185.

Conn, H. J. (1948) ‘The most abundant groups of bacteria in soil’, *Bacteriological reviews*, 12(3), pp. 257–273.

Crack, J. C. *et al.* (2009) ‘Characterization of [4Fe-4S]-containing and cluster-free forms of Streptomyces WhiD’, *Biochemistry*, 48(51), pp. 12252–12264.

Dalton, K. A. *et al.* (2007) ‘A novel compartment, the “subapical stem” of the aerial hyphae, is the location of a sigN-dependent, developmentally distinct transcription in Streptomyces coelicolor’, *Molecular microbiology*, 64(3), pp. 719–737.

Daniel, R. A. and Errington, J. (2003) ‘Control of cell morphogenesis in bacteria: two distinct ways to make a rod-shaped cell’, *Cell*, 113(6), pp. 767–776.

Datsenko, K. A. and Wanner, B. L. (2000) ‘One-step inactivation of chromosomal genes in Escherichia coli K-12 using PCR products’, *Proceedings of the National Academy of Sciences of the United States of America*, 97(12), pp. 6640–6645.

Davis, N. K. and Chater, K. F. (1990) ‘Spore colour in Streptomyces coelicolor A3(2) involves the developmentally regulated synthesis of a compound biosynthetically related to polyketide antibiotics’, *Molecular microbiology*, 4(10), pp. 1679–1691.

Davis, N. K. and Chater, K. F. (1992) ‘The Streptomyces coelicolor whiB gene encodes a small transcription factor-like protein dispensable for growth but essential for sporulation’, *Molecular & general genetics: MGG*, 232(3), pp. 351–358.

Decatur, A. L. and Losick, R. (1996) ‘Three sites of contact between the Bacillus subtilis transcription factor sigmaF and its antisigma factor SpoIIAB’, *Genes & development*, 10(18), pp. 2348–2358.

DeMaio, J. *et al.* (1996) ‘A stationary-phase stress-response sigma factor from Mycobacterium tuberculosis’, *Proceedings of the National Academy of Sciences of the United States of America*, 93(7), pp. 2790–2794.

Den Hengst, C. D. *et al.* (2010) 'Genes essential for morphological development and antibiotic production in Streptomyces coelicolor are targets of BldD during vegetative growth', *Molecular microbiology*, 78(2), pp. 361–379.

Derouaux, A. *et al.* (2004) 'Deletion of a cyclic AMP receptor protein homologue diminishes germination and affects morphological development of Streptomyces coelicolor', *Journal of bacteriology*, 186(6), pp. 1893–1897.

Di Berardo, C. *et al.* (2008) 'Function and redundancy of the chaplin cell surface proteins in aerial hypha formation, rodlet assembly, and viability in Streptomyces coelicolor', *Journal of bacteriology*, 190(17), pp. 5879–5889.

Diederich, B. *et al.* (1994) 'Role of interactions between SpoIIAA and SpoIIAB in regulating cell-specific transcription factor sigma F of Bacillus subtilis', *Genes & development*, 8(21), pp. 2653–2663.

Diederich, B. *et al.* (1994) 'Role of interactions between SpoIIAA and SpoIIAB in regulating cell-specific transcription factor σ F of Bacillus subtilis', *Genes & Development*, pp. 2653–2663. doi: 10.1101/gad.8.21.2653.

Ditkowski, B. *et al.* (2013) 'Dynamic interplay of ParA with the polarity protein, Scy, coordinates the growth with chromosome segregation in Streptomyces coelicolor', *Open biology*, 3(3), p. 130006.

Doroghazi, J. R. and Buckley, D. H. (2014) 'Intraspecies comparison of Streptomyces pratensis genomes reveals high levels of recombination and gene conservation between strains of disparate geographic origin', *BMC genomics*, 15, p. 970.

Dufour, A. and Haldenwang, W. G. (1994) 'Interactions between a Bacillus subtilis anti-sigma factor (RsbW) and its antagonist (RsbV)', *Journal of bacteriology*, 176(7), pp. 1813–1820.

Duncan, L. and Losick, R. (1993) 'SpoIIAB is an anti-sigma factor that binds to and inhibits transcription by regulatory protein sigma F from Bacillus subtilis', *Proceedings of the National Academy of Sciences of the United States of America*, 90(6), pp. 2325–2329.

Dutta, R. and Inouye, M. (2000) 'GHKL, an emergent ATPase/kinase superfamily', *Trends in biochemical sciences*, 25(1), pp. 24–28.

Eccleston, M. *et al.* (2002) 'Structural and genetic analysis of the BldB protein of Streptomyces coelicolor', *Journal of bacteriology*, 184(15), pp. 4270–4276.

Eccleston, M. *et al.* (2006) 'Critical residues and novel effects of overexpression of the Streptomyces coelicolor developmental protein BldB: evidence for a critical interacting partner', *Journal of bacteriology*, 188(23), pp. 8189–8195.

Ehrlich, J. *et al.* (1948) 'Streptomyces venezuelae, n. sp., the source of chloromycetin', *Journal of bacteriology*, 56(4), pp. 467–477.

Elliot, M. A. *et al.* (2003) 'The chaplins: a family of hydrophobic cell-surface proteins involved in aerial mycelium formation in Streptomyces coelicolor', *Genes & development*, 17(14), pp. 1727–1740.

Elliot, M. A. and Leskiw, B. K. (1999) 'The BldD protein from Streptomyces coelicolor is a DNA-binding protein', *Journal of bacteriology*, 181(21), pp. 6832–6835.

Essuman, K. *et al.* (2018) 'TIR Domain Proteins Are an Ancient Family of NAD-Consuming Enzymes', *Current biology: CB*, 28(3), pp. 421–430.e4.

Facey, P. D. *et al.* (2009) 'Streptomyces coelicolor Dps-like proteins: differential dual roles in response to stress during vegetative growth and in nucleoid condensation during reproductive cell division', *Molecular microbiology*, 73(6), pp. 1186–1202.

Fernández Martínez, L. *et al.* (2009) 'Osmoregulation in Streptomyces coelicolor: modulation of SigB activity by OsaC', *Molecular microbiology*, 71(5), pp. 1250–1262.

Fernández-Moreno, M. A. *et al.* (1991) 'The act cluster contains regulatory and antibiotic export genes, direct targets for translational control by the bldA tRNA gene of Streptomyces', *Cell*, 66(4), pp. 769–780.

Fernández-Moreno, M. A. *et al.* (1992) 'abaA, a new pleiotropic regulatory locus for antibiotic production in Streptomyces coelicolor', *Journal of bacteriology*, 174(9), pp. 2958–2967.

Flärdh, K. (2003) 'Essential role of DivIVA in polar growth and morphogenesis in Streptomyces coelicolor A3(2)', *Molecular microbiology*, 49(6), pp. 1523–1536.

Flärdh, K. and Buttner, M. J. (2009) 'Streptomyces morphogenetics: dissecting differentiation in a filamentous bacterium', *Nature reviews. Microbiology*, 7(1), pp. 36–49.

Flärdh, K., Findlay, K. C. and Chater, K. F. (1999) 'Association of early sporulation genes with suggested developmental decision points in Streptomyces coelicolor A3(2)', *Microbiology*, 145 (Pt 9), pp. 2229–2243.

Flärdh, K. and McCormick, J. R. (2017) 'The Streptomyces O-B one connection: a force within layered repression of a key developmental decision', *Molecular microbiology*, 104(5), pp. 695–699.

Flett, F., Mersinias, V. and Smith, C. P. (1997) 'High efficiency intergeneric conjugal transfer of plasmid DNA from Escherichia coli to methyl DNA-restricting streptomycetes', *FEMS microbiology letters*, 155(2), pp. 223–229.

Fraikin, N., Goormaghtigh, F. and Van Melderen, L. (2020) 'Type II Toxin-Antitoxin Systems: Evolution and Revolutions', *Journal of bacteriology*, 202(7). doi: 10.1128/JB.00763-19.

Fröjd, M. J. and Flärdh, K. (2019) 'Apical assemblies of intermediate filament-like protein FilP are highly dynamic and affect polar growth determinant DivIVA in Streptomyces venezuelae', *Molecular microbiology*, 112(1), pp. 47–61.

Fuchino, K. *et al.* (2013) 'Dynamic gradients of an intermediate filament-like cytoskeleton are recruited by a polarity landmark during apical growth', *Proceedings of the National Academy of Sciences of the United States of America*, 110(21), pp. E1889–97.

Fuchino, K. *et al.* (2017) 'Cell-Biological Studies of Osmotic Shock Response in Streptomyces spp', *Journal of bacteriology*, 199(1). doi: 10.1128/JB.00465-16.

Fyans, J. K. *et al.* (2013) 'The ESX/type VII secretion system modulates development, but not virulence, of the plant pathogenStreptomyces scabies', *Molecular Plant Pathology*, pp. 119–130. doi: 10.1111/j.1364-3703.2012.00835.x.

Gallagher, K. A. *et al.* (2020) 'c-di-GMP Arms an Anti-σ to Control Progression of Multicellular Differentiation in Streptomyces', *Molecular cell*, 77(3), pp. 586–599.e6.

Gaskell, A. A. *et al.* (2007) 'RsmA is an anti-sigma factor that modulates its activity through a [2Fe-2S] cluster cofactor', *The Journal of biological chemistry*, 282(43), pp. 31812–31820.

Gaur, N. K., Dubnau, E. and Smith, I. (1986) 'Characterization of a cloned Bacillus subtilis gene that inhibits sporulation in multiple copies', *Journal of bacteriology*, 168(2), pp. 860–869.

Gaur, N. K., Oppenheim, J. and Smith, I. (1991) 'The Bacillus subtilis sin gene, a regulator of alternate developmental processes, codes for a DNA-binding protein', *Journal of bacteriology*, 173(2), pp. 678–686.

Gehring, A. M. *et al.* (2000) 'Genomewide insertional mutagenesis in Streptomyces coelicolor reveals additional genes involved in morphological differentiation', *Proceedings of the National Academy of Sciences of the United States of America*, 97(17), pp. 9642–9647.

Gerber, N. N. (1967) 'Geosmin, an earthy-smelling substance isolated from actinomycetes', *Biotechnology and bioengineering*, 9(3), pp. 321–327.

Gerdes, K., Christensen, S. K. and Løbner-Olesen, A. (2005) 'Prokaryotic toxin-antitoxin stress response loci', *Nature reviews. Microbiology*, 3(5), pp. 371–382.

Gibson, D. G. *et al.* (2009) 'Enzymatic assembly of DNA molecules up to several hundred kilobases', *Nature methods*, 6(5), pp. 343–345.

Girard, G. *et al.* (2014) 'Analysis of novel kitasatosporae reveals significant evolutionary changes in conserved developmental genes between Kitasatospora and Streptomyces', *Antonie van Leeuwenhoek*, 106(2), pp. 365–380.

Godinez, O. *et al.* (2015) 'Targeting the Osmotic Stress Response for Strain Improvement of an Industrial Producer of Secondary Metabolites', *Journal of microbiology and biotechnology*, 25(11), pp. 1787–1795.

Gomez-Escribano, J. P. *et al.* (2021) 'Streptomyces venezuelae NRRL B-65442: genome sequence of a model strain used to study morphological differentiation in filamentous actinobacteria', *Journal of Industrial Microbiology and Biotechnology*. doi: 10.1093/jimb/kuab035.

González-Cerón, G., Miranda-Olivares, O. J. and Servín-González, L. (2009) 'Characterization of the methyl-specific restriction system of Streptomyces coelicolor A3(2) and of the role played by laterally acquired nucleases', *FEMS microbiology letters*, 301(1), pp. 35–43.

Gray, D. I., Gooday, G. W. and Prosser, J. I. (1990) 'Apical hyphal extension in Streptomyces coelicolor A3(2)', *Journal of general microbiology*, 136(6), pp. 1077–1084.

Grinberg, I. *et al.* (2006) 'The Streptomyces NrdR transcriptional regulator is a Zn ribbon/ATP cone protein that binds to the promoter regions of class Ia and class II ribonucleotide reductase operons', *Journal of bacteriology*, 188(21), pp. 7635–7644.

Gubbens, J. *et al.* (2017) 'Identification of glucose kinase-dependent and -independent pathways for carbon control of primary metabolism, development and antibiotic production in Streptomyces coelicolor by quantitative proteomics', *Molecular microbiology*, 105(1), p. 175.

Guindon, S. *et al.* (2010) 'New algorithms and methods to estimate maximum-likelihood phylogenies: assessing the performance of PhyML 3.0', *Systematic biology*, 59(3), pp. 307–321.

Gust, B. *et al.* (2003) 'PCR-targeted Streptomyces gene replacement identifies a protein domain needed for biosynthesis of the sesquiterpene soil odor geosmin', *Proceedings of the National Academy of Sciences of the United States of America*, 100(4), pp. 1541–1546.

Haldenwang, W. G. and Losick, R. (1979) 'A modified RNA polymerase transcribes a cloned gene under sporulation control in Bacillus subtilis', *Nature*, 282(5736), pp. 256–260.

Hanahan, D. (1983) 'Studies on transformation of Escherichia coli with plasmids', *Journal of Molecular Biology*, pp. 557–580. doi: 10.1016/s0022-2836(83)80284-8.

Harasym, M. *et al.* (1990) 'The Streptomyces coelicolor A3(2) bldB region contains at least two genes involved in morphological development', *Journal of general microbiology*, 136(8), pp. 1543–1550.

Haswell, E. S., Phillips, R. and Rees, D. C. (2011) 'Mechanosensitive Channels: What Can They Do and How Do They Do It?', *Structure*, pp. 1356–1369. doi: 10.1016/j.str.2011.09.005.

Hecker, M., Pané-Farré, J. and Uwe, V. (2007) 'SigB-Dependent General Stress Response in Bacillus subtilis and Related Gram-Positive Bacteria', *Annual Review of Microbiology*, pp. 215–236. doi: 10.1146/annurev.micro.61.080706.093445.

Heijna, M. C. R. *et al.* (2007) 'Spherulitic growth of hen egg-white lysozyme crystals', *The journal of physical chemistry. B*, 111(7), pp. 1567–1573.

Hempel, A. M. *et al.* (2008) 'Assemblies of DivIVA Mark Sites for Hyphal Branching and Can Establish New Zones of Cell Wall Growth in Streptomyces coelicolor', *Journal of Bacteriology*, pp. 7579–7583. doi: 10.1128/jb.00839-08.

Hempel, A. M. *et al.* (2012) 'The Ser/Thr protein kinase AfsK regulates polar growth and hyphal branching in the filamentous bacteria Streptomyces', *Proceedings of the National Academy of Sciences of the United States of America*, 109(35), pp. E2371–9.

Herrick, J. and Sclavi, B. (2007) 'Ribonucleotide reductase and the regulation of DNA replication: an old story and an ancient heritage', *Molecular Microbiology*, pp. 22–34. doi: 10.1111/j.1365-2958.2006.05493.x.

Hindra *et al.* (2014) 'Complex intra-operonic dynamics mediated by a small RNA in Streptomyces coelicolor', *PloS one*, 9(1), p. e85856.

Holmes, N. A. *et al.* (2013) 'Coiled-coil protein Scy is a key component of a multiprotein assembly controlling polarized growth in Streptomyces', *Proceedings of the National Academy of Sciences of the United States of America*, 110(5), pp. E397–406.

Homerova, D. *et al.* (2012) 'Regulation of an alternative sigma factor σI by a partner switching mechanism with an anti-sigma factor PrsI and an anti-anti-sigma factor ArsI in Streptomyces coelicolor A3(2)', *Gene*, pp. 71–80. doi: 10.1016/j.gene.2011.11.011.

Hong, H.-J. *et al.* (2005) 'The role of the novel Fem protein VanK in vancomycin resistance in Streptomyces coelicolor', *The Journal of biological chemistry*, 280(13), pp. 13055–13061.

Hopwood, D. A. (1967) ‘Genetic analysis and genome structure in Streptomyces coelicolor’, *Bacteriological reviews*, 31(4), pp. 373–403.

Hopwood, D. A. and Wright, H. M. (1983) ‘CDA is a new chromosomally-determined antibiotic from Streptomyces coelicolor A3(2)’, *Journal of general microbiology*, 129(12), pp. 3575–3579.

Ho, Y. S. J., Burden, L. and Hurley, J. (2001) ‘Structure of the GAF domain, a ubiquitous signaling motif and a new class of cyclic GMP receptor’, *The EMBO Journal*, pp. 1483–1483. doi: 10.1093/emboj/20.6.1483.

Hunt, A. C. *et al.* (2005) ‘The bldC developmental locus of Streptomyces coelicolor encodes a member of a family of small DNA-binding proteins related to the DNA-binding domains of the MerR family’, *Journal of bacteriology*, 187(2), pp. 716–728.

Hutchings, M. I., Truman, A. W. and Wilkinson, B. (2019) ‘Antibiotics: past, present and future’, *Current Opinion in Microbiology*, pp. 72–80. doi: 10.1016/j.mib.2019.10.008.

Hwang, S. *et al.* (2021) ‘Elucidating the Regulatory Elements for Transcription Termination and Posttranscriptional Processing in the Streptomyces clavuligerus Genome’, *mSystems*, 6(3). doi: 10.1128/mSystems.01013-20.

Jakimowicz, P. *et al.* (2005) ‘Evidence That the Streptomyces Developmental Protein WhiD, a Member of the WhiB Family, Binds a [4Fe-4S] Cluster’, *Journal of Biological Chemistry*, pp. 8309–8315. doi: 10.1074/jbc.m412622200.

Jones, S. E. *et al.* (2017) ‘Streptomyces exploration is triggered by fungal interactions and volatile signals’, *eLife*. doi: 10.7554/elife.21738.

Jones, S. E. *et al.* (2019) ‘Streptomyces Volatile Compounds Influence Exploration and Microbial Community Dynamics by Altering Iron Availability’, *mBio*. doi: 10.1128/mbio.00171-19.

Kaiser, B. K. and Stoddard, B. L. (2011) ‘DNA recognition and transcriptional regulation by the WhiA sporulation factor’, *Scientific reports*, 1, p. 156.

Kang, C. M., Vijay, K. and Price, C. W. (1998) ‘Serine kinase activity of a Bacillus subtilis switch protein is required to transduce environmental stress signals but not to activate its target PP2C phosphatase’, *Molecular microbiology*, 30(1), pp. 189–196.

Karimova, G. *et al.* (1998) ‘A bacterial two-hybrid system based on a reconstituted signal transduction pathway’, *Proceedings of the National Academy of Sciences*, 95(10), pp. 5752–5756.

Karimova, G., Ullmann, A. and Ladant, D. (2000) ‘Bordetella pertussis adenylate cyclase toxin as a tool to analyze molecular interactions in a bacterial two-hybrid system’, *International journal of medical microbiology: IJMM*, 290(4-5), pp. 441–445.

Karoonuthaisiri, N. *et al.* (2005) ‘Regional organization of gene expression in Streptomyces coelicolor’, *Gene*, 353(1), pp. 53–66.

Kearns, D. B. *et al.* (2004) ‘A master regulator for biofilm formation by Bacillus subtilis’, *Molecular Microbiology*, pp. 739–749. doi: 10.1111/j.1365-2958.2004.04440.x.

Keijser, B. J. F. *et al.* (2002) ‘Developmental regulation of the Streptomyces lividans ram genes: involvement of RamR in regulation of the ramCSAB operon’, *Journal of bacteriology*, 184(16), pp. 4420–4429.

Kelemen, G. H. *et al.* (1996) 'The positions of the sigma-factor genes, whiG and sigF, in the hierarchy controlling the development of spore chains in the aerial hyphae of Streptomyces coelicolor A3(2)', *Molecular Microbiology*, pp. 593–603. doi: 10.1111/j.1365-2958.1996.tb02567.x.

Kelemen, G. H. *et al.* (1998) 'Developmental regulation of transcription of whiE, a locus specifying the polyketide spore pigment in Streptomyces coelicolor A3 (2)', *Journal of bacteriology*, 180(9), pp. 2515–2521.

Kelemen, G. H. *et al.* (2001) 'A connection between stress and development in the multicellular prokaryote Streptomyces coelicolor A3(2)', *Molecular microbiology*, 40(4), pp. 804–814.

Kelemen, G. H. and Buttner, M. J. (1998) 'Initiation of aerial mycelium formation in Streptomyces', *Current opinion in microbiology*, 1(6), pp. 656–662.

Kieser, T. *et al.* (2000) *Practical Streptomyces Genetics*.

Kim, E. S. *et al.* (2008) 'A possible extended family of regulators of sigma factor activity in Streptomyces coelicolor', *Journal of bacteriology*, 190(22), pp. 7559–7566.

Kim, T. J., Gaidenko, T. A. and Price, C. W. (2004) 'In Vivo Phosphorylation of Partner Switching Regulators Correlates with Stress Transmission in the Environmental Signaling Pathway of Bacillus subtilis', *Journal of bacteriology*, 186(18), pp. 6124–6132.

Kim, Y. J. *et al.* (2008) 'Acidic pH shock induces the expressions of a wide range of stress-response genes', *BMC genomics*, 9, p. 604.

King-Scott, J. *et al.* (2011) 'Structural characterization of the multidomain regulatory protein Rv1364c from Mycobacterium tuberculosis', *Structure* , 19(1), pp. 56–69.

Kirby, R. *et al.* (2012) 'Draft genome sequence of the human pathogen Streptomyces somaliensis, a significant cause of actinomycetoma', *Journal of bacteriology*, 194(13), pp. 3544–3545.

Kirby, R. and Hopwood, D. A. (1977) 'Genetic determination of methylenomycin synthesis by the SCP1 plasmid of Streptomyces coelicolor A3(2)', *Journal of general microbiology*, 98(1), pp. 239–252.

Knizewski, L. and Ginalski, K. (2007) 'Bacterial DUF199/COG1481 proteins including sporulation regulator WhiA are distant homologs of LAGLIDADG homing endonucleases that retained only DNA binding', *Cell cycle* , 6(13), pp. 1666–1670.

Kodani, S. *et al.* (2004) 'The SapB morphogen is a lantibiotic-like peptide derived from the product of the developmental gene ramS in Streptomyces coelicolor', *Proceedings of the National Academy of Sciences of the United States of America*, 101(31), pp. 11448–11453.

Komatsu, M. *et al.* (2003) 'Cloning of the conserved regulatory operon by its aerial mycelium-inducing activity in an amfR mutant of Streptomyces griseus', *Gene*, pp. 79–89. doi: 10.1016/s0378-1119(03)00405-0.

Komatsu, M. *et al.* (2006) 'Proteins encoded by the conservon of Streptomyces coelicolor A3(2) comprise a membrane-associated heterocomplex that resembles eukaryotic G protein-coupled regulatory system', *Molecular microbiology*, 62(6), pp. 1534–1546.

Konopka, M. C. *et al.* (2009) 'Cytoplasmic protein mobility in osmotically stressed Escherichia coli', *Journal of bacteriology*, 191(1), pp. 231–237.

Koo, B. M. *et al.* (2017) 'Construction and Analysis of Two Genome-Scale Deletion Libraries for Bacillus subtilis', *Cell systems*, 4(3), pp. 291–305.e7.

Koprowski, P. *et al.* (2015) 'Cytoplasmic Domain of MscS Interacts with Cell Division Protein FtsZ: A Possible Non-Channel Function of the Mechanosensitive Channel in Escherichia Coli', *PloS one*, 10(5), p. e0127029.

Kormanec, J. *et al.* (1999) 'A new gene, sigG, encoding a putative alternative sigma factor of Streptomyces coelicolor A3(2)', *FEMS microbiology letters*, 172(2), pp. 153–158.

Kormanec, J. *et al.* (2000) 'Identification and transcriptional characterization of the gene encoding the stress-response sigma factor sigma(H) in streptomyces coelicolor A3(2)', *FEMS microbiology letters*, 189(1), pp. 31–38.

Kormanec, J. and Sevcikova, B. (2002) 'The stress-response sigma factor σH controls the expression of ssgB, a homologue of the sporulation-specific cell division gene ssgA, in Streptomyces coelicolor A3(2)', *Molecular Genetics and Genomics*, pp. 536–543. doi: 10.1007/s00438-002-0687-0.

Kozlowski, L. P. (2017) 'Proteome-pI: proteome isoelectric point database', *Nucleic acids research*, 45(D1), pp. D1112–D1116.

Labeda, D. P. *et al.* (2017) 'Phylogenetic relationships in the family Streptomycetaceae using multi-locus sequence analysis', *Antonie van Leeuwenhoek*, 110(4), pp. 563–583.

Lal, D. *et al.* (2016) 'Codon usage bias in phylum Actinobacteria: relevance to environmental adaptation and host pathogenicity', *Research in microbiology*, 167(8), pp. 669–677.

Lambert, S. *et al.* (2014) 'Altered desferrioxamine-mediated iron utilization is a common trait of bald mutants of Streptomyces coelicolor', *Metallomics: integrated biometal science*, 6(8), pp. 1390–1399.

Langmead, B. and Salzberg, S. L. (2012) 'Fast gapped-read alignment with Bowtie 2', *Nature methods*, 9(4), pp. 357–359.

Latoscha, A. *et al.* (2020) 'c-di-AMP hydrolysis by the phosphodiesterase AtaC promotes differentiation of multicellular bacteria', *Proceedings of the National Academy of Sciences of the United States of America*, 117(13), pp. 7392–7400.

Lee, E.-J. *et al.* (2004) 'Regulation of σB by an anti- and an anti-anti-sigma factor in Streptomyces coelicolor in response to osmotic stress', *Journal of bacteriology*, 186(24), pp. 8490–8498.

Lee, E.-J. *et al.* (2005) 'A master regulator σB governs osmotic and oxidative response as well as differentiation via a network of sigma factors in Streptomyces coelicolor', *Molecular microbiology*, 57(5), pp. 1252–1264.

Leskiw, B. K. *et al.* (1991) 'TTA codons in some genes prevent their expression in a class of developmental, antibiotic-negative, Streptomyces mutants', *Proceedings of the National Academy of Sciences*, 88(6), pp. 2461–2465.

Leskiw, B. K. and Mah, R. (1995) 'The bldA-encoded tRNA is poorly expressed in the bldI mutant of Streptomyces coelicolor A3(2)', *Microbiology*, 141 (Pt 8), pp. 1921–1926.

Letunic, I. and Bork, P. (2019) ‘Interactive Tree Of Life (iTOL) v4: recent updates and new developments’, *Nucleic acids research*. doi: 10.1093/nar/gkz239.

Lewis, R. J. *et al.* (1998) ‘An evolutionary link between sporulation and prophage induction in the structure of a repressor:anti-repressor complex’, *Journal of molecular biology*, 283(5), pp. 907–912.

Liao, Y., Smyth, G. K. and Shi, W. (2013) ‘The Subread aligner: fast, accurate and scalable read mapping by seed-and-vote’, *Nucleic acids research*, 41(10), p. e108.

Liebal, U. W. *et al.* (2013) ‘Simulations of stressosome activation emphasize allosteric interactions between RsbR and RsbT’, *BMC systems biology*, 7, p. 3.

Li, L. *et al.* (2019) ‘Actinomadura craniellae sp. nov., isolated from a marine sponge in the South China Sea’, *International journal of systematic and evolutionary microbiology*, 69(4), pp. 1207–1212.

Li, M.-S. *et al.* (2004) ‘Increased transcription of a potential sigma factor regulatory gene Rv1364c in Mycobacterium bovis BCG while residing in macrophages indicates use of alternative promoters’, *FEMS microbiology letters*, 233(2), pp. 333–339.

Liu, X. *et al.* (2019) ‘Overexpression of the diguanylate cyclase CdgD blocks developmental transitions and antibiotic biosynthesis in Streptomyces coelicolor’, *Science China. Life sciences*, 62(11), pp. 1492–1505.

Liu, Y. *et al.* (2020) ‘Structural Insights Into the Transcriptional Regulation of HigBA Toxin–Antitoxin System by Antitoxin HigA in Pseudomonas aeruginosa’, *Frontiers in Microbiology*. doi: 10.3389/fmicb.2019.03158.

Loening, U. E. (1968) ‘Molecular weights of ribosomal RNA in relation to evolution’, *Journal of molecular biology*, 38(3), pp. 355–365.

Loria, R. *et al.* (1997) ‘Plant pathogenicity in the genus Streptomyces’, *Plant disease*, 81(8), pp. 836–846.

Lucet, I. *et al.* (2000) ‘Direct interaction between the cell division protein FtsZ and the cell differentiation protein SpoIIE’, *The EMBO journal*, 19(7), pp. 1467–1475.

Lun, A. T. L., Chen, Y. and Smyth, G. K. (2016) ‘It’s DE-licious: A Recipe for Differential Expression Analyses of RNA-seq Experiments Using Quasi-Likelihood Methods in edgeR’, *Methods in Molecular Biology*, pp. 391–416. doi: 10.1007/978-1-4939-3578-9_19.

Lu, Y. *et al.* (2011) ‘An orphan histidine kinase, OhkA, regulates both secondary metabolism and morphological differentiation in Streptomyces coelicolor’, *Journal of bacteriology*, 193(12), pp. 3020–3032.

MacNeil, D. J. *et al.* (1992) ‘Analysis of Streptomyces avermitilis genes required for avermectin biosynthesis utilizing a novel integration vector’, *Gene*, 111(1), pp. 61–68.

Magnin, T. *et al.* (1996) ‘Establishing differential gene expression in sporulating Bacillus subtilis: phosphorylation of SpoIIAA (anti-anti-sigmaF) alters its conformation and prevents formation of a SpoIIAA/SpoIIAB/ADP complex’, *Molecular microbiology*, 19(4), pp. 901–907.

Ma, H. and Kendall, K. (1994) ‘Cloning and analysis of a gene cluster from Streptomyces coelicolor that causes accelerated aerial mycelium formation in Streptomyces lividans’, *Journal of bacteriology*, 176(12), pp. 3800–3811.

Makarova, K. S., Wolf, Y. I. and Koonin, E. V. (2009) 'Comprehensive comparative-genomic analysis of type 2 toxin-antitoxin systems and related mobile stress response systems in prokaryotes', *Biology direct*, 4, p. 19.

Malpartida, F. and Hopwood, D. A. (1984) 'Molecular cloning of the whole biosynthetic pathway of a Streptomyces antibiotic and its expression in a heterologous host', *Nature*, 309(5967), pp. 462–464.

Mandic-Mulec, I., Doukhan, L. and Smith, I. (1995) 'The Bacillus subtilis SinR protein is a repressor of the key sporulation gene spo0A', *Journal of bacteriology*, 177(16), pp. 4619–4627.

Mao, X.-M., Zhou, Z., Cheng, L.-Y., *et al.* (2009) 'Involvement of SigT and RstA in the differentiation of Streptomyces coelicolor', *FEBS letters*, 583(19), pp. 3145–3150.

Mao, X.-M., Zhou, Z., Hou, X.-P., *et al.* (2009) 'Reciprocal regulation between SigK and differentiation programs in Streptomyces coelicolor', *Journal of bacteriology*, 191(21), pp. 6473–6481.

Marles-Wright, J. *et al.* (2008) 'Molecular architecture of the "stressosome," a signal integration and transduction hub', *Science*, 322(5898), pp. 92–96.

Marton, E. (2008) 'Investigation of the BldB homologues of Streptomyces coelicolor: regulators of development and antibiotic production', M.Sc Thesis, McMaster University, Toronto, Canada

Mazurakova, V. *et al.* (2006) 'Cascade of sigma factors in streptomycetes: identification of a new extracytoplasmic function sigma factor sigmaJ that is under the control of the stress-response sigma factor sigmaH in Streptomyces coelicolor A3(2)', *Archives of microbiology*, 186(6), pp. 435–446.

McCormick, J. R. *et al.* (1994) 'Growth and viability of Streptomyces coelicolor mutant for the cell division gene ftsZ', *Molecular microbiology*, 14(2), pp. 243–254.

McDonnell, G. E. *et al.* (1994) 'Genetic control of bacterial suicide: regulation of the induction of PBSX in Bacillus subtilis', *Journal of bacteriology*, 176(18), pp. 5820–5830.

McDonnell, G. E. and McConnell, D. J. (1994) 'Overproduction, isolation, and DNA-binding characteristics of Xre, the repressor protein from the Bacillus subtilis defective prophage PBSX', *Journal of bacteriology*, 176(18), pp. 5831–5834.

McLean, T. C. *et al.* (2019) 'Sensing and responding to diverse extracellular signals: an updated analysis of the sensor kinases and response regulators of Streptomyces species', *Microbiology*, pp. 929–952. doi: 10.1099/mic.0.000817.

Mendez, C. and Chater, K. F. (1987) 'Cloning of whiG, a gene critical for sporulation of Streptomyces coelicolor A3(2)', *Journal of bacteriology*, 169(12), pp. 5715–5720.

Merrick, M. J. (1976) 'A morphological and genetic mapping study of bald colony mutants of Streptomyces coelicolor', *Journal of general microbiology*, 96(2), pp. 299–315.

Mika, J. T. *et al.* (2010) 'Molecular sieving properties of the cytoplasm of Escherichia coli and consequences of osmotic stress', *Molecular microbiology*, 77(1), pp. 200–207.

Mingyar, E. *et al.* (2014) 'The σ(F)-specific anti-sigma factor RsfA is one of the protein kinases that phosphorylates the pleiotropic anti-anti-sigma factor BldG in Streptomyces coelicolor A3(2)', *Gene*, 538(2), pp. 280–287.

Min, K.-T. *et al.* (1993) 'σF, the first compartment-specific transcription factor of B. subtilis, is regulated by an anti-σ factor that is also a protein kinase', *Cell*, 74(4), pp. 735–742.

Mishig-Ochiriin, T. *et al.* (2003) 'Biophysical and structural property of the putative DNA-binding protein, BldB, from Streptomyces lividans', *Biopolymers*, 69(3), pp. 343–350.

Molle, V. *et al.* (2000) 'WhiD and WhiB, homologous proteins required for different stages of sporulation in Streptomyces coelicolor A3(2)', *Journal of bacteriology*, 182(5), pp. 1286–1295.

Molle, V. and Buttner, M. J. (2000) 'Different alleles of the response regulator gene bldM arrest Streptomyces coelicolor development at distinct stages', *Molecular microbiology*, 36(6), pp. 1265–1278.

Morris, A. R. and Visick, K. L. (2013) 'The response regulator SypE controls biofilm formation and colonization through phosphorylation of the syp-encoded regulator SypA in Vibrio fischeri', *Molecular microbiology*, 87(3), pp. 509–525.

Morth, J. P. *et al.* (2004) 'The crystal and solution structure of a putative transcriptional antiterminator from Mycobacterium tuberculosis', *Structure* , 12(9), pp. 1595–1605.

Muok, A. R., Claessen, D. and Briegel, A. (2021) 'Microbial hitchhiking: how Streptomyces spores are transported by motile soil bacteria', *The ISME journal*, 15(9), pp. 2591–2600.

Nguyen, K. T. *et al.* (2002) 'A central regulator of morphological differentiation in the multicellular bacterium Streptomyces coelicolor', *Molecular microbiology*, 46(5), pp. 1223–1238.

Nguyen, K. T. *et al.* (2003) 'Colonial differentiation in Streptomyces coelicolor depends on translation of a specific codon within the adpA gene', *Journal of bacteriology*, 185(24), pp. 7291–7296.

Nieselt, K. *et al.* (2010) 'The dynamic architecture of the metabolic switch in Streptomyces coelicolor', *BMC genomics*, 11, p. 10.

Nodwell, J. R. *et al.* (1999) 'Extracellular complementation and the identification of additional genes involved in aerial mycelium formation in Streptomyces coelicolor', *Genetics*, 151(2), pp. 569–584.

Nodwell, J. R. and Losick, R. (1998) 'Purification of an extracellular signaling molecule involved in production of aerial mycelium by Streptomyces coelicolor', *Journal of bacteriology*, 180(5), pp. 1334–1337.

Nodwell, J. R., McGovern, K. and Losick, R. (1996) 'An oligopeptide permease responsible for the import of an extracellular signal governing aerial mycelium formation in Streptomyces coelicolor', *Molecular microbiology*, 22(5), pp. 881–893.

Noens, E. E. *et al.* (2007) 'Loss of the controlled localization of growth stage-specific cell-wall synthesis pleiotropically affects developmental gene expression in an ssgA mutant of Streptomyces coelicolor', *Molecular Microbiology*, pp. 1244–1259. doi: 10.1111/j.1365-2958.2007.05732.x.

Notredame, C., Higgins, D. G. and Heringa, J. (2000) 'T-Coffee: A novel method for fast and accurate multiple sequence alignment', *Journal of molecular biology*, 302(1), pp. 205–217.

O'Connor, T. J., Kanellis, P. and Nodwell, J. R. (2002) 'The ramC gene is required for morphogenesis in Streptomyces coelicolor and expressed in a cell type-specific manner under the direct control of RamR', *Molecular Microbiology*, pp. 45–57. doi: 10.1046/j.1365-2958.2002.03004.x.

O'Rourke, S. *et al.* (2009) 'Extracellular signalling, translational control, two repressors and an activator all contribute to the regulation of methylenomycin production in Streptomyces coelicolor', *Molecular microbiology*, 71(3), pp. 763–778.

Paget, M. S. *et al.* (1999) 'Evidence that the extracytoplasmic function sigma factor sigmaE is required for normal cell wall structure in Streptomyces coelicolor A3(2)', *Journal of bacteriology*, 181(1), pp. 204–211.

Parashar, A. *et al.* (2009) 'BldG and SCO3548 interact antagonistically to control key developmental processes in Streptomyces coelicolor', *Journal of bacteriology*, 191(8), pp. 2541–2550.

Parida, B. K. *et al.* (2005) 'Interactions of anti-sigma factor antagonists of Mycobacterium tuberculosis in the yeast two-hybrid system', *Tuberculosis* , 85(5-6), pp. 347–355.

Park, C. J. *et al.* (2021) 'Unexpected genomic, biosynthetic and species diversity of Streptomyces bacteria from bats in Arizona and New Mexico, USA', *BMC genomics*, 22(1), p. 247.

Park, D. M. *et al.* (2013) 'The bacterial response regulator ArcA uses a diverse binding site architecture to regulate carbon oxidation globally', *PLoS genetics*, 9(10), p. e1003839.

Park, D. M. and Kiley, P. J. (2014) 'The influence of repressor DNA binding site architecture on transcriptional control', *mBio*, 5(5), pp. e01684–14.

Park, H.-S. *et al.* (2005) 'Accumulation of S-adenosylmethionine induced oligopeptide transporters including BldK to regulate differentiation events in Streptomyces coelicolor M145', *FEMS microbiology letters*, 249(2), pp. 199–206.

Passantino, R., Puglia, A.-M. and Chater, K. (1991) 'Additional copies of the actII regulatory gene induce actinorhodin production in pleiotropic bld mutants of Streptomyces coelicolor A3(2)', *Journal of general microbiology*, 137(9), pp. 2059–2064.

Passot, F.M., Cantlay, S. and Flärdh, K. (2021) 'Protein phosphatase SppA regulates apical growth and dephosphorylates cell polarity determinant DivIVA in Streptomyces coelicolor', *Molecular microbiology*, doi:10.1111/mmi.14856.

Persson, J., Chater, K. F. and Flärdh, K. (2013) 'Molecular and cytological analysis of the expression of Streptomyces sporulation regulatory gene whiH', *FEMS microbiology letters*, 341(2), pp. 96–105.

Pohle, S. *et al.* (2011) 'Biosynthetic gene cluster of the non-ribosomally synthesized cyclodepsipeptide skyllamycin: deciphering unprecedented ways of unusual hydroxylation reactions', *Journal of the American Chemical Society*, 133(16), pp. 6194–6205.

Pope, M. K., Green, B. D. and Westpheling, J. (1996) 'The bld mutants of Streptomyces coelicolor are defective in the regulation of carbon utilization, morphogenesis and cell--cell signalling', *Molecular microbiology*, 19(4), pp. 747–756.

Pope, M. K., Green, B. and Westpheling, J. (1998) ‘The bldB Gene Encodes a Small Protein Required for Morphogenesis, Antibiotic Production, and Catabolite Control in Streptomyces coelicolor’, *Journal of Bacteriology*, pp. 1556–1562. doi: 10.1128/jb.180.6.1556-1562.1998.

Pope, M. K., Green, B. and Westpheling, J. (1998) ‘The bldB gene encodes a small protein required for morphogenesis, antibiotic production, and catabolite control in Streptomyces coelicolor’, *Journal of bacteriology*, 180(6), pp. 1556–1562.

Potúcková, L. *et al.* (1995) ‘A new RNA polymerase sigma factor, sigma F, is required for the late stages of morphological differentiation in Streptomyces spp’, *Molecular microbiology*, 17(1), pp. 37–48.

Preu, J. *et al.* (2012) ‘The sensor region of the ubiquitous cytosolic sensor kinase, PdtaS, contains PAS and GAF domain sensing modules’, *Journal of structural biology*, 177(2), pp. 498–505.

Pullan, S. T. *et al.* (2011) ‘Genome-wide analysis of the role of GlnR in Streptomyces venezuelae provides new insights into global nitrogen regulation in actinomycetes’, *BMC genomics*, 12, p. 175.

Ramakrishnan, G. *et al.* (2015) ‘Enriching the annotation of Mycobacterium tuberculosis H37Rv proteome using remote homology detection approaches: Insights into structure and function’, *Tuberculosis*, pp. 14–25. doi: 10.1016/j.tube.2014.10.009.

Ramesh, M. *et al.* (2021) ‘Intracellular localization of the mycobacterial stressosome complex’, *Scientific reports*, 11(1), p. 10060.

Ramos-León, F. *et al.* (2021) ‘A conserved cell division protein directly regulates FtsZ dynamics in filamentous and unicellular actinobacteria’, *eLife*, 10. doi: 10.7554/eLife.63387.

Review on Antimicrobial Resistance (2014) *Antimicrobial Resistance: Tackling a Crisis for the Health and Wealth of Nations*.

Rezuchová, B., Barák, I. and Kormanec, J. (1997) ‘Disruption of a sigma factor gene, sigF, affects an intermediate stage of spore pigment production in Streptomyces aureofaciens’, *FEMS microbiology letters*, 153(2), pp. 371–377.

Rioseras, B. *et al.* (2018) ‘Quantitative Proteome and Phosphoproteome Analyses of Reveal Proteins and Phosphoproteins Modulating Differentiation and Secondary Metabolism’, *Molecular & cellular proteomics: MCP*, 17(8), pp. 1591–1611.

Rodríguez-García, A. *et al.* (2007) ‘Genome-wide transcriptomic and proteomic analysis of the primary response to phosphate limitation inStreptomyces coelicolor M145 and in a ΔphoP mutant’, *Proteomics*, pp. 2410–2429. doi: 10.1002/pmic.200600883.

Rojas, E. R. and Huang, K. C. (2018) ‘Regulation of microbial growth by turgor pressure’, *Current opinion in microbiology*, 42, pp. 62–70.

Rojas, E. R., Huang, K. C. and Theriot, J. A. (2017) ‘Homeostatic Cell Growth Is Accomplished Mechanically through Membrane Tension Inhibition of Cell-Wall Synthesis’, *Cell systems*, 5(6), pp. 578–590.e6.

Rojas, E., Theriot, J. A. and Huang, K. C. (2014) ‘Response of Escherichia coli growth rate to osmotic shock’, *Proceedings of the National Academy of Sciences of the United States of America*, 111(21), pp. 7807–7812.

Romero-Rodríguez, A., Robledo-Casados, I. and Sánchez, S. (2015) 'An overview on transcriptional regulators in Streptomyces', *Biochimica et biophysica acta*, 1849(8), pp. 1017–1039.

Ruddick, S. M. and Williams, S. T. (1972) 'Studies on the ecology of actinomycetes in soil V. Some factors influencing the dispersal and adsorption of spores in soil', *Soil Biology and Biochemistry*, pp. 93–103. doi: 10.1016/0038-0717(72)90046-6.

Rutledge, P. J. and Challis, G. L. (2015) 'Discovery of microbial natural products by activation of silent biosynthetic gene clusters', *Nature reviews. Microbiology*, 13(8), pp. 509–523.

Ryding, N. J. *et al.* (1998) 'A developmentally regulated gene encoding a repressor-like protein is essential for sporulation in Streptomyces coelicolor A3(2)', *Molecular microbiology*, 29(1), pp. 343–357.

Ryding, N. J. *et al.* (1999) 'New sporulation loci in Streptomyces coelicolor A3(2)', *Journal of bacteriology*, 181(17), pp. 5419–5425.

Santamaría, R. I. *et al.* (2018) 'The XRE-DUF397 Protein Pair, Scr1 and Scr2, Acts as a Strong Positive Regulator of Antibiotic Production in', *Frontiers in microbiology*, 9, p. 2791.

Santos-Beneit, F. *et al.* (2017) 'A mechanism for FtsZ-independent proliferation in Streptomyces', *Nature communications*, 8(1), p. 1378.

Santos, C. L. *et al.* (2009) 'A phylogenomic analysis of bacterial helix-turn-helix transcription factors', *FEMS microbiology reviews*, 33(2), pp. 411–429.

Schatz, A., Bugle, E. and Waksman, S. A. (1944) 'Streptomycin, a Substance Exhibiting Antibiotic Activity Against Gram-Positive and Gram-Negative Bacteria.*', *Experimental biology and medicine*, 55(1), pp. 66–69.

Schlimpert, S. *et al.* (2017) 'Two dynamin-like proteins stabilize FtsZ rings during sporulation', *Proceedings of the National Academy of Sciences of the United States of America*, 114(30), pp. E6176–E6183.

Schlimpert, S., Flärdh, K. and Buttner, M. (2016) 'Fluorescence Time-lapse Imaging of the Complete S. venezuelae Life Cycle Using a Microfluidic Device', *Journal of visualized experiments: JoVE*, (108), p. 53863.

Schmidt, R. *et al.* (1990) 'Control of developmental transcription factor sigma F by sporulation regulatory proteins SpoIIAA and SpoIIAB in Bacillus subtilis', *Proceedings of the National Academy of Sciences of the United States of America*, 87(23), pp. 9221–9225.

Schumacher, M. A. *et al.* (2009) 'Molecular mechanisms of HipA-mediated multidrug tolerance and its neutralization by HipB', *Science*, 323(5912), pp. 396–401.

Schumacher, M. A. *et al.* (2017) 'The Streptomyces master regulator BldD binds c-di-GMP sequentially to create a functional BldD2-(c-di-GMP)4 complex', *Nucleic acids research*, 45(11), pp. 6923–6933.

Schumacher, M. A., Bush, M. J., *et al.* (2018) 'The crystal structure of the RsbN–σBldN complex from Streptomyces venezuelae defines a new structural class of anti-σ factor', *Nucleic Acids Research*, pp. 7467–7468. doi: 10.1093/nar/gky616.

Schumacher, M. A., den Hengst, C. D., *et al.* (2018) 'The MerR-like protein BldC binds DNA direct repeats as cooperative multimers to regulate Streptomyces development', *Nature communications*, 9(1), p. 1139.

Schumacher, M. A. *et al.* (2021) 'Evolution of a σ-(c-di-GMP)-anti-σ switch', *Proceedings of the National Academy of Sciences of the United States of America*, 118(30). doi: 10.1073/pnas.2105447118.

Seipke, R. F. *et al.* (2011) 'A single Streptomyces symbiont makes multiple antifungals to support the fungus farming ant Acromyrmex octospinosus', *PloS one*, 6(8), p. e22028.

Sevciková, B. *et al.* (2001) 'Stress-response sigma factor sigma(H) is essential for morphological differentiation of Streptomyces coelicolor A3(2)', *Archives of microbiology*, 177(1), pp. 98–106.

Sevcikova, B. *et al.* (2010) 'The Anti-Anti-Sigma Factor BldG Is Involved in Activation of the Stress Response Sigma Factor H in Streptomyces coelicolor A3(2)', *Journal of Bacteriology*, pp. 5674–5681. doi: 10.1128/jb.00828-10.

Sevcikova, B. and Kormanec, J. (2002) 'Activity of the Streptomyces coelicolor stress-response sigma factor sigmaH is regulated by an anti-sigma factor', *FEMS microbiology letters*, 209(2), pp. 229–235.

Ševčíková, B., Mazuráková, V. and Kormanec, J. (2005) 'Characterization of the alternative sigma factor σG in Streptomyces coelicolor A3(2)', *Folia microbiologica*, 50(1), p. 47.

Sexton, D. L. and Tocheva, E. I. (2020) 'Ultrastructure of Exospore Formation in Revealed by Cryo-Electron Tomography', *Frontiers in microbiology*, 11, p. 581135.

Skjerning, R. B. *et al.* (2019) 'The RES domain toxins of RES-Xre toxin-antitoxin modules induce cell stasis by degrading NAD+', *Molecular microbiology*, 111(1), pp. 221–236.

Šmídová, K. *et al.* (2019) 'DNA mapping and kinetic modeling of the HrdB regulon in Streptomyces coelicolor', *Nucleic acids research*, 47(2), pp. 621–633.

Smith, M. C. M. *et al.* (2013) 'Evolutionary Relationships among Actinophages and a Putative Adaptation for Growth in Streptomyces spp', *Journal of bacteriology*, 195(21), pp. 4924–4935.

Smollett, K. L. *et al.* (2012) 'Global Analysis of the Regulon of the Transcriptional Repressor LexA, a Key Component of SOS Response in Mycobacterium tuberculosis', *Journal of Biological Chemistry*, pp. 22004–22014. doi: 10.1074/jbc.m112.357715.

Sola-Landa, A. *et al.* (2005) 'Binding of PhoP to promoters of phosphate-regulated genes in Streptomyces coelicolor: identification of PHO boxes', *Molecular microbiology*, 56(5), pp. 1373–1385.

Sola-Landa, A. *et al.* (2008) 'Target genes and structure of the direct repeats in the DNA-binding sequences of the response regulator PhoP in Streptomyces coelicolor', *Nucleic acids research*, 36(4), pp. 1358–1368.

Soliveri, J. A. *et al.* (2000) 'Multiple paralogous genes related to the Streptomyces coelicolor developmental regulatory gene whiB are present in Streptomyces and other actinomycetes', *Microbiology*, 146 (Pt 2), pp. 333–343.

Stevenson, C. E. M. *et al.* (2013) 'Investigation of DNA sequence recognition by a streptomycete MarR family transcriptional regulator through surface plasmon resonance and X-ray crystallography', *Nucleic acids research*, 41(14), pp. 7009–7022.

Stevenson, C. E. M. and Lawson, D. M. (2021) 'Analysis of Protein–DNA Interactions Using Surface Plasmon Resonance and a ReDCaT Chip', *Protein-Ligand Interactions*, pp. 369–379. doi: 10.1007/978-1-0716-1197-5_17.

Stewart, M. Y. Y. *et al.* (2020a) 'Interaction of the Streptomyces Wbl protein WhiD with the principal sigma factor σHrdB depends on the WhiD [4Fe-4S] cluster', *Journal of Biological Chemistry*, pp. 9752–9765. doi: 10.1074/jbc.ra120.012708.

Stewart, M. Y. Y. *et al.* (2020b) 'Interaction of the Wbl protein WhiD with the principal sigma factor σ depends on the WhiD [4Fe-4S] cluster', *The Journal of biological chemistry*, 295(28), pp. 9752–9765.

Stuttard, C. (1979) 'Transduction of Auxotrophic Markers in a Chloramphenicol-producing Strain of Streptomyces', *Journal of General Microbiology*, pp. 479–482. doi: 10.1099/00221287-110-2-479.

Stuttard, C. (1982) 'Temperate Phages of Streptomyces venezuelae: Lysogeny and Host Specificity Shown by Phages SV1 and SV2', *Microbiology*, 128(1), pp. 115–121.

Sun, D. *et al.* (2017) 'An Alternative σ Factor, σ8, Controls Avermectin Production and Multiple Stress Responses in Streptomyces avermitilis', *Frontiers in microbiology*, 8, p. 736.

Sun, J. *et al.* (1999) 'Green fluorescent protein as a reporter for spatial and temporal gene expression in Streptomyces coelicolor A3(2)', *Microbiology*, 145 (Pt 9)(9), pp. 2221–2227.

Takano, E. *et al.* (2003) 'A rare leucine codon in adpA is implicated in the morphological defect of bldA mutants of Streptomyces coelicolor', *Molecular microbiology*, 50(2), pp. 475–486.

Takano, H. *et al.* (2003) 'Involvement of sigma(H) and related sigma factors in glucose-dependent initiation of morphological and physiological development of Streptomyces griseus', *Gene*, 320, pp. 127–135.

Takano, H. *et al.* (2007) 'Role of sigmaH paralogs in intracellular melanin formation and spore development in Streptomyces griseus', *Gene*, 393(1-2), pp. 43–52.

Takano, H. *et al.* (2011) 'Cross-interaction of anti-σH factor RshA with BldG, an anti-sigma factor antagonist in Streptomyces griseus', *FEMS microbiology letters*, 314(2), pp. 158–163.

Tanaka, Y. and Omura, S. (1990) 'Metabolism and products of actinomycetes. An introduction', *Nihon Hosenkin Gakkai shi = Actinomycetologica*, 4(1), pp. 13–14.

Taylor, B. L. and Zhulin, I. B. (1999) 'PAS domains: internal sensors of oxygen, redox potential, and light', *Microbiology and molecular biology reviews: MMBR*, 63(2), pp. 479–506.

Thanapipatsiri, A. *et al.* (2016) 'Discovery of Unusual Biaryl Polyketides by Activation of a Silent Streptomyces venezuelae Biosynthetic Gene Cluster', *Chembiochem: a European journal of chemical biology*, 17(22), pp. 2189–2198.

Tian, Y. *et al.* (2007) 'An unusual response regulator influences sporulation at early and late stages in Streptomyces coelicolor', *Journal of bacteriology*, 189(7), pp. 2873–2885.

Tiessen, A., Pérez-Rodríguez, P. and Delaye-Arredondo, L. J. (2012) 'Mathematical modeling and comparison of protein size distribution in different plant, animal, fungal and microbial species reveals a negative correlation between protein size and protein number, thus providing insight into the evolution of proteomes', *BMC research notes*, 5, p. 85.

Traxler, M. F. *et al.* (2012) 'Interspecies modulation of bacterial development through iron competition and siderophore piracy', *Molecular microbiology*, 86(3), pp. 628–644.

Tschowri, N. *et al.* (2014) 'Tetrameric c-di-GMP mediates effective transcription factor dimerization to control Streptomyces development', *Cell*, 158(5), pp. 1136–1147.

Tzanis, A. *et al.* (2014) 'A sporulation-specific, sigF-dependent protein, SspA, affects septum positioning in Streptomyces coelicolor', *Molecular microbiology*, 91(2), pp. 363–380.

Umeyama, T., Naruoka, A. and Horinouchi, S. (2000) 'Genetic and biochemical characterization of a protein phosphatase with dual substrate specificity in Streptomyces coelicolor A3(2)', *Gene*, 258(1-2), pp. 55–62.

Vijay, K. *et al.* (2000) 'A PP2C phosphatase containing a PAS domain is required to convey signals of energy stress to the sigmaB transcription factor of Bacillus subtilis', *Molecular microbiology*, 35(1), pp. 180–188.

Viollier, P. H. *et al.* (2001) 'Role of acid metabolism in Streptomyces coelicolor morphological differentiation and antibiotic biosynthesis', *Journal of bacteriology*, 183(10), pp. 3184–3192.

Viollier, P. H., Weihofen, A., *et al.* (2003) 'Post-transcriptional Regulation of the Streptomyces coelicolor Stress Responsive Sigma Factor, SigH, Involves Translational Control, Proteolytic Processing, and an Anti-sigma Factor Homolog', *Journal of Molecular Biology*, pp. 637–649. doi: 10.1016/s0022-2836(02)01280-9.

Viollier, P. H., Kelemen, G. H., *et al.* (2003) 'Specialized osmotic stress response systems involve multiple SigB-like sigma factors in Streptomyces coelicolor', *Molecular microbiology*, 47(3), pp. 699–714.

Voelker, U. *et al.* (1997) 'Stress activation of Bacillus subtilis sigma B can occur in the absence of the sigma B negative regulator RsbX', *Journal of bacteriology*, 179(6), pp. 1980–1984.

Vollmer, B. *et al.* (2019) 'Role of the Streptomyces spore wall synthesizing complex SSSC in differentiation of Streptomyces coelicolor A3(2)', *International journal of medical microbiology: IJMM*, 309(6), p. 151327.

Vora, T., Hottes, A. K. and Tavazoie, S. (2009) 'Protein occupancy landscape of a bacterial genome', *Molecular cell*, 35(2), pp. 247–253.

Waksman, S. A. (1957) 'Species concept among the actinomycetes with special reference to the genus Streptomyces', *Bacteriological reviews*, 21(1), pp. 1–29.

Wang, C. *et al.* (2010) 'SigN is responsible for differentiation and stress responses based on comparative proteomic analyses of Streptomyces coelicolor wild-type and sigN deletion strains', *Microbiological research*, 165(3), pp. 221–231.

Wang, L. *et al.* (2007) 'Role of an FtsK-like protein in genetic stability in Streptomyces coelicolor A3(2)', *Journal of bacteriology*, 189(6), pp. 2310–2318.

White, J. and Bibb, M. (1997) ‘bldA dependence of undecylprodigiosin production in Streptomyces coelicolor A3(2) involves a pathway-specific regulatory cascade’, *Journal of bacteriology*, 179(3), pp. 627–633.

Willey, J. *et al.* (1991) ‘Extracellular complementation of a developmental mutation implicates a small sporulation protein in aerial mycelium formation by S. coelicolor’, *Cell*, 65(4), pp. 641–650.

Willey, J., Schwedock, J. and Losick, R. (1993) ‘Multiple extracellular signals govern the production of a morphogenetic protein involved in aerial mycelium formation by Streptomyces coelicolor’, *Genes & development*, 7(5), pp. 895–903.

Wood, H. E., Devine, K. M. and McConnell, D. J. (1990) ‘Characterisation of a repressor gene (xre) and a temperature-sensitive allele from the Bacillus subtilis prophage, PBSX’, *Gene*, 96(1), pp. 83–88.

Worsley, S. F. *et al.* (2020) ‘Endophytes Promote Host Health and Enhance Growth across Plant Species’, *Applied and environmental microbiology*, 86(16). doi: 10.1128/AEM.01053-20.

Wright, L. F. and Hopwood, D. A. (1976) ‘Identification of the antibiotic determined by the SCP1 plasmid of Streptomyces coelicolor A3(2)’, *Journal of general microbiology*, 95(1), pp. 96–106.

Wu, F. *et al.* (2019) ‘Cell Boundary Confinement Sets the Size and Position of the E. coli Chromosome’, *Current Biology*, pp. 2131–2144.e4. doi: 10.1016/j.cub.2019.05.015.

Wu, L. J., Feucht, A. and Errington, J. (1998) ‘Prespore-specific gene expression in Bacillus subtilis is driven by sequestration of SpoIIE phosphatase to the prespore side of the asymmetric septum’, *Genes & Development*, pp. 1371–1380. doi: 10.1101/gad.12.9.1371.

Xu, H. *et al.* (2008) ‘A cellulose synthase-like protein involved in hyphal tip growth and morphological differentiation in streptomyces’, *Journal of bacteriology*, 190(14), pp. 4971–4978.

Yagüe, P. *et al.* (2014) ‘Transcriptomic analysis of liquid non-sporulating Streptomyces coelicolor cultures demonstrates the existence of a complex differentiation comparable to that occurring in solid sporulating cultures’, *PloS one*, 9(1), p. e86296.

Yamazaki, H., Ohnishi, Y. and Horinouchi, S. (2000) ‘An A-factor-dependent extracytoplasmic function sigma factor (sigma(AdsA)) that is essential for morphological development in Streptomyces griseus’, *Journal of bacteriology*, 182(16), pp. 4596–4605.

Yamazaki, H., Ohnishi, Y. and Horinouchi, S. (2003) ‘Transcriptional Switch On of ssgA by A-Factor, Which Is Essential for Spore Septum Formation in Streptomyces griseus’, *Journal of bacteriology*, 185(4), pp. 1273–1283.

Yang, X. *et al.* (1996) ‘Opposing pairs of serine protein kinases and phosphatases transmit signals of environmental stress to activate a bacterial transcription factor’, *Genes & development*, 10(18), pp. 2265–2275.

Yang, Z. *et al.* (2020) ‘Exploration and genome mining of natural products from marine Streptomyces’, *Applied microbiology and biotechnology*, 104(1), pp. 67–76.

Yao, T. *et al.* (2018) ‘Characterization of the biosynthetic gene cluster of the polyene macrolide antibiotic reedsmycins from a marine-derived Streptomyces strain’, *Microbial cell factories*, 17(1), p. 98.

Yim, G., Wang, H. and Davies, J. (2007) ‘Antibiotics as signalling molecules’, *Philosophical transactions of the Royal Society of London. Series B, Biological sciences*, 362(1483), pp. 1195–1200.

Yu, T. W. and Hopwood, D. A. (1995) ‘Ectopic expression of the Streptomyces coelicolor whiE genes for polyketide spore pigment synthesis and their interaction with the act genes for actinorhodin biosynthesis’, *Microbiology*, 141 (Pt 11), pp. 2779–2791.

Zhu, Y. *et al.* (2020) ‘A novel XRE family regulator that controls antibiotic production and development in Streptomyces coelicolor’, *Applied microbiology and biotechnology*, 104(23), pp. 10075–10089.